Graph decomposition techniques for quantum spin systems with multi-spin interactions

Graphzerlegungstechniken für Quantenspinsysteme mit Multi-Spin Wechselwirkungen

Der Naturwissenschaftlichen Fakultät
der Friedrich-Alexander-Universität
Erlangen-Nürnberg
zur
Erlangung des Doktorgrades Dr. rer. nat.
vorgelegt von

Matthias Mühlhauser

Als Dissertation genehmigt
von der Naturwissenschaftlichen Fakultät
der Friedrich-Alexander-Universität Erlangen-Nürnberg

Tag der mündlichen Prüfung: 6. Dezember 2024
Gutachter: Prof. Dr. Kai Phillip Schmidt
Prof. Dr. Daniel Burgarth

Abstract

This thesis, titled “Graph decomposition techniques for quantum spin systems with multi-spin interactions”, introduces an approach to formulate perturbative linked-cluster expansions via full hypergraph decompositions for quantum spin systems at zero temperature where the unperturbed part of the problem is local and the elementary perturbations couple more than two sites. The approach is then employed to investigate ground-state and excitation energies of several physical models, most of them featuring some kind of topological order.

With the presented approach the established method of linked-cluster expansions via a full graph decomposition is extended to problems with perturbations which couple multiple sites. The first step is to find all subclusters of the system which are relevant for the calculation of the desired quantity. In the next step the subclusters are sorted into equivalence classes, such that two subclusters in the same equivalence class, have the same reduced contribution to the desired quantity. It is actually this step where the presented method differs from conventional graph decompositions. For problems with a local unperturbed part and a perturbation consisting of two-spin couplings a graph representation of the subclusters appears natural: The vertices represent the sites and the edges represent the couplings between the sites. Finally, the equivalence of subclusters relates to isomorphism of the representing graphs. For perturbations with multi-spin couplings, such a graph representation is not as obvious, whereas a representation in terms of hypergraphs appears natural. In the end, we use a graph representation of these hypergraphs, the König representation, to distinguish equivalence classes of subclusters. As for conventional graph decompositions, this allows to calculate the reduced contribution to the desired quantity once for each class, instead of once for each subcluster. Considering highly symmetric lattice models, this typically reduces the calculational effort significantly.

It is the main focus of this thesis to explain hypergraph decompositions in a rather general way considering also minor complications like non-symmetric interactions or the presence of several different types of couplings. We encounter these aspects in the treatment of the various physical problems within this thesis. Importantly, we also use hypergraph decompositions to calculate series expansions in the topological phase of the toric code in a magnetic field. While we only slightly extend the previously known series, we explain how to systematically include the non-local effects of the anyonic statistics into a full hypergraph decomposition. Further considered models include the X-Cube model in a parallel magnetic field and a model which puts the X-Cube model and the 3D toric code into competition.

Zusammenfassung

Diese Arbeit, mit dem Titel „Graphzerlegungstechniken für Quantenspinsysteme mit Multi-Spin Wechselwirkungen“, beschreibt ein Verfahren perturbative Linked-Cluster Entwicklungen für Quantenspinsysteme am Temperaturnullpunkt mithilfe vollständiger Hypergraphzerlegungen zu formulieren, wobei der ungestörte Teil des Problems lokal ist und die elementare Störung mehr als zwei Plätze koppelt. Der Ansatz wird schließlich verwendet um Grundzustands- und Anregungsenergien verschiedener physikalischer Modelle zu berechnen, von denen die meisten eine Art topologischer Ordnung aufweisen.

Mithilfe des vorgestellten Verfahrens wird die etablierte Methode von Linked-Cluster Entwicklungen mittels vollständiger Graphzerlegung auf Probleme erweitert, bei denen Störterme mehrere Plätze koppeln. Der erste Schritt ist es alle Untercluster des Systems zu finden, die für die Berechnung der zu bestimmenden Größe relevant sind. Im nächsten Schritt werden die Untercluster in Äquivalenzklassen eingeteilt, so dass zwei Untercluster aus der selben Äquivalenzklasse den gleichen reduzierten Beitrag zu der zu bestimmenden Größe liefern. Tatsächlich, ist es dieser Schritt, wo sich die Methode von konventionellen Graphzerlegungen unterscheidet. Für Probleme mit einem lokalen ungestörten Teil und einer Störung die aus Zwei-Spin-Kopplungen besteht, ist eine Graphdarstellung der Untercluster offensichtlich: Die Vertices stellen die Plätze und die Kanten die Kopplungen zwischen den Plätzen dar. Die Äquivalenz von Unterclustern steht in enger Beziehung zur Isomorphie der entsprechenden Graphen. Für Störungen mit Multi-Spin-Kopplungen ist eine solche Graphdarstellung nicht mehr so offensichtlich, wohingegen eine Darstellung mithilfe von Hypergraphen naheliegend erscheint. Letztlich, nutzen wir eine Graphdarstellung dieser Hypergraphen, die Königdarstellung, um Äquivalenzklassen von Unterclustern zu unterscheiden. Wie bei herkömmlichen Graphzerlegungen, erlaubt dies den reduzierten Beitrag zur zu berechnenden Größe nur einmal für jede Äquivalenzklasse zu berechnen, anstatt einmal für jeden Untercluster. Im Bereich hochsymmetrischer Gittermodelle reduziert dies den Rechenaufwand typischerweise erheblich.

Es ist der Hauptfokus dieser Arbeit Hypergraphzerlegungen in einer relativ allgemeinen Weise zu erklären, und dabei auch kleinere Schwierigkeiten, wie nicht symmetrische Wechselwirkungen oder die Existenz mehrerer verschiedener Kopplungstypen miteinzubeziehen. Wir stoßen bei der Behandlung der verschiedenen physikalischen Modelle innerhalb dieser Arbeit auf diese Aspekte.

Ein wichtiger Punkt ist die Verwendung von Hypergraphzerlegungen, um Reihenenwicklungen für den Toric Code im Magnetfeld innerhalb der topologischen Phase zu berechnen. Insbesondere erklären wir, wie man die nicht-lokalen Effekte der anyonischen Statistik in eine volle Hypergraphzerlegung einbezieht. Weitere Modelle, die in dieser Arbeit behandelt werden, beinhalten das X-Cube Modell in einem parallelen magnetischen Feld, sowie ein Modell, welches das

X-Cube Modell und den 3D Toric Code in einem Hamiltonoperator kombiniert.

Contents

Chapter 1

Introduction

Quantum spin models play an important role in theoretical condensed matter physics in order to describe magnetic systems. Furthermore, they can be experimentally realized in quantum optical platforms [1–5]. In this thesis we consider quantum spin models on infinite lattices at zero temperature, which implies the absence of thermal fluctuations. Two well known quantum spin models are the transverse-field Ising model (TFIM) and the Heisenberg model. Both of these models have in common that they feature two-spin interactions, capturing the intuition that most interactions in nature are two-body interactions. The TFIM is a relatively simple model featuring a quantum phase transition (QPT), a phase transition driven by quantum fluctuations [6, 7]. Consequently, it is commonly used as an introductory example for a quantum phase transitions [7–9]. The Hamiltonian of the TFIM reads

$$H^{\mathrm{TFIM}} = -J \sum_{\langle i,j \rangle} \sigma_i^x \sigma_j^x - h \sum_{i \in \mathcal{L}} \sigma_i^z \tag{1.1}$$

where σ_i^α are the usual Pauli matrices acting at site i and $\langle i, j \rangle$ indicates that the sum runs over pairs of next neighbors on the underlying lattice $\mathcal{L}$. The coefficients J and h are real numbers. Notably, the model can be solved analytically on a chain [10]. The Hamiltonian is invariant under $\sigma^x \mapsto -\sigma^x$ [9]. For $h > 0$ and $J = 0$ the ground state is a polarized state, where all spins are pointing in positive z-direction, while for the opposite limit $h = 0$ and $J > 0$ there are two ground states for which all spins point simultaneously either in positive or negative x-direction. The phase for small h/J is called the magnetically ordered phase, whereas the phase at large h/J is called disordered paramagnetic phase [8, 9]. The phases can be distinguished via the ground-state expectation value of the magnetization in x-direction $m_x = \langle \sigma_i^x \rangle_{\mathrm{gs}}$. While $m_x = 0$ in the paramagnetic phase, in the magnetically ordered phase one has $m_x \neq 0$ [9]. In between these two phases a QPT of second order occurs [8, 9].

In contrast to the magnetically ordered quantum phases in the TFIM, a topologically ordered [11–13] phase can not be characterized by a local order parameter [7], like the m_x for the TFIM before, because topological phase transitions go beyond Landau's theory of symmetry breaking [14]. Instead, topologically ordered phases are characterized by a ground state which features a robust topological degeneracy [12] as well as a non-trivial topological entanglement entropy [15, 16]. Furthermore, the topological excitations feature an exotic mutual statistics [15–17] like the well known anyons in the toric code model [18].

Quantum spin models which feature topological order include the toric code [18] and its three

dimensional counterpart [19,20] which are paradigmatic examples of exactly solvable models which feature topological order. The two dimensional toric code is defined on a square lattice where spin-1/2 degrees of freedom are located on the links of the lattice [18]

$$H^{\mathrm{tc}} = -J_{+}\sum_{+} X_{+} - J_{\square}\sum_{\square} Z_{\square} \tag{1.2}$$

with the star operators X_{+} and the plaquette operators $Z_{\square}$

$$X_{+} = \prod_{i\in+} \sigma_i^x \,, \qquad Z_{\square} = \prod_{i\in\square} \sigma_i^z \,, \tag{1.3}$$

where the products run over the four spins surrounding a vertex of the lattice or the four spins at the edges of a plaquette, respectively, as illustrated in Fig. 1.1. These operators commute mutually and thus the problem is exactly solvable. Note that unlike the TFIM this model contains multi-spin interactions. However, the Kitaev honeycomb model is an example for a model with two-spin interactions which features topological order [21]. Notably, the ground state of the toric code model has been realized on a superconducting quantum processor, the topological entanglement entropy has been measured and the mutual statistics of charges and fluxes has been simulated [22].

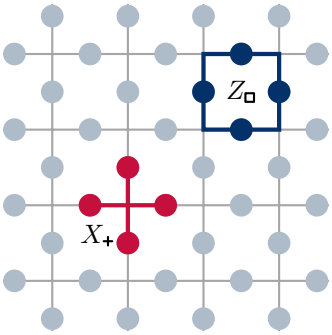

Figure 1.1: Illustration of the stabilizer operators X_{+} and $Z_{\square}$ of the toric code model. The image is taken from Ref. [23].

Interestingly, also many fracton models [24–27] are formulated as quantum spin models with multi-spin interactions. These models are typically defined in three or higher dimensions [24–26]. In contrast to conventional topological order, the ground-state degeneracy of fracton models does not only depend on the topology but also on geometrical properties of the system like the system size [25, 26, 28, 29]. Furthermore, for some fracton models it has been shown, that also the topological entanglement entropy of the ground state scales with the size of the considered subsystem [30, 31].

The elementary topological excitations in these fracton models are immobile [26], in the sense that they cannot move without creating additional excitations [27, 32]. In fracton phases of type I there are topological excitations formed by composites of fractons which can move within lower dimensional subsystems, whereas in fracton phases of type II there are no mobile topological excitations at all [26].

In order to investigate phase transitions out of topological phases one can add additional perturbations like an external field to the exactly solvable models [33–39]. The resulting models are

typically not exactly solvable in the thermodynamic limit any more. However, one wants to calculate properties of the models for various strengths of the perturbation in order to extract critical points and possibly also critical exponents in the case of a continuous quantum phase transition.

One possibility is to approximate the thermodynamic limit by exact numeric calculations on finite systems, this approach is called exact diagonalization (ED) [40, 41]. For small systems one could indeed just calculate the Hamiltonian matrix, which is often sparse, and calculate its eigenvalues and eigenvectors. But this approach is strongly limited by the dimension of the Hilbert space, which is 2^N for N spin-$1/2$ degrees of freedom, and thus the matrix has 2^{2N} entries, which very quickly becomes intractable even for modern supercomputers. However, using techniques like the Lanczos algorithm [42, 43] to calculate only the desired eigenvalues instead of the full spectrum and wisely exploiting symmetries gives access to larger systems [40, 41]. High-end calculations reach system sizes of 48 spin-$1/2$ degrees of freedom [44]. Nevertheless, even the best ED studies are strongly limited in the size of the considered systems.

Another important method to treat quantum spin systems is density matrix renormalization group (DMRG) [45–48]. DMRG is one of the best methods to study one-dimensional quantum lattice models [47], whereas the treatment of higher dimensional systems is more challenging [48, 49]. However, DMRG has been applied to two and three dimensional quantum lattice models [50, 51]. In these studies the reached system sizes are still limited, albeit significantly larger than the system sizes accessible to ED.

Interestingly, the states generated by DMRG are matrix product states (MPS) [52–54] which are a class of tensor network (TN) states particularly useful for one dimensional systems [55]. Generalizing TN methods to higher dimensions leads to projected entangled pair states (PEPS) [56], which are a higher dimensional generalization of MPS [55]. Interestingly, these TN states reflect the structure of entanglement of low-energy eigenstates of local gapped Hamiltonians (area law), whereas most of the states in the Hilbert space have a different structure of entanglement (volume law) [55, 57]. Hence, TN states characterize the exponentially small corner of states relevant for the low-energy physics of a quantum many-body problem within the Hilbert space [55, 58].

As a consequence, TNs permit an efficient variational ansatz to approximate low-energy properties of quantum many body Hamiltonians [58]. Notably, TN methods are also suitable to simulate systems in the thermodynamic limit [59]. One problem of TN methods is that for higher dimensional systems the contraction of tensor networks, and hence, the calculation of observables is usually extremely time consuming [54, 60]. However, there are approaches to efficiently contract such higher dimensional TNs [61, 62] and TNs have been used to simulate exotic two and three dimensional quantum spin systems [63, 64].

Another important class of methods for the simulation of quantum spin systems are Quantum Monte Carlo (QMC) methods [41, 65–68]. An important QMC method for the simulation of quantum spin systems is the method of stochastic series expansions (SSE) [68–70]. The SSE method makes it possible to efficiently calculate thermal expectation values on large finite systems [71]. Still one can simulate low enough temperatures to effectively obtain zero-temperature properties of the system and finite-size scaling allows to extrapolate finite-size results to the thermodynamic limit, effectively allowing the simulation of quantum many body systems in the thermodynamic limit and at $T = 0$ [70,72,73]. A well known limitation of QMC methods is the sign problem [41,74–77]. This sign problem is commonly present for frustrated quantum spin models [75,76]. Still it turned out that some of these frustrated problems can be formulated in a way such that no sign problem occurs [75,78–81] or such that the sign problem is sufficiently reduced to still permit efficient QMC

simulations [82, 83].

In the context of topological order, QMC methods have been applied to the toric code in a parallel magnetic field [34, 36]. Furthermore, SSE calculations have been employed to calculate the phase diagram of the X-Cube model in a parallel magnetic field [84]. Moreover, QMC methods have been used to calculate dynamic structure factors and correlation functions of several topological excitations of the X-Cube model in an external magnetic field [85] as well as to determine the type of the phase transition in the quantum Newman-Moore model in a transverse field [63, 86].

Further numerical approaches to quantum many body problems include continuous unitary transformations (CUTs) [87–89], variational wave functions based on neural networks [90–92] and hybrid quantum classical algorithms like the variational quantum eigensolver (VQE) [93, 94].

The method we consider in this thesis are series expansions [95–97]. Series expansions have a long tradition in the study of quantum phase transitions [98–105]. The aim is to find a power series expansion of a desired quantity

$$O(\lambda) = \sum_{j=0}^{k} a_j \lambda^j \tag{1.4}$$

up to an order k in the hope that the calculated terms provide useful information for the problem at hand [97]. Note that usually the coefficients a_j can be calculated exactly [97] so actually series expansions are not a numerical method. From a practical perspective, the functions in a physical context are typically well behaved around $\lambda = 0$ and so the first coefficients $a_0 \dots a_k$ of the series are assumed to provide significant information about the quantity $O(\lambda)$ [97].

Clearly, series expansions rely on perturbative expansions, and hence, need an unperturbed starting point, where the system is exactly solvable. For the TFIM given in Eq. (1.1) both limiting cases can be used as a perturbative starting point, and indeed both of these starting points have been used in investigations of the TFIM on several lattices [98–100, 106]. Notably, series expansions are commonly employed to investigate critical behavior [33,35,98–100,102,103,106–114]. Although the bare series cannot capture critical behavior, there are established extrapolation techniques which allow for a quantitative investigation of second-order quantum phase transitions [115, 116]. Series expansions proved to be a powerful tool to quantitatively investigate quantum phase transitions of various quantum spin systems, like the TFIM on several lattices [98–100, 106], the three-state Potts model [101] the TFIM with long-range interactions [71, 109, 110] and frustrated systems [103, 104, 117]. Interestingly, the method has also been applied to higher dimensional problems like the TFIM on the hypercubic lattice [108]. Furthermore, also phase transitions out of topological and fracton phases have been investigated using series expansions [33, 35, 39, 105, 107, 118, 119]. One way to approach series expansions is to execute a particular calculation on a single finite system. Interestingly, finite-order series expansions for several quantities like the ground-state energy and irreducible excitation energies can be obtained in the thermodynamic limit from calculations on such a finite system as long as the interactions of the system are of finite range [103, 120–122]. This is due to the fact that this finite system hosts all relevant perturbative fluctuations in the desired perturbation order (possibly up to translational symmetry) [123].

Another well established approach to series expansions is the method of linked-cluster expansions (LCEs) via a full graph decomposition [95–99, 124]. In this approach to LCEs the calculation of a quantity on the full system is decomposed into calculations on connected subclusters of the system [95, 96]. Typically, many of these subclusters have equivalent structure and one can iden-

tify classes of subclusters which have the same contribution to the desired quantity [95, 96, 99]. Obviously, it suffices to evaluate the contribution of each class once, which is then weighed with the number of instances of this class which need to be considered [95–99]. Typically, this saves a lot of time and memory and makes much higher perturbation orders accessible. From a technical point of view the subclusters are represented by graphs, where the vertices represent physical sites and the edges represent couplings of these sites within the Hamiltonian [95–97, 123]. The classes of subclusters correspond to isomorphism classes of the representing graphs. In the end one rewrites the quantity as a sum of appropriately weighed contributions of all relevant isomorphism classes [95–99].

Interestingly, LCEs via a full graph decompositions have also been used in conjunction with numerical methods instead of perturbative series expansions. This is commonly referred to as numerical linked-cluster expansions (NLCEs) [125, 126]. Examples of methods used with graph decompositions include ED [125, 127], CUTs [128] and recently also VQE [129].

The step to full hypergraph decompositions [130] presented in this thesis is motivated by the fact that a graph representation of subclusters is not as obvious when couplings between multiple sites have to be considered. In contrast, hypergraphs, a generalization of graphs where an edge can join an arbitrary number of vertices [131], naturally capture this kind of structure. Interestingly, hypergraphs can be represented by bipartite graphs such that the hypergraph isomorphism problem can be relegated to graph isomorphism [132,133]. Notably, hypergraphs and their representation in terms of bipartite graphs have also been used to distinguish complex chemical structures [134–136].

It is the main motivation of this thesis to thoroughly describe the method of hypergraph decompositions [130] and consider its application to several physical problems.

In Chap. 2 we cover some elements of graph and hypergraph theory which we find helpful in the context of graph and hypergraph decompositions.

In Chap. 3 we motivate and recapitulate the method of LCEs via a full graph decomposition [95–99,124] before we finally consider the generalization to hypergraph decompositions. As the method of hypergraph decompositions is introduced in Ref. [130], the corresponding section, Sect. 3.6, is essentially based on this reference. After introducing hypergraph decompositions we consider their application to series expansions about the low-field limit of the plaquette Ising model [137–140] in a transverse field on the cubic lattice. As in Ref. [130] this part serves as an example to get more familiar with the method. The corresponding section, Sect. 3.7, is closely based on Ref. [130].

Next, the two-dimensional toric code in an arbitrary homogeneous magnetic field is investigated. The corresponding chapter, Chap. 4, essentially corresponds to Ref. [23]. An in-detail explanation is given how the effects of the non-local interactions due to the anyonic statistics can be incorporated into a full hypergraph decomposition for the ground-state energy and the one-particle excitation gaps. The particularities of such a decomposition are addressed.

In Chap. 5 the ground-state energy of the X-Cube model in a parallel magnetic field is approached in order to confirm the ground-state phase diagram of the model, which is already known from QMC simulations [84]. In a sense this is the natural next step from the results of Ref. [39], where two specific field directions, which are well suited for perturbative expansions, are considered. These series are extended in this thesis, before the more general case of an arbitrary parallel field is investigated. While we can calculate series expansions from both, the high- and the low-field limit in this case, we cannot deduce a reliable estimate for the phase transition point from our results due to convergence issues of the resulting series.

Moreover, the phase diagram of a Hamiltonian combining the fractonic X-Cube model and the topologically ordered three dimensional toric code is explored by calculating the ground-state energies in various perturbative limits. The corresponding chapter, Chap. 6, is closely based on Ref. [118], though we integrate some variational calculations which are not covered in Ref. [118].

Lastly, in Chap. 7 the method of hypergraph decompositions is used to calculate the ground-state energy in the low-field limit of the TFIM on the triangular and the square lattice, using also a non-perturbative method to calculate the contributions of the subclusters. We use a duality mapping [121] in order to keep the formalism of the high-field type LCEs, at the expense of having effective multi-spin interactions. The obtained non-perturbative results are in good agreement with the known perturbative series [100] which use the low-field type formalism. Even beyond the phase transition the NLCE results are actually in agreement with the high-field series [99], even though convergence gets worse for higher fields.

Chapter 2

Elements of graph theory

In the context of linked-cluster expansions it is crucial to determine whether a cluster is structurally equivalent to another one, but also if and how often it is contained in a specific lattice [96, 97]. For the linked-cluster expansions where the perturbation terms are acting on two sites these tasks can be straightforwardly formulated in terms of graph and subgraph isomorphism. Both of these problems are computationally challenging [141–143], however, practically efficient algorithms to tackle graph isomorphism [133, 144–147], as well as subgraph isomorphism exist [142, 148–154]. Importantly, generic software libraries implementing common graph algorithms exist, which also include implementations of graph and subgraph isomorphism algorithms. For example there are the Boost Graph library (C++) or NetworkX (python).

In this chapter we introduce some elements of graph theory which are relevant in the context of this thesis. We start with some basic definitions which can be found in graph theory textbooks like Refs. [155–157]. We continue with the definitions of graph isomorphism and subgraph isomorphism and briefly introduce graph automorphisms and some related concepts which are helpful in order to access the symmetries of graphs. Finally, we add some notes about hypergraphs [131] which naturally arise when we generalize linked-cluster expansions to the case where perturbations act on multiple sites simultaneously. We mention some generalized versions of hypergraphs [158–161] to motivate a variant of hypergraphs which captures the structures we are considering within the application to physical problems. In order to access structural equivalence of hypergraphs we need to discuss hypergraph isomorphism. Importantly, the isomorphism problem for hypergraphs is equivalent to the isomorphism problem of simple bipartite graphs [132, 133] which are referred to as the König representation of a hypergraph [132].

2.1 Graphs

A graph $g = (V, E)$ is an ordered pair of finite sets, the set of vertices V and the set of edges E. In order to clearly denote to which graph the respective sets belong one can write $V(g)$ and $E(g)$. For a graph with n vertices we usually use $V = \{0, 1, 2, \ldots, n-1\}$. Each edge is a pair of vertices, called the end vertices of this edge. The edge is said to join its end vertices. An edge whose end vertices are identical is called a loop. The end vertices of a given edge are said to be incident to this edge. The degree of a vertex is the number of edges incident to this vertex (loops are counted

twice). Two distinct vertices are called neighbors or adjacent to each other if they are joined by an edge. Similarly, two edges are adjacent if they share at least one end vertex. In a simple graph every edge has two distinct end vertices and each pair of end vertices occurs maximally once in the set of edges. A graph where a given pair of end vertices can appear multiple times in the set of edges is called a multigraph. A graph whose edges are ordered pairs is a directed graph. As examples we illustrate a directed and an undirected graph in Fig. 2.1. From now on the term graph refers to simple undirected graphs, and we explicitly specify when we consider directed graphs or multigraphs, unless it is clear from the context.

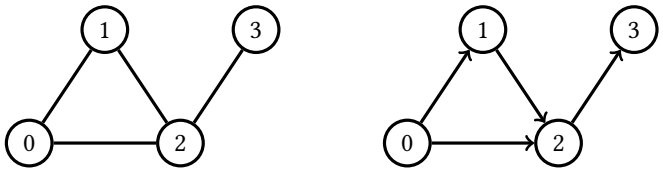

Figure 2.1: In the left part a (simple undirected) graph $g_1 = (V_1, E_1)$ is shown. The vertices given by $V_1 = \{0, 1, 2, 3\}$ are represented by circles and the edges $E_1 = \big\{\{0, 1\}, \{0, 2\}, \{1, 2\}, \{2, 3\}\big\}$ are visualized by lines. In the right part a simple directed graph $g_2 = (V_2, E_2)$ with the vertices $V_2 = \{0, 1, 2, 3\}$ is shown. The directed edges $E_2 = \big\{(0, 1), (0, 2), (1, 2), (2, 3)\big\}$ are visualized by arrows.

Additionally, colors can be assigned to edges and vertices of a graph. Formally, these colors are just an additional (integer) label assigned to the vertices or edges. However, in a graphical representation often actual colors are used. We use the term color to distinguish these additional labels from the labels assigned in order to name vertices and edges. An important representation of graphs is the adjacency matrix, where the rows and columns correspond to vertices. If an edge from u to v exists then $\mathcal{A}_{uv} = 1$ otherwise $\mathcal{A}_{uv} = 0$ [155]. Accordingly the adjaceny matrix is symmetric for undirected graphs. For the graphs illustrated in Fig. 2.1 the adjacency matrices are given by

$$\mathcal{A}(g_1) = \begin{bmatrix} 0 & 1 & 1 & 0 \\ 1 & 0 & 1 & 0 \\ 1 & 1 & 0 & 1 \\ 0 & 0 & 1 & 0 \end{bmatrix} \qquad \mathcal{A}(g_2) = \begin{bmatrix} 0 & 1 & 1 & 0 \\ 0 & 0 & 1 & 0 \\ 0 & 0 & 0 & 1 \\ 0 & 0 & 0 & 0 \end{bmatrix}. \tag{2.1}$$

2.1.1 Subgraphs and induced subgraphs

A subgraph $g = (V, E)$ of a graph $g' = (V', E')$ is a graph with $V \subseteq V'$ and $E \subseteq E'$ [157]. One writes $g \subseteq g'$ for a subgraph and $g \subset g'$ for a proper subgraph, which is a subgraph which fulfills $g \neq g'$. An induced subgraph additionally obeys that all vertices of the subgraph which are not adjacent in the subgraph g, are also not adjacent in the original graph g' [142]

$$\{u, v\} \notin E \Rightarrow \{u, v\} \notin E' \; \forall u, v \in V \tag{2.2}$$

Two examples for subgraphs are shown in Fig. 2.2. Moreover, if g is a subgraph of g', the graph g' is said to be a supergraph of g [162].

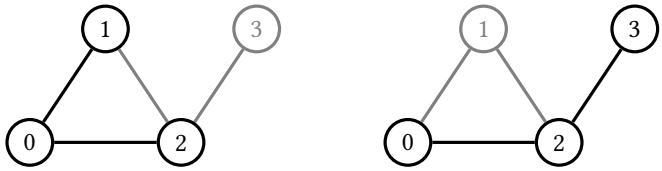

Figure 2.2: The image shows two graphs with opaque and transparent vertices and edges. The opaque vertices and edges indicate subgraphs of the respective graphs. In the left part the indicated subgraph is not an induced subgraph of the given graph, because the edge $\{1, 2\}$ is not present in the subgraph, although the vertices 1 and 2 are contained in the subgraph. In contrast, in the right part the indicated subgraph is an induced subgraph of the given graph, because it contains all edges of the graph which join vertices of the subgraph.

2.1.2 Paths and connectedness

The notion of connectedness is important for us as linked clusters are represented by connected graphs. A walk in a graph $g = (V, E)$ is an alternating sequence $(v_0, e_1, \ldots, e_n, v_n)$ of $v_i \in V$ edges $e_i \in E$ and vertices with $e_i = \{v_{i-1}, v_i\}$ [155, 157]. If all the vertices within such a walk are distinct it is called a path [155, 156]. The path $(v_0, \ldots, v_n)$ is then said to join the vertices v_0 and v_n and the vertices v_0 and v_n are said to be connected [162]. A graph g is called connected if for each pair of vertices $u, v \in V(g)$ a path connecting these vertices exists [155, 157]. If two vertices are joined by a path, they are in the same connected component of g (Otherwise, they are in different connected components of g). This relation is actually an equivalence relation partitioning the vertex set $V(g)$ into different equivalence classes [131, 162]. The connected components are the maximal connected subgraphs in the graph g, in the sense that there is no other connected subgraph of g containing these graphs [157].

2.1.3 Chromatic number

The chromatic number $\chi(g)$ of a graph g is the minimal number of vertex colors necessary to obtain a feasible vertex coloring of the graph g [163]. A feasible vertex coloring assigns colors to the vertices of a graph such that two adjacent vertices never have the same color [163]. An example for a feasible coloring of a graph can be found in Fig. 2.3. Interestingly, a graph with $\chi(g) = 2$ is also a bipartite graph and vice-versa [163].

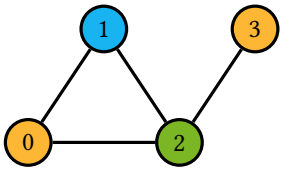

Figure 2.3: An example for a feasible vertex coloring. Adjacent vertices never have the same color. The chromatic number of the graph is 3.

2.1.4 Graph and subgraph isomorphism

Given two graphs $g = (V, E)$ and $g' = (V', E')$ there are several types of mappings $\varphi : V \to V'$ which are relevant for this thesis. As we name the vertices of a graph with integers $0, 1, 2, \ldots, n-1$, we explicitly specify such a mapping by $(\varphi(0), \varphi(1), \varphi(2), \ldots, \varphi(n-1))$, where n is the number

of vertices in the graph g. Note that φ induces a mapping from E to E' which takes each edge $\{u, v\} \in E$ to the edge $\{\varphi(u), \varphi(v)\} \in E'$.

For all of these mappings we require that they preserve the colors of edges and vertices, so vertices are only mapped to vertices with the same color and edges are only mapped to edges with the same color [142].

Graph isomorphism

A bijective mapping $\varphi : V \to V'$ with

$$\{u, v\} \in E \Leftrightarrow \{\varphi(u), \varphi(v)\} \in E' \tag{2.3}$$

is called graph isomorphism [143, 157]. If there is an isomorphism between two graphs g and g' they are said to be isomorphic and one writes $g \cong g'$. Intuitively, two isomorphic graphs have the same structure, they may only differ in the names of the vertices and be drawn differently as illustrated in Fig. 2.4. Graph isomorphism is an equivalence relation on the set of graphs and thus isomorphic graphs belong to the same isomorphism class [155,157]. Isomorphism classes of graphs are also informally referred to as unlabeled graphs [157] and accordingly isomorphic graphs may be addressed as the same unlabeled graph in some contexts.

Figure 2.4: Two isomorphic graphs. An isomorphism from the left graph to the right graph is given by the mapping $(0, 1, 4, 2, 3)$. This example is also given in Ref. [157] with different names for the vertices.

Subgraph isomorphism

An injective mapping $\varphi : V \to V'$ with

$$\{u, v\} \in E \Rightarrow \{\varphi(u), \varphi(v)\} \in E' \tag{2.4}$$

is called a subgraph isomorphism [142]. A subgraph isomorphism maps a graph g to a subgraph of g' which is isomorphic to g.

A subgraph isomorphism $\varphi : V \to V'$ with

$$\{u, v\} \notin E \Rightarrow \{\varphi(u), \varphi(v)\} \notin E' \tag{2.5}$$

is called an induced subgraph isomorphism [142, 164]. An induced subgraph isomorphism maps the graph g to an induced subgraph of g' which is isomorphic to g [164]. A subgraph isomorphism is also called subgraph monomorphism in order to distinguish it from the induced subgraph isomorphism [142, 164].

Importantly, the number of (induced) subgraph isomorphisms from g to g' is not necessarily equal to the number of (induced) subgraphs of g' which are isomorphic to g. Indeed, multiple (induced) subgraph isomorphisms may take the graph g to the same identical (induced) subgraph. The number of (induced) subgraph isomorphisms per (induced) subgraph isomorphic to g is equal to the size of the automorphism group of the graph g (see also Subsect. 2.1.6). Accordingly, the number of (induced) subgraphs isomorphic to g in g' is obtained by dividing the number of (induced) subgraph isomorphisms from g to g' by the number of automorphisms mapping g to itself [165].

2.1.5 Graph invariants

A graph invariant is a property of a graph g which is invariant under isomorphism [141, 155, 166–168]. Though some authors require graph invariants to be scalar properties [155, 166], we also consider multidimensional quantities as Ref. [167]. As it is invariant under isomorphism, a graph invariant does not depend on the labels assigned to name the vertices or edges but only on the structural properties of the graph [141, 168]. Clearly, for two isomorphic graphs each graph invariant agrees, while two graphs which differ in any graph invariant cannot be isomorphic. However, in general also two non-isomorphic graphs can agree in a given graph invariant [141].

Simple examples for graph invariants are the number of edges or the number of vertices of a graph [141, 166]. As a consequence two graphs which differ in these numbers cannot be isomorphic. Still one easily constructs an example for two graphs which agree in the number of edges and the number of vertices. Such an example is given in Fig. 2.5. Nevertheless, the idea of deciding isomorphism via a simple graph invariant is tempting. Such a graph invariant, which is different for each pair of non-isomorphic graphs, is called a complete graph invariant [141, 167].

As an isomorphism also conserves the degrees of the vertices, one can construct graph invariants based on the vertex degrees. A simple invariant based on vertex degrees is the ordered degree sequence [141, 166], which consists of the degrees of all the vertices in the graph in non-increasing order [141, 157]. An example is given in Fig. 2.5.

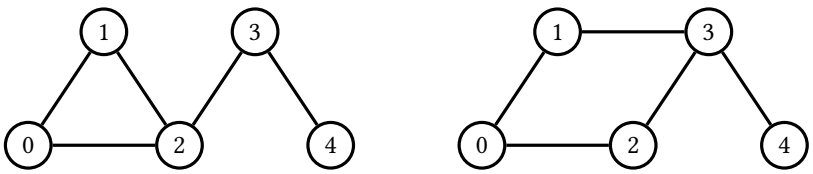

ODS: $(3, 2, 2, 2, 1)$
NDS: $(13, 13, 12, 10, 4)$

ODS: $(3, 2, 2, 2, 1)$
NDS: $(13, 13, 9, 9, 8)$

Figure 2.5: Two non-isomorphic graphs which have the same number of edges and vertices. Even the ordered degree sequences (ODS) agree. However, a different graph invariant (NDS) can be defined, which distinguishes the graphs. To calculate this invariant one determines the sum of the squared degrees of all the neighbors of a given vertex. The resulting values are arranged in a non-increasing sequence.

2.1.6 Graph automorphism

For a graph $g = (V, E)$ an isomorphism from g to itself $\gamma : V \to V$ is called a graph automorphism [143]. An automorphism is hence a permutation of the vertices V which preserves adjacency [155]. All the automorphisms of g together with composition form the automorphism group $\mathrm{Aut}(g)$ of g [143, 147]. The size of the automorphism group $|\mathrm{Aut}(g)|$ is equal to the number of symmetries of g and also referred to as symmetry number of g in the literature [97, 115]. Interestingly, for two isomorphic graphs $g \cong g'$ and an arbitrary isomorphism $\varphi : V(g) \to V(g')$, the set of all isomorphisms from g to g' can be written as [169, 170]

$$\mathrm{Iso}(g, g') = \{\varphi \circ \gamma \,|\, \gamma \in \mathrm{Aut}(g)\}. \tag{2.6}$$

Accordingly, the number of isomorphisms from g to g' is equal to the size of the automorphism group of g.

Automorphism orbits and stabilizers

Formally, acting with an automorphism on a graph g corresponds to the action of an element of the automorphism group on the vertex set $V(g)$ of the graph. Accordingly, some concepts of group theory (see e.g. [171]) may be helpful for the understanding of automorphism groups and the symmetries of graphs.

The set of the vertices to which a vertex $v \in V$ can be mapped by automorphisms of g is called the orbit $\mathrm{Orb}_{\mathrm{Aut}(g)}(v)$ of the vertex v under the automorphism group $\mathrm{Aut}(g)$. The set of all such orbits partitions the set V into disjoint subsets [171].

The automorphisms which map a vertex v to itself are called the stabilizers of v and form a subgroup $\mathrm{Aut}_v(g)$ of $\mathrm{Aut}(g)$. In Figs. 2.6 and 2.7 we explicitly give the elements of the automorphism group for two examples with some comments on orbits and stabilizers in the description of the images. By the orbit-stabilizer property (for finite groups) the cardinality of the stabilizer subgroup multiplied with the size of the orbit of the stabilized vertex equals the cardinality of the entire group [171].

$$|\mathrm{Aut}(g)| = |\mathrm{Orb}_{\mathrm{Aut}(g)}(v)| \cdot |\mathrm{Aut}_v(g)|\,. \tag{2.7}$$

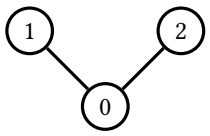

Automorphisms:

$(0, 1, 2)$
$(0, 2, 1)$

Figure 2.6: A simple example for the automorphisms of a graph g. Apart from the identity the only feasible automorphism maps vertex 1 to vertex 2 and vice versa. The automorphism orbits are $\mathrm{Orb}_{\mathrm{Aut}(g)}(1) = \mathrm{Orb}_{\mathrm{Aut}(g)}(2) = \{1, 2\}$ and $\mathrm{Orb}_{\mathrm{Aut}(g)}(0) = \{0\}$.

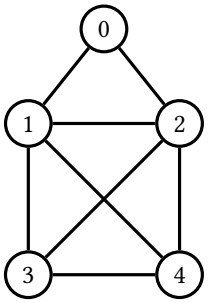

Automorphisms:

$(0, 1, 2, 3, 4)$
$(0, 1, 2, 4, 3)$
$(0, 2, 1, 3, 4)$
$(0, 2, 1, 4, 3)$

Figure 2.7: Another graph with a more complicated automorphism group. The orbits are $\{1, 2\}$, $\{3, 4\}$ and $\{0\}$. There are two stabilizers of the vertex 1, namely $(0, 1, 2, 3, 4)$, $(0, 1, 2, 4, 3)$.

2.2 Hypergraphs

Hypergraphs are a generalization of a graphs. In a hypergraph an edge is not necessarily a pair, instead an edge can be any non-empty subset of the vertex set with arbitrary cardinality [131, 172, 173]. These subsets are called hyperedges, or simply edges if it is clear from the context that actually hyperedges are meant. Within a hypergraph the edges are not necessarily distinct, and so the edges of a hypergraph actually form a family instead of a set [131, 172, 173]. Hypergraphs with distinct hyperedges are referred to as simple hypergraphs [131]. Formally, a hypergraph is an ordered pair (V, E) with a finite vertex set V and a family $E = (e_i)_{i \in I}$ of non-empty subsets of V called hyperedges [173]. I is a finite index set used to index the hyperedges. More concretely, for a hypergraph with n vertices and m edges we use $V = \{0, 1, \ldots, n-1\}$ and $E = \{e_0, e_1, \ldots, e_{m-1}\}$.

The notions of adjacency and incidence in a hypergraph are analogous to the notions for conventional graphs. Two vertices are adjacent if there is an hyperedge containing both of these vertices [131, 173]. Two edges which share at least one vertex are adjacent to each other [131] and a vertex is incident to a hyperedge if it is contained in this hyperedge [136, 174]. The degree of a vertex in a hypergraph is the number of hyperedges incident to this vertex [172, 174, 175]. Hypergraphs are of particular interest for us because they naturally model relations between multiple vertices. An example for a hypergraph $h = (V, E)$ is given by

$$\begin{aligned} &V = \{0, 1, 2, 3, 4, 5\}, \quad E = \{e_0, e_1, e_2\} \\ &e_0 = \{0, 1, 2\}, \quad e_1 = \{2, 3, 4\}, \quad e_2 = \{2, 3, 5\}. \end{aligned} \tag{2.8}$$

Formally one can represent a hypergraph $h = (V, E)$ by its incidence matrix $\mathcal{I}(h)$ [172] with the matrix elements

$$\mathcal{I}_{ij}(h) = \begin{cases} 0 & \text{if} \quad i \notin e_j \\ 1 & \text{if} \quad i \in e_j \end{cases} \tag{2.9}$$

In this matrix the columns represent the edges, and the rows represent the vertices [158, 172, 175].

For the hypergraph defined in Eq. 2.8 and illustrated in Fig. 2.8 the incidence matrix is

$$\mathcal{I}(h) = \begin{matrix} e_0 & e_1 & e_2 & \\ \end{matrix} \begin{bmatrix} 1 & 0 & 0 \\ 1 & 0 & 0 \\ 1 & 1 & 1 \\ 0 & 1 & 1 \\ 0 & 1 & 0 \\ 0 & 0 & 1 \end{bmatrix} \begin{matrix} 0 \\ 1 \\ 2 \\ 3 \\ 4 \\ 5\,. \end{matrix} \tag{2.10}$$

2.2.1 Hypergraph isomorphism

For hypergraphs with distinct hyperedges a hypergraph isomorphism is a bijective mapping between the vertex sets of two hypergraphs $h = (V, E)$ and $h' = (V', E')$ which preserves the edge structure $e \in E \Leftrightarrow \varphi(e) = \{\varphi(v) \mid v \in e\} \in E'$ [173], analogously to the definition for simple graphs. More generally, for two hypergraphs $h = (V, E = (e_i)_{i\in I})$ and $h' = (V', E' = (e_j)_{j\in J})$ an isomorphism consists of two bijective mappings [132, 133, 173]

$$\varphi_1 :\ V \to V'\,, \qquad \varphi_2 :\ E \to E'\,, \tag{2.11}$$

which fulfill

$$v \in e \Leftrightarrow \varphi_1(v) \in \varphi_2(e) \quad \forall v \in V,\ \forall e \in E\,. \tag{2.12}$$

Note that the edges are distinguished by the indices, so the mapping φ_2 is actually induced by a bijection between the index sets $\pi : I \to J$ [173].

Interestingly, two hypergraphs are isomorphic if and only if their König representations are isomorphic [132, 133]. The König representation of a hypergraph is a simple bipartite graph. One part of the vertices of the graph represents the vertices of the original hypergraph (vertex-part), the other part represents the edges of the original hypergraph (edge-part). The information to which part a vertex belongs is part of the König representation and can be incorporated using vertex colors. Two vertices are joined by an edge if and only if they represent an edge and a vertex which are incident in the original hypergraph. For the hypergraph $h = (V, E)$ the König representation $K(h)$ reads [132, 133]

$$\begin{aligned} K(h) &= (V_K, E_K)\,, \qquad V_K = V \cup E\,, \\ E_K &= \big\{\{e, v\} \,\big|\, v \in V, e \in E, v \in e\big\}, \end{aligned} \tag{2.13}$$

where the parts V, E are distinguished by vertex colors. This distinction is necessary to ensure that a graph isomorphism $\varphi : V \cup E \to V' \cup E'$ between two König graphs $K(h)$ and $K(h')$ respects $\varphi(V) = V'$ and $\varphi(E) = E'$ [133] ensuring that vertices which represent vertices of the original hypergraph are never mapped to vertices which represent hyperedges and vice versa. As a consequence the mapping φ actually consists of two bijections $\varphi_1 : V \to V'$ and $\varphi_2 : E \to E'$, one for each part, which fulfill

$$\{v, e\} \in E_K \Leftrightarrow \{\varphi_1(v), \varphi_2(e)\} \in E'_K \quad \forall v \in V \quad \forall e \in E. \tag{2.14}$$

Recalling that $\{v, e\} \in E_K$ is equivalent to $v \in e$ within the hypergraph one quickly notes the equivalence of isomorphism of hypergraphs and isomorphism of the respective König graphs,

which are simple bipartite graphs. A hypergraph $h = (V, E)$

$$\begin{aligned} V &= \{0,1,2,3,4,5\}\,, \quad E = \{e_0, e_1, e_2\}\,, \\ e_0 &= \{0,1,2\}\,, \quad e_1 = \{2,3,4\}\,, \quad e_2 = \{2,3,5\} \end{aligned} \tag{2.15}$$

and its König representation $K(h) = (V_K, E_K)$

$$\begin{aligned} V_K =& \{0,1,2,3,4,5,e_0,e_1,e_2\} \\ E_K =& \big\{\{0,e_0\},\{1,e_0\},\{2,e_0\},\{2,e_1\}, \\ & \{3,e_1\},\{4,e_1\},\{2,e_2\},\{3,e_2\},\{5,e_2\}\big\} \end{aligned} \tag{2.16}$$

are illustrated in Fig. 2.8. It is also interesting to look at the adjacency matrix of the König representation which corresponds to

$$\mathcal{A}(K(h)) = \begin{matrix} \\ E \\ V \end{matrix} \begin{matrix} \begin{matrix} E & \quad V \end{matrix} \\ \begin{bmatrix} 0 & \mathcal{I}^T(h) \\ \mathcal{I}(h) & 0 \end{bmatrix} \end{matrix} \tag{2.17}$$

where $\mathcal{I}(h)$ is the incidence matrix of h and $\mathcal{I}^T(h)$ denotes its transpose.

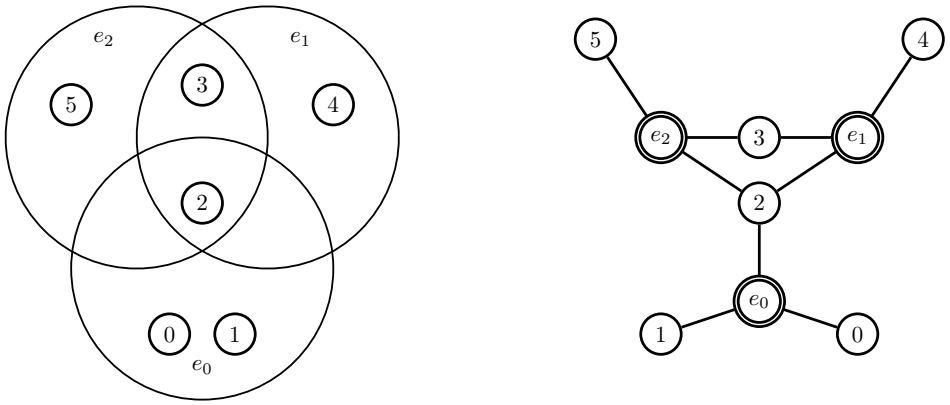

Figure 2.8: In the left part an example for a hypergraph is illustrated. The hyperedges are illustrated by drawing circles around the contained vertices. On the right the König representation of the hypergraph is given. The vertices corresponding to edges are represented by double circles to distinguish them from the other vertices.

2.2.2 Paths and Connectedness

Similar to the definition for graphs one can define paths for hypergraphs. Such a path is an alternating sequence of vertices and hyperedges $(v_0, e_{j_1}, v_1, \ldots, e_{j_n}, v_n)$ which contains each edge and each vertex only once and obeys $v_i, v_{i-1} \in e_{j_i}\ \forall i \in \{1,\ldots,n\}$ [131, 173]. As for graphs such a path is said to connect the vertices v_0 and v_n.

The relation of connectedness is an equivalence relation among the sets of vertices of a hypergraph and the respective equivalence classes are the connected components [131, 173]. Note that these connected components also contain all the edges which contain at least one vertex of the respective component. If each pair of vertices within a hypergraph is connected, the hypergraph has only one connected component and is said to be connected [173].

2.2.3 Some variants of hypergraphs

Directed hypergraphs are a generalization of hypergraphs, where the hyperedges are an ordered pair of disjoint sets of vertices, these subsets are referred to as head and tail of the hyperedge [158, 176]. This can be seen as a generalization of directed graphs allowing edges which join an arbitrary number of vertices.

Sequence hypergraphs are another generalization of hypergraphs where the edges are sequences of distinct vertices [159]. Similar definitions referred to as oriented hypergraphs or oriented k-uniform hypergraphs are given in [177, 178]. Also sequence hypergraphs can be interpreted as a generalization of directed graphs with edges which allow to join an arbitrary number of vertices.

In a sense, each vertex in a sequence hyperedge is assigned a unique role within this edge, while each vertex in a directed hyperedge is assigned one of two roles. However, for our applications we would like to assign a role to each vertex within a hyperedge such that several vertices within an hyperedge can be assigned the same role within the edge. In other words, we would like to assign a color to each incident hyperedge-vertex pair.

Interestingly, hypergraphs where an integer or real coefficient is assigned to each hyperedge-vertex pair are defined in the literature [160, 161]. In this case the entries of the incidence matrix are not restricted to $\{0, 1\}$ but can be any integer or even real number, depending on the definition. Typically, in these definitions a coefficient of 0 is equivalent to non-incidence as in the incidence matrix of a conventional hypergraph. Note that these oriented hypergraphs can represent sequence hypergraphs as well as directed hypergraphs. For sequence hypergraphs one can assign the position of the vertex within the sequence hyperedge to the respective hyperedge-vertex pair. Similarly, for directed hypergraphs one can incorporate the fact whether a vertex is in the head or the tail of a directed hyperedge into the respective entry of the incidence matrix. In a sense these definitions of hypergraphs allow to assign weights to edge-vertex pairs, though conceptually these weights are still related to the strength of the incidence.

So, instead of an oriented hypergraph, we consider a conventional hypergraph, with edges E and vertices V. To incorporate the role of the vertices within the edges, we define an incidence-type function

$$\theta : \Xi \to \mathbb{N}_0 \qquad \text{with} \quad \Xi = \{(v, e) \in V \times E \mid v \in e\} \tag{2.18}$$

which assigns a positive integer to each incident edge-vertex pair. With this we define the incidence-colored hypergraph $h = (V, E, \theta)$. As example for an incidence-colored hypergraph $h = (V, E, \theta)$ we write

$$\begin{aligned} &V = \{0, 1, 2, 3, 4, 5\}\,, \quad E = \{e_0, e_1, e_2\} \\ &e_0 = \{0, 1, 2\}\,, \quad e_1 = \{4, 2, 3\}\,, \quad e_2 = \{2, 3, 5\}\,, \end{aligned} \tag{2.19}$$

where we incorporate the values of θ using colors for the numbers inside the edges (black, red and blue). A vertex v which has color c inside edge e corresponds to $\theta(v, e) = c$. Isomorphism of

incidence-colored hypergraphs should preserve the incidence types so in addition to the condition in Eq. 2.12 one requests

$$v \in e \Rightarrow \theta^{(h)}(v,e) = \theta^{(h')}(\varphi_1(v), \varphi_2(e)) \quad \forall v \in V \quad \forall e \in E, \tag{2.20}$$

where $\theta^{(h)}$ denotes the incidence-type function of the incidence-colored hypergraph h. One can straightforwardly adapt the König representation to incidence-colored hypergraphs by encoding the incidence-types by edge colors in the bipartite graph as illustrated in Fig. 2.9. Considering that edges in the König representation indicate incidence in the original hypergraph, it is very natural to represent the type of the incidence by the color of the respective edge.

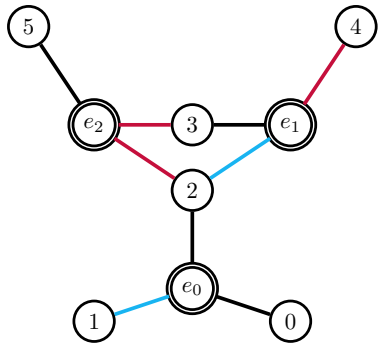

Figure 2.9: The König representation of the incidence colored hypergraph $h = (V, E, \theta)$ defined in Eq. (2.19). The incidence-types are represented by the colors of the edges.

Chapter 3

Linked-cluster expansions

3.1 Introduction

Graph decomposition techniques are a well established method to derive high-order series expansions for quantum lattice models at zero temperature [96, 97]. Importantly, the method of graph decompositions has been introduced much earlier in the context of high-temperature series expansions for quantum many-body systems [96,115]. The first appearance of a linked-cluster expansion (LCE) with a full graph decomposition for a quantum spin model at $T = 0$ is probably the work of Marland [97, 98], where perturbative series expansions for zero-temperature ground-state properties of the transverse-field Ising model are calculated. In this work and other works from that time [127, 179, 180] and later [99, 100] the method is attributed to B. G. Nickel.

For non-extensive quantities, like the excitation gap, graph decomposition techniques were already known [99, 100, 127], though these schemes required the use of disconnected clusters, and hence, cannot be considered as linked-cluster expansions. Some years later Gelfand described how to set up a true linked-cluster expansion for the one-quasiparticle dispersion [97,123,124]. However, Gelfand's approach was based on the assumption that the one-quasiparticle states are in a different symmetry sector than the ground state [96, 97, 124]. In the adverse case, it is still possible to do linked-cluster expansions. However, the evaluation of the contributions of individual clusters must be done with a method which guarantees that only connected clusters need to be considered, which is not the case for all methods [97, 181].

The treatment of two-particle excited states followed shortly afterwards [182, 183] and also the calculation of dynamic structure factors is described in the literature [96, 184]. Typically, LCEs are done perturbatively to obtain high-order series expansions. Though also a variant called numerical linked-cluster expansions (NLCEs) is established [125, 127, 128, 181, 185]. Here, we focus on the perturbative approach. We give a short discussion of the numerical approach in the context of a low-field expansion for the ferromagnetic transverse-field Ising model (TFIM) in Chap. 7. In order to access properties of two-particle excited states with LCEs, an orthogonal transformation, called multi-block orthogonal transformation (MBOT) [97], was developed [182,183]. This method leads to an effective Hamiltonian which conserves the number of quasiparticles [182, 183]. Such an effective Hamiltonian can also be obtained by perturbative continuous unitary transformations (pCUTs) [103, 120]. Importantly, the structure of these effective Hamiltonians allows systematic

calculations of irreducible n-quasiparticle quantities [120]. Both methods, pCUT and MBOT, lead to a cluster additive effective Hamiltonian, which is an effective Hamiltonian that can be written as a sum of contributions from connected subclusters of the system [181, 186, 187]. Accordingly, evaluating matrix elements of such an effective Hamiltonian on a large system can already be seen as an LCE. Indeed, choosing an appropriately designed finite cluster, it is possible to obtain results which are valid in the thermodynamic limit up to a given finite perturbation order [103, 120–122].

However, for lattice models typically a lot of subclusters have equivalent structure. This structural equivalence can be exploited to write the LCE as a sum over all structurally distinct subclusters [95–97]. To this end the structural information of the subclusters is usually incorporated into a graph, where the vertices represent the sites and the edges represent the couplings between sites corresponding to the bonds of the cluster [95–97, 123]. Structural equivalence of subclusters then corresponds to isomorphism of these graphs, and the LCE can be written as a sum over isomorphism classes of connected graphs [95–97]. In the literature this sum is often referred to as a sum over all (unlabeled) graphs or all distinct clusters [95–97].

In a perturbative setting there are typically two different limits in such a setup. While in expansions of the *high-field type* the perturbation is given by the couplings and the local terms are the unperturbed part, it is the other way around in expansions of the *low-field type* [96]. In the literature these types are also called high- or low-temperature (type) expansions respectively [96, 97, 99, 100]. Here, we focus on expansions of the high-field type, whereas in Chap. 7 we shortly address expansions of the low-field type.

3.2 General setup

As a starting point we consider a typical perturbation theory set up with a lattice Hamiltonian H of the form

$$H = H_0 + \mathcal{V} \tag{3.1}$$

where H_0 is the unperturbed part and $\mathcal{V}$ is the perturbation. First, we assume that H_0 can be written as sum over diagonal local operators which are defined identically for every site i of the lattice $\mathcal{L}$ [123]

$$H_0 = \sum_{i\in\mathcal{L}} H_{0,i} = \sum_{i\in\mathcal{L}} \left[e_0^{(0)} + \sum_{\alpha} n_i^{\alpha} \right] = E_0^{(0)} + Q, \tag{3.2}$$

where the operators n_i^{α} are local occupation number operators which count the number of quasiparticles of type α at site i, $E_0^{(0)} = N e_0^{(0)}$ is the unperturbed ground-state energy, Q counts the total number of quasiparticles in the system, and N is the number of lattice sites. Furthermore, we assume that $\mathcal{V}$ can be written as a sum of operators which act on the bonds b

$$\mathcal{V} = \sum_{b} \mathcal{V}_b \,. \tag{3.3}$$

In a general setting the bonds b are just sequences of distinct sites. These bonds indicate on which sites the *elementary perturbation operators* $\mathcal{V}_b$ act, and the order of the sequence indicates how $\mathcal{V}_b$ acts on these sites, as $\mathcal{V}_b$ might not act equivalently on all sites in b. Note that the bonds may contain more than two sites, if the perturbation features multi-site interactions. In the simplest case the perturbation $\mathcal{V}$ is given by

$$\mathcal{V} = \lambda V \,, \tag{3.4}$$

where $\mathcal{V}_b = \lambda V_b$ is defined equivalently for all bonds in the system. However, we also consider problems with several types of perturbation operators [123]

$$\mathcal{V} = \sum_i \mathcal{V}^{(i)} = \sum_i \lambda_i V^{(i)}\,, \tag{3.5}$$

where the different types of perturbation operators $V^{(i)}$ are associated to perturbation parameters λ_i. Clearly, different types of perturbation operators $V^{(i)}$ and $V^{(j)}$ can be associated with the same perturbation parameter by setting $\lambda_i = \lambda_j$. Importantly, the perturbation operators $V^{(i)}$ act only on bonds of type i, and accordingly

$$V^{(i)} = \sum_{b\in\mathcal{B}_i} V_b^{(i)}\,, \tag{3.6}$$

where the elementary perturbation $V_b^{(i)}$ is defined equivalently for all bonds of type i which we denote by $\mathcal{B}_i$. Note that this also implies that for each bond of type i the operator $\mathcal{V}_b$ corresponds simply to $\lambda_i V_b^{(i)}$. Finally, we remark that any two operators in the Hamiltonian, which do not act on at least one common site, do commute as we are considering quantum spin systems. The states of the system are elements of a product Hilbert space

$$\mathcal{H} = \bigotimes_{i\in\mathcal{L}} \mathcal{H}_i, \tag{3.7}$$

where $\mathcal{H}_i$ labels the local Hilbert space at site i. We refer to the states within this local Hilbert space using a subscript, e.g., $|0\rangle_i$ indicates that the state on site i is the unperturbed local ground state. Note that we frequently omit this index, if it is clear from the context to which site the local states belong. The global unperturbed ground state of the system is uniquely given by the product state $|0\rangle = \bigotimes_i |0\rangle_i$, and thus a perturbation series for the ground-state energy can be obtained using non-degenerate perturbation theory. The excited eigenstates of $H_{0,i}$ can be specified by the occupation numbers of the operators n_i^α. In particular, we denote an elementary excitation by a local state $|1_\alpha\rangle_i$. The flavor α distinguishes elementary excitations of the same unperturbed energy at the same site, which can be interpreted as quasiparticles of different flavor α.

Conversely to the ground state, the lowest excited state of the unperturbed system is not unique, because a quasiparticle can be located at any site of the lattice, and in general two quasiparticles of different flavors can have the same energy. As a consequence, the excited states have to be treated with degenerate perturbation theory by calculating an effective Hamiltonian H_{eff} which is block diagonal with respect to the unperturbed energies.

There are several methods to obtain such effective Hamiltonians. Importantly, one distinguishes between two-block [97,183] and multi-block diagonalization schemes [97,103,120,182,183]. Some of these methods are described in Sect. 3.4. In a two-block diagonalization scheme the effective Hamiltonian conserves the number of quasiparticles only within a selected eigenspace of the unperturbed Hamiltonian [183]. Conversely, a multi-block diagonalization results in an effective Hamiltonian which conserves the number of quasiparticles $[H_{\text{eff}}, Q] = 0$. Accordingly, the effective Hamiltonian has a block of size 1×1 which corresponds to the perturbed ground-state energy. Another block contains the matrix elements between the energetically lowest unperturbed states. These are the states which host exactly one quasiparticle. Yet another block contains the two-quasiparticle matrix elements and so on [120, 182, 183]. In general, unless specified explicitly,

or implicitly by naming a particular method, the effective Hamiltonians we consider in this thesis have this multi-block structure.

For the unperturbed case ($\lambda = 0$) the eigenbasis of the Hamiltonian is given by product states of eigenstates of the local operators $H_{0,i}$. The unique unperturbed ground state is denoted as

$$|0\rangle = |0\rangle \otimes |0\rangle \otimes \dots , \tag{3.8}$$

and for the one-quasiparticle sector we use the notation

$$|i, 1_\alpha\rangle = |0\rangle_0 \otimes \dots \otimes |0\rangle_{i-1} \otimes |1_\alpha\rangle_i \otimes |0\rangle_{i+1} \otimes \dots , \tag{3.9}$$

where the only excitation is located at site i. A paradigmatic example for such a setup is the transverse-field Ising model (TFIM) in the high field limit $h \gg J$

$$H^{\mathrm{TFIM}} = -h \sum_{i \in \mathcal{L}} \sigma_i^z - J \sum_{\langle i,j \rangle} \sigma_i^x \sigma_j^x , \tag{3.10}$$

where the operators σ_i^x and σ_i^z are the known Pauli matrices. To obtain the form given in Eq. (3.2) one can simply divide the Hamiltonian of the TFIM by $2h$ and consider the rescaled Hamiltonian

$$\frac{H^{\mathrm{TFIM}}}{2h} = -\frac{1}{2} \sum_{i \in \mathcal{L}} \sigma_i^z - \frac{J}{2h} \sum_{\langle i,j \rangle} \sigma_i^x \sigma_j^x . \tag{3.11}$$

In this example $H_{0,i}$ is given by $-\sigma_i^z/2$, which has the eigenvalues $\pm 1/2$ and $J/(2h)$ corresponds to the perturbation parameter λ. Moreover, the ground state is given by $|0\rangle = \bigotimes_i |\uparrow\rangle_i$ and a quasiparticle corresponds to a local spin flip.

3.2.1 Clusters and graphs

In the context of this thesis the term cluster refers to a system of sites and bonds, where the sites are real physical sites [97] and the bonds represent couplings of these sites within the Hamiltonian [123]. So we define a cluster $C = (S, B)$ as an ordered pair of sets[1], with the sites S and the bonds B analogously to the definition of graphs and hypergraphs [23, 123]. When it is not clear to which cluster the respective sets refer, we denote the sites and bonds of a cluster C by $S(C)$ and $B(C)$, respectively. Conversely to graphs or hypergraphs, we understand a cluster as an actual physical system where each site has coordinates in real space and the bonds represent couplings of sites within the Hamiltonian [23, 123]. If necessary, different types of couplings in the Hamiltonian might be reflected by different types of bonds. If the couplings are not symmetric, the bonds also need to encode which role a given site plays within the coupling. Typically, not all the information about a cluster is relevant for calculations. It is extremely helpful to represent clusters by graphs or hypergraphs in order to focus on their structural properties and identify structurally equivalent clusters. Indeed, the fact that the restriction of a lattice Hamiltonian onto structurally equivalent subclusters of the lattice leads to the same Hamiltonian up to a renumbering of the sites is a crucial ingredient of LCEs [96].

Consequently, we use terms from graph and hypergraph theory, like *isomorphic* or *connected* in the context of clusters. These terms can then be understood on the level of the graphs or hypergraphs representing the structure of the clusters. Importantly, often the term *linked* is used,

[1] In a more general definition B can contain multiple identical bonds, and accordingly B is a family instead of a set.

instead of the term connected. Also the term subcluster is understood analogously to the definition in graph theory. Given two clusters C_1 and C_2, C_1 is a subcluster of C_2 if $B(C_1) \subseteq B(C_2)$ and $S(C_1) \subseteq S(C_2)$. In this case we write $C_1 \subseteq C_2$. If additionally $C_1 \neq C_2$, we write $C_1 \subset C_2$ and call C_1 a proper subcluster of C_2.

3.2.2 Assigning contributions to subclusters

An important concept for LCEs is to decompose a scalar quantity O on a given cluster C into contributions from all subclusters of the cluster C [95, 96]

$$O(C) = \sum_{c \subseteq C} o(c) = o(C) + \sum_{c \subset C} o(c)\,. \tag{3.12}$$

The quantity $o(c)$ is called the *reduced contribution* of the cluster c to the quantity $O(C)$ [97, 123]. In this thesis we mainly consider LCEs for the ground-state energy and matrix elements of the effective Hamiltonian. Note that Eq. (3.12) is already a cluster expansion of the quantity $O(C)$. If we could find some argument that the reduced contributions $o(c)$ vanish for disconnected clusters it would be a linked-cluster expansion. These reduced contributions play an important role in the formalism of LCEs [95–97, 99]. Usually, the definitions in the literature are given in terms of graphs exploiting the structural equivalence of various subclusters [97, 99]. Here, we postpone the argument of structural equivalence to Subsect. 3.5.1 in order to attribute contributions to actual subclusters of the system. The reduced contribution $o(C)$ of a cluster C is obtained via [95, 96]

$$o(C) = O(C) - \sum_{c \subset C} o(c)\,. \tag{3.13}$$

The reduced contributions $o(C)$ can be determined iteratively, starting from the clusters which do not have any proper subclusters [97, 99]. For such a cluster $o(C) = O(C)$ as the sum over all proper subclusters in Eq. (3.13) vanishes. To make the concept of the reduced contribution more explicit, we consider it within a perturbative calculation of the quantity $O(C)$, where C is an arbitrary cluster. For the sake of simplicity we assume that the unperturbed part $O^{(0)}(C)$ is strictly local

$$O^{(0)}(C) = \sum_{i \in S(C)} o^{(0)}(i) = \sum_{i \in S(C)} O^{(0)}(i)\,, \tag{3.14}$$

where $o^{(0)}(i)$ labels the reduced contribution to $O^{(0)}(C)$ of the cluster consisting only of the site i. Furthermore, let us consider a lattice Hamiltonian as described in Subsect. 3.2

$$H = H_0 + \lambda V\,, \tag{3.15}$$

and follow the argumentation of Ref. [96] and rewrite the lattice Hamiltonian (3.15) on the cluster C as

$$H^C = \sum_{i \in S(C)} H_{0,i} + \sum_{b \in B(C)} \lambda_b V_b\,. \tag{3.16}$$

Note, that we formally introduce an individual perturbation parameter λ_b for each bond b. Calculating $O(C)$ in perturbation theory up to order k with these distinguished perturbation parameters λ_b results in

$$O(C) = O^{(0)}(C) + \sum_{\Lambda \in \mathcal{M}} \Big(\prod_{b, m_\Lambda(b) \neq 0} \lambda_b^{m_\Lambda(b)} \Big) w(\Lambda), \tag{3.17}$$

where $\mathcal{M}$ contains all combinations[2] of bonds containing from one up to k bonds. In any of these combinations, bonds are allowed to occur multiple times and the order of the elements does not matter. The number of occurrences of a bond b in a combination Λ is labeled by $m_\Lambda(b)$, whereas $w(\Lambda)$ is a weight associated with the combination Λ. Importantly, the monomial in the parameters λ_b clearly indicates which perturbation operators V_b are involved how many times to obtain the respective contribution. Interestingly, a combination Λ defines a subcluster $c \subseteq C$ by just considering the set of the bonds which are contained in Λ at least once and the sites contained in these bonds

$$B(c) = \left\{ b \in B(C) \;\middle|\; m_\Lambda(b) \neq 0 \right\}, \tag{3.18}$$

$$S(c) = \left\{ s \in S(C) \;\middle|\; \exists\, b \in B(c) \;:\; s \in b \right\}. \tag{3.19}$$

In this way we associate a subcluster to a set of combinations. Note that in principle these clusters can be disconnected. Rewriting equation (3.17) in terms of these clusters gives

$$O(C) = O^{(0)}(C) + \sum_{c \subseteq C} \sum_{\Lambda, \Lambda \mapsto c} \Big(\prod_{b, m_\Lambda(b) \neq 0} \lambda_b^{m_\Lambda(b)} \Big) w(\Lambda), \tag{3.20}$$

The first sum runs over all the subclusters of C, the second sum runs over all the combinations Λ which are associated with the cluster c. This can be further simplified to

$$O(C) = O^{(0)}(C) + \sum_{c \subseteq C, B(c) \neq \emptyset} o(c)\,, \tag{3.21}$$

where the sum runs over all clusters which contain at least one bond. Comparing Eqs. (3.20) and (3.21) it is apparent, that for each cluster with at least one bond, $o(c)$ consists of the perturbative corrections where λ_b from each bond inside the cluster c appears at least once (and no λ_b from outside the cluster appears). In this way the perturbative corrections are associated with clusters in an intuitive way and we have a clear prescription how to calculate the reduced contributions $o(c)$. The unperturbed part results from reduced contributions of subclusters which consist of only one site (and no bonds). Associating the contributions of the unperturbed part to the respective clusters one again obtains

$$O(C) = \sum_{c \subseteq C} o(c)\,, \tag{3.22}$$

which corresponds to Eq. 3.12.

3.3 Calculations on finite systems

A straightforward approach to perturbation theory in the context of lattice models is to calculate series expansions for a quantity of interest on a large finite cluster [103, 121]. To this end, we need to define the restriction of the lattice Hamiltonian H on a cluster $C = (S, B)$, also called cluster Hamiltonian. Within this cluster Hamilton we consider only the sites S and the bonds B of the

[2] Actually, these combinations are multisets (see e.g. [188]) over the set of bonds $B(C)$. A multiset over a set A is a pair (A, m), where m is a mapping from A to $\mathbb{N}_0$ which assigns a multiplicity $m(a)$ to each $a \in A$. Here the multisets $\Lambda = (B(C), m_\Lambda)$ consist of the bonds $B(C)$ together with a mapping m_Λ which assigns a multiplicity to each bond $b \in B(C)$. The set $\mathcal{M}$ contains all such multisets with $0 < \sum_b m_\Lambda(b) \leq k$.

cluster C [96]. Consequently, restricting a lattice Hamiltonian as introduced in Sect. 3.2 to the sites and bonds of the cluster C one obtains the cluster Hamiltonian

$$H^C = \sum_{i \in S} H_{0,i} + \sum_{b \in B} \mathcal{V}_b \,. \tag{3.23}$$

An effective Hamiltonian derived from this restricted Hamiltonian is denoted H^C_{eff}. In general, we allow that such a restricted operator O^C acts on any cluster which contains the cluster C. In this case the operator O^C acts as identity outside of the cluster C. Interestingly, for a suitable quantity, one can obtain a series expansion which is valid in the thermodynamic limit up to any finite perturbation order from calculations on a single appropriately designed finite cluster [103, 120–122]. In the following we consider such a calculation and review how contributions are assigned to subclusters for the ground-state energy and one-particle matrix elements of the effective Hamiltonian using the concept of the reduced contribution of a cluster, which is usually introduced in the context of full graph decompositions [96, 97, 99].

3.3.1 Ground-state energy

In an LCE the ground-state energy of a cluster C is written as a sum of reduced contributions $\epsilon_0(c)$ over all subclusters of C [96]

$$E_0(C) = \epsilon_0(C) + \sum_{c \subset C} \epsilon_0(c) \,. \tag{3.24}$$

In a perturbative setting the reduced contribution $\epsilon_0(c)$ can be thought of as the perturbative contributions which involve all bonds in the cluster c and no other bond [96]. Accordingly, clusters consisting of a single site (and no bond), only have reduced contributions of order zero. To obtain the reduced ground-state energy $\epsilon_0(C)$ of the cluster C one can rewrite Eq. (3.24) as [96]

$$\epsilon_0(C) = E_0(C) - \sum_{c \subset C} \epsilon_0(c) \,. \tag{3.25}$$

This expression can be evaluated iteratively, starting from clusters which do not have any proper subclusters, whose reduced contribution $\epsilon_0(c)$ is equal to the ground-state energy $E_0(c)$. Considering perturbation theory in order k, it is clear that $\epsilon_0(C) = 0$ for any cluster C which has more than k bonds [96]. Now, consider a disconnected cluster $C = C_1 \cup C_2$, with two disjoint subclusters C_1 and C_2. This means the clusters C_1 and C_2 do not share any sites and there is no bond in the cluster C which links a site in cluster C_1 to a site in cluster C_2. The ground-state energy E_0 is an extensive quantity, and hence, the ground-state energy on C is given by [96, 97, 99]

$$E_0(C) = E_0(C_1) + E_0(C_2) \,. \tag{3.26}$$

Furthermore, combining the fact that the ground-state energy is extensive with Eq. 3.24 yields [99]

$$E_0(C) = E_0(C_1) + E_0(C_2) = \sum_{c \subseteq C_1} \epsilon_0(c) + \sum_{c \subseteq C_2} \epsilon_0(c) \,. \tag{3.27}$$

Indeed, introducing an individual perturbation parameter for each bond in the cluster C as done in Eq. (3.16), Eq. (3.27) can only be fulfilled if the reduced ground-state energy of all subclusters $c \subseteq C$ which obey neither $c \subseteq C_1$ nor $c \subseteq C_2$ vanishes [95]. This also proves that the reduced ground-state energy of all disconnected clusters vanishes [95–99].

As a consequence, we only need to consider linked clusters in expression (3.24) and thus it is indeed a linked-cluster expansion. Next, evaluating the ground-state energy up to order k in perturbation theory, the clusters which have a non-vanishing reduced contribution have k or less bonds [96]. Recalling that only connected clusters can have a non-vanishing reduced contribution and considering bonds of finite range, we can conclude that the spatial extension of all contributing clusters is also finite, and hence, the ground-state energy in the thermodynamic limit can be calculated on a finite cluster [103, 120]. This cluster is conveniently designed as a periodic cluster, such that no connected subcluster with k or less bonds can go around this cluster, to avoid wrap-around effects [97, 103]. In this way any connected subcluster of this cluster with k or less bonds lies within a region of this cluster that cannot be distinguished from a corresponding part of the infinite lattice $\mathcal{L}$.

3.3.2 One-quasiparticle matrix elements

Suppose we have a quasiparticle number conserving effective Hamiltonian H_{eff}^{C} on a cluster C and aim to evaluate the one-quasiparticle matrix elements of this effective Hamiltonian. To this end we consider a matrix element of the effective Hamiltonian with respect to single-particle states in the product basis

$$m_{i,j}(C) = \langle i, 1_\alpha |\, H_{\text{eff}}^{C} \,| j, 1_\alpha \rangle \ . \tag{3.28}$$

For the sake of simplicity we consider only one particle type α here. Such a matrix element can be decomposed according to the formula (3.12) similar to the ground-state energy in Eq. (3.24)

$$m_{i,j}(C) = \sum_{c \subseteq C} \mu_{i,j}(c)\,, \tag{3.29}$$

where $\mu_{i,j}(c)$ is the reduced contribution of the cluster c to the matrix element $m_{i,j}(C)$. Again, we can write the reduced matrix element explicitly as

$$\mu_{i,j}(C) = m_{i,j}(C) - \sum_{c \subset C} \mu_{i,j}(c), \tag{3.30}$$

which can also be evaluated iteratively. In general not every subcluster $c \subset C$ contains the sites i and j. For a cluster c which contains neither the site i nor the site j one has

$$m_{i,j}(c) = \langle i, 1_\alpha |\, H_{\text{eff}}^{c} \,| j, 1_\alpha \rangle = \langle 0 |_c \, H_{\text{eff}}^{c} \, | 0 \rangle_c \times \langle i, 1_\alpha |_{\bar{c}}\, j, 1_\alpha \rangle_{\bar{c}} = \delta_{i,j} E_0(c), \tag{3.31}$$

where $\delta_{i,j}$ is the Kronecker symbol, and $E_0(c)$ is the ground-state energy of the cluster c. The subscript c indicates that the state is defined only on the sites of the subcluster c while a subscript $\bar{c}$ indicates a state within the Hilbert space on the remaining sites

$$\mathcal{H}^{\bar{c}} = \bigotimes_{i \in S(C) \setminus S(c)} \mathcal{H}_i\,. \tag{3.32}$$

The contributions of clusters which contain either i or j (but not both) vanish because the scalar product on $\mathcal{H}^{\bar{c}}$ yields zero in this case. So actually, we can write the matrix element as

$$m_{i,j}(C) = \sum_{c \subseteq C, c \not\ni i,j} \mu_{i,j}(c) + \sum_{c \subseteq C, c \ni i,j} \mu_{i,j}(c)\,. \tag{3.33}$$

If a cluster c does not contain neither i nor j, then the reduced contribution of the cluster to the matrix element $\mu_{i,j}(c)$ reads

$$\mu_{i,j}(c) = \delta_{i,j}\epsilon_0(c) \qquad i,j \notin c \tag{3.34}$$

where $\epsilon_0(c)$ is the reduced ground-state energy of the cluster c. Plugging Eq. (3.34) into Eq. (3.33) we obtain

$$m_{i,j}(C) = \sum_{c\subseteq C, c\not\ni i,j} \delta_{i,j}\epsilon_0(c) + \sum_{c\subseteq C, c\ni i,j} \mu_{i,j}(c). \tag{3.35}$$

We can now incorporate Gelfand's idea [124] by subtracting the ground-state energy as written in Eq. (3.24) from the matrix element $m_{i,j}$ given in Eq. (3.35)

$$\begin{aligned} t_{i,j}(C) &= m_{i,j}(C) - \delta_{i,j}E_0(C) \\ &= \sum_{c\subseteq C, c\not\ni i,j} \delta_{i,j}\big[\epsilon_0(c) - \epsilon_0(c)\big] + \sum_{c\subseteq C, c\ni i,j} \big[\mu_{i,j}(c) - \delta_{i,j}\epsilon_0(c)\big] \\ &= \sum_{c\subseteq C, c\ni i,j} \big[\mu_{i,j}(c) - \delta_{i,j}\epsilon_0(c)\big]\,. \end{aligned} \tag{3.36}$$

This sum contains only contributions from clusters which contain the sites i and j. Consequently, in our setup, all irreducible one-quasiparticle matrix elements $\langle i,1_\alpha| H_{\text{eff}} - E_0 |j,1_\alpha\rangle$ can be written as sums over subclusters which contain the sites i and j [183]. Note, that in other setups this must not always be the case [23, 187].

Conversely to the calculations for the ground-state energy, we have no guarantee that the sum will run over connected subclusters only [97]. In general this is the case if the effective Hamiltonian is cluster additive [186] (see Subsect. 3.3.4). If the bonds have finite range, the connected subclusters up to k bonds of the lattice which contain the site i can be found within a finite part of the lattice. So given a cluster additive effective Hamiltonian one can again obtain results for $t_{i,j}$ in the thermodynamic limit up to any finite perturbation order k on an appropriately designed finite cluster [103, 120–122]. This cluster is typically just a finite part of the lattice which contains any connected subcluster of the lattice up to k bonds containing the sites i and j.

3.3.3 Diagonalizing the one-quasiparticle sector

Let us assume that the quasiparticle number conserving effective Hamiltonian is cluster additive and consider the single-particle matrix elements on a lattice $\mathcal{L}$

$$t_{i,j}^{\alpha,\beta} = \langle i,1_\alpha| H_{\text{eff}} - E_0 |j,1_\beta\rangle\ . \tag{3.37}$$

For the sake of simplicity we assume that the lattice has a unit cell which contains only one lattice site. Even in this case there are extensively many matrix elements $t_{i,j}^{\alpha,\beta}$. So we need to exploit the translational symmetry of the system using the Fourier transform [183]

$$|\vec{k},1_\alpha\rangle = \frac{1}{\sqrt{N}} \sum_{i\in\mathcal{L}} \mathrm{e}^{\mathrm{i}\vec{k}\vec{r}_i} |i,1_\alpha\rangle\,, \tag{3.38}$$

where N is the number of sites in the lattice, $\vec{r}_i$ is the position of site i, and $\vec{k}$ is a vector of the reciprocal lattice. Another consequence of translational symmetry is that the value of a matrix

element does not depend on the actual positions of the sites but only on the relative position $\vec{\delta} = \vec{r}_i - \vec{r}_j$ [183]

$$t_{i,j}^{\alpha,\beta} = t_{\vec{\delta}}^{\alpha,\beta} \qquad \forall i,j \;\text{ with }\; \vec{\delta} = \vec{r}_i - \vec{r}_j \,. \tag{3.39}$$

A matrix element in momentum space is given by

$$\langle \vec{k}, 1_\alpha | \, H_{\text{eff}} - E_0 \, | \vec{k}', 1_\beta \rangle = \delta_{\vec{k},\vec{k}'} \sum_{\vec{\delta}} \mathrm{e}^{-\mathrm{i}\vec{k}\vec{\delta}} t_{\vec{\delta}}^{\alpha,\beta} = \delta_{\vec{k},\vec{k}'} \Omega^{\alpha,\beta}(\vec{k}), \tag{3.40}$$

where the sum runs over all relative positions $\vec{\delta}$. If the interactions $\mathcal{V}_b$ of the Hamiltonian are of finite range this sum contains only a finite number of non-vanishing hopping elements $t_{\vec{\delta}}^{\alpha,\beta}$ in any finite perturbation order. In general the size of the matrix $\Omega(\vec{k})$ is determined by the number of involved quasiparticle types and the size of the unit cell. Diagonalizing the matrix yields the eigenvalues $\omega_n(\vec{k})$. The minimum of these eigenvalues in the Brillouin zone is the excitation gap.

As we have seen in Subsect. 3.3.2, all relevant hopping elements $t_{i,j}^{\alpha,\beta}$ can be evaluated in any finite perturbation order k on appropriately designed finite clusters, if the bonds have finite range and the effective Hamiltonian is cluster additive [103,120–122]. Actually, all hopping elements $t_{i,j}^{\alpha,\beta}$ in order k can be evaluated on a cluster C which is a section of the infinite lattice given by one site i and all other sites and bonds lying within a distance of up to k bonds. The calculations can be further optimized, by designing a cluster for each single $t_{i,j}^{\alpha,\beta}$. The most straightforward way is to generate all connected subclusters up to k bonds which contain the sites i and j. All sites and bonds which are contained in at least one of these subclusters together form a cluster which suffices for the calculation [189]. Even in higher particle sectors only clusters which host at least one quasiparticle can contribute to matrix elements of $H_{\text{eff}} - E_0$. However, in the two-quasiparticle sector there are typically contributions from clusters which only host one quasiparticle. The other quasiparticle is then allowed to be at any site within the remaining Hilbert space leading to extensively many one-quasiparticle contributions. By appropriately subtracting these one-quasiparticle contributions one can also calculate two-quasiparticle energies [183]. Finally, this scheme can be continued to irreducible interaction energies of an arbitrary number of quasiparticles [120].

3.3.4 Cluster additivity

Cluster additivity is a crucial property to obtain results which are valid in the thermodynamic limit from calculations on finite clusters [120, 186, 187]. Consider a cluster $C = C_1 \cup C_2$, consisting of two disjoint subclusters C_1 and C_2. Accordingly, the clusters C_1 and C_2 do not share any sites and there is no bond in the cluster C which links a site in cluster C_1 to a site in cluster C_2. A quantity M^C is called *cluster additive* if it can be written as [120]

$$M^C = M^{C_1} + M^{C_2} = M^{C_1} \otimes \mathbb{1}^{C_2} + \mathbb{1}^{C_1} \otimes M^{C_2} \,. \tag{3.41}$$

for any disconnected cluster C. This means that M^C can be arranged in a sum which does not contain any term which acts non-trivially on C_1 and C_2 simultaneously. In the end, this allows to write the quantity M^C as a sum over all connected components $\mathcal{K}(C)$ of C

$$M^C = \sum_{X \in \mathcal{K}(C)} M^X \,, \tag{3.42}$$

where the contributions M^X contain all terms of M^C which act non-trivially only within the connected cluster $X \in \mathcal{K}(C)$. This implies that the reduced contribution of C to any matrix element of M^C vanishes [186]. Consequently, if an effective Hamiltonian H_{eff} is cluster additive it can be written as a sum of terms which act only on linked clusters. So, the reduced contribution of any disconnected cluster to any matrix element of this effective Hamiltonian vanishes [186].

3.4 Perturbation Theory

Perturbation theory is a standard technique in quantum mechanics, and thus, it is described in standard texts like [190, 191]. Here, we consider time independent perturbation theory for a time independent lattice Hamiltonian

$$H = H_0 + \mathcal{V} \,. \tag{3.43}$$

The operator H_0 is the unperturbed part and the perturbation $\mathcal{V}$ is defined as

$$\mathcal{V} = \sum_i \lambda_i V^{(i)} \,, \tag{3.44}$$

where λ_i are real valued perturbation parameters. For the unperturbed part H_0 the problem is solved in the sense that the eigenvalues $E_n^{(0)}$ and eigenvectors $|\Psi_n^{(0)}\rangle$ of H_0 are known [190]. The number of different perturbation parameters depends on the problem. In the simplest case we have only a single perturbation parameter λ, and write

$$H = H_0 + \lambda V \,, \tag{3.45}$$

where we omitted the index i of the perturbation V and the perturbation parameter λ. In the non-degenerate case the aim is to find approximations to the eigenvalue

$$E_n = \sum_{r=0}^{\infty} \lambda^r E_n^{(r)} \tag{3.46}$$

and the corresponding eigenstate

$$|\Psi_n\rangle = \sum_{r=0}^{\infty} \lambda^r \, |\Psi_n^{(r)}\rangle \tag{3.47}$$

of the full Hamiltonian (3.45). In the degenerate case one typically derives an effective Hamiltonian which is block diagonal with respect to an eigenspace L of the unperturbed Hamiltonian

$$H_{\text{eff}} = \Gamma^\dagger H \Gamma, \tag{3.48}$$

where Γ is a transformation. To obtain such a transformation several methods are known [103, 181–183, 192]. Some of these methods like perturbative continuous transformations (pCUTs) [103, 120] and the multi-block orthogonal transformation (MBOT) [182, 183] yield an effective Hamiltonian which is block diagonal with respect to all unperturbed energy levels

$$[H_{\text{eff}}, H_0] = 0 \,. \tag{3.49}$$

Other methods like Takahashi's perturbation theory [192] or perturbative cluster additive transformations (pCAT) [181] construct an effective Hamiltonian for a selected eigenspace of H_0. In

this section we review some of these methods. We also comment how these methods can be used together with a bookkeeping technique in order to directly obtain the reduced contributions of a given cluster needed in LCEs. For pCUTs such a bookkeeping technique is described in Ref. [123]. Here, we also address bookkeeping techniques for Löwdin's partitioning technique and Takahashi's perturbation theory [193].

3.4.1 Perturbative continuous unitary transformations

Perturbative continuous unitary transformations (pCUTs) are a perturbative method to transform a quantum many-body Hamiltonian of the form $H = H_0 + \mathcal{V}$ to an effective Hamiltonian H_{eff} which conserves the number of quasiparticles [103, 120]. The method is applicable if the unperturbed Hamiltonian has an equidistant spectrum which is bounded from below [103]

$$H_0 = E_0^{(0)} + \sum_{i \in \mathcal{L}} \sum_{\alpha} n_i^{\alpha} = E_0^{(0)} + Q \,, \tag{3.50}$$

where $E_0^{(0)}$ is the unperturbed ground-state energy, the n_i^{α} are local quasiparticle counting operators, which count excitations of flavor α at site i, and the operator Q counts the total number of quasiparticles in the system. Furthermore, the perturbation must be of the form [103]

$$\mathcal{V} = \sum_{n=-N}^{N} \mathcal{T}_n \,, \tag{3.51}$$

where the operators $\mathcal{T}_n$ create n particles

$$[Q, \mathcal{T}_n] = n\mathcal{T}_n \,. \tag{3.52}$$

For negative values of n this means that $\mathcal{T}_n$ annihilates $|n|$ particles.

As pCUTs are a perturbative variant of continuous unitary transformations (CUTs) which have been introduced by Wegner [87] and Glazek and Wilson [88], we review the main ideas of CUTs before we proceed to pCUTs. The basic idea of CUTs is to transform the Hamiltonian in a continuous way into a (block-)diagonal effective Hamiltonian [87]. For a given non-negative continuous parameter ℓ the flowing Hamiltonian is defined as [89]

$$H(\ell) = U^{\dagger}(\ell) H U(\ell), \tag{3.53}$$

where $U(\ell)$ is a unitary transformation. The flow starts at $\ell = 0$ with the original Hamiltonian $H = H(0)$, whereas the effective Hamiltonian corresponds to $H_{\text{eff}} = H(\infty)$ [103]. Taking the derivative of $H(\ell)$ with respect to ℓ yields the flow equation [87]

$$\frac{\mathrm{d}H(\ell)}{\mathrm{d}\ell} = [\eta(\ell), H(\ell)] \,, \tag{3.54}$$

where $\eta(\ell) = -U^{\dagger}(\ell)\frac{\mathrm{d}U(\ell)}{\mathrm{d}\ell}$ is the anti-Hermitian generator of the unitary transformation $U(\ell)$ [89, 194]. The transformation $U(\ell)$ is equivalent to the application of infinitely many infinitesimal unitary transformations $\exp(-\eta(\ell)\mathrm{d}\ell)$ [89, 194]. There are several choices for the generator $\eta(\ell)$. The generator proposed by Wegner [87] is not optimal for problems where the initial Hamiltonian has a band diagonal structure, as the generator does not preserve this structure during

the flow [103, 195]. Note that the form of H_0 and $\mathcal{V}$ specified in Eqs. (3.50) and (3.51) implies a band-diagonal structure. Mielke proposed a generator which preserves band diagonality of the Hamiltonian during the flow [195]. Finally, a generator leading to an effective Hamiltonian which conserves the number of quasiparticles has been introduced in Ref. [103]. This generator is also referred to as Mielke-Knetter-Uhrig (MKU) generator and reads in the eigenbasis of Q [89]

$$\eta_{ij}(\ell) = \mathrm{sgn}(q_{i,i} - q_{j,j}) h_{i,j}(\ell), \tag{3.55}$$

where $h_{i,j}(\ell)$ are the matrix elements of $H(\ell)$, $q_{i,j}$ are the matrix elements of the operator Q, and sgn denotes the sign function. Accordingly, $q_{i,i}$ is simply the quasiparticle number of the i-th eigenstate of H_0. A proof that the generator (3.55) leads indeed to a quasiparticle number conserving effective Hamiltonian $[H_{\text{eff}}, Q] = 0$ is given in [103]. In order to obtain perturbative expansions of the effective Hamiltonian one expands the operators $\eta(\ell)$ and $H(\ell)$ [103, 196]

$$H(\ell) = E_0^{(0)} + Q + \sum_{k=1}^{\infty} \sum_{\vec{m}, |\vec{m}|=k} \mathcal{F}(\ell, \vec{m}) \mathcal{T}(\vec{m}) \tag{3.56}$$

$$\eta(\ell) = \sum_{k=1}^{\infty} \sum_{\vec{m}, |\vec{m}|=k} \mathrm{sgn}(M(\vec{m})) \mathcal{F}(\ell, \vec{m}) \mathcal{T}(\vec{m}), \tag{3.57}$$

where $\mathcal{F}(\ell, \vec{m})$ are unknown real functions. The notation for a sequence $\vec{m} = (m_1, m_2, \ldots, m_k)$ is explained as follows

$$m_i \in \{0, \pm 1, \ldots, \pm N\} \tag{3.58}$$

$$|\vec{m}| = \dim(\vec{m}) = k \tag{3.59}$$

$$\mathcal{T}(\vec{m}) = \mathcal{T}_{m_1} \mathcal{T}_{m_2} \ldots \mathcal{T}_{m_k} \tag{3.60}$$

$$M(\vec{m}) = \sum_{i=1}^{k} m_i \,. \tag{3.61}$$

The property that the band-diagonality of the Hamiltonian is preserved during the flow is reflected by the fact that $\mathcal{F}(\ell, \vec{m}) = 0$ if $|M(\vec{m})| > N$ [103, 196]. Plugging the expressions (3.56) and (3.57) into the flow equation (3.54) yields differential equations for the functions $\mathcal{F}(\ell, \vec{m})$. With these equations the functions $\mathcal{F}(\ell, m)$ can be determined order by order [103, 196]. After taking the limit $\ell \to \infty$ one obtains the quasiparticle number conserving effective Hamiltonian [103, 196]

$$H_{\text{eff}} = E_0^{(0)} + Q + \sum_{k=1}^{\infty} \sum_{\substack{\vec{m}, |\vec{m}|=k \\ M(\vec{m}=0)}} \mathcal{C}(\vec{m}) \mathcal{T}(\vec{m}) \,, \tag{3.62}$$

where $\mathcal{C}(\vec{m}) = \lim_{\ell \to \infty} \mathcal{F}(\ell, \vec{m})$ are model independent rational coefficients. The operators $\mathcal{T}_n$ are sums of bond-local operators [121, 123]

$$\mathcal{T}_n = \sum_b \mathcal{T}_{n,b} \,, \tag{3.63}$$

where an operator $\mathcal{T}_{n,b}$ acts only on the bond b. With these operators the effective Hamiltonian can then be rewritten as [123]

$$H_{\text{eff}} = E_0^{(0)} + Q + \sum_{k=1}^{\infty} \sum_{\vec{b}, |\vec{b}|=k} \sum_{\substack{\vec{m}, |\vec{m}|=k \\ M(\vec{m}=0)}} \mathcal{C}(\vec{m}) \mathcal{T}(\vec{m}, \vec{b}) \,, \tag{3.64}$$

where $\vec{b}$ are sequences of bonds, which can contain any bond an arbitrary number of times and the notation is explained as

$$\vec{b} = (b_1, \dots b_k) \tag{3.65}$$

$$|\vec{b}| = \dim(\vec{b}) = k \tag{3.66}$$

$$\mathcal{T}(\vec{m}, \vec{b}) = \mathcal{T}_{m_1,b_1} \dots \mathcal{T}_{m_k,b_k} \tag{3.67}$$

The contributions from all the bond sequences $\vec{b}$ which involve all bonds of the cluster C (and no other bond) correspond to the reduced contribution of the cluster C to the effective Hamiltonian [121,123]. This does not apply to clusters without bonds. However, these are only relevant in order zero, where the solution of the considered problem is anyway already known.

Accordingly, the reduced contribution of a cluster can be evaluated without explicit subcluster subtraction. Instead, one can employ a bookkeeping scheme which identifies the relevant terms by tracking on which bonds the individual operators $\mathcal{T}_{n,b}$ acted during the evaluation of the sequences $\mathcal{T}(\vec{m})$ [123].

An important feature of pCUTs is, that the reduced contribution of any disconnected cluster to the effective Hamiltonian vanishes [123]. As a consequence, we only need to consider processes $\mathcal{T}(\vec{m}, \vec{b})$, where the bonds in $\vec{b}$ together with the sites contained in these bonds form a linked cluster. One can see this because the effective Hamiltonian (3.62) can be written in terms of nested commutators of $\mathcal{T}$-operators [121]. Furthermore, the cluster additivity of the effective Hamiltonian can be proven directly [186]. To this end consider a cluster C consisting of two disjoint clusters A and B as described in Subsect. 3.3.4. If $\eta(0)$ and $H(0)$ are both cluster additive

$$H^C(0) = H^A(0) + H^B(0)\,, \tag{3.68}$$

$$\eta^C(0) = \eta^A(0) + \eta^B(0)\,, \tag{3.69}$$

the flow equation can be decomposed into a flow equation on cluster A and on cluster B [186,187]

$$\begin{aligned} \frac{\mathrm{d}H^C(\ell)}{\mathrm{d}\ell} &= \frac{\mathrm{d}H^A(\ell)}{\mathrm{d}\ell} + \frac{\mathrm{d}H^B(\ell)}{\mathrm{d}\ell} \\ &= \left[\eta^A(\ell), H^A(\ell)\right] + \left[\eta^B(\ell), H^B(\ell)\right] = \left[\eta^C(\ell), H^C(\ell)\right]\,. \end{aligned} \tag{3.70}$$

3.4.2 Takahashi's perturbation theory

For the described general setup in Sect. 3.2 one could also use Takahashi's perturbation theory [192]. In contrast to pCUTs it does not require H_0 to have an equidistant spectrum. We describe the method following the supplemental material of Ref. [197]. Again, the idea is to transform a many body Hamiltonian of the form $H = H_0 + \mathcal{V}$ into an effective Hamiltonian $H_{\text{eff}} = \Gamma^\dagger H \Gamma$. The transformation Γ yields an effective Hamiltonian which acts only on the eigenspace L of H_0 which corresponds to the eigenvalue $E_L^{(0)}$. To this end one defines the projection operator P which projects onto the space L. Furthermore, the projector $\tilde{P}$ projects onto the perturbed eigenspace $\tilde{L}$, which is spanned by the perturbed eigenstates from the space L [192]. The transformation is defined by [192]

$$\Gamma = \tilde{P}P(P\tilde{P}P)^{-1/2} \tag{3.71}$$

and the projector $\tilde{P}$ can be written as [192, 198]

$$\tilde{P} = P - \sum_{n=1}^{\infty} \sum_{k_1+\ldots+k_{n+1}=n} S^{k_1} \mathcal{V} S^{k_2} \mathcal{V} \ldots \mathcal{V} S^{k_{n+1}} \tag{3.72}$$

with $S^0 = -P$ and $S^k = \left(\frac{1-P}{E_L^{(0)} - H_0}\right)^k$ for $k \neq 0$. Furthermore, one can expand the expression [192]

$$(P\tilde{P}P)^{-1/2} = P + \sum_{n=1}^{\infty} \frac{(2n-1)!!}{(2n)!!} (P(P-\tilde{P})P)^n, \tag{3.73}$$

where !! denotes the double factorial

$$\begin{aligned} (2n)!! &= 2n \cdot (2n-2) \cdot (2n-4) \cdot \ldots \cdot 2\,, \\ (2n-1)!! &= (2n-1) \cdot (2n-3) \cdot (2n-5) \cdot \ldots \cdot 1\,. \end{aligned} \tag{3.74}$$

With these definitions the transformation Γ and the effective Hamiltonian can be written in terms of the operators P, $\mathcal{V}$ and S [197]. The effective Hamiltonian in order $n+1$ for $n \geq 0$ is of the form [199]

$$H_{\text{eff}}^{(n+1)} = \sum_{k_1+\ldots+k_n=n} f(k_1, \ldots, k_n) P \mathcal{V} S^{k_1} \mathcal{V} S^{k_2} \ldots S^{k_n} \mathcal{V} P\,, \tag{3.75}$$

where the coefficients $f(k_1, \ldots, k_{n-1})$ are obtained from explicit expansions of Γ in terms of the operators S, $\mathcal{V}$ and P and the zeroth order effective Hamiltonian is just H_0. As before we can write the effective Hamiltonian in terms of bond-local operators $\mathcal{V}_b$ and obtain

$$H_{\text{eff}}^{(n+1)} = \sum_{\vec{b}, |\vec{b}|=n+1} \sum_{k_1+\ldots+k_n=n} f(k_1, \ldots, k_n) P \mathcal{V}_{b_1} S^{k_1} \mathcal{V}_{b_2} S^{k_2} \ldots S^{k_n} \mathcal{V}_{b_{n+1}} P\,. \tag{3.76}$$

Also here the contributions from all bond sequences which exactly correspond to a cluster C sum up to the reduced contribution of this cluster, and thus one can implement a bookkeeping technique to directly obtain the reduced contribution [193] as for pCUTs [123]. In contrast to pCUTs, here also bond sequences corresponding to disconnected clusters can contribute, as the effective Hamiltonian is in general not cluster additive [181, 200]. Note that for the setup described in Sect. 3.2 we can evaluate the operators S and P on the individual cluster defined by the bonds $\vec{b}$ because the unperturbed energy from the rest of the system is not changed by acting with $\mathcal{V}_b$ on any bond in the cluster C.

3.4.3 Löwdin's partitioning technique

Another way to approach perturbation theory is Löwdin's partitioning technique [201]. The review given here is based on Refs. [202–205]. Given a Hamiltonian of the form $H = H_0 + \mathcal{V}$ with perturbed eigenstates

$$(H_0 + \mathcal{V}) |\Psi_i\rangle = E_i |\Psi_i\rangle\,, \tag{3.77}$$

we denote the unperturbed eigenstates as

$$H_0 |\Phi_i\rangle = E_i^{(0)} |\Phi_i\rangle\ . \tag{3.78}$$

Now consider an eigenspace L of this unperturbed Hamiltonian and define the projection operator P which projects onto this space, and the projection operator $\bar{P} = 1 - P$ which projects onto the orthogonal complement $\bar{L}$ of this space. We denote the projection of the perturbed state $|\Psi_i\rangle$ onto the subspaces L and $\bar{L}$ as

$$P\,|\Psi_i\rangle = |\Psi_i\rangle_p \qquad \bar{P}\,|\Psi_i\rangle = |\Psi_i\rangle_{\bar{p}}\,. \tag{3.79}$$

In order to obtain the perturbative corrections $E_i - E_i^{(0)}$ to the unperturbed energy $E_i^{(0)}$ one can derive an eigenvalue equation in the eigenspace L of the unperturbed Hamiltonian H_0

$$\Theta\,|\Psi_i\rangle_p = (E_i - E_i^{(0)})\,|\Psi_i\rangle_p\,, \tag{3.80}$$

In the non-degenerate case $\dim(L) = 1$ the state $|\Psi_i\rangle_p$ corresponds to the unperturbed eigenstate $|\Phi_i\rangle$ and one can determine the perturbative corrections to $E_i^{(0)}$ by evaluating the action of the operator Θ on the unperturbed eigenstate $|\Psi_i\rangle_p$.

We now give the derivation of the operator Θ following Ref. [203]. First, the decomposition (3.79) is inserted into the time-independent Schrödinger equation

$$(H_0 + \mathcal{V})\,|\Psi_i\rangle_p + (H_0 + \mathcal{V})\,|\Psi_i\rangle_{\bar{p}} = E_i\,|\Psi_i\rangle_p + E_i\,|\Psi_i\rangle_{\bar{p}}\,. \tag{3.81}$$

Applying the projection operators P and $\bar{P}$ to this equation yields

$$(E_i^{(0)} + P\mathcal{V}P)\,|\Psi_i\rangle_p + P\mathcal{V}\bar{P}\,|\Psi_i\rangle_{\bar{p}} = E_i\,|\Psi_i\rangle_p\,, \tag{3.82}$$

$$\bar{P}\mathcal{V}P\,|\Psi_i\rangle_p + (H_0 + \bar{P}\mathcal{V}\bar{P})\,|\Psi_i\rangle_{\bar{p}} = E_i\,|\Psi_i\rangle_{\bar{p}}\,. \tag{3.83}$$

From Eq. (3.83) one obtains

$$|\Psi_i\rangle_{\bar{p}} = (E_i - H_0 - \bar{P}\mathcal{V}\bar{P})^{-1}\bar{P}\mathcal{V}P\,|\Psi_i\rangle_p\,. \tag{3.84}$$

Inserting this into Eq. (3.82) yields

$$(E_i^{(0)} + P\mathcal{V}P)\,|\Psi_i\rangle_p + P\mathcal{V}\bar{P}(E_i - H_0 - \bar{P}\mathcal{V}Q)^{-1}\bar{P}\mathcal{V}P\,|\Psi_i\rangle_p = E_i\,|\Psi_i\rangle_p\,. \tag{3.85}$$

This can be rearranged as

$$\left[P\mathcal{V}P - P\mathcal{V}\bar{P}(E_i - H_0 - \bar{P}\mathcal{V}\bar{P})^{-1}\bar{P}\mathcal{V}P\right]|\Psi_i\rangle_p = (E_i - E_i^{(0)})\,|\Psi_i\rangle_p \tag{3.86}$$

which has exactly the form of Eq. (3.80), and thus the operator Θ is given by

$$\Theta = P\mathcal{V}P - P\mathcal{V}\bar{P}(E_i - H_0 - \bar{P}\mathcal{V}\bar{P})^{-1}\bar{P}\mathcal{V}P\,. \tag{3.87}$$

In order to use this expression for perturbation theory it has to be expanded in powers of $\mathcal{V}$. To this end the expression

$$(E_i - H_0 - \bar{P}\mathcal{V}\bar{P})^{-1} = (1 - (E_i - H_0)^{-1}\bar{P}\mathcal{V}\bar{P})^{-1}\,(E_i - H_0)^{-1} \tag{3.88}$$

is expanded with the help of a Neumann series [204]

$$(E_i - H_0 - \bar{P}\mathcal{V}\bar{P})^{-1} = \sum_{m=0}^{\infty}\left[(E_i - H_0)^{-1}\bar{P}\mathcal{V}\bar{P}\right]^m (E_i - H_0)^{-1}\,. \tag{3.89}$$

Expanding the energies $E_i = E_i^{(0)} + \sum_{k=1}^{\infty} E_i^{(k)}$, where $E_i^{(k)}$ is the perturbative energy correction in order k, leads to

$$\begin{aligned}(E_i - H_0)^{-1} &= \Big(E_i^{(0)} + \sum_{k=1}^{\infty} E_i^{(k)} - H_0\Big)^{-1} \\ &= \Big[(E_i^{(0)} - H_0)\big(1 + (E_i^{(0)} - H_0)^{-1} \sum_{k=1}^{\infty} E_i^{(k)}\big)\Big]^{-1} \\ &= \Big(1 + (E_i^{(0)} - H_0)^{-1} \sum_{k=1}^{\infty} E_i^{(k)}\Big)^{-1} (E_i^{(0)} - H_0)^{-1} \\ &= \Lambda\Omega\,,\end{aligned} \tag{3.90}$$

with the operators

$$\Omega = (E_i^{(0)} - H_0)^{-1}\,, \tag{3.91}$$

$$\Lambda = \big(1 + \Omega \sum_{k=1}^{\infty} E_i^{(k)}\big)^{-1}\,. \tag{3.92}$$

Note that Ω is easily evaluated for any eigenstate of H_0, while Λ can again be expanded as a Neumann series [204]

$$\Lambda = \sum_{j=0}^{\infty} \Big[- \Omega \sum_{k=1}^{\infty} E_i^{(k)}\Big]^j\,. \tag{3.93}$$

Now these results can be used to rewrite

$$\Theta = P\mathcal{V}P - P\mathcal{V}\bar{P} \sum_{m=0} \Big[\Lambda\Omega\bar{P}\mathcal{V}\bar{P}\Big]^m \Lambda\Omega\bar{P}\mathcal{V}P\,. \tag{3.94}$$

Using the fact that $\bar{P}$ commutes with Λ and Ω this can be rearranged to [203, 204]

$$\Theta = P\mathcal{V}P - P\mathcal{V} \sum_{m=0}^{\infty} \Big[\Lambda\Omega\bar{P}\mathcal{V}\Big]^m \Lambda\Omega\bar{P}\mathcal{V}P = P\mathcal{V} \sum_{m=0}^{\infty} \Big[\Lambda\Omega\bar{P}\mathcal{V}\Big]^m P\,. \tag{3.95}$$

Inserting Λ explicitly results in [204, 205]

$$\Theta = P\mathcal{V} \sum_{m=0}^{\infty} \Big[\sum_{j=0}^{\infty} \Big(- \Omega \sum_{k=1}^{\infty} E_i^{(k)}\Big)^j \Omega\bar{P}\mathcal{V}\Big]^m P\,. \tag{3.96}$$

In order to evaluate this operator up to order k only the $E_i^{(k)}$ up to order $k-2$ are needed, and hence, this operator can be iteratively evaluated up to any desired order k [204]. As $\bar{P} = \bar{P}^2$ it is straightforward to write the operator Θ in terms of the operators $S = \frac{\bar{P}}{E_i^{(0)} - H_0}$ which we also use in Takahashi's perturbation theory

$$\Theta = P\mathcal{V} \sum_{m=0}^{\infty} \Big[\sum_{j=0}^{\infty} \Big(- S \sum_{k=1}^{\infty} E_i^{(k)}\Big)^j S\mathcal{V}\Big]^m P\,. \tag{3.97}$$

If one expands this explicitly [204] one finds a strong similarity between the effective Hamiltonian of Takahashi's perturbation theory and the operator Θ [187]. In fact one can interpret the operator

Θ as a variant of the effective Hamiltonian of Takahashi's approach where the terms $P \dots P$ are evaluated and collected such that the coefficients can be written in terms of the energy corrections $E_i^{(k)}$ [187]. It is clear that the operator Θ can be written in terms of bond-local operators $\mathcal{V}_b$. However, in general the energy corrections $E_i^{(k)}$ are calculated on the whole system, and hence, the reduced contribution for a subcluster C is not determined by considering only the terms where the $\mathcal{V}_b$ act on all bonds in the cluster C. Instead, one can decompose the energy $E_i^{(k)}$ into reduced contributions from different subclusters [96]

$$E_i^{(k)} = \sum_{c \subseteq \mathcal{L}} \epsilon_i^{(k)}(c) \,. \tag{3.98}$$

We can use this decomposition together with the bond-local operators $\mathcal{V}_b$ to write

$$\Theta = P \sum_{m=0}^{\infty} \sum_{\vec{b}, |\vec{b}|=m+1} \mathcal{V}_{b_1} \left[\prod_{i=2}^{m+1} \left[\sum_{j=0}^{\infty} \Big(- S \sum_{k=1}^{\infty} \sum_{c \subseteq \mathcal{L}} \epsilon_i^{(k)}(c) \Big)^j S \mathcal{V}_{b_i} \right] \right] P \,. \tag{3.99}$$

Now the reduced contribution of a subcluster C is obtained by considering only the terms where the clusters, whose reduced energy corrections $\epsilon_i^{(k)}(c)$ are contained in the respective term and the sequence $\vec{b}$ together contain all the bonds of the subcluster C, and no other bonds. In other words, for the bookkeeping the appearance of a term $\epsilon_i^{(k)}(c)$ indicates that the perturbation acted on all bonds in c. One can understand this by explicitly inserting all energy corrections $\epsilon_i^{(k)}(c)$ as expressions in P, $\mathcal{V}$ and S into Eq. (3.99). Technically this bookkeeping is rather easy to implement, because one just needs to store the $\epsilon_i^{(k)}(c)$ broken down by the information from which bonds they have been obtained.

3.4.4 Matrix perturbation theory

Matrix perturbation theory [95–97] is a very efficient method to obtain high-order series expansions, especially for problems where only one perturbation parameter is considered. Generalizations to multiple perturbation parameters can be found in the literature [96, 206]. We describe this method closely following Ref. [97]. As a starting point consider the perturbative setup

$$H = H_0 + \lambda V \,, \tag{3.100}$$

where H_0 is the unperturbed Hamiltonian, λ is a perturbation parameter and V is the perturbation. Let $E_0^{(0)}$ be the unperturbed ground-state energy and $|0\rangle$ be the non-degenerate unperturbed ground state

$$H_0 \, |0\rangle = E_0^{(0)} \, |0\rangle \,. \tag{3.101}$$

Considering that all local Hilbert spaces are of finite dimension also the Hilbert space on any finite cluster is of finite dimension, and so H_0, V and H can be represented by square matrices. In order to find the relevant Hilbert space one acts repeatedly with V on the unperturbed ground state $|0\rangle$. The resulting states are decomposed into eigenstates of H_0. Importantly, it is sufficient to consider only those eigenstates which are obtained within $k/2$ actions of V on the ground state in order to obtain the series up to order k in λ. Note that the number of relevant unperturbed eigenstates can be significantly lower than the dimension of the full Hilbert space. In the following we label the eigenstates of H_0 by $|j\rangle$, where $|0\rangle$ corresponds to the non-degenerate unperturbed ground

state, and the other states $j \neq 0$ correspond to excited states. We now aim to find the ground state-energy E_0 and the ground-state $|\Psi\rangle$ of the operator H

$$H\,|\Psi\rangle = E_0\,|\Psi\rangle\ . \tag{3.102}$$

In a perturbative approach these quantities are expanded as series in the perturbation parameter

$$E_0 = \sum_{r=0}^{\infty} \lambda^r E_0^{(r)}\,, \tag{3.103}$$

$$|\Psi\rangle = \sum_{r=0}^{\infty} \lambda^r\,|\Psi^{(r)}\rangle\ , \tag{3.104}$$

where we choose the perturbative corrections to the unperturbed ground state $|0\rangle$ such that they fulfill $\langle 0|\Psi^{(r)}\rangle = 0$ for all $r \neq 0$ [95]. Inserting (3.103) and (3.104) into the Schrödinger Eq. (3.102) yields

$$(H_0 + \lambda V)\Big[\sum_{r=0}^{\infty} \lambda^r\,|\Psi^{(r)}\rangle\Big] = \Big[\sum_{r=0}^{\infty} \lambda^r E_0^{(r)}\Big]\Big[\sum_{s=0}^{\infty} \lambda^s\,|\Psi^{(s)}\rangle\Big]\,. \tag{3.105}$$

Collecting the terms which are proportional to λ^r leads to

$$H_0\,|\Psi^{(r)}\rangle + V\,|\Psi^{(r-1)}\rangle = \sum_{s=0}^{r} E_0^{(r-s)}\,|\Psi^{(s)}\rangle\ . \tag{3.106}$$

Additionally, the zeroth order term can be moved out of the sum on the right hand side

$$(H_0 - E_0^{(0)})\,|\Psi^{(r)}\rangle + V\,|\Psi^{(r-1)}\rangle = \sum_{s=0}^{r-1} E_0^{(r-s)}\,|\Psi^{(s)}\rangle\ . \tag{3.107}$$

Multiplying the unperturbed ground state $|0\rangle$ from the left side leads to

$$\langle 0|\,V\,|\Psi^{(r-1)}\rangle = E_0^{(r)}. \tag{3.108}$$

Expanding $|\Psi^{(r)}\rangle$ in the eigenbasis of H_0

$$|\Psi^{(r)}\rangle = \sum_j |j\rangle\,\langle j|\Psi^{(r)}\rangle = \sum_j c_{j,r}\,|j\rangle \tag{3.109}$$

with $c_{j,r} = \langle j|\Psi^{(r)}\rangle$, Eq. (3.108) can be rewritten as

$$E_0^{(r)} = \sum_j V_{0,j} c_{j,r-1}\,, \tag{3.110}$$

where $V_{j,k} = \langle j|\,V\,|k\rangle$ denotes the matrix elements of V in the unperturbed basis. Finally, Eq. (3.110) gives the energy correction in order r in terms of the state corrections in smaller perturbation orders. If instead we multiply with an unperturbed energy eigenstate $|j\rangle$ which is different from $|0\rangle$, we obtain

$$(E_j^{(0)} - E_0^{(0)})\,c_{j,r} + \langle j|\,V\,|\Psi^{(r-1)}\rangle = \sum_{s=0}^{r-1} E_0^{(r-s)} c_{j,s}\,, \tag{3.111}$$

where $E_j^{(0)}$ denotes the unperturbed energy of the state $|j\rangle$. Writing $|\Psi^{(r-1)}\rangle$ as a superposition of eigenstates of H_0 we get

$$(E_j^{(0)} - E_0^{(0)})\, c_{j,r} + \sum_i V_{j,i}\, c_{i,r-1} = \sum_{s=0}^{r-1} E_0^{(r-s)} c_{j,s}\,. \tag{3.112}$$

With some further rearrangements one finally obtains the state corrections

$$c_{j,r} = \frac{1}{E_j^{(0)} - E_0^{(0)}} \left(\sum_{s=0}^{r-1} E_0^{(r-s)} c_{j,s} - \sum_i V_{j,i} c_{i,r-1} \right). \tag{3.113}$$

With Eqs. (3.110) and (3.113) the strategy is now to iteratively compute the perturbative corrections order by order. Once we have calculated these quantities for a given order r we can proceed with the calculation of the energy correction $E_0^{(r+1)}$ in order $r+1$ using Eq. (3.110). Afterwards, one can use the result to obtain the state correction calculating the coefficients $c_{j,r+1}$ in order $r+1$ from Eq. (3.113).

Technically, the coefficients $c_{j,r}$ can be stored in vectors (one for each perturbation order), whereas the perturbation V is stored in a sparse matrix. Additionally, the unperturbed energies $E_j^{(0)}$ are easily precalculated. While for the other methods we considered some bookkeeping techniques in order to extract the reduced contribution directly, this appears difficult for matrix perturbation theory. So in order to obtain reduced ground-state energy of a cluster with matrix perturbation theory we subtract the reduced contributions of all proper subclusters [95–97].

3.4.5 Matrix based approaches to block-diagonalization

There exist also matrix based approaches to perturbation theory to extract single and multi-particle properties. One is the two-block orthogonal transformation (TBOT) method [97, 183]. The TBOT method determines an effective Hamiltonian

$$H_{\text{eff}} = O^{-1} H O\,, \tag{3.114}$$

where O is an orthogonal transformation. As in Takahashi's perturbation theory [192] the effective Hamiltonian is block diagonal in the sense that there is one block containing all matrix elements with respect to the states of the unperturbed basis with the selected energy. This method is very efficient because only a part of the whole orthogonal transformation needs to be calculated explicitly in order to obtain the effective Hamiltonian in the sector of interest [97]. In Ref. [181] it has been shown that the transformation obtained by TBOT is actually equivalent to the one used in Takahashi's perturbation theory [192] presented in Subsect. 3.4.2. Unfortunately, the effective Hamiltonian obtained by this method is not necessarily cluster additive, and hence, in general the effective Hamiltonian obtained with this method has contributions associated with disconnected clusters [181,200]. This explains the observation that it is not always possible to set up a correct LCE with this method [97,183]. Another method called multi-block orthogonal transformation (MBOT) was developed which generates an effective Hamiltonian which is block diagonal with respect to all unperturbed energies [182,183]. This effective Hamiltonian is actually cluster additive [181], but the method is less efficient than TBOT [183]. Finally, a method named projective cluster additive transformation (pCAT) which combines cluster additivity and an efficiency comparable to TBOT is introduced in Ref. [181].

3.4.6 Discussion

We conclude this section with a short discussion of the advantages and disadvantages of methods formulated in terms of matrices and methods based on evaluating the operator sequences of the effective Hamiltonian (or the operator Θ for Löwdin's method) directly. Such a discussion is also given in Ref. [200]. Notably, Takahashi's method and TBOT are equivalent as they use the same transformation [181, 200]. However, Takahashi's method is formulated in terms of operator sequences while TBOT is formulated in terms of matrices. A description of the implementation of the pCUT method can be found in Refs. [196] and [71]. Let us quickly review the basics of an implementation of methods like pCUT, Takahashi's perturbation theory or Löwdin's partitioning technique [207].

In such an implementation the model is defined by the local operators $H_{0,i}$ and the bond-local operators $\mathcal{T}_{n,b}$ or $\mathcal{V}_b$, respectively. The operators $\mathcal{T}_{n,b}$ as well as the operators $\mathcal{V}_b$ act equivalently on all bonds of the same type. So it is sufficient to define the action of these operators on the unperturbed local basis states once for every bond type. Also $H_{0,i}$ needs to be stored only once, as it is the same for all sites in the system. The bonds where the operators $\mathcal{T}_{n,b}$ or $\mathcal{V}_b$ act are specified separately. A state is then represented by an associative container (e.g. dictionaries in python or maps in C++) which has bit arrays (which encode the unperturbed basis states) as keys and the associated amplitudes as values [71, 123]. The amplitudes contain the perturbation parameters explicitly as polynomials in one or more variables. The operators $\mathcal{T}_{n,b}$ as well as $\mathcal{V}_b$ map every unperturbed basis state in such a container to another state, written in the unperturbed basis. Such a mapping involves the manipulation of bit arrays and the evaluation of products of polynomials. In the end the action of an operator $\mathcal{T}_n$ consists of two loops, one over all basis states in the superposition the operator acts on, and another one over all bonds [71]. The action of $\mathcal{V}$ can be implemented analogously. The resulting basis states are again stored in an associative container.

For Takahashi's perturbation theory and Löwdin's partitioning technique also the operators S and P need to be defined in this framework. However, the unperturbed energy of the basis states and thus also the resolvents in the operators S are easily evaluated using the operators $H_{0,i}$. So the action of these operators basically corresponds to the removal of basis states or adjustments of amplitudes according to the obtained unperturbed energies of the involved states.

One can then evaluate matrix elements of the respective effective Hamiltonians or the operator Θ for Löwdin's method, by evaluating all operator sequences weighed with the appropriate coefficients, which have been calculated beforehand. For pCUT there can be a lot of different operator sequences to evaluate, even for moderately many different n in the operators $\mathcal{T}_n$ [103, 121].

In the matrix based methods one typically generates the parts of the matrices relevant for the calculations and stores them in sparse matrices. The states are usually represented by vectors in the unperturbed product basis. All the operations in the method are then represented by the usual linear algebra operations for matrices and vectors.

The advantage of the methods formulated in terms of matrices is that they are extremely efficient on small systems, like the clusters which are considered in a graph decomposition, with one or few perturbation parameters. For example the ground-state energy of the TFIM on the square lattice in the low-field limit has been calculated up to order 14 in Ref. [121] with pCUT, while it has been calculated up to order 26 almost twenty years before [100]. In contrast, the local implementation of the perturbation operators to evaluate the sequences permits to easily imple-

ment bookkeeping techniques in order to calculate the reduced contributions directly [123]. For the matrix-based methods such bookkeeping techniques appear to be less straightforward, and we are not aware of any implementation. Of course the usual subcluster subtraction schemes can be employed for these methods [95–97]. Furthermore, the local implementation allows to easily incorporate several perturbation parameters. While this is in principle also possible for the matrix based methods it is not as straightforward [206].

In the end it is important to know about the advantages and disadvantages of the methods and use the method which is most suited for the problem. Typically, the number of perturbation parameters, but also whether we require a cluster additive effective Hamiltonian or not is of interest. Finally, the pCAT method introduced in Ref. [181] allows to find a cluster additive effective Hamiltonian with very good efficiency (comparable to TBOT), so there is in principle no reason to use methods which result in an effective Hamiltonian which is not cluster additive, apart from the availability of an implementation.

3.5 Linked-cluster expansions via graph decompositions

In the following we review the basics of the method of LCEs via a full graph decomposition [95–97, 99] before we approach the generalization to perturbations which include many-site interactions [130]. Here we consider the operators $\mathcal{V}_b$ to be symmetric two-site interactions. For the sake of simplicity we assume that we have only one type of interaction in the Hamiltonian, so we have only one bond type and $\mathcal{V}_b = \lambda V_b$ is defined equivalently for all bonds in the system. Additionally, we assume that there are no two bonds containing the same pair of sites.

The aim of this section is to describe the calculation of basic quantities like the ground-state energy and one-quasiparticle irreducible hopping elements for simple systems with the established method of LCEs via a full graph decomposition [95–97, 99].

3.5.1 Exploiting structural equivalence

In the previous parts of this chapter we have seen that we can write suitable quantities as the ground-state energy or irreducible one-quasiparticle matrix elements of the effective Hamiltonian as an LCE. For such a quantity O an LCE can be written as [96]

$$O(\mathcal{L}) = \sum_{C \subseteq \mathcal{L}} o(C), \tag{3.115}$$

where the sum runs only over the connected subclusters of the lattice $\mathcal{L}$ and $o(C)$ is the reduced contribution of the cluster C. Note that, instead of the lattice $\mathcal{L}$, one can use an appropriately designed finite cluster such that the results are valid in the thermodynamic limit [103, 120–122] as also explained in Sect. 3.3. An important observation is that many of the subclusters of $\mathcal{L}$ have equivalent structure. For example two subclusters can be related by translational or rotational symmetries of the lattice. Furthermore, subclusters can have the same structure, with the only difference that the elements of these clusters are arranged differently in real space.

The idea of a graph decomposition is to identify classes of subclusters which have the same reduced contribution due to structural equivalence [96, 99]. To this end also other information like the actual states involved in a matrix element or coordinate differences of certain sites might be

necessary. In the end the aim is to define equivalence classes $\mathcal{E}$ of clusters such that [96, 105, 187]

$$o(C) = o(\mathcal{E}) \quad \forall C \in \mathcal{E}\,. \tag{3.116}$$

Then one rewrites Eq. (3.115) as a sum over all equivalence classes $\mathcal{E}$ of subclusters in the lattice [95–99]

$$O(\mathcal{L}) = \sum_{\mathcal{E}\subseteq\mathcal{L}} \mathcal{N}(\mathcal{E},\mathcal{L}) \cdot o(\mathcal{E})\,, \tag{3.117}$$

where the contribution $o(\mathcal{E})$ is calculated only once (on any cluster of the class $\mathcal{E}$) for each equivalence class, and the number $\mathcal{N}(\mathcal{E},\mathcal{L})$ accounts for how many subclusters in the lattice belong to the class $\mathcal{E}$. Often these are extensively many subclusters due to translational symmetry. In this case one normalizes $\mathcal{N}(\mathcal{E},\mathcal{L})$ dividing it by the number of sites (or other suitable units) in the system and then obtains the desired quantity per site (or unit). Note that also for the calculation of $o(\mathcal{E})$ the equivalence of subclusters can be exploited. Instead of [95, 96]

$$o(C) = O(C) - \sum_{c\subset C} o(c)\,, \tag{3.118}$$

one usually calculates [96, 97, 99]

$$o(\mathcal{E}) = O(\mathcal{E}) - \sum_{\mathcal{E}'\subset\mathcal{E}} \mathcal{N}(\mathcal{E}',\mathcal{E}) \cdot o(\mathcal{E}')\,, \tag{3.119}$$

where the sum runs over all classes of proper subclusters of a cluster in $\mathcal{E}$ and $\mathcal{N}(\mathcal{E}',\mathcal{E})$ denotes the number of subclusters of class $\mathcal{E}'$ contained in any cluster of class $\mathcal{E}$. To understand the effect of structural equivalence better, consider two subclusters $C = (S, B)$ and $C' = (S', B')$ of the lattice with the respective cluster Hamiltonians

$$H^C = \sum_{i\in S} H_{0,i} + \lambda \sum_{b\in B} V_b\,, \tag{3.120}$$

$$H^{C'} = \sum_{i\in S'} H_{0,i} + \lambda \sum_{b\in B'} V_b\,. \tag{3.121}$$

Now we interpret the clusters as graphs where the edges correspond to the bonds and the vertices to the sites. Obviously, in this way we discard most of the spatial information about the clusters and just keep the information about the connectivity. If two clusters correspond to isomorphic graphs there is a bijection $\varphi : S \to S'$ which preserves the bond structure

$$\{i, j\} \in B \Leftrightarrow \{\varphi(i), \varphi(j)\} \in B'\,. \tag{3.122}$$

In the case of several bond types the isomorphism φ preserves the types of the bonds which correspond to edge colors in the representing graphs. We denote such clusters as *isomorphic* or *structural equivalent* clusters and call the respective graphs the representing graphs of the isomorphism class. For two isomorphic clusters we can relabel the indices in H^C such that both Hamiltonians are the same [96]

$$H^{\varphi(C)} = H^{C'}, \tag{3.123}$$

where $\varphi(C)$ just denotes the cluster C with appropriately relabeled sites $i \mapsto \varphi(i)$. This equivalence also translates to the restrictions of the quasiparticle number conserving effective Hamiltonian

$$H_{\text{eff}}^{\varphi(C)} = H_{\text{eff}}^{C'}\,. \tag{3.124}$$

Now, suppose we wish to evaluate matrix elements $\langle\Phi|\, H_{\text{eff}}\, |\Psi\rangle$ of the effective Hamiltonian in perturbation theory, with product states

$$|\Phi\rangle = \bigotimes_{i\in\mathcal{L}} |\Phi_i\rangle\ , \qquad |\Psi\rangle = \bigotimes_{i\in\mathcal{L}} |\Psi_i\rangle \tag{3.125}$$

where we may assume $|\Phi_i\rangle \in \{|0\rangle, |1\rangle\}$ and $|\Psi_i\rangle \in \{|0\rangle, |1\rangle\}$ for simplicity. Because of Eq. (3.124) we have

$$\langle\Phi|\, H_{\text{eff}}^{C}\, |\Psi\rangle = \langle\Phi|\, H_{\text{eff}}^{\varphi(C)}\, |\Psi\rangle = \langle\Phi|\, H_{\text{eff}}^{C'}\, |\Psi\rangle \tag{3.126}$$

if also the states on the clusters C and C' are equivalent. This means there is an isomorphism $\varphi : S \to S'$ which fulfills

$$|\Phi_i\rangle = |\Phi_{\varphi(i)}\rangle \quad \text{and} \quad |\Psi_i\rangle = |\Psi_{\varphi(i)}\rangle \qquad \forall i \in S\,. \tag{3.127}$$

If such an isomorphism exists the clusters C and C' are *equivalent* in the context of a calculation of the matrix element $\langle\Phi|\, H_{\text{eff}}\, |\Psi\rangle$. For the ground-state energy all local states are equivalent $|\Psi\rangle = |\Phi\rangle = |0\rangle = \bigotimes_{i\in\mathcal{L}} |0\rangle_i$, condition (3.127) is trivially fulfilled, and structurally equivalent clusters have the same reduced contribution [96, 99]

$$\epsilon_0(\mathcal{E}) = \epsilon_0(C) \quad \forall\, C \in \mathcal{E}, \tag{3.128}$$

for any isomorphism class of clusters $\mathcal{E}$, where

$$\epsilon_0(C) = \langle 0|\, H_{\text{eff}}^{C}\, |0\rangle - \sum_{c\subset C} \epsilon_0(c)\,. \tag{3.129}$$

Accordingly, the ground-state energy can be written as [96, 97, 99]

$$E_0(\mathcal{L}) = \langle 0|\, H_{\text{eff}}\, |0\rangle = \sum_{C\subseteq\mathcal{L}} \epsilon_0(C) = \sum_{\mathcal{E}\subseteq\mathcal{L}} \mathcal{N}(\mathcal{E},\mathcal{L})\cdot\epsilon_0(\mathcal{E})\,, \tag{3.130}$$

where $\mathcal{N}(\mathcal{E},\mathcal{L})$ is the number of clusters $C \in \mathcal{E}$ contained in the lattice $\mathcal{L}$. For the calculation of the reduced contribution one can again exploit structural equivalence as given in Eqs. (3.119) [97, 99]. Typically, Eq. (3.130) is than written as the sum over all non-isomorphic connected graphs [95–97]

$$E_0(\mathcal{L}) = \sum_{g} \mathcal{N}(g,G)\cdot\epsilon_0(g)\,, \tag{3.131}$$

where G is the (possibly infinite) *lattice graph* which represents the lattice. The reduced contribution $\epsilon_0(g) = \epsilon_0(\mathcal{E})$ corresponds to the reduced contribution of any cluster of the class represented by g, and the factor $\mathcal{N}(g,G) = \mathcal{N}(\mathcal{E},\mathcal{L})$ is the number of subgraphs of G which are isomorphic to g [115]. For translationally symmetric systems, $\mathcal{N}(g,G)$ is typically extensively large, and one would calculate the ground-state energy per site (or some other suitable unit) [96, 97].

In the more complicated case where $|\Phi\rangle$ and $|\Psi\rangle$ are excited states we aim to calculate

$$\langle\Phi|\, H_{\text{eff}}\, |\Psi\rangle = \sum_{C\subseteq\mathcal{L}} \mu(C) = \sum_{\mathcal{E}\subseteq\mathcal{L}} \mathcal{N}(\mathcal{E},\mathcal{L})\cdot\mu(\mathcal{E})\,. \tag{3.132}$$

Here, the classes $\mathcal{E}$ are designed such that

$$\mu(\mathcal{E}) = \mu(C) \quad \forall\, C \in \mathcal{E} \tag{3.133}$$

where the reduced contribution $\mu(C)$ of the cluster C is given by

$$\mu(C) = \langle\Phi| H_{\text{eff}}^{C} |\Psi\rangle - \sum_{c\subset C} \mu(c). \tag{3.134}$$

In contrast to an LCE for the ground-state energy discussed before, here the states $|\Psi\rangle$ and $|\Phi\rangle$ in the matrix element need to be considered for the definition of the equivalence classes $\mathcal{E}$ in order to adhere to the constraint (3.127). This means it is in general not sufficient to identify isomorphic clusters but the states on the sites of these clusters also need to be equivalent. We use additional vertex colors within the representing graphs to incorporate the local states on the sites of the clusters within the states $|\Phi\rangle$ and $|\Psi\rangle$. The equivalence relation then corresponds to isomorphism of these graphs, which now represent an equivalence class of clusters in the context of the calculation of the considered matrix element. Again, the reduced contribution is

$$\mu(C) = \langle\Phi| H_{\text{eff}}^{C} |\Psi\rangle - \sum_{c\subset C} \mu(c)\,. \tag{3.135}$$

However, in practice, we use a bookkeeping technique in order to obtain the reduced contributions to individual hopping elements [123]. Note that while for the ground-state energy the reduced contributions of disconnected clusters (graphs) vanish [95–98] one cannot rely on this for the hopping elements. Instead, this depends on the perturbation theory method employed to evaluate the reduced contributions of the clusters [97, 181]. Clearly, for LCEs we need to use a method which guarantees, that only connected clusters have a non-vanishing reduced contribution to the desired matrix elements, and indeed, methods which yield non vanishing reduced contributions only on connected clusters (graphs) do exist [103, 121, 181–183].

In practice, one is typically interested in one- or few-quasiparticle hopping elements in the thermodynamic limit. How a single one-quasiparticle hopping element can be calculated using an LCE is described in Refs. [97, 208]. For the calculation of matrix elements of the effective Hamiltonian with $|\Phi\rangle \neq |\Psi\rangle$ one only needs to consider subclusters including all sites where the local states change. In the case $|\Phi\rangle = |\Psi\rangle$ the term $\langle\Phi| H_{\text{eff}} |\Phi\rangle$ contains extensively many vacuum fluctuations as $\mu(C) = \epsilon_0(C)$ if no excitations are on the cluster C within the state $|\Phi\rangle$. In order to get rid of these vacuum fluctuations they are simply subtracted [124]

$$\begin{aligned}
\langle\Phi| H_{\text{eff}} - E_0 |\Phi\rangle &= \langle\Phi| H_{\text{eff}} |\Phi\rangle - \langle 0| H_{\text{eff}} |0\rangle \\
&= \sum_{C\subseteq\mathcal{L}} \mu(C) - \sum_{C\subseteq\mathcal{L}} \epsilon_0(C) \\
&= \sum_{C\subseteq\mathcal{L}} [\mu(C) - \epsilon_0(C)] \\
&= \sum_{\mathcal{E}\subseteq\mathcal{L}} \mathcal{N}(\mathcal{E},\mathcal{L})\,[\mu(\mathcal{E}) - \epsilon_0(\mathcal{E})]\,,
\end{aligned} \tag{3.136}$$

where we used that equivalence of clusters in the context of a matrix element $\langle\Phi| H_{\text{eff}} |\Psi\rangle$ also implies isomorphism of these clusters and hence $\epsilon_0(C) = \epsilon_0(\mathcal{E})$ for all clusters in the class $\mathcal{E}$. Here, one observes that only clusters hosting at least one excitation need to be taken into account. In the one-quasiparticle sector the subtraction of the ground-state energy leads to the irreducible one-quasiparticle matrix elements of the effective Hamiltonian (see also Subsect. 4.2.3) [124]. In general one can also derive irreducible matrix elements for higher quasiparticle numbers by appropriately

subtracting irreducible matrix elements from lower quasiparticle sectors [120,183]. In this thesis we do not calculate irreducible matrix elements for more than one quasiparticle, so we do not further elaborate on this topic here. In principle, a matrix element of the effective Hamiltonian can also be written in terms of graphs [97, 208]

$$\begin{aligned} \langle \Phi | \, H_{\text{eff}} \, | \Psi \rangle &= \sum_g \mathcal{N}(g, G) \cdot \mu(g) \,, \\ \langle \Phi | \, H_{\text{eff}} - E_0 \, | \Phi \rangle &= \sum_g \mathcal{N}(g, G) [\mu(g) - \epsilon_0(g)] \,, \end{aligned} \tag{3.137}$$

where, again, the reduced contributions $\mu(g)$ and $\epsilon_0(g)$ correspond to the reduced contributions of the respective equivalence class. However, here the sums run over all non-isomorphic connected graphs with several vertex colors, and also the lattice graph has several vertex colors to incorporate the local states $|\Phi_i\rangle$ and $|\Psi_i\rangle$ on all sites of the lattice. As before $\mathcal{N}(g, G)$ is the number of subgraphs of G isomorphic to g. We stress again, that we require a graph isomorphism to preserve edge and vertex colors. Obviously, generating all non-isomorphic connected graphs with various vertex colors is an expensive combinatorial task, and thus, it may be more efficient to identify the relevant subclusters on the lattice and sort them into equivalence classes to obtain an individual hopping element.

Typically, one does not set up a graph decomposition to calculate a single irreducible one-quasiparticle hopping element. Instead, a scheme to efficiently obtain all hopping elements needed to calculate the one-quasiparticle dispersion is described in the literature [96, 97, 124]. In particular, this scheme can be formulated in terms of isomorphism classes of clusters, and hence, in terms of non-isomorphic connected graphs without the need to distinguish several vertex colors [97, 124].

Now, we are essentially ready for the calculation of ground-state energies and one particle-hopping elements in this setting. The remaining tasks are to determine the relevant graphs or subclusters, and the corresponding embedding factors.

3.5.2 Equivalence classes and embedding factors

In the previous subsection we discussed, how to calculate the ground-state energy and matrix elements of the effective Hamiltonian with a LCE via a full graph decomposition. In order to set up such an LCE we need to find the relevant equivalence classes of subclusters and their embedding factors.

In principle we know of two possibilities to obtain the relevant equivalence classes of subclusters and their embedding factors. The first possibility is to find all relevant connected subclusters of the lattice and sort them into isomorphism classes keeping track of the occurrences [96]. Here, the graph representation serves to distinguish the several equivalence classes of subclusters. Alternatively, one can determine all non-isomorphic connected graphs and calculate their embedding factors $\mathcal{N}(g, G)$ [96,97]. In order to obtain the embedding factors also the lattice is represented by a graph, which is referred to as the *lattice graph*. Within this subsection we assume that the unit cell of the lattice consists of a single site. Note that, any vertex within this lattice graph represents an actual site of the lattice, so each subgraph of the lattice graph corresponds to an actual subcluster of the system. The ground-state energy or an irreducible one-quasiparticle matrix element of the effective Hamiltonian can be calculated on a single finite cluster up to a desired perturbation order

in the thermodynamic limit [103, 120–122]. Accordingly, the lattice graph is usually chosen to be a finite graph representing such a cluster [97].

In general, the approach to generate all non-isomorphic graphs and determine their embedding factors, can be regarded as standard for all problems which can be efficiently formulated in terms of isomorphism classes of clusters [96, 97]. Though, in some cases more information than just the embedding factor of a given graph are required. For example, the scheme to calculate all relevant one-quasiparticle hopping elements necessary to obtain the dispersion within a single graph decomposition requires information about the subgraphs isomorphic to a given graph, which can be found in the lattice graph [97, 124].

Notwithstanding, the approach to find all relevant subclusters and sort them into equivalence classes has advantages for the generalization of graph decompositions to perturbation terms with multi-site interactions [130]. Interestingly, this approach is also established in the field of NLCEs, where other elements than bonds may be used as basic building blocks of the considered clusters [126, 209]. However, this approach is discussed in the context of hypergraph decompositions in Sect. 3.6. Accordingly, we focus more on the graph based approach in this subsection.

Finding all non-isomorphic connected graphs

In order to determine all relevant isomorphism classes of subclusters one first generates all non-isomorphic connected graphs up to k edges, where k is the desired perturbation order [96, 97]. Note that we consider isomorphism classes of clusters, so the generated graphs are not supposed to have several vertex colors. To assert that the graphs actually correspond to subclusters of the lattice one also needs to check whether there is a subgraph of the respective isomorphism class in the lattice graph [97, 210].

The generation of all non-isomorphic connected graphs up to a given number of edges can be done in a simple way. Starting from a list of all non-isomorphic connected graphs with k edges one can obtain all non-isomorphic connected graphs with $k+1$ edges by simply appending an edge in every possible way to every graph in the list (also considering to append an edge and a vertex at the same time) [96, 210]. As a starting point for this iterative procedure one can use a graph consisting of only one vertex [210]. In general, this procedure discovers several graphs which are isomorphic to each other. As a consequence, one has to check, whether an isomorphic graph has already been discovered, before accepting a newly generated graph [96]. This can be done either by calculating a canonical label [96, 97] or by checking for isomorphism against all previously accepted graphs. We mention here that more elaborate techniques to generate isomorph-free sets of graphs [211] and also very efficient algorithms to calculate canonical labels are known [133, 147].

In our implementation we actually check each newly obtained graph for isomorphism against other graphs using the RI algorithm [142, 164] which we describe in Subsect. 3.5.3. As it is unfeasible to explicitly check a newly generated graph against all non-isomorphic graphs obtained so far, we use a graph invariant to keep the number of explicit isomorphism checks low. The usage of graph invariants to reduce the number of explicit isomorphism checks is described in the literature [166, 212, 213]. A quick explanation of graph invariants is provided in Subsect. 2.1.5. For LCEs one is interested to find all non-isomorphic connected graphs with $\mathcal{N}(g, G) \neq 0$. These graphs are called *embeddable* into the lattice. Several simple checks can be employed before an explicit check, whether a given graph is embeddable into the lattice, is performed [97, 210]. In particular a graph is not embeddable into the lattice if [97, 210]

- The degree of any vertex of the graph exceeds the degree of each vertex of the lattice graph.
- An isomorphic graph has already been found to be not embeddable into the lattice.
- A subgraph of the given graph is not embeddable into the lattice.

Note that the third point also implies, that all the graphs found by appending edges to a non-embeddable graph are also not embeddable, which typically simplifies the generation of the relevant graphs a lot. Altogether, with these insights it is usually pretty efficient to find all graphs which are embeddable into a given lattice.

Normalized embedding factors

Here, we address how to find the number of subgraphs in the lattice graph G which are isomorphic to g, normalized to the number of vertices of the lattice graph N. In practice, this lattice graph represents a cluster which is equivalent to the infinite system in a sufficiently large environment instead of an infinite lattice. To this end it is convenient to choose periodic boundary conditions, so such an environment exists around every site in this cluster. This periodic cluster must be large enough, such that the subclusters relevant for the calculation and their normalized embedding factors are not affected by the periodic boundary conditions [97, 115]. Typically, in a perturbative calculation up to order k, these are the connected subclusters with k or less bonds [96]. Accordingly, one has to design a periodic cluster, such that no subclusters up to k bonds can go around the cluster [97]. This cluster is then represented by the finite lattice graph G in the obvious manner.

In order to find the normalized embedding factor $\mathcal{N}(g, G)/N$ we can determine all subgraph monomorphisms $\mathrm{Mon}(g, G)$ from g to G. An algorithm to explicitly determine these monomorphisms is discussed in Subsect. 3.5.3. The number of subgraphs isomorphic to g is given by the number of monomorphisms $|\mathrm{Mon}(g, G)|$ divided by the number of symmetries of g, which is given by the size of the automorphism group $|\mathrm{Aut}(g)|$. If necessary, one can extract all information about the subclusters of a given isomorphism class by considering the monomorphisms $|\mathrm{Mon}(g, G)|$ of the representing graph g to the lattice graph G.

In principle one can determine $|\mathrm{Mon}(g, G)|$ and divide it by N to obtain the embedding factor per site, but typically it is much more efficient to exploit translational symmetry and directly calculate the embedding factor per site [96, 97]. To this end we fix a vertex in the subgraph monomorphisms and require each monomorphism φ to obey [96]

$$\varphi(0) = 0\,, \tag{3.138}$$

where we suppose that the vertices in $V(g)$ and $V(G)$ are numbered by subsequent integers starting from 0. We denote the monomorphisms from g to G which fulfill this condition by $\mathrm{Mon}_{(0,0)}(g, G)$. Now, consider a subgraph $g' \subset G$, and let there be a monomorphism $\varphi' \in \mathrm{Mon}_{(0,0)}(g, G)$ taking the graph g to the subgraph g'. Clearly, g' is isomorphic to g and the number of monomorphisms in $\mathrm{Mon}_{(0,0)}(g, G)$ taking g to g' is given by the size of the stabilizer subgroup $|\mathrm{Aut}_0(g)|$. If the vertex 0 has a trivial orbit $\mathrm{Orb}_{\mathrm{Aut}(g)}(0) = \{0\}$ this is exactly the number of automorphisms $|\mathrm{Aut}(g)|$. Conversely, if the vertex 0 has non-trivial orbit $|\mathrm{Orb}_{\mathrm{Aut}(g)}(0)| \neq 1$ this is not the case. However, in this case there is an ambiguity in the assignment of the subgraph g' to a site. Indeed, we find a subgraph monomorphism mapping g to the subgraph g' under any of the conditions $\varphi(0) = x$ for all $x \in \mathrm{Orb}_{\mathrm{Aut}(g')}(0)$. In order to obtain the number of subgraphs per site, we must correct this,

dividing by the size of the orbit $|\mathrm{Orb}_{\mathrm{Aut}(g)}(0)|$. This leads to the formula for the embedding factor per site [96, 214]

$$\mathcal{N}(g,G)/N = \frac{|\mathrm{Mon}_{(0,0)}(g,G)|}{|\mathrm{Aut}_0(g)| \cdot |\mathrm{Orb}_{\mathrm{Aut(g)}}(0)|} = \frac{|\mathrm{Mon}_{(0,0)}(g,G)|}{|\mathrm{Aut}(g)|}\,. \tag{3.139}$$

It is also common to fix two vertices in the monomorphisms [97]

$$\varphi(0) = 0 \qquad \varphi(n_0) = n_0\,, \tag{3.140}$$

where n_0 denotes a neighbor of the vertex 0, in g and in G. This leads to [97]

$$\mathcal{N}(g,G)/N = \frac{|\mathrm{Mon}_{(0,0),(n_0,n_0)}(g,G)|}{|\mathrm{Aut}(g)|} \cdot q, \tag{3.141}$$

where $\mathrm{Mon}_{(0,0),(n_0,n_0)}(g,G)$ denotes the monomorphisms from g to G which take 0 to 0 and n_0 to n_0, and q is the coordination number of the lattice.

Let us now consider the example of the isomorphic graphs g_1, g_2 and the lattice graph G illustrated in Fig. 3.1. For each of these graphs we find 30 monomorphisms which obey the constraint

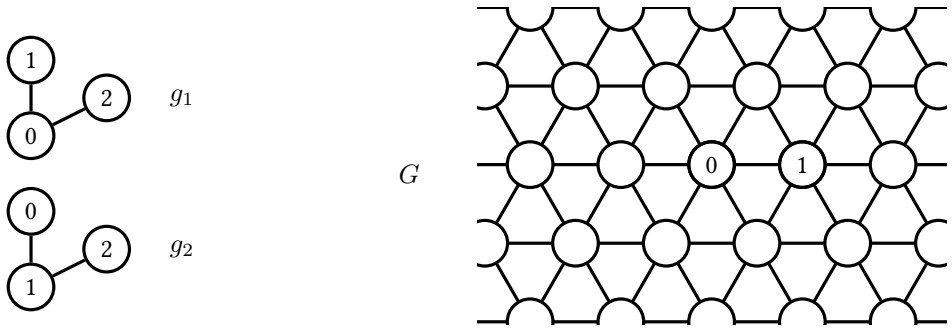

Figure 3.1: The image shows two isomorphic graphs (left) and a part of the triangular lattice (right) which are considered in the example discussed in the main text.

$\varphi(0) = 0$. Any of these monomorphisms maps one of these graphs to a subgraph of G. The monomorphisms take g_1 to 15 different subgraphs of G, but twice to each of them. This is illustrated in Fig. 3.2. These subgraphs are clearly associated to the vertex 0 of the lattice graph, as no monomorphism with $\varphi(0) = x \neq 0$ would map g_1 to the same subgraphs. In contrast, the graph g_2 is mapped to 30 different subgraphs, once to each of them. However, for any of these subgraphs, we can find another monomorphism with $\varphi(0) \neq 0$ which maps g_2 to the same subgraph. This is illustrated in Fig. 3.3. So for g_1 the ambiguity is given by the fact that multiple monomorphisms take g_1 to the same subgraph, because $|\mathrm{Aut}_0(g_1)| \neq 1$. Instead, for g_2 the ambiguity comes from the fact, that there are vertices in the graph which can not be distinguished from vertex 0 on a structural level $|\mathrm{Orb}_{\mathrm{Aut}(g_2)(0)}| \neq 1$. Note that both types of ambiguities are taken into account in Eq. 3.139 dividing by the size of the automorphism group.

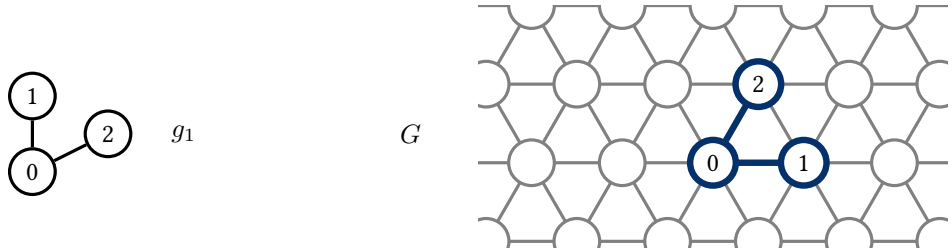

Figure 3.2: The graph g_1 (left) and a part of the lattice graph G (right) are illustrated. A particular subgraph of this lattice graph is highlighted in blue. The graph g_1 can be taken to this subgraph by a monomorphism which fulfills $\varphi(0) = 0$. Because of the reflection symmetry around the vertex 0, there are actually two monomorphisms fulfilling this condition.

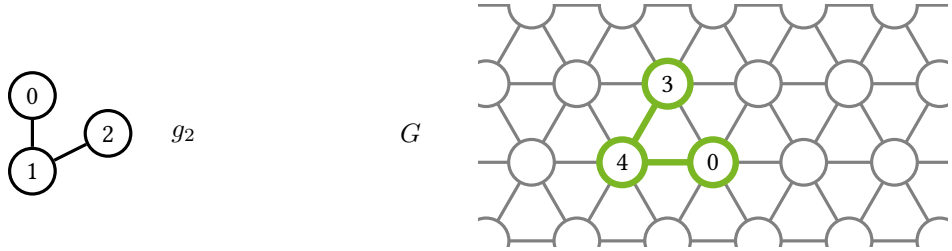

Figure 3.3: The graph g_2 (left) and a part of the lattice graph G (right) are illustrated. A particular subgraph of the lattice graph is highlighted in green. The graph g_2 can be taken to this subgraph by a monomorphism such that $\varphi(0) = 0$. Here, there is only one monomorphism fulfilling this condition, but there would be another monomorphism with $\varphi(0) = 3$ to the same subgraph.

Unnormalized embedding factors

Next, we consider unnormalized embedding factors in the context of the calculation of a one-particle hopping element from site j to site i on the lattice

$$t_{i,j}^{\alpha,\beta} = \langle i, 1_\alpha | \, H_{\text{eff}} - E_0 \, | j, 1_\beta \rangle \ . \tag{3.142}$$

Importantly, we need to take into account the subclusters which contain the sites i and j and have up to k bonds, where again k is the desired perturbation order. In practice, the infinite lattice is then replaced by a finite cluster which contains all these subclusters. The lattice graph G represents this finite cluster including the information about the states $|i, 1_\alpha\rangle$, $|j, 1_\beta\rangle$. This information is incorporated using vertex colors within the lattice graph G to reflect the local states on the sites of this cluster.

Importantly, also the graphs representing equivalence classes of subclusters incorporate the information about the local states on the sites of the clusters within the states $|i, 1_\alpha\rangle$, $|j, 1_\beta\rangle$ using vertex colors. For a given graph g we then determine and count all subgraph monomorphisms to the lattice graph and divide this number by the symmetry number

$$\mathcal{N}(g, G) = \frac{|\text{Mon}(g, G)|}{|\text{Aut}(g)|} \tag{3.143}$$

to obtain the embedding factor of the respective equivalence class $\mathcal{N}(\mathcal{E}, \mathcal{L}) = \mathcal{N}(g, G)$. Recall that the monomorphisms and automorphisms preserve the vertex colors which encode the local states on the sites before and after the hopping process.

Obviously, generating all non-isomorphic connected graphs up to a given number of edges becomes much more expensive when several vertex colors are involved, so these embedding factor might be obtained more easily by generating the subclusters of the lattice and assigning them to the respective classes, based on isomorphism of the representing graphs. In practice, these unnormalized embedding factors are of low relevance for graph decompositions as one rarely needs to calculate a single irreducible one-quasiparticle hopping element on the lattice. Instead, one uses a scheme to determine all irreducible hopping elements needed to calculate the one-quasiparticle dispersion within a single graph decomposition [96, 97, 124].

3.5.3 RI algorithm for (sub)graph isomorphism

As the embedding factors needed in LCEs via a full graph decomposition are closely related to subgraph monomorphism, and the equivalence of clusters is often determined using graph isomorphism, we present a simple but efficient algorithm to approach graph isomorphism, subgraph isomorphism and subgraph monomorphism.

The RI algorithm developed by Bonnici et al. [142,164] is an algorithm to find all (subgraph) isomorphisms $\varphi : V \to V'$ from a given pattern graph $g = (V, E)$ to a target graph $g' = (V', E')$. The algorithm can handle induced subgraph isomorphism, subgraph monomorphism and also graph isomorphism, although it is not primarily designed for the latter [164]. As a first step the algorithm determines an ordering of the vertices V of the pattern graph, which is called the matching order μ. We denote the n-th vertex in the matching order by μ_n. In a second step the possible mappings are explored using a backtracking algorithm. The idea is to choose the matching order such that many constraints are introduced as early as possible. For all three considered types of mappings -

induced subgraph isomorphism, subgraph monomorphism and graph isomorphism - two vertices which are adjacent within the pattern graph are required to be mapped to adjacent vertices in the target graph. So the basic idea is to design the matching order μ such that each vertex μ_n in μ has as many neighbors in $\mu_1, \ldots, \mu_{n-1}$ as possible, in order to introduce constraints early on within the backtracking algorithm. In this way one aims to prune away infeasible solutions as early as possible and reduce the size of the search tree which is traversed by the algorithm.

Greatest constraint first

The matching order μ is determined in the following way. We start with μ being an empty sequence. For each vertex in the pattern graph we keep track of the following ordered triple [164]

1. The number of neighbors which are contained in μ.
2. The number of neighbors which are not in μ but adjacent to at least one vertex in μ.
3. The degree of the vertex[3].

The next vertex to be appended to μ is the vertex with the lexicographically largest triple which is not already contained in μ. If two vertices have the same triple one of them is picked arbitrarily. Of course, after the insertion of a vertex the triples of all vertices not yet contained in μ have to be updated. Furthermore, for each vertex which is not yet in μ we keep track of the parent vertex during this procedure. The parent vertex is the vertex μ_n which has the minimum index n among all the neighbors of v which are contained in μ. From this definition it is clear, that not every vertex must have a parent, e.g., the vertex μ_1 cannot have a parent. We refer to the parent of a vertex v as $p(v)$ and once v is inserted into μ at the n-th position, i.e., $\mu_n = v$, we will employ the notation $p(\mu_n) = p_n$. This means p is a sequence where the n-th element corresponds to the parent of the n-th element in the sequence μ. Vertices are appended to the sequence μ according to these rules, until every vertex of the pattern graph is contained in μ. An example for the whole procedure with explanations is given in Fig. 3.4. Let us note that details in the definitions of the triple will not influence the correctness of the algorithm as long as μ contains every vertex of the pattern graph once and only once, and the parent of each vertex μ_n is always either a neighbor of μ_n which appears in μ at position $m < n$, or μ_n has no parent at all.

A step by step example how the matching order is determined is given in Fig. 3.4. We briefly comment on the several steps. In the first step no vertex is in μ so the vertex with the highest degree is chosen. The vertices 1 and 2 both have the highest degree so we arbitrarily choose vertex 1 and append it to μ. In the second step the vertex 2 is appended, because it has the highest number of green neighbors together with the vertices 0 and 3, but it has a larger amount of orange neighbors compared to these vertices. In the third step the vertex 0 is chosen, as it has more green neighbors than vertex 4, and a higher degree than vertex 3 (which has the same number of green and orange neighbors). Then in the situation in the bottom left the vertex 3 is appended to μ because it has more green neighbors than vertex 4. This vertex is appended afterwards, as it is the only vertex which is not in μ. One observes that at any point of the above procedure the green vertices which are already considered in the matching order are well connected within the pattern graph.

[3] In the literature [142, 164] the number of neighbors which are not in μ and do not have a neighbor in μ is used.

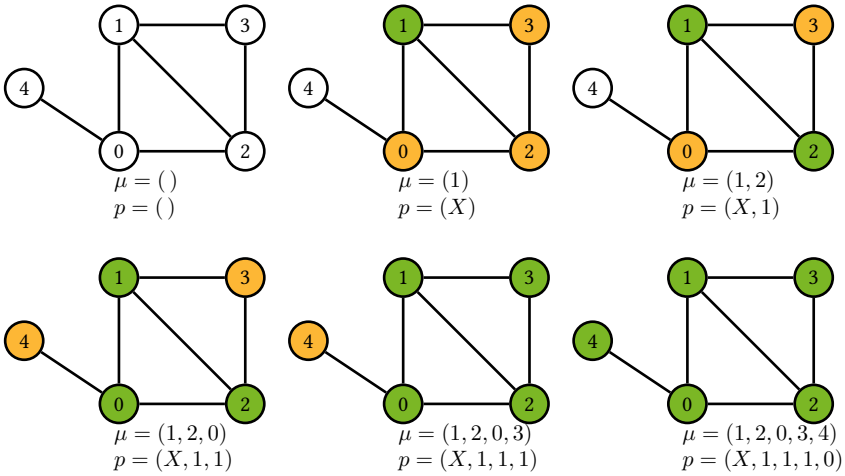

Figure 3.4: The image illustrates how to determine the greatest constraint first matching order. Vertices in μ are green, vertices adjacent to at least one vertex in μ are orange. The current status of μ and the vertex parents are given below the images, where p_i is the vertex parent of μ_i, and the symbol X stands for "no parent". The triples used for the selection of the next vertex to be appended to μ can be easily determined by counting the green, the orange and all neighbors of the vertices which are not yet in μ (i.e., not green). The several steps starting from an empty μ up to the final matching order are given from the top left to the bottom right.

The matching process

The idea of the search process is to to start from the state where no vertex in μ is mapped to a vertex in g' and extend a partial mapping φ_{cur} by adding pairs of vertices (μ_n, v), indicating that μ_n is mapped to v in the current partial solution, to this mapping in a depth-first manner. As the matching order μ is fixed the algorithm just has to find feasible assignments for $\varphi_{\text{cur}}(\mu_n)$. For a given μ_n the vertices considered for this assignment are the neighbors of the vertex $\varphi_{\text{cur}}(p(\mu_n))$. We call these vertices candidates in the following. If μ_n does not have a parent vertex, all vertices of g' are considered as candidates. In order to find a valid assignment $\varphi_{\text{cur}}(\mu_n)$ the algorithm iterates over the candidates and checks for each candidate whether the partial mapping can still be extended to a valid subgraph isomorphism after adding the corresponding pair. In the following we consider a pair (μ_n, v) which shall be added to the mapping. The algorithm accepts the pair only if the new partial mapping fulfills several criteria. These criteria are different for subgraph monomorphism, induced subgraph isomorphism and graph isomorphism. For subgraph monomorphism they read:

1. $v \neq \varphi_{\text{cur}}(\mu_m) \quad \forall m < n$
2. $\deg(\mu_n) \leq \deg(v)$
3. $\{\mu_n, \mu_m\} \in E \Rightarrow \{v, \varphi_{\text{cur}}(\mu_m)\} \in E' \quad \forall m < n.$

For induced subgraph isomorphism one additionally has the condition

4. $\{\mu_n, \mu_m\} \notin E \Rightarrow \{v, \varphi_{\text{cur}}(\mu_m)\} \notin E' \quad \forall m < n,$

or equivalently

4. $\{v, \varphi_{\mathrm{cur}}(\mu_m)\} \in E' \Rightarrow \{\mu_n, \mu_m\} \in E \quad \forall m < n.$

For graph isomorphism one requests $|V| = |V'|$ from the beginning and uses the criteria

1. $v \neq \varphi_{\mathrm{cur}}(\mu_m) \quad \forall m < n,$
2. $\deg(\mu_n) = \deg(v),$
3. $\{\mu_n, \mu_m\} \in E \Rightarrow \{v, \varphi_{\mathrm{cur}}(\mu_m)\} \in E' \quad \forall m < n.$

If the graphs have vertex or edge colors we request that these are preserved by φ_{cur}. If the respective conditions are fulfilled the partial mapping φ_{cur}, then it is extended by assigning $v = \varphi_{\mathrm{cur}}(\mu_n)$ and the algorithm continues with the first candidate vertex for $\varphi_{\mathrm{cur}}(\mu_{n+1})$, otherwise the next candidate for $\varphi_{\mathrm{cur}}(\mu_n)$ is tried. If no candidate is left to be tried for $\varphi_{\mathrm{cur}}(\mu_n)$ and $n > 1$, the algorithm removes the pair $(\mu_n, \varphi_{\mathrm{cur}}(\mu_n))$ from the partial mapping φ_{cur} and tries the next candidate for $\varphi_{\mathrm{cur}}(\mu_{n-1})$. If no candidate is left to be tried for $\varphi_{\mathrm{cur}}(\mu_1)$ the algorithm explored all relevant partial mappings φ_{cur} and terminates.

Obviously, after verifying the respective criteria for $n = |V|$ the partial mapping φ_{cur} cannot be extended any more because all vertices in μ have been matched to a vertex in the target graph and φ_{cur} is a valid solution. If one is interested in testing whether a solution exists, one can terminate the algorithm at this point. If, instead, one desires to find all possible solutions the algorithm removes the pair $(\mu_n, \varphi_{\mathrm{cur}}(\mu_n))$ and tries the next candidate for $\varphi_{\mathrm{cur}}(\mu_n)$. In Fig. 3.5 this matching process is illustrated for a simple example.

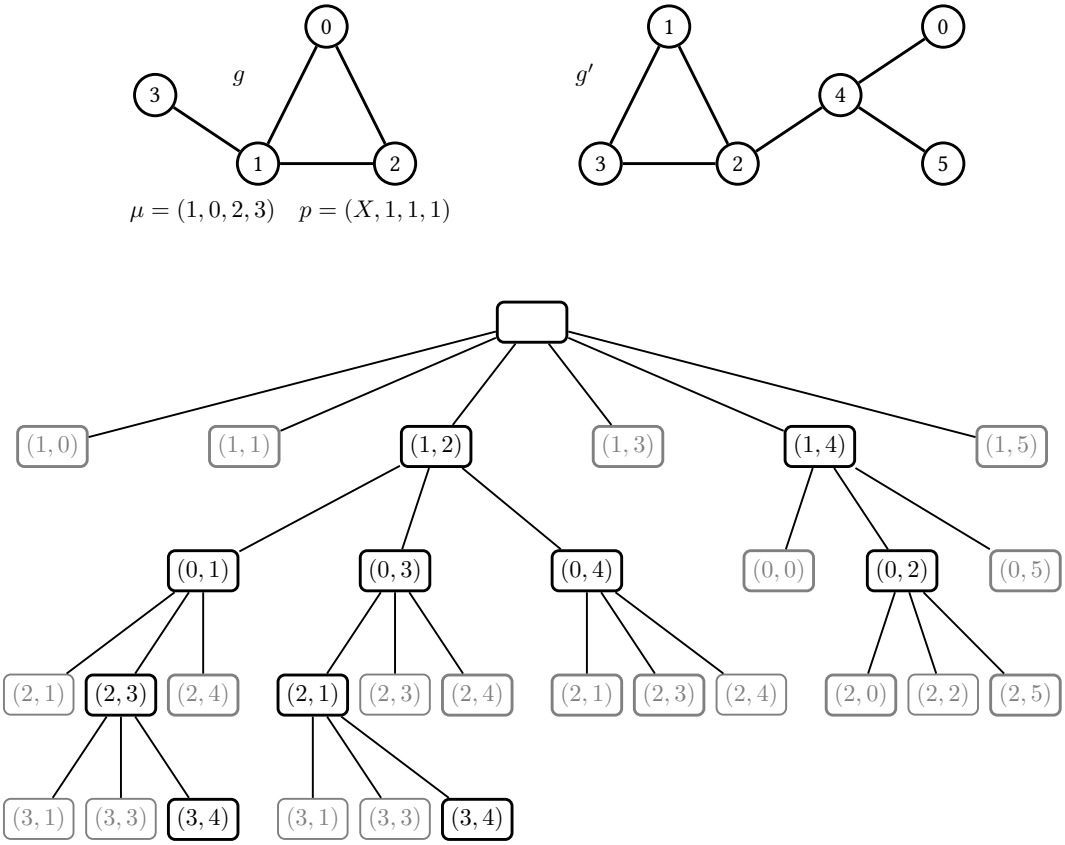

Figure 3.5: An example for the search tree explored by the RI algorithm during the matching process in order to find the subgraph monomorphisms from g to g'. The opaque nodes are accepted by the algorithm, while the less opaque ones are rejected. Nodes which are rejected because they lead to a mapping which is not injective have thinner boundaries. A path from the empty root node to any other node in the tree corresponds to a partial mapping. A path from the root node to an opaque leaf node corresponds to a solution.

3.5.4 Identifying non-contributing graphs

Another important technique in the context of LCEs via graph decompositions is to identify graphs whose reduced contribution is zero in the desired perturbation order although they are embeddable into the lattice graph. If the reduced contribution of a graph to the desired quantity is zero in the considered perturbation order and all lower orders, we refer to the graph as *non-contributing*. Such graphs can often be identified without an actual calculation of the reduced contribution by applying heuristic selection rules [97, 99, 108, 215]. These rules go well beyond the obvious fact, that clusters which contain more than k bonds cannot have a reduced contribution in order k or less [96]. However, these selection rules are model dependent and for some models no such rule can be found. Here, we give a rather general overview formulating conditions when the different selection rules hold. However, we assume that all considered models comply with the general setup, and that the perturbation features only pairwise interactions. Importantly, there are two main types of selection rules. One type can identify only the given graph as non-contributing, whereas the other type can identify the given graph and all supergraphs of the given graph as non-contributing. The latter type is named transitive heuristics in Ref. [130], while the first type is called intransitive heuristics.

Selection rules for the ground-state energy

We begin with selection rules for the calculation of the ground-state energy. Let us start with the transitive rules which are typically based on the vertex degrees of the given graph [97].

As a preliminary remark, recall that the reduced contribution of a graph consists of the processes where the perturbation operators act at least once on every edge in the graph. The graphs we consider for these selection rules are connected graphs, which have at least one edge.

Let us start with a rather weak condition on the model: Any operator $\mathcal{V}_b$ maps the unperturbed local ground state to an unperturbed local excited state on all sites in the bond b. Accordingly, in every perturbative process relevant for the reduced contribution, the perturbation needs to act at least twice on each vertex within the considered graph. Each process which acts only once on any vertex in the graph results in a state which is orthogonal to the unperturbed ground-state. Every process which acts zero times on any vertex in the graph, does not act on all edges of the graph, and hence, is not relevant for the reduced contribution of this graph. Overall, this implies, that for each vertex of degree one, the perturbation has to act at least twice on one of the edges adjacent to this vertex. So a connected graph g with $|E(g)|$ edges and $N_{\text{one}}(g)$ vertices of degree one can only have a non-vanishing reduced contribution in order k if

$$N_{\text{one}}(g) \leq 2 \cdot (k - |E(g)|)\,. \tag{3.144}$$

The factor of two comes from the fact that an edge joins two vertices, and thus, a perturbation operator acting on a single edge, can act on two vertices of degree one simultaneously. Importantly, if g is identified as non-contributing, then each supergraph $g' \supset g$ can not contribute as well. To see this, consider a supergraph g' which has $x > 0$ edges more than g. Every additional edge reduces the number of degree-one vertices at most by two. So for any $g' \supset g$ we have

$$N_{\text{one}}(g') \geq N_{\text{one}}(g) - 2x\,, \qquad |E(g')| = |E(g)| + x\,. \tag{3.145}$$

And we obtain

$$N_{\text{one}}(g) - 2x > 2 \cdot (k - |E(g)|) - 2x \quad \Rightarrow \quad N_{\text{one}}(g') > 2 \cdot (k - |E(g')|)\,. \tag{3.146}$$

With another rearrangement we obtain the desired result

$$N_{\text{one}}(g) > 2 \cdot (k - |E(g)|) \quad \Rightarrow \quad N_{\text{one}}(g') > 2 \cdot (k - |E(g')|)\,. \tag{3.147}$$

Next, we consider a stronger condition: Acting an odd number of times with (potentially different) elementary perturbation operators on any site in the unperturbed local ground state takes this site to a state which has zero overlap with the unperturbed local ground state. This implies that only processes where the perturbation acts an even number of times on each vertex of a given graph are relevant for the reduced contribution of this graph, as all other processes result in a state which has zero overlap with the unperturbed ground state. Accordingly, for any vertex of odd degree the perturbation has to act twice on at least one edge adjacent to this vertex.

An example for such a model is the TFIM in the high-field limit, for which this selection rule is described in Ref. [97]. Also in this case one action of the perturbation at an edge can involve two vertices of odd degree at the same time. So up to order k in perturbation theory, one only needs to take into account graphs which obey

$$N_{\text{odd}}(g) \leq 2 \cdot (k - |E(g)|) \tag{3.148}$$

where $N_{\text{odd}}(g)$ is the number of vertices of odd degree in the graph g. Also this selection rule is transitive. The proof is completely analogue to the proof given before.

Let us now come to the intransitive heuristics. One is described in Ref. [99] for the TFIM in the high-field limit[4]. Similar to the selection rules discussed before, it is designed for cases where the perturbation has to act an even number of times on each vertex in the graph, in order to reobtain the unperturbed ground state. The idea is to calculate the minimum number $N_{\text{min}}^{\text{dup}}(g)$ of edges which have to be duplicated in the graph g under investigation, such that the resulting multigraph has no vertices of odd degree. Accordingly, up to order k we only need to consider graphs which fulfill

$$N_{\text{min}}^{\text{dup}}(g) \leq k - |E(g)|\,. \tag{3.149}$$

An analogous selection rule can be formulated in terms of vertices with degree one. Another intransitive heuristics is described in Refs. [108, 215]. This selection rule applies, if the action of any $\mathcal{V}_b$ conserves the total parity of the number of excitations but changes the parity of the number of excitations at each side of the edge where the perturbation acts. If a single edge is connecting two parts of a graph, acting only once on this edge will lead to an odd number of elementary excitations in both parts. However, the unperturbed ground state has an even number of elementary excitations in both parts, namely zero. In order to restore the parities the perturbation has to act at least twice on this edge. An edge whose removal increases the number of connected components of a graph is called a bridge [156]. In the case of a connected graph, the removal of the edge results in a disconnected graph. Accordingly, this selection rule is based on finding bridges in a graph. Every such bridge corresponds to an edge where the $\mathcal{V}_b$ has to act twice in order to reobtain the unperturbed ground state. Accordingly, in order k perturbation theory, one needs to consider only graphs with

$$N_{\text{bridges}}(g) \leq k - |E(g)|, \tag{3.150}$$

where $N_{\text{bridges}}(g)$ is the number of bridges in g.

[4] In Ref. [99] the selection rule is described for the calculation of another observable, but the adaption to the ground-state energy is straightforward.

Selection rules for one-particle hopping elements

For hopping elements these selection rules can be adapted. We restrict ourselves to the selection rules formulated in terms of odd-degree vertices, as the adaption works analogously for the selection rules in terms of vertices of degree one. The selection rules have been motivated by assumptions about the action of the perturbation on sites which are in the unperturbed local ground state. Obviously, these assumptions do not need to hold for vertices which host an excitation before (start vertex) or after (end vertex) the hopping process. A simple idea is to just not consider these vertices, when we list vertices of odd degree in the context of the selection rule. Accordingly, in the transitive selection rule we do not count the start and the end vertices, whereas in the intransitive selection rule, they are allowed to have odd degree in the multigraph which results from duplicating edges. The selection rule based on parity conservation of excitation numbers requires some more thought, as the parity on both sides of the bridge can change in a hopping process. So we count only the bridges between parts whose parity is not changed by the hopping process, i.e., where the excitation is on the same side of the bridge before and after the hopping process [216].

Example

As an example we consider the TFIM in the high-field limit, with the rescaled Hamiltonian

$$\frac{H^{\text{TFIM}}}{2h} = -\sum_{i\in\mathcal{L}} \sigma_i^z - \lambda \sum_{\langle i,j\rangle} \sigma_i^x \sigma_j^x, \tag{3.151}$$

where $\lambda = J/(2h)$ is the perturbation parameter, σ_i^x and σ_i^z are the usual Pauli matrices and $\langle i,j\rangle$ indicates that the respective sum goes over pairs of next neighbors. Next, we check in which order the graph given in Fig. 3.6 can have a non-vanishing reduced contribution to the ground-state energy according to the different selection rules. Let us start with the obvious observation that the

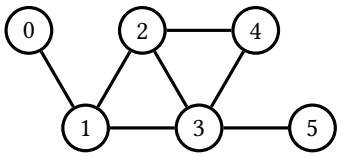

Figure 3.6: The graph g used in the presented example.

graph cannot contribute in perturbation orders smaller than seven, because it has seven edges. As already mentioned before, we have the constraint that the perturbation has to act an even number of times on each vertex in order to obtain the same local states again. Accordingly, we can use the selection rules formulated in terms of vertices of odd degree given in Eq. (3.148). The graph has four vertices of odd degree $(0, 1, 2, 5)$. So we have $N_{\text{odd}}(g) = 4$ and $|E(g)| = 7$. Plugging this in the selection rule (3.148) leads to the conclusion that this graph (and any supergraph of it) can have a non-vanishing reduced contribution to the ground-state energy only in orders $k \geq 9$. Next, we consider selection rule (3.149). To this end we infer that the edges $\{0, 1\}, \{3, 5\}$ have to be duplicated in order to obtain even degrees on the vertices 0 and 5. After duplicating said edges the vertices 0, 1 and 5 have even degree but the vertices 2 and 3 have odd degree, so we also need to duplicate the edge $\{2, 3\}$. So, in total we need to duplicate three edges, and hence, we can be

sure to get a reduced contribution to the ground-state energy only in orders $k \geq 10$. Note that by adding edges $\{0, 2\}$ and $\{1, 5\}$ we obtain a graph without vertices of odd degree, which illustrates that supergraphs of g might have a non-vanishing reduced contribution at orders $k < 10$.

We continue with selection rule (3.150). It is clear, that the elementary perturbation changes the number of excitations by one at each side of an edge, the perturbation acts on. However, it does not change the parity of the total excitation number. If this edge is a bridge, the only way to restore the parity number on the different sites of the bridge is that the perturbation acts again on this edge. By inspection we find two bridges $\{0, 1\}$ and $\{3, 5\}$ where the perturbation has to act at least twice. This leads to the conclusion that g can have a non-vanishing reduced contribution to the ground-state energy in orders $k \geq 9$. Note that this is a weaker statement compared to the selection rule (3.149). However, the selection rule (3.150) can be applied in cases where (3.149) can not be applied.

Next we investigate a hopping element from vertex 0 to vertex 5 on the graph. For the transitive selection rule (3.148) we do not count the vertices 0 and 5 as vertices of odd degree, and hence, we obtain that the graph can have a non-vanishing reduced contribution to this hopping element in orders $k \geq 8$, because there are only two other vertices of odd degree, namely 1 and 2. For the selection rule (3.149) based on duplicating edges it is sufficient to add an edge $\{1, 2\}$ in order to get rid of all vertices of odd degree apart from 0 and 5. From this one can also conclude that the graph has non-vanishing reduced contribution in orders $k \geq 8$. The selection rules based on bridges (3.150) states that the graph can have a non-vanishing contribution in orders $k \geq 7$ which is already obvious from the number of edges, because all bridges are necessary to connect the vertices 0 and 5.

3.6 Linked-cluster expansions via hypergraph decompositions

After discussing LCEs based on graph decompositions [95–99] in the previous section, we come to the generalization to perturbations which contain couplings of an arbitrary number of lattice sites [130]. As this generalization has been introduced in Ref. [130], this section is largely based on this publication. A shorter introduction to hypergraph decompositions is also found in the appendix of Ref. [105]. Multi-spin couplings are present in several quantum spin models. In two dimensions examples include Kitaev's toric code [18] and the quantum Newman-Moore model [86, 217]. In three dimensions the three dimensional toric code [19, 20] as well as fracton models like the X-Cube model [26] or Haah's cubic code [24] feature such couplings.

Considering a setup as described in Sect. 3.2 we can write a scalar quantity like the ground-state energy and matrix elements of the quasiparticle number conserving effective Hamiltonian in the unperturbed eigenbasis [96–99]

$$O(\mathcal{L}) = \sum_{\mathcal{E} \subseteq \mathcal{L}} \mathcal{N}(\mathcal{E}, \mathcal{L}) \cdot o(\mathcal{E}) \,, \tag{3.152}$$

where $\mathcal{E}$ are equivalence classes of subclusters of the lattice $\mathcal{L}$ and $o(\mathcal{E})$ corresponds to the reduced contribution of any cluster of the class $\mathcal{E}$ to the quantity $O(\mathcal{L})$ [96, 105, 187]

$$o(\mathcal{E}) = o(C) \quad \forall\, C \in \mathcal{E} \,. \tag{3.153}$$

The reduced contribution of a cluster can be calculated, as in LCEs with only two-site interactions, either via subcluster subtraction [95–97] (see Eq. (3.13)) or a bookkeeping technique [123]. What actually changes by the introduction of multi-site interactions in the perturbation terms, is how the equivalence of subclusters is accessed and consequently also how the embedding factors of the equivalence classes are obtained [130]. For graph decompositions with only pairwise interactions a representation of clusters in terms of graphs is straightforward, and the equivalence of clusters corresponds to isomorphism of the representing graphs. Such a graph representation is not obvious for the case of perturbations which feature multi-site interactions, although some problem specific formulations of graph decompositions with multi-site interactions exist in the context of topologically ordered phases [107, 187, 218].

However, for perturbations with couplings of more than two sites the clusters can be naturally represented by hypergraphs [130]. As mentioned in Sect. 2.2, these hypergraphs can be represented by simple bipartite graphs, called the König representation [132]. Importantly, two hypergraphs are isomorphic if and only if their representing König graphs are isomorphic [132, 133]. Accordingly, the equivalence of subclusters in the context of hypergraph decompositions corresponds to isomorphism of the representing König graphs [130]. Interestingly, hypergraphs and their König representation have already been used to represent chemical structures [134–136]. First, we describe how to obtain the connected subclusters relevant for the calculation using an algorithm presented in Ref. [219]. Next, we discuss how to sort these subclusters into equivalence classes such that equivalent clusters have the same contribution to the desired matrix element. We explain how these subclusters are represented by hypergraphs, and how the König representation of these hypergraphs is obtained. We also describe how the information about local states on the sites within a subcluster are incorporated into the König representation if necessary. Further, we address how to obtain the embedding factors of all relevant equivalence classes of subclusters up to a given number of bonds. Finally, we discuss how to identify non-contributing subclusters as early as possible during the calculation which is analogous to the known methods for conventional graph decompositions [97, 99, 108, 215].

3.6.1 Subcluster generation

For the generation of subclusters we use an algorithm [219] originally designed to enumerate all connected subgraphs of a given graph. As it simply identifies a subgraph by the involved edges, it is not limited to conventional graphs and perfectly applicable for our purpose to find all relevant connected subclusters of a given cluster, excluding clusters consisting of a single site.

The algorithm basically transverses a search tree in a depth-first manner [220]. It starts from a single bond and tries to extend the current subcluster by adding one of the adjacent bonds, which are not already part of the current subcluster. If an adjacent bond can be added the algorithm has discovered a new subcluster. If no adjacent bond can be added the algorithm backtracks, i.e., it removes the last appended bond. This bond must not be added any more to the cluster to which the algorithm backtracked and all the clusters obtained by extending it. The bond will be available again once the algorithm backtracks one level further. Thinking in terms of search trees, it is forbidden to append the removed bond in the remaining subtree rooted in the node to which the algorithm backtracked. When the algorithm leaves this subtree (by backtracking further) this bond is allowed to be added again. Overall, considering all child nodes of a given node of the search tree, the bond represented by a given child node must not be appended in the subtrees descendant from

the other child nodes which are visited after this node. This is illustrated for an example in Fig 3.7.

In this way the algorithm ensures that all paths descendant from a given node differ in at least one bond and hence every connected subcluster containing the initial bond is found once and only once. Obviously, one can also apply this scheme with the empty cluster as a root node, allowing

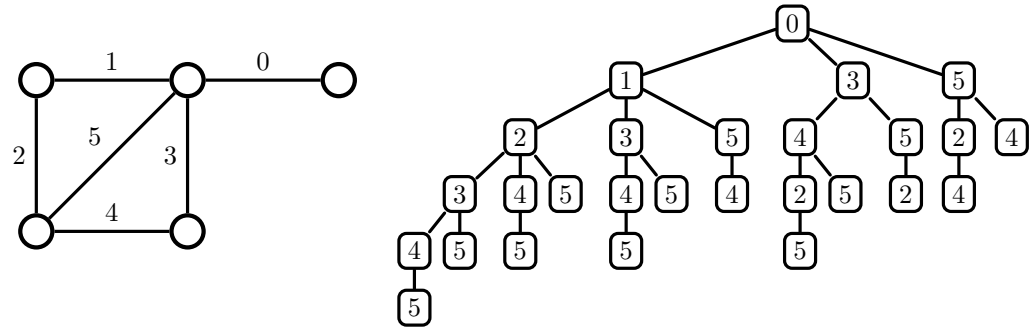

Figure 3.7: A cluster with indices naming the bonds and a potential search tree starting from the bond 0. The leftmost branches are visited first. Note that for any two child nodes of the same node, the bond represented by the child node which is further left is not contained in the subtree descendant from the other child node.

every bond to be added to the empty cluster. This corresponds to restarting the search from all the bonds in the cluster while excluding the bonds from which we have started the search before. Limiting the size of the subclusters obtained by this algorithm can be easily incorporated into an additional condition for backtracking. As in the original paper [219] we give an example which we also illustrate in Fig. 3.7 where we show a cluster and the corresponding search tree traversed by the algorithm starting at bond 0. The obtained subclusters in terms of bonds are given in Tab. 3.1. Continuing with bond 1 as root node we have to exclude bond 0 and obtain the clusters given in Tab. 3.2.

Here, we traversed the search tree by always appending the bond with the lowest index first (but the order is not important). As a consequence, we can use this algorithm to find all subclusters of a given cluster which contain a given bond or one bond out of a set of bonds. In the case of LCEs for extensive ground-state energies this helps to find only the clusters which have a bond in a given unit cell. This still does not exclude that we generate clusters which are related by translational symmetry. This issue is addressed in Subsubsect. 3.6.3.

In the case of hopping elements this helps to find only the clusters with reduced contributions different from the reduced ground-state energy by enforcing that all starting bonds of the algorithm are adjacent to some site which is occupied before the hopping process, and induce backtracking when any site which changes its local state in the hopping element under consideration is not reachable by extending the cluster up to k bonds.

subclusters (given as sets of bonds)						Forbidden
{0}	{0,1}	{0,1,2}	{0,1,2,3}	{0,1,2,3,4}	{0,1,2,3,4,5}	{ }
				{0,1,2,3,5}		{4}
			{0,1,2,4}	{0,1,2,4,5}		{3}
			{0,1,2,5}			{3,4}
		{0,1,3}	{0,1,3,4}	{ 0,1,3,4,5}		{2}
			{0,1,3,5}			{2,4}
		{0,1,5}	{0,1,5,4}			{2,3}
	{0,3}	{0,3,4}	{0,3,4,2}	{0,3,4,2,5}		{1}
			{0,3,4,5}			{1,2}
		{0,3,5}	{0,3,5,2}			{1,4}
	{0,5}	{0,5,2}	{0,5,2,4}			{1,3}
		{0,5,4}				{1,2,3}

Table 3.1: The sets in the left part of the table are sets of bonds, which specify all connected subclusters which contain the bond 0. Every line corresponds to the algorithm appending bonds. On a line-break one or more backtracks occur and the first given cluster is the result of the first appending operation. In the rightmost column we denote the bonds which cannot be appended in a given line because they have been removed before.

subclusters (given as sets of bonds)					Forbidden
{1}	{1,2}	{1,2,3}	{1,2,3,4}	{1,2,3,4,5}	{0}
			{1,2,3,5}		{0,4}
		{1,2,4}	{1,2,4,5}		{0,3}
		{1,2,5}			{0,4}
	{1,3}	{1,3,4}	{1,3,4,5}		{0,2}
		{1,3,5}			{0,2,4}
	{1,5}	{1,5,4}			{0,2,3}

Table 3.2: The subclusters obtained with 1 as root node without the subclusters containing bond 0. The format is the same as in Tab. 3.1.

3.6.2 Cluster classification

A key element of LCEs is the structural equivalence of clusters. In conventional LCEs clusters are represented by graphs, and once these graphs are isomorphic the Hamiltonians on the respective clusters can be shown to be equivalent [96] as also shown in Subsect. 3.5.1. Clearly, deciding whether two clusters are structurally equivalent is also desirable in the context of LCEs with perturbations which act on multiple sites simultaneously. A straightforward representation of the clusters is given by hypergraphs. Indeed, using such a hypergraph representation we can proceed analogously to Subsect. 3.5.1.

Given a cluster $C = (S, B)$, we interpret this cluster as a hypergraph, where the vertices represent the sites and the hyperedges represent the bonds. For simplicity, we assume that clusters do not have duplicate bonds. One can again distinguish different bond types by edge colors and the roles of sites within different bonds using incidence colored hypergraphs as introduced in Subsect. 2.2.3. Importantly, structural equivalence or isomorphism of clusters is again given by isomorphism of the corresponding hypergraphs. Accordingly, for two isomorphic clusters $C = (S, B)$ and $C' = (S', B')$ we have a bijective mapping of the sites $\varphi : S \to S'$

$$i \in b \Leftrightarrow \varphi(i) \in \varphi(b) = \{\varphi(i) \,|\, i \in b\} \quad \forall i \in S,\ \forall b \in B\,, \tag{3.154}$$

and hence, the respective effective cluster Hamiltonians are equivalent

$$H_{\text{eff}}^{\varphi(C)} = H_{\text{eff}}^{C'}\,, \tag{3.155}$$

where $\varphi(C)$ is the cluster obtained by renaming the sites according to the isomorphism φ. In the case of different bond types the isomorphism φ is required to preserve the bond types. Finally, also the roles of sites within the bonds must be preserved by φ. Due to Eq. 3.155 isomorphic clusters have the same reduced contribution to the ground-state energy. For the calculation of matrix elements $\langle\Phi|\, H_{\text{eff}}\, |\Psi\rangle$ with respect to unperturbed basis states

$$|\Phi\rangle = \bigotimes_{i\in\mathcal{L}} |\Phi_i\rangle\,, \qquad |\Psi\rangle = \bigotimes_{i\in\mathcal{L}} |\Psi_i\rangle\,, \tag{3.156}$$

the isomorphism needs to obey

$$|\Phi_i\rangle = |\Phi_{\varphi(i)}\rangle \quad \text{and} \quad |\Psi_i\rangle = |\Psi_{\varphi(i)}\rangle \qquad \forall i \in S\,, \tag{3.157}$$

in order to guarantee that

$$\langle\Phi|\, H_{\text{eff}}^{C}\, |\Psi\rangle = \langle\Phi|\, H_{\text{eff}}^{\varphi(C)}\, |\Psi\rangle = \langle\Phi|\, H_{\text{eff}}^{C'}\, |\Psi\rangle\,, \tag{3.158}$$

and hence, the reduced contributions of the clusters C and C' to the matrix element $\langle\Phi|\, H_{\text{eff}}\, |\Psi\rangle$ agree. In this case we call the clusters C and C' *equivalent* in the context of the calculation of this matrix element. As this equivalence also implies that C and C' are isomorphic, also their reduced contributions to the matrix element $\langle\Phi|\, H_{\text{eff}} - E_0\, |\Psi\rangle$ agree.

As explained in Sect. 2.2 hypergraphs can be represented by simple bipartite graphs, which are also referred to as the König representation of a hypergraph [132]. Importantly, two hypergraphs are isomorphic if and only if the respective König representations are isomorphic [132, 133], so the problem of hypergraph isomorphism is relegated to the isomorphism of simple graphs.

Using this König representation, a cluster is represented by the bipartite graph where the vertices represent the sites and bonds of the cluster. In the following we refer to vertices representing sites as *site vertices* and to vertices representing bonds as *bond vertices*. Whether a vertex is a site or bond vertex has to be clearly distinguishable in the graph. A bond vertex is joined to a site vertex if and only if the respective site is contained in the respective bond. There are no edges joining two site vertices or two bond vertices, so the graph is bipartite. To distinguish different bond types we assign colors to the bond vertices, keeping in mind that site and bond vertices remain distinguishable. Similarly, we can use edge colors to distinguish the role of vertices within a bond, if this is necessary. Up to now, this representation captures only the structure of a subcluster not the local states involved in a given matrix element. However, we still need to adhere to condition (3.157). While for a calculation of the ground-state energy this condition is trivially fulfilled as $|\Phi\rangle = |\Psi\rangle = \bigotimes_{i\in\mathcal{L}} |0\rangle$, this is not the case for other matrix elements $\langle\Phi| H_{\text{eff}} |\Psi\rangle$ of the effective Hamiltonian, like one-quasiparticle matrix elements. In this case the local states $|\Phi_i\rangle$ and $|\Psi_i\rangle$ on the sites of the subclusters need to be incorporated into the König representation using additional vertex colors for the site vertices.

From a more practical perspective, bonds with the same bond type always act on the same number of sites. As a consequence, we can further simplify the graph representation by omitting site vertices of degree one as long as the corresponding sites are not occupied in the product states $|\Phi\rangle$ and $|\Psi\rangle$ of the desired matrix element $\langle\Phi| H_{\text{eff}} |\Psi\rangle$. Obviously, for a calculation of the ground-state energy all of these site vertices can be omitted.

Examples

In order to make the graph representation of clusters more accessible we present two examples. As the bonds are actually representing the couplings of a lattice Hamiltonian, we provide a lattice Hamiltonian for each example. We then specify a small cluster, which can be regarded as the subcluster of a lattice, and the matrix element we consider on this lattice. Then we give a graph representation of the cluster, which is designed such, that any two clusters represented by isomorphic graphs have the same reduced contribution to this matrix element. We start with the lattice Hamiltonian

$$H^{\text{ex1}} = -\sum_{i\in\mathcal{L}} \sigma_i^z - \lambda \sum_{b\in\mathcal{B}} \prod_{i\in b} \sigma_i^x, \tag{3.159}$$

where $\mathcal{B}$ is the set of all bonds in the system. We assume that all of these bonds b contain four different sites, so we deal with four spin interactions. Now, consider the cluster $C = (S, B)$ in the context of an evaluation of the ground-state energy per site of H^{ex1}

$$\begin{aligned} S &= \{0,1,2,3,4,5\}\,, \quad B = \{b_0, b_1\}\,, \\ b_0 &= \{0,1,2,3\}\,, \quad b_1 = \{2,3,4,5\}\,. \end{aligned} \tag{3.160}$$

Clearly, we do not need to distinguish any bond types here, and the order within the bonds does not play any role, because the interaction is symmetric as it acts equivalently on every site in the bond. The representations of the cluster by a hypergraph, its König representation and the reduced König representation are given in Fig. 3.8. Finally, using this reduced König representation, two clusters represented by isomorphic graphs have the same reduced contribution to the ground-state energy.

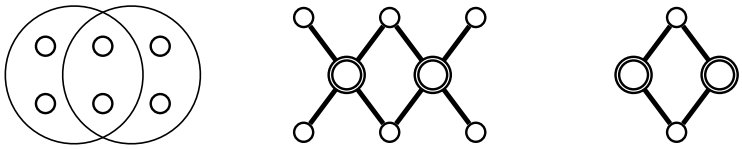

Figure 3.8: Representation of the cluster C by a hypergraph (left): The small circles correspond to the vertices of the hypergraph, i.e., to the sites of the cluster. The large circles are the hyperedges, which represent the bonds of the cluster. The (full) König representation (center) of the cluster C: The double circles illustrate the bond vertices and the single circles represent the site vertices. The reduced König representation of the cluster C (right): With respect to the full König graph the site vertices of degree one and edges adjacent to these vertices have been dropped.

Next, we continue with a more complicated example, considering the lattice Hamiltonian

$$H^{\text{ex2}} = -\sum_{i\in\mathcal{L}} \sigma_i^z - \lambda \sum_{b\in\mathcal{B}} \sigma_i^x \sigma_j^x \sigma_k^z - \lambda \sum_{b\in\mathcal{B}} \sigma_i^z \sigma_j^x \sigma_k^z \tag{3.161}$$

where all bonds contain three different sites i, j, k. However, as the elementary perturbation terms do not act equivalently on all sites within a bond, we deal with non-symmetric three spin interactions. Additionally, we also have several types of bonds in the system. Clearly, the unperturbed ground state is a z-polarized state, and the elementary excitation corresponds to a spin pointing in negative z-direction. Now, let us consider a cluster C in the context of an evaluation of a hopping element $\langle 1, \vec{r}_3 | \, H_{\text{eff}}^{\text{ex2}} - E_0 \, | 1, \vec{r}_1 \rangle$ of a spin-flip excitation from site 1 to site 3. The cluster C is given by

$$\begin{aligned} S &= \{0,1,2,3,4\}\,, \quad B = \{b_0, b_1\} \\ b_0 &= \{0,1,2\}\,, \quad b_1 = \{2,3,4\}\,, \end{aligned} \tag{3.162}$$

where we distinguish the bond types by the colors of the respective bonds in the set B. Furthermore, we also incorporate the different roles of the sites within the bonds, because the interactions are not symmetric and act differently on the three sites within the bond. Here, we choose the colors such, that σ^x acts on the red numbers and σ^z on the black numbers within the bonds. Further, the local states on the sites within the states $|1, \vec{r}_1\rangle$ and $|1, \vec{r}_3\rangle$ are incorporated using the vertex colors

$$\begin{array}{c} \\ \langle 0| \\ \langle 1| \end{array} \begin{array}{c} \begin{array}{cc} |0\rangle & |1\rangle \end{array} \\ \left[\begin{array}{cc} \circ & \bullet \\ \bullet & \bullet \end{array} \right] \end{array} . \tag{3.163}$$

The König representation and the reduced König representation of the cluster together with the information about the local states on the cluster are given in Fig. 3.9. Again, using the reduced König representation, two clusters have the same reduced contribution to the matrix element $\langle 1, \vec{r}_3 | \, H_{\text{eff}}^{\text{ex2}} - E_0 \, | 1, \vec{r}_1 \rangle$ if the representing graphs are isomorphic.

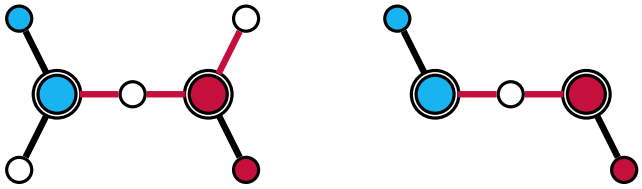

Figure 3.9: The (full) König representation of the cluster C (left): The site vertices are colored according to their occupation before and after the hopping process. The color of the edges reflects the role of the vertices within the bonds. Here, a red edge indicates that within the given bond σ^x is acting on this vertex, whereas the black edges are indicating actions of σ^z. The reduced König representation of the cluster C (right): Here the site vertices of degree one which are neither occupied in the initial nor in the final state and their adjacent edges have been dropped.

Practical considerations

In a practical implementation one would typically just use integer numbers to assign colors to the edges and vertices, in a way which still allows to tell apart site vertices from bond vertices. For the site vertices one could impose the following scheme for a given matrix element $\langle\Phi| H_{\text{eff}} - E_0 |\Psi\rangle$ on a cluster C. For any site in the cluster label every local unperturbed eigenstate in $|\Psi\rangle$ by an integer $s_i^{\text{right}} \in \{0, s^{\max}\}$ and similarly use an integer $s_i^{\text{left}} \in \{0, s_i^{\max}\}$ for the state $|\Phi\rangle$. Then the color c_i of the site vertex representing site i is

$$c_i = s_i^{\text{left}} \cdot s^{\max} + s_i^{\text{right}} \,. \tag{3.164}$$

For four different local states ($s^{\max} = 3$) this yields the vertex colors

	$\|0\rangle$	$\|1\rangle$	$\|2\rangle$	$\|3\rangle$
$\langle 0\|$	0	1	2	3
$\langle 1\|$	4	5	6	7
$\langle 2\|$	8	9	10	11
$\langle 3\|$	12	13	14	15

. (3.165)

In order to keep vertices representing sites distinguishable from vertices representing bonds, one needs to use different colors for site and bond vertices. One possibility is to assign positive integers (without zero) to the bond vertices and negative integers (including zero) to the site vertices.

Once all necessary information is included into the graphs, we can simply check for equivalence of clusters using appropriate algorithms to access the isomorphism of the representing graphs. Recall that we require isomorphism to preserve edge and vertex colors. We use the RI algorithm [142,164] which is also described in Subsect. 3.5.3 for explicit isomorphism checks. Again, it is helpful to use a set of graph invariants to strongly reduce the necessity of explicit checks for isomorphism. The typical situation is that we have a set of non-isomorphic graphs, and want to check whether a newly discovered graph is isomorphic to any graph in this set. We first distinguish the graphs by the number of bond vertices. For each number of bond vertices we store key-value

pairs in a suitable data structure (e.g. a map from the C++ standard library). The keys of this data structure are given by another graph invariant. This invariant is based on degree information and possibly on the colors of the vertices. The value associated with a key is again a small list of a all graphs which coincide in this graph invariant. So, instead of checking a newly obtained graph for isomorphism against all previously found graphs, we only check it against a, typically very limited, set of graphs with the same invariant.

3.6.3 Embedding factors

We have already explained how to obtain the relevant subclusters and how to sort them into equivalence classes. Here, we address how to obtain the embedding factor $\mathcal{N}(\mathcal{E}, \mathcal{L})$ for a given equivalence class. As we already determined the potentially relevant subclusters and sorted them into equivalence classes, the remaining task is to count them properly. For the normalized embedding factor of an equivalence class of clusters per unit of the lattice $\mathcal{N}(\mathcal{E}, \mathcal{L})/N_{\mathrm{unit}}$, one counts the subclusters of each equivalence class modulo translational symmetry, which requires some attention. For the unnormalized embedding factors $\mathcal{N}(\mathcal{E}, \mathcal{L})$ counting of the subclusters in each equivalence class is sufficient. For both cases we also address the question, which subclusters need to be generated at all.

Normalized embedding factors

We aim to exploit the translational symmetry of the lattice and calculate the ground-state energy with respect to some suitable unit. This unit may be a single bond of the lattice, but it can also contain several bonds. Accordingly, we aim to calculate the embedding factor per unit $\mathcal{N}(\mathcal{E}, \mathcal{L})/N_{\mathrm{unit}}$, where N_{unit} is the number of such units in the lattice. The algorithm from Ref. [219] as described in Subsect. 3.6.1 finds all connected subclusters (up to a specified number of bonds) which contain at least one of the bonds in this unit.

For now we assume that all bonds in the lattice are symmetry equivalent and thus also of the same type. Accordingly, we can calculate the ground-state energy per bond. The subcluster generation algorithm finds all connected subclusters which contain a given bond b_0. We refer to these subclusters as $\mathcal{S}_{b_0}$. However, when a subcluster contains a second bond b_1, it will also be contained in the set of all connected subclusters which contain b_1, which we denote $\mathcal{S}_{b_1}$. Obviously, this leads to an overcounting of the subclusters and the number of subclusters belonging to an equivalence class with k bonds is overcounted k times [187]. Accordingly, the simplest strategy is to count all the instances of a given equivalence class in $\mathcal{S}_{b_0}$ and divide by the number of bonds contained in a subcluster of this class. However, this means that we have to sort all instances of $\mathcal{S}_{b_0}$ into equivalence classes, although in general only a fraction of them is counted towards the embedding factors.

In order to improve this, we count only instances where b_0 is always in a specific position within the subclusters. Let us use v_0 to refer to the vertex representing b_0 in the reduced König representation of each subcluster. In a first step we require that v_0 obeys some condition based on isomorphism invariant vertex properties of the bond vertices. Importantly, one has to make sure that at least one bond vertex fulfills this condition for any subcluster. For example one could only count subclusters where v_0 has maximum degree among all bond vertices. The subclusters which do not fulfill this requirement do not need to be assigned to an equivalence class as they are not

counted towards the embedding factors anyways. Still, other subclusters obtained by extending them, might be counted towards embedding factors of other classes. Note that this saves a lot of isomorphism checks, as the over-counting is reduced to the number of bond vertices in the reduced König representation which fulfill this condition, at almost no computational expense. The embedding factor is then given by the number of counted instances divided by the number of bond vertices in the reduced König representation which fulfill the condition. Additionally, one can ensure that for a given equivalence class v_0 is always in equivalent automorphism orbits[5]. The first subcluster which is counted towards the embedding factor of an equivalence class is used as the representative for this class. Further instances belonging to this class are only counted if there is an isomorphism from this representative to the newly discovered instance, which maps the vertices v_0 to each other. In this way we ensure that v_0 is in equivalent automorphism orbits for all counted instances of a given class. Accordingly, the over-counting is reduced to the number of vertices in this automorphism orbit. In practice, this check is actually done during the sorting of the subclusters into isomorphism classes, where we do not only test if there is an isomorphism, but also if there is an isomorphism which maps the vertices representing b_0 to each other. If there is an isomorphism, but no isomorphism which fulfills this condition, the subcluster is not counted. Conversely, if there is no isomorphism at all, the subclusters belong to a different equivalence classes.

In summary, for a given equivalence class we only count instances where v_0 is in a specific automorphism orbit. If this orbit is non-trivial we are still over-counting the number of clusters by the size of this orbit. Note the similarity of this approach to the procedure in conventional graph decompositions, where we consider only the monomorphisms where one specific vertex (pair of neighboring vertices) of the graph is mapped to a specific vertex (pair of neighboring vertices) of the lattice graph [96, 97]. Details about this procedure are also discussed in Subsubsect. 3.5.2.

Next, let us consider the case where all bonds in the chosen unit cell are of different type, still assuming that bonds of the same type are symmetry equivalent within the lattice. We start with the subclusters which contain the bond b_0 which we define to be of bond type 0, and determine the embedding factors. One can still count only instances where v_0 is in equivalent automorphism orbits. Again, one has to correct the over-counting dividing by the size of the respective orbit. However, when we use a criterion based on properties of bond vertices to reduce the number of subclusters which need to be counted, we have to make sure to base this criterion only on the properties of the vertices representing bonds of type 0, such that a least one of these vertices fulfills the condition. In this way we get all the embedding factors for the isomorphism classes containing at least one bond of type 0.

After we have obtained the embedding factors for all isomorphism classes containing a bond of type 0, we consider all subclusters which contain a specific bond b_1 of type 1 and no bond of type 0. We do not need to consider any subclusters which contain a bond of type 0 here, as they belong to isomorphism classes which we already considered before. Again we count only instances where the vertex representing b_1 is in equivalent automorphism orbits, and hence, also need to correct for the size of the respective orbit. Here, any condition to exclude subclusters from the counting based on properties of bond vertices, needs to make sure that at least one vertex representing a

[5]Given two graphs $g \cong g'$ with an isomorphism $\varphi : V(g) \to V(g')$ the automorphism orbit under $\mathrm{Aut}(g')$ equivalent to $\mathrm{Orb}_{\mathrm{Aut}(g)}(v)$ is $\varphi(\mathrm{Orb}_{\mathrm{Aut}(g)}(v)) = \mathrm{Orb}_{\mathrm{Aut}(g')}(\varphi(v))$.

bond of type 1 fulfills the condition. This scheme is continued considering clusters which contain bond b_n of type n but no bond of the types 0 to $n-1$. From a practical perspective one can restart the cluster generation algorithm from bond b_n with a system where all bonds of type 0 to $n-1$ have been deleted. If multiple bonds of the same type are in the chosen unit and all of these bonds are symmetry equivalent, one can determine the embedding factor of an isomorphism class per bond of this type. The embedding factor per unit is then obtained by multiplying this factor with the number of bonds of this type in the chosen unit.

Unnormalized embedding factors

To calculate a hopping element $\langle\Phi| H_{\text{eff}} - E_0 |\Psi\rangle$ we aim to find all subclusters which can have a non-vanishing reduced contribution to this matrix element. These are typically all subclusters which contain at least one site which is occupied within the product states $|\Phi\rangle$ and $|\Psi\rangle$ and each site where the states $|\Phi\rangle$ and $|\Psi\rangle$ have different local states. It is sufficient to sort these subclusters into equivalence classes and count how many subclusters belong to each equivalence class. Note that here the equivalence of clusters takes into account the local states on the sites of the respective clusters within the states $|\Phi\rangle$ and $|\Psi\rangle$ as explained in Subsect. 3.6.2. On a more technical level, the positions (and possibly also the types) of the excitations are incorporated into the representing graphs using additional vertex colors for the site vertices, and equivalence of the clusters is given by (color preserving) isomorphism of these graphs.

3.6.4 Identifying non-contributing clusters

The selection rules [97, 99, 108, 215] discussed in Subsect. 3.5.4 can be adapted for clusters which contain bonds which couple multiple sites. Also here we consider only connected clusters which contain at least one bond. Interestingly, this can be done with only very minor modifications. We discuss only the generalizations of the selection rules based on vertices of odd degree to the case of perturbations which include multi-site interactions for calculations of the ground-state energy. As in Subsect. 3.5.4 we also briefly address how to apply such rules to hopping elements. In this subsection we do not give examples. Instead, we relegate them to Subsect. 3.7.4 where we consider a concrete example in the context of the high-field limit of the plaquette Ising model [137–140] in a transverse field on the cubic lattice.

Selection rules for the ground-state energy

Let us first consider how to adapt the transitive selection rule (3.148) based on vertices of odd degree. Instead of counting odd-degree vertices of a graph, we count the sites in the subcluster which are contained in an odd number of bonds (sites of odd degree). The vertices in the König representation corresponding to sites of odd degree also have odd degree, and they are clearly distinguishable from vertices which represent bonds. As in Subsect. 3.5.4 we require the elementary perturbation operators to act an even amount of times on each site in the cluster, to restore the unperturbed ground state (or any state which has overlap with it). Recalling, that only processes which act on all bonds of a cluster (and no bond outside) contribute to its reduced contribution, each site of odd degree requires that the elementary perturbation acts at least twice on a bond which contains this site. Again one needs to consider, that a bond can contain an arbitrary number of sites of odd degree, and hence, this requirement can be fulfilled for multiple sites of odd degree

by acting twice on a single bond. Accordingly the reduced contribution of a subcluster C (and each connected cluster obtained by expanding it) needs to be calculated only if

$$N_{\mathrm{odd}}(C) \leq c_{\max} \cdot (k - N_{\mathrm{bonds}}(C)) \tag{3.166}$$

where $N_{\mathrm{odd}}(C)$ is the number of sites of odd degree and $N_{\mathrm{bonds}}(C)$ is the number of bonds in the subcluster C, $c_{\max}$ is the maximum cardinality of a bond in the entire system and k is the desired perturbation order. The proof that this selection rule is indeed transitive is analogous to the one given in Subsect. 3.5.4. The intransitive selection rule which searches for the minimum number of edges which need to be duplicated such that no vertex of odd degree is left in the resulting multigraph can also be generalized in order to determine whether a given subcluster C can have a non-vanishing reduced contribution. To this end one searches the minimum number of bonds $N_{\mathrm{dup}}(C)$ in the cluster C which have to be duplicated such that no sites of odd degree are left in the resulting cluster. The subcluster needs to be included in the calculation only if

$$N_{\mathrm{dup}}(C) \leq (k - N_{\mathrm{bonds}}(C)) \,. \tag{3.167}$$

All these rules can be used on the level of actual subclusters but also on the level of isomorphism classes. Typically, it is most efficient to use the transitive rules during the generation of subclusters, to get rid of entire branches of the search tree, and then use the intransitive rules afterwards on the level of the isomorphism classes.

In [130] another transitive heuristics is introduced which depends on the actual realization of the subcluster under investigation within the lattice. It is closely related to the transitive heuristics based on counting the sites of odd degree. Importantly, for this heuristic we need to calculate beforehand, which sites within the system are contained in the same bond, and which are not. Then, given the odd-degree sites of the subcluster, we estimate how many bonds (from all the bonds which are in the system) we need to cover all of these odd degree sites, such that every odd degree site is contained in at least one of these bonds.

As a motivation consider a subcluster with two sites of odd degree, but there is no bond in the lattice joining these two sites. As the perturbation has to act twice on each of these sites, but it cannot act simultaneously on both sites, it has to act two additional times on the subcluster (compared to the number of bonds present in the subcluster). To make this estimate more formal, we create an auxiliary graph g_{aux}, whose vertices represent the sites of odd degree. Whenever, two sites are not contained simultaneously in any bond within the lattice, the representing vertices are connected by an edge. Accordingly, neighboring vertices in this graph, cannot be in the same bond, and thus they need to be in different bonds. Now, let us assign colors to the vertices, with the constraint that neighboring vertices cannot have the same color. Accordingly, sites which have no common bond within the system correspond to vertices with different colors in the auxiliary graphs. In order to find a lower bound for the number of bonds needed to cover all sites of odd degree in this subcluster, we can simply employ a graph coloring algorithm and calculate the chromatic number $\chi(g_{\mathrm{aux}})$ of the auxiliary graph (see Subsect. 2.1.3). The cluster in question can have a non-vanishing reduced contribution only if

$$\chi(g_{\mathrm{aux}}) \leq k - N_{\mathrm{bonds}} \tag{3.168}$$

where again k is the desired perturbation order and N_{bonds} is the number of bonds in the considered cluster. Interestingly, also this selection rule is transitive, and hence, all the subclusters obtained by further expanding a subcluster which is discarded due to this selection rule can also be discarded.

Selection rules for hopping elements

For hopping elements the selection rules can be easily adapted. For the heuristics based on odd-degree vertices a feasible approach is to simply allow sites which are occupied in the left or right state of the matrix element to have odd degree in the sense that they need not to be counted or covered within the selection rules. Instead, they are just treated, as if they had even degree.

3.7 Plaquette Ising model in a transverse field

In this section we aim to make the details of the hypergraph decomposition method more explicit by considering the example of the three dimensional plaquette Ising model [137–140] in a transverse magnetic field (TFPIM). This example is also considered in Ref. [130]. Accordingly, this section is closely based on the respective parts of Ref. [130]. We consider the TFPIM on a cubic lattice with the Hamiltonian

$$H^{\mathrm{TFPIM}} = -\sum_i \sigma_i^z - \lambda \sum_{\square} \sigma_{i_1}^x \sigma_{i_2}^x \sigma_{i_3}^x \sigma_{i_4}^x \,, \tag{3.169}$$

where the first sum runs over all sites of the cubic lattice, and the second sum runs over all plaquettes. The indices i_1 to i_4 refer to the four sites at the corners of the given plaquette and λ is a perturbation parameter. We focus on calculating the ground-state energy per plaquette, but also briefly comment on the modifications which are necessary to calculate hopping elements and give results for the ground-state energy per plaquette and the excitation gap as obtained in Ref. [130].

3.7.1 Subcluster generation

The first step is to define a cluster which is suitably large and periodically coupled such that a calculation of the ground-state energy in the thermodynamic limit can be done on this cluster up to the desired perturbation order k. For each bond in this cluster we store the bonds adjacent to it. Then we choose a starting bond, and run the algorithm from Ref. [219] (see also Subsect. 3.6.1) to find all relevant subclusters. It does not matter from which bond we start the algorithm because any two bonds are related by translation and rotation. Obviously, we need to incorporate the desired perturbation order k into the algorithm. Basically, subclusters with k bonds are not allowed to be expanded further. As a consequence, the algorithm finds all connected subclusters, which contain the starting bond b_0 and have k or less bonds. Not all of these clusters contribute to the final result, and it is helpful to apply transitive selection rules [97, 130] during the subcluster generation in order to discard branches of the search tree which contain only non-contributing clusters as early as possible.

3.7.2 Cluster Classification

A very important consideration of graph decomposition techniques is to classify subclusters, such that every subcluster in a class has the same contribution. In graph decomposition techniques this is typically done by representing the subclusters by graphs and checking the graphs for isomorphism [95–97]. For models where the perturbation operators act on two sites, the graph representation of a subcluster is obvious. However, this is not the case for the plaquette Ising model in a transverse magnetic field. At this point it is tempting to consider simple graph representations of the clusters, and sort the clusters into isomorphism classes based on these representations.

As an example consider that we represent each plaquette by a vertex, and join two vertices by an edge whenever these bonds share one or more sites. Furthermore, we assign colors to these edges in order to take into account that two overlapping plaquettes can share one or two sites. This representation does not correctly distinguish the clusters. An example for two clusters which are not correctly classified is given in Fig. 3.10, where two structurally distinct clusters - note that they have different numbers of sites - lead to the same naive graph representation, but to different König representations. Of course at this point one could start to improve on the mapping until it successfully distinguishes the clusters. However, then the question arises at which point we can be sure, that the given mapping discriminates clusters correctly and whether we artificially distinguish clusters which have equivalent structure. It is clear that the approach with the König and the

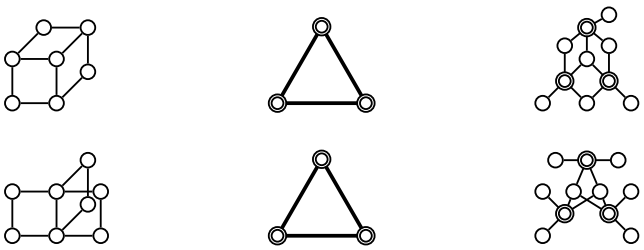

Figure 3.10: In the left column two clusters consisting of three plaquette bonds which are erroneously classified as isomorphic by the naive mapping which is given in the central column. In the central column the plaquettes are represented by double circles. These are connected by edges if the corresponding plaquettes have common sites. Here overlapping plaquettes always share two sites which we represent by thick black edges. The resulting graphs in the central column are isomorphic, but the clusters on the left side are obviously not. In contrast, the graphs in the right column are the König representations of the clusters which successfully distinguish the non-isomorphic clusters. This figure has been redesigned from Ref. [130].

reduced König representation has some calculational overhead compared to a simple mapping and simple mappings which avoid this overhead are expected to be more efficient. However, the König representation incorporates the entire structural information of a cluster in the presented setup into a representing graph. Here we have undirected interactions as the elementary perturbation acts equivalently on all four sites within a plaquette. This means that we do not have to distinguish different roles of the sites within a single plaquette. In a calculation of the ground-state energy the local states on all sites are equivalent, so we do not need to further distinguish the sites in the graph representation. For this scenario we list the isomorphism classes of clusters and the corresponding König representations up to three plaquettes in Figs. 3.11 and 3.12. The figures also illustrate that removing the vertices which correspond to sites which are contained in only a single plaquette, leads to a much simpler representation. Typically, this also leads to significant reduction of the symmetries of the graph representation, which is helpful in the next step, when we need to determine the embedding factors (per plaquette).

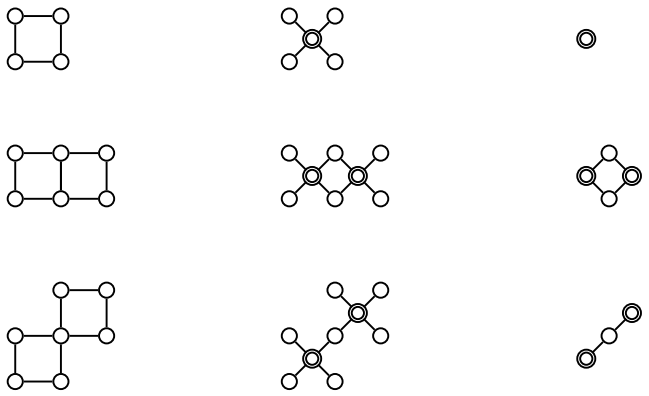

Figure 3.11: Isomorphism classes of connected clusters with two bonds (plaquettes) for a calculation of the ground-state energy in the high-field limit of the TFPIM. In the left column a representative cluster is given. The corresponding König representation is given in the central column. The double circles illustrate vertices which represent bonds (plaquettes) of the original cluster, while the single circles illustrate vertices which represent sites of the original cluster. The reduced König representation is illustrated in the right column. It is obtained by omitting the vertices of degree one which represent sites and the edges adjacent to these vertices. This figure has been redrawn from Ref. [130].

3.7.3 Embedding factors

From the cluster generation we obtain all subclusters which contain a given plaquette p_0 of the cubic lattice. While we sort these clusters into isomorphism classes, we keep track of the embedding factors. The simplest way of calculating the embedding factor is to count the instances of the isomorphism class and divide by the number of plaquettes of the isomorphism class under investigation. However, one can reduce the calculational effort by employing a simple condition for the vertex v_0 which represents p_0 within the reduced König representation of a subcluster. For example, we can request that v_0 has the maximum degree among all vertices representing plaquettes in the reduced König representation. All the subclusters which do not fulfill this condition are not counted towards the embedding factor and not sorted into isomorphism classes, saving lots of explicit isomorphism checks. Obviously, at this stage the embedding factor is overcounted. For a given isomorphism class, this can be corrected dividing by the number of bond vertices in the respective subcluster which fulfill the employed condition. Though, typically at this stage we do not correct the embedding factors, and use this heuristic approach only as a prefiltering.

Instead, for a given isomorphism class of subclusters we usually count only the instances where the plaquette p_0 is in an equivalent position within the considered subcluster, and then divide by the number of plaquettes in the subcluster which are structurally indistinguishable from p_0. This canonical position of p_0 within the subclusters of an isomorphism class, is determined by the first instance which is counted for the respective class. This instance has also passed the prefiltering stage, and thus the canonical position is compatible with the condition imposed in the prefiltering.

In the end, for the subclusters counted towards the embedding factor of a given isomorphism class, the vertex v_0 is in equivalent automorphism orbits of the reduced König representations. The

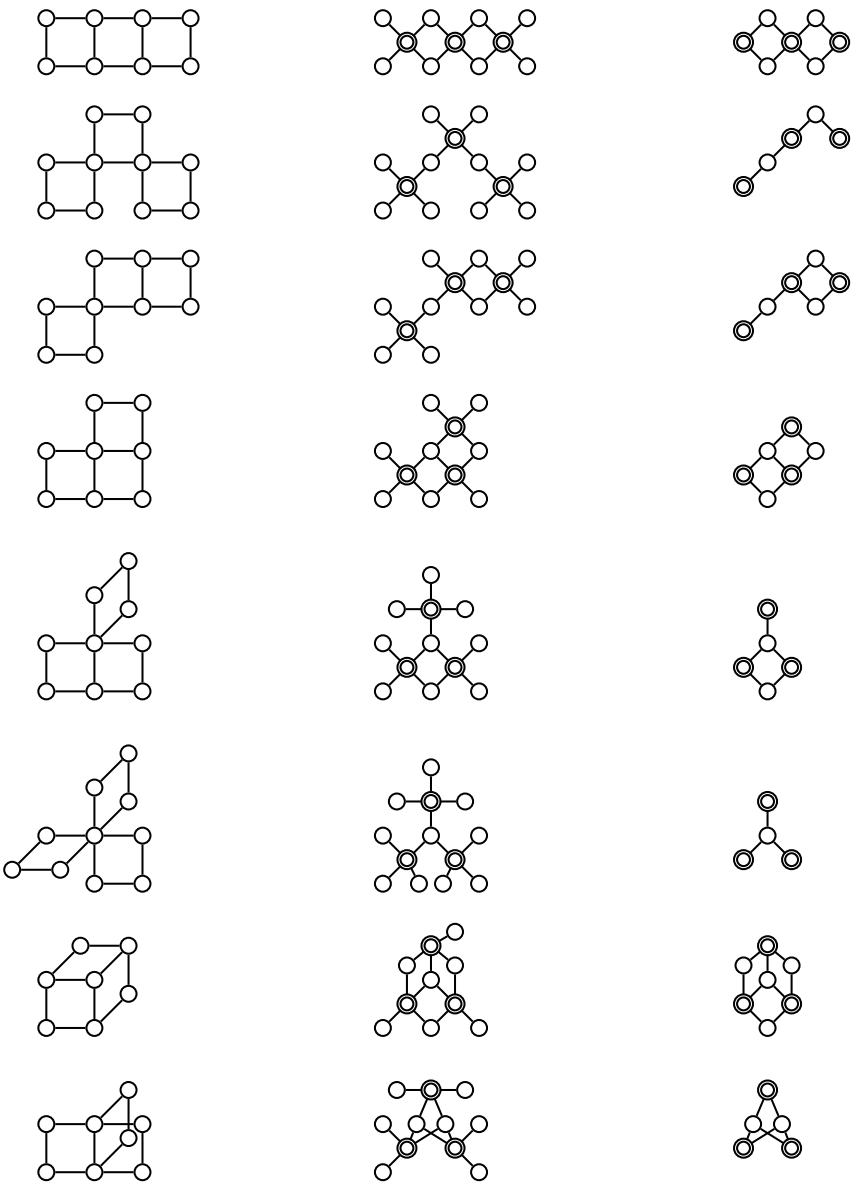

Figure 3.12: Isomorphism classes of connected clusters with three bonds (plaquettes) for a calculation of the ground-state energy in the high-field limit of the TFPIM. In the left column the connected clusters with three plaquettes are illustrated. In the central column the König representation is shown, and in the right column the reduced König representation is illustrated. This figure has been redrawn from Ref. [130].

embedding factor per plaquette is then obtained dividing the number of counted subclusters by the size of the respective automorphism orbit of v_0 in the reduced König representation. Conceptually, this is very similar to fixing a vertex in the monomorphisms from a graph to the lattice graph and dividing by the number of automorphisms of the graph as done in conventional LCEs [96, 97].

Let us consider the second line in Fig. 3.11 as an example. The cluster generation finds all twelve subclusters which belong to this isomorphism class and contain the plaquette p_0. Consider one of these subclusters, and call the other plaquette in this subcluster p_1. Clearly, p_0 and p_1 are structurally indistinguishable within the subcluster. Obviously, this subcluster also belongs to the twelve subclusters within the isomorphism class which contain the plaquette p_1. So, in a sense the two plaquettes share the subcluster, and hence, the embedding factor of the isomorphism class per plaquette is equal to six. Next, consider the first line in Fig. 3.12 as another example. Also here

Figure 3.13: Two clusters of the same isomorphism class (first line) with their reduced König representation (second line). Structurally equivalent plaquettes within a cluster are given in the same color as well as bond vertices which are in the same or equivalent automorphism orbits of the reduced König representation. For this concrete example p_0 can be in the center (orange) or on one of the outer plaquettes (blue). On the structural level the outer plaquettes are indistinguishable, and the respective vertices of the reduced König representations are in equivalent orbits (blue).

the cluster generation scheme will provide all clusters in this isomorphism class which contain the plaquette p_0. There are 54 such clusters, 18 where p_0 corresponds to the central plaquette and 36 where p_0 corresponds to one of the outer plaquettes. Within the cluster the central plaquette is structurally distinguishable from the other two plaquettes (see Fig. 3.13). In the reduced König representation the automorphism orbit of the corresponding vertex is trivial. If we only consider the subclusters, where p_0 is in the central position, we can just count them and we obtain the correct embedding factor per plaquette. If instead, we require p_0 to be one of the outer plaquettes, the embedding factor obtained by just counting all subclusters of this isomorphism class (where p_0 is on one of the outer plaquettes) has to be corrected dividing by a factor of two, to correct for the fact that the outer plaquettes are indistinguishable on the structural level. For any counted subcluster the other outer plaquette corresponds to another plaquette in the cubic lattice. Accordingly, the subcluster is not only associated to the plaquette p_0 but also to this other plaquette, which explains the factor of two.

3.7.4 Identifying non-contributing clusters

For this model we can apply the selection rules given in Subsect. 3.6.4, which are based on the vertices of odd degree which represent sites in the König representation of the cluster. We refer to such sites as sites of odd degree or odd-degree sites. The main idea behind all these techniques is that $\mathcal{V}_b$ just flips the eigenvalues of all spin degrees of freedom in the bond b. In particular it maps the unperturbed local ground state to an unperturbed local excited state and vice versa on all sites in the respective bond. So the elementary perturbation has to act an even amount of times on any site to obtain the same local state again. However, in perturbative processes contributing to the reduced contribution of a given cluster the elementary perturbation has to act at least once on every bond in the cluster. The local ground state on a site of odd degree cannot be restored, if the perturbation acts once on every bond. Instead, any site of odd degree requires that the perturbation acts twice on at least one bond which contains this site. However, for the present problem, four sites of odd degree can be in the same bond, and hence, this requirement can be fulfilled for four sites, with one additional action of the elementary perturbation. In this subsection we consider the isomorphism class of clusters illustrated in the first line of Fig. 3.12. In the following we go through the selection rules and determine in which order the cluster can contribute according to these rules.

Counting sites of odd degree

First we check the selection rule given in Eq. (3.166). We count four vertices in the vertex part of the König representation which have odd degree. The cluster contains three plaquettes, and the maximum cardinality of bonds in the system is four as all plaquettes contain four sites. So according to the selection rule, the clusters from this isomorphism class and all clusters obtained by adding further bonds to such clusters contribute in order four or higher. Note that for some subclusters of this class, it is possible to add a bond linking the four sites of odd degree. This results in a cluster without any site of odd degree as illustrated in Fig. 3.14.

Figure 3.14: Adding a single plaquette to the cluster on the left, results in a cluster where any site is contained in an even number of bonds (right). The newly added plaquette is highlighted by thick red lines.

Covering sites of odd degree

The previous selection rule was based on the isomorphism class and did not exploit properties of the actual subcluster. To this end consider the two different realizations of a cluster from this isomorphism class within the cubic lattice given in Fig. 3.15. In this example the cluster which consists of three plaquettes, all oriented in the same way (see left part of Fig. 3.15), can not be turned into a cluster which has no sites of odd degree by adding a single plaquette from the cubic

Figure 3.15: Two clusters from the same isomorphism class. Consider these clusters inside a cubic lattice. For the left cluster we cannot get rid of the sites of odd degree by adding one plaquette of the surrounding cubic lattice, while for the right one this is certainly possible.

lattice. Instead, for the cluster which is bent (see right part of Fig. 3.15) this is definitely possible. We try to formalize this idea by calculating which sites within the entire system do share a common bond and which do not. We then build an auxiliary graph, where any site of odd degree within the cluster is represented by a vertex. Two vertices in this auxiliary graph are joined by an edge if and only if the corresponding sites do not share any bond in the entire system. Note, that by entire system we mean the full lattice, or the finite cluster which we use instead of the full lattice, respectively. We show these auxiliary graphs for the clusters from Fig. 3.15 in Fig. 3.16. The idea

Figure 3.16: The two auxiliary graphs (opaque) for the clusters (low opacity) in Fig. 3.15. The vertices of the auxiliary graph represent the sites of odd degree from the respective clusters. In the auxiliary graph two vertices are joined by an (opaque) edge if and only if the respective sites are not contained in the same bond within the the cubic lattice. The colors of the vertices of the auxiliary graph correspond to a feasible graph coloring with as few colors as possible. Accordingly, the number of different vertex colors within each auxiliary graph corresponds to the chromatic number of the respective graph.

is that odd-degree sites which are not contained in the same bond (within the full system), can not be joined by adding a single bond (of the full system) to the subcluster. Note that by considering all the bonds of the system, we also allow to duplicate a bond which is contained in the subcluster.

This is then translated into a graph coloring problem (see Subsect. 2.1.3). Here, the sites of odd degree which must be in different bonds are represented by adjacent vertices of the auxiliary graph, and a lower bound on the number of bonds needed to cover the sites of odd degree is given by the chromatic number of this auxiliary graph.

In Fig. 3.16 the chromatic number of the left graph equals two, whereas it is one for the right graph. This gives a lower bound for the numbers of bonds which need to be added to the cluster or duplicated within the cluster such that all sites of odd degree are contained in at least one of these bonds. In the present case, two bonds need to be duplicated in the left cluster in Fig. 3.15, as the odd-degree sites are not contained in a single bond of the cubic lattice. Instead, in the right cluster in the same figure all the four sites of odd degree are contained in one bond of the cubic lattice. After adding this bond the four sites of odd degree have even degree. So we find that the left cluster

in Fig. 3.15 (and all clusters including it) can only have a non-vanishing reduced contribution in perturbation order five or higher, whereas the right cluster in Fig. 3.15 (and all subclusters including it) may already have a non-vanishing reduced contribution in order four. For the left cluster we also observe that sites of odd degree remain, after adding or duplicating two bonds. This could actually be an interesting direction to improve on this selection rule.

Duplicating bonds

Lastly, we apply the selection rule given in Eq. (3.167). We consider again the sites of odd degree in a cluster of the equivalence class under investigation. In order to get rid of odd-degree sites, we duplicate bonds within the cluster which contain these sites. So we definitely need to duplicate the two outer bonds, which contain the sites of odd degree. However, after these bonds are duplicated, the four sites in the center have degree three. This can be resolved by duplicating the central plaquette as well. The duplication of the plaquettes is illustrated in Fig. 3.17. In total we need to duplicate three plaquettes and hence we conclude that any cluster of this isomorphism class can contribute only in order six or higher. In contrast to the two selection rules considered before, here we do not make any statement about clusters obtained by adding further bonds to a cluster of this class.

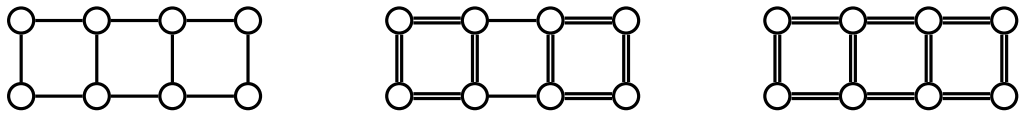

Figure 3.17: The image illustrates the duplication of the plaquettes as described in the main text.

Calculating hopping elements

The main difference in the calculation of the hopping elements $\langle\Phi| H_{\text{eff}} - E_0 |\Psi\rangle$ with respect to product states $|\Psi\rangle$ and $|\Phi\rangle$ is that we incorporate the local states $|\Psi_i\rangle$ and $|\Phi_i\rangle$ of the sites of the subclusters within the hypergraph representation. Equivalence of subclusters corresponds to color preserving isomorphism of these hypergraphs. If $|\Phi\rangle \neq |\Psi\rangle$ the subclusters to be considered need to contain all sites i where the local states differ, i.e., $|\Psi_i\rangle \neq |\Phi_i\rangle$. If instead $|\Psi\rangle = |\Phi\rangle$, they must contain at least one site which is occupied. Otherwise the reduced contribution of the subcluster to the matrix element $\langle\Phi| H_{\text{eff}} - E_0 |\Psi\rangle$ vanishes. The embedding factors of the classes just correspond to the number of subclusters which belong to the respective class. The selection rules can be adapted by observing that a site of odd degree with $|\Phi_i\rangle \neq |\Psi_i\rangle$ does not require the perturbation to act at least twice on an adjacent bond. A simple approach is to only consider sites of odd degree for which $|\Psi_i\rangle = |\Phi_i\rangle = |0\rangle$ to be relevant for the selection rules. The other sites of odd degree are treated within the selection rule as if they had even degree.

3.7.5 Results

Using a hypergraph decomposition and evaluating the reduced contributions of the considered clusters with Löwdin's method [201, 205] (explained in Subsect. 3.4.3) one obtains [130]

$$\begin{aligned} e_0 = &-\frac{1}{3}-\frac{\lambda^2}{8}-\frac{113\lambda^4}{1536}-\frac{21427\lambda^6}{163840}-\frac{87959384893\lambda^8}{254803968000} \\ &-\frac{1151818046218646 39\lambda^{10}}{102736959897600000} \\ &-\frac{1199864820008961969940451\lambda^{12}}{28996479561498624000000 0}\,, \end{aligned} \tag{3.170}$$

for the ground-state energy per plaquette. The excitation gap of two adjacent spin flips Δ_2 is located at $\vec{k}=0$, and one obtains [130]

$$\begin{aligned} \Delta_2 =&4-4\lambda-3\lambda^2-\frac{17\lambda^3}{8}-\frac{1151\lambda^4}{192}-\frac{37165\lambda^5}{9216} \\ &-\frac{2591423\lambda^6}{122880}-\frac{6264944713\lambda^7}{530841600} \\ &-\frac{5707377242657\lambda^8}{63700992000}-\frac{2114517232207\lambda^9}{53084160000} \\ &-\frac{2169534326790862117\lambda^{10}}{5136847994880000}\,, \end{aligned} \tag{3.171}$$

using the method of perturbative continuous transformations [103, 120] explained in Subsect. 3.4.1 to determine the reduced contributions of the considered clusters to the relevant hopping elements. The reduced contributions to both, the ground-state energy and the relevant hopping elements, have been evaluated using a bookkeeping technique [123, 130]. Note that two adjacent spin flips correspond to a quasiparticle which can only move within a plane [27, 39, 221, 222]. The dispersion of this excitation is obtained by calculating all necessary irreducible hopping elements $t_{\vec{\delta}}$ of this quasiparticle in the plane, and summing them up weighted with the appropriate phase factors $\exp(-\mathrm{i}\vec{k}\vec{\delta})$ as described in Subsect. 3.3.3. After appropriate rearrangements the obtained results agree with the series expansions from Ref. [39] up to the orders available in this reference.

Chapter 4

Incorporating anyonic statistics into a linked-cluster expansion

This chapter is taken, in large parts verbatim, from Ref. [23] including images, tables and captions. Still, we incorporated some changes and rearrangements where we found this appropriate.

In this chapter we describe how to set up a hypergraph decomposition in the topological phase of Kitaev's toric code [18] in a field. Kitaev's toric code represents an exactly solvable model, which realizes a non-trivial topological phase with a highly entangled ground state and Abelian anyons as elementary excitations. As a consequence, it has been an attractive starting point for many investigations to understand the physical properties of topologically ordered quantum matter, e.g., the effect of external perturbations and the properties of induced quantum phase transitions [33–36, 223–230], the consequences of thermal fluctuations [231–233], the properties of entanglement measures [234, 235] or dynamical correlation functions [37] as well as non-equilibrium properties [236, 237].

One prominent method which has been applied successfully to determine the quantum-critical properties of the 2D toric code in the presence of a uniform magnetic field [33,35,226,238] are high-order series expansions applying the method of perturbative continuous unitary transformations [103, 120]. In these works the excitation energies of elementary charges and fluxes have been calculated as a series in the low-field limit. The non-local effects of the braiding statistics have been taken into account in a post-processing procedure by correctly incorporating the winding of charges around fluxes (or vice versa). This has been done with large clusters but also with Enting's finite-lattice method [121,239], in order to define particle strings in a fixed gauge-invariant way so that the particle as well as the relevant fluctuations are both present on each cluster.

In this chapter, we explain how to adapt the formalism of hypergraph expansions [130] presented in Sect. 3.6 to calculate series expansions for the ground-state energy and irreducible one-quasiparticle matrix elements in the low-field topological phase of the toric code in a homogeneous magnetic field. For this problem, a particular challenge of such a hypergraph decomposition is to take the non-local mutual anyonic statistics of the excitations into account. How this can be done on large clusters, or with Enting's finite-lattice method [121,239], is explained in the literature [238] where high-order series expansions in this phase have been derived [33, 35, 226, 238]. Still, to the best of our knowledge, we are the first to apply a full hypergraph decomposition for this model [23].

Although we only achieve a slight extension of the previously known series expansions, the main merit of Ref. [23] and this chapter is the formulation of a full graph decomposition which correctly takes into account the exotic mutual statistics.

4.1 Kitaev's toric code in a field

We investigate the perturbed topological phase of the toric code in a uniform field. The Hamiltonian of this model is therefore the sum of the toric code H^{tc} and a general uniform magnetic field

$$H^{\mathrm{tcf}} = H^{\mathrm{tc}} - \sum_i \vec{h} \cdot \vec{\sigma}_i, \tag{4.1}$$

where $\vec{h} = (h_x, h_y, h_z)^T \in \mathbb{R}^3$ and $\vec{\sigma} = (\sigma^x, \sigma^y, \sigma^z)^T$. In contrast to the bare toric code described in Subsect. 4.1.1, this model is not exactly solvable and displays a rich quantum phase diagram [35]. For the special case of a magnetic field pointing in x- or z-direction the model is isospectral to the well-known transverse field Ising model on the dual square lattice in the relevant low-energy sector [223, 224] displaying a second-order quantum phase transition in the 3D Ising universality class. The quantum phase diagram of the toric code in a magnetic field in the xz-plane is obtained with series expansion methods [33], quantum Monte Carlo simulations [34, 36], and tensor networks [227]. Notably, the universality class of the quantum phase transition remains 3D Ising except for the symmetric case $h_x = h_z$ where a multicritical point is expected [33–35]. In contrast, for a magnetic field pointing in transverse y-direction, the model is dual to the Xu-Moore model [240] as well as to the quantum compass model [241] and the nature of the phase transition is strongly first order [226]. The full extent of the topological phase in the presence of a general uniform magnetic field has been determined by combining high-order series expansions and tensor network algorithms [35] displaying rich physical behavior depending on the magnetic field direction. This includes planes of first- and second-order quantum phase transitions as well as multicritical lines.

In this work we focus on the perturbed topological phase at finite fields and we describe how to set up high-order series expansions. Consequently, we describe the non-trivial unperturbed limit $\vec{h} = 0$ of the bare toric code next.

4.1.1 Kitaev's toric code

Kitaev's toric code is defined on a square lattice with spin-$1/2$ degrees of freedom on the edges of the lattice [18]. The Hamiltonian is given by

$$H^{\mathrm{tc}} = -\frac{1}{2}\sum_{+} X_{+} - \frac{1}{2}\sum_{\square} Z_{\square}\,. \tag{4.2}$$

The star operators X_{+} and the plaquette operators $Z_{\square}$ are both defined as products of four Pauli matrices

$$X_{+} = \prod_{i\in+} \sigma_i^x, \qquad\qquad Z_{\square} = \prod_{i\in\square} \sigma_i^z\,, \tag{4.3}$$

where σ_i^x, σ_i^z are the usual Pauli matrices. The first product runs over the four sites surrounding a vertex, the second one over the four sites at the edges of a plaquette as illustrated in Fig. 4.1.

As these stabilizer operators are products of Pauli matrices their eigenvalues $x_{✚}, z_{□}$ are equal to ± 1 [18]. Furthermore, all these operators commute mutually

$$\begin{aligned} [X_{✚}, X_{✚'}] &= 0 \quad \forall ✚, ✚', \\ [X_{✚}, Z_{□}] &= 0 \quad \forall ✚, □\,, \\ [Z_{□}, Z_{□'}] &= 0 \quad \forall □, □'\,. \end{aligned} \tag{4.4}$$

As a consequence, one can construct a state where all eigenvalues $x_{✚}, z_{□}$ are equal to $+1$, which corresponds to a ground state

$$|\mathrm{GS}\rangle = \mathcal{N} \prod_{✚} (1 + X_{✚}) \prod_{□} (1 + Z_{□}) \, |\mathrm{ref}\rangle \,, \tag{4.5}$$

where $\mathcal{N}$ is a normalization factor and $|\mathrm{ref}\rangle$ is a reference states. This reference state has to be chosen such that it is not orthogonal to the ground-state space. For example, the states $|\Uparrow\rangle$ or $|\Rightarrow\rangle$, where all spins point in positive z- or x-direction can be used. The ground state $|\mathrm{GS}\rangle$ is unique on an open plane. However, the ground-state manifold features a non-trivial topological degeneracy which equals 4^g on a compact orientable surface of genus g indicating topological order [18]. Importantly, all operators $X_{✚}$ and $Z_{□}$ act trivially on the ground state. Furthermore, any contractible loop of σ^x or σ^z matrices is equal to the product of operators $X_{✚}$ or $Z_{□}$ contained in the loop respectively [18]. The ground-state energy is given by $E_0^{\mathrm{tc}} = -N/2$ with N the number of spins which equals the total number of plaquettes and stars.

Acting with σ_i^x (σ_i^z) on site i of the ground state creates two flux (charge) excitations corresponding to $z_{□} = -1$ ($x_{✚} = -1$) adjacent to site i. These topological excitations are located at the plaquettes (vertices) of the lattice and behave like hardcore bosons with a mutual anyonic statistics [18, 35, 37]. More generally, acting with string operators

$$S_z = \prod_{i \in p} \sigma_i^z, \qquad S_x = \prod_{i \in \bar{p}} \sigma_i^x, \tag{4.6}$$

on the ground state, where p ($\bar{p}$) are open paths on the (dual) lattice, creates two excitations at the end of the respective path [18]. Examples for two such operators are illustrated in the right panel of Fig. 4.1. Note that it is not possible to have an odd number of excitations on the torus [18]. However, on an open plane, one can create a pair of excitations and move one of them to infinity [33, 35]. A single charge $x_{✚} = -1$ at position $\vec{r}$ is denoted by the state $|\vec{r}, ✚\rangle$. This state is uniquely defined up to the concrete operator which creates the excitation from the ground state. In order to define such an excited state unambiguously we define it by a sequence of Pauli operators acting on the reference ground state $|\mathrm{GS}\rangle$

$$|\vec{r}, ✚\rangle = \prod_{i \in p_{\vec{r}}} \sigma_i^z \, |\mathrm{GS}\rangle \,, \tag{4.7}$$

where $p_{\vec{r}}$ is a straight open path which goes from the excitation to infinity in negative x-direction as illustrated in the left panel of Fig. 4.2. This way we fixed the gauge freedom to define these states uniquely. In the following we call these states *canonical one-charge states*. In the same fashion one can define *canonical one-flux states*

$$|\vec{r}, □\rangle = \prod_{i \in \bar{p}_{\vec{r}}} \sigma_i^x \, |\mathrm{GS}\rangle \,, \tag{4.8}$$

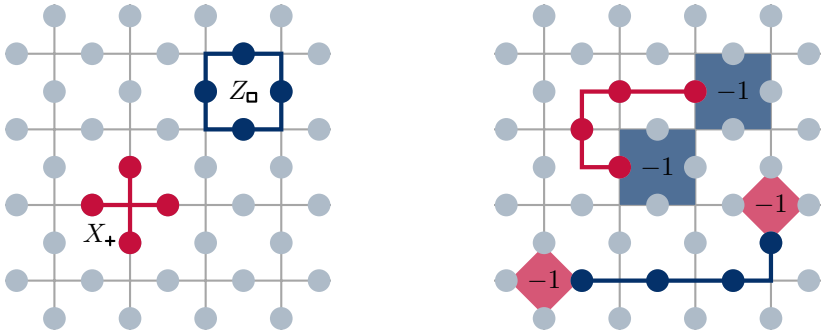

Figure 4.1: *L*eft: The spin-1/2 degrees of freedom are depicted in light blue at the edges of the square lattice. The operators X_+ and $Z_\square$ are illustrated in red or blue respectively. Blue (red) circles indicate that the illustrated operator acts with σ^z (σ^x) on the respective spin. *R*ight: Two examples for string operators of the type S_x (S_z) in red (blue). Actions of σ^x (σ^z) on spin degrees of freedom are represented by red (blue) circles. The flux (charge) excitations at the end of the string operator S_x (S_z) are illustrated as blue (red) squares labeled with -1 indicating the negative eigenvalue $z_\square$ (x_+) of $Z_\square$ (X_+). This image is taken from Ref. [23].

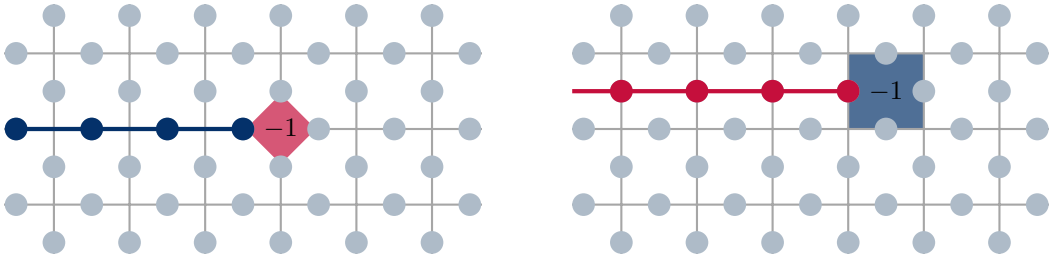

Figure 4.2: Canonical one-particle states. *Left*: A single charge excitation is obtained by creating two charges from the ground state and moving one to infinity. This procedure results in a semi-infinite string attached to the charge (indicated in blue). *Right*: A single flux excitation is obtained by creating two fluxes from the ground state and moving one to infinity. This procedure results in a semi-infinite string attached to the flux (indicated in red). This image is taken from Ref. [23].

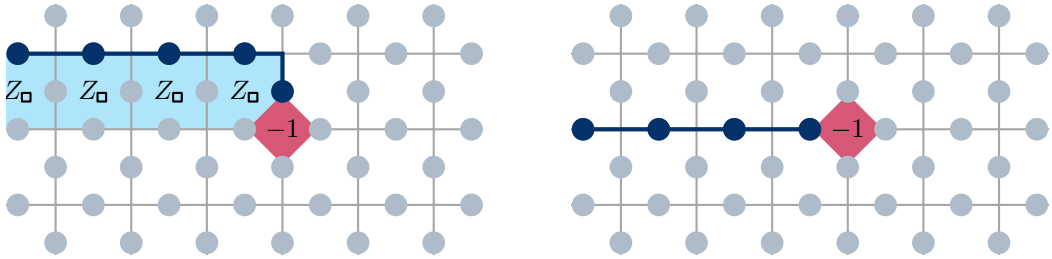

Figure 4.3: The left figure illustrates a non-canonical one-charge state. The product of a contractible loop operator of σ^z with a non-canonical string operator (left) is equal to a canonical string operator (right). Recall that a contractible loop of σ^z is equivalent to a product of operators $Z_\square$. This image is taken from Ref. [23].

where $\bar{p}_{\vec{r}}$ is a straight open path on the dual lattice which is going straight into negative x-direction from the position $\vec{r}$ of the flux excitation to infinity as illustrated in the right panel of Fig. 4.2. We stress that non-canonical one-particle states with a different string can always be transformed into canonical states by exploiting

$$Z_\square \left|\mathrm{GS}\right\rangle = X_+ \left|\mathrm{GS}\right\rangle = \left|\mathrm{GS}\right\rangle \qquad \forall \square, + . \tag{4.9}$$

For a non-canonical one-charge state obtained by acting with σ_i^z along an open path $l_{\vec{r}} \neq p_{\vec{r}}$ from infinity to $\vec{r}$ this can be achieved in the following way

$$\prod_{i\in l_{\vec{r}}} \sigma_i^z \left|\mathrm{GS}\right\rangle = \prod_{i\in l_{\vec{r}}} \sigma_i^z \prod_{\square\in\Gamma_z} Z_\square \left|\mathrm{GS}\right\rangle = \prod_{i\in p_{\vec{r}}} \sigma_i^z \left|\mathrm{GS}\right\rangle = \left|\vec{r},+\right\rangle , \tag{4.10}$$

where Γ_z is chosen such that

$$\prod_{i\in l_{\vec{r}}} \sigma_i^z \prod_{\square\in\Gamma_z} Z_\square = \prod_{i\in p_{\vec{r}}} \sigma_i^z . \tag{4.11}$$

One specific example is illustrated for the case of a one-charge state in Fig. 4.3. The analogue procedure can be done for one-flux states.

More generally, applying the same procedure and conventions, one can generate multi-particle states with an arbitrary number of charges and fluxes. This can be done by successively acting with the corresponding (canonical) string operators on the ground state $\left|\mathrm{GS}\right\rangle$. The concept of canonical one- and multi-particle states including a description how non-canonical states can be transformed to canonical states is described in Ref. [238].

Next, we introduce a specific representation of these canonical multi-particle basis states which is convenient for high-order series expansions discussed in the following sections. To this end we consider as reference states $\left|\mathrm{ref}\right\rangle$ the fully polarized states $\left|\Uparrow\right\rangle$ and $\left|\Rightarrow\right\rangle$ in z- and x-direction, respectively. Once the reference state is chosen, all canonical states are uniquely defined including the overall phase. Let us consider an arbitrary multi-particle state with energy

$$E^{\mathrm{tc}}(\{x_+\},\{z_\square\}) = -\frac{1}{2}\sum_+ x_+ - \frac{1}{2}\sum_\square z_\square \tag{4.12}$$

only depending on the eigenvalues of plaquettes and stars. In our construction these states can be written as the product of $\prod_+(1\pm X_+)\prod_\square(1\pm Z_\square)$ and the action of string operators (for each

particle one) on the reference state $|\text{ref}\rangle$. The second part of this product corresponds to a spin product state which we call spin background. It can be described by the set of spin eigenvalues $\{s_i\}$ with $s_i \in \{\pm 1\}$ on all sites i. For the specific case of a two-particle state with one charge and one flux, one has

$$\begin{aligned} |\vec{r}_{1,+}, \vec{r}_{2,\square}\rangle &= \prod_{i \in p_{\vec{r}_1}} \sigma_i^z \prod_{i \in \bar{p}_{\vec{r}_2}} \sigma_i^x |\text{GS}\rangle \,, \\ &= \mathcal{N} \left(\prod_{+ \neq +_1} (1 + X_+)(1 - X_{+_1}) \prod_{\square \neq \square_2} (1 + Z_\square)(1 - Z_{\square_2}) \right) \left(\prod_{i \in p_{\vec{r}_1}} \sigma_i^z \prod_{i \in \bar{p}_{\vec{r}_2}} \sigma_i^x |\text{ref}\rangle \right) \\ &\equiv |\{x_+\}, \{z_\square\}, \{s_i\}\rangle \end{aligned} \tag{4.13}$$

where $+_1$ is the star at position $\vec{r}_1$, $\square_2$ is the plaquette located at $\vec{r}_2$, and $\prod_{i \in p_{\vec{r}_1}} \sigma_i^z \prod_{i \in \bar{p}_{\vec{r}_2}} \sigma_i^x |\text{ref}\rangle$ is the spin background. In general, we keep track of the three sets $\{x_+\}$, $\{z_\square\}$, and $\{s_i\}$ of $\mathbb{Z}_2$ degrees of freedom. This way we over-parametrize the states. However, keeping track of the spin background and the positions of the particles is crucial to derive high-order series expansions in the low-field phase of the toric code in a general field [33]. As a consequence, the spin background will turn out to be useful in the next sections to treat the non-trivial statistics of charges and fluxes within the high-order series expansions.

4.2 Series expansions in the perturbed topological phase

Our goal is to describe a systematic way how to incorporate non-local anyonic statistics into a high-order series expansion exploiting a full graph decomposition considering the topological phase of the toric code as the unperturbed starting point. How high-order series expansions for arbitrary field directions can be derived using finite clusters is explained in [238], where also Enting's finite lattice method [121, 239] has been applied. Such series expansions have been applied successfully to the toric code in a field [33,35,226]. However, to the best of our knowledge no full graph decomposition has been performed for general field directions. In this section we review how to calculate the ground-state energy and one-quasiparticle excitation energies in the topological phase using perturbation theory about the low-field limit. To this end we consider perturbative calculations on finite clusters which are sufficiently large to contain the relevant physical properties in the thermodynamic limit [120–122]. The discussion of the full graph decomposition of the perturbed topological phase is then presented in Sect. 4.3.

4.2.1 Setup

We perform perturbative calculations about the limit $\vec{h} = 0$. We therefore take the canonical states $|\{x_+\}, \{z_\square\}, \{s_i\}\rangle$ with energy $E^{\text{tc}}(\{x_+\}, \{z_\square\})$ as unperturbed basis (see Subsect. 4.1.1 for details). We stress again that the unperturbed energies of these basis states do not depend on the spin background $\{s_i\}$. The perturbation $\mathcal{V} \equiv -\sum_i \vec{h} \cdot \vec{\sigma}_i$ is a sum over local terms acting on individual sites i. Locally, besides the obvious action on the spin at site i, the Pauli matrix σ_i^x (σ_i^z) flips the two eigenvalues $z_\square$ (x_+) attached to site i while the Pauli matrix σ_i^y flips all four eigenvalues of star and plaquette operators containing site i. We can therefore split the perturbation $\mathcal{V}$ as follows

$$\mathcal{V} = \mathcal{T}_0 + \mathcal{T}_{-2} + \mathcal{T}_{+2} + \mathcal{T}_{-4} + \mathcal{T}_{+4} \tag{4.14}$$

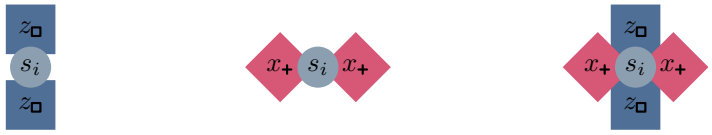

$b^{(x)}$ $b^{(z)}$ $b^{(y)}$

Figure 4.4: An illustration of the three different bond types $b^{(\alpha)}$ with $\alpha \in \{x, y, z\}$. These bonds contain the charge and flux sites which are affected by the action of Pauli matrices σ_i^x, σ_i^z and σ_i^y as well as the respective spin site i. This image is taken from Ref. [23].

so that $[H^{\text{tc}}, \mathcal{T}_n] = n\mathcal{T}_n$ and n corresponding to the net change of the total charge and flux particle number due to the action of $\mathcal{T}_n$. Consequently, at finite fields, the system becomes a challenging quantum many-body problem where the bare number of charges and fluxes is not conserved and the elementary charge and flux excitations gain a finite dispersion and interact.

The properties of the unperturbed toric code as well as the decomposition Eq. 4.14 meet all the requirements to apply the method of perturbative continuous transformation (pCUTs) [103, 120], which has been done in a series of works [33, 35, 226]. The pCUT method allows to map (4.1) to an effective quasiparticle number conserving Hamiltonian H_{eff} perturbatively exact up to the calculated order in the parameters h_x, h_y, and h_z. This effective Hamiltonian obeys $[H^{\text{tc}}, H_{\text{eff}}] = 0$, i.e., the effective Hamiltonian is block-diagonal and the quantum many-body problem reduces to a few-body problem in terms of dressed charge and flux excitations. Specifically, H_{eff} can be written as follows

$$H_{\text{eff}} = H^{\text{tc}} + \sum_{k=1}^{\infty} \sum_{\substack{|\mathbf{m}|=k,\\ M(\mathbf{m})=0}} C(\mathbf{m})\mathcal{T}(\mathbf{m}) \tag{4.15}$$

where $\mathbf{m} \equiv (m_1, \ldots, m_k)$ with $m_i \in \{0, \pm 2, \pm 4\}$, $\mathcal{T}(\mathbf{m}) = \mathcal{T}_{m_1}\mathcal{T}_{m_2}\mathcal{T}_{m_3}\ldots\mathcal{T}_{m_k}$ is a product of k operators $\mathcal{T}_n$ in order k perturbation theory, $M(\mathbf{m}) = \sum m_i$, and $C(\mathbf{m})$ are rational numbers. We highlight that the $C(\mathbf{m})$ are model independent and we refer to Ref. [103] for their calculation and values. In each perturbative order k one therefore has a weighted sum of quantum fluctuations described by the perturbative processes $\mathcal{T}(\mathbf{m})$, which are quasiparticle number conserving so that $M(\mathbf{m}) = 0$.

The $\mathcal{T}(\mathbf{m})$ and therefore the effective Hamiltonian (4.15) are not normal ordered so that physical properties can not be extracted directly. The normal ordering is most efficiently done by calculating matrix elements on finite clusters as only linked processes can have a non-vanishing contribution to these matrix elements. Indeed, if a finite cluster is sufficiently large so that all linked processes of a given perturbative order fit on this cluster for a specific matrix element, then this matrix element can be calculated and is directly valid in the thermodynamic limit. This therefore allows to obtain the normal-ordered form of the effective Hamiltonian.

The appearance of linked processes can be directly seen by introducing $\mathcal{T}_n = -\sum_{b^{(\alpha)}} h_\alpha T_{n,b^{(\alpha)}}$ where $T_{n,b^{(\alpha)}}$ acts on bonds $b^{(\alpha)}$ with $\alpha \in \{x, y, z\}$. These different bond types are illustrated in Fig. 4.4. The bond $b^{(\alpha)}$ contains the charge sites $+$, flux sites $\square$, and spin sites i on which the

operator $T_{n,b^{(\alpha)}}$ acts. For the three bonds containing the site i we can rewrite the σ_i^α as

$$\sigma_i^x = T_{-2,b^{(x)}} + T_{0,b^{(x)}} + T_{2,b^{(x)}} \,, \tag{4.16}$$

$$\sigma_i^y = T_{-4,b^{(y)}} + T_{-2,b^{(y)}} + T_{0,b^{(y)}} + T_{2,b^{(y)}} + T_{4,b^{(y)}} \,, \tag{4.17}$$

$$\sigma_i^z = T_{-2,b^{(z)}} + T_{0,b^{(z)}} + T_{2,b^{(z)}} \,. \tag{4.18}$$

As the relevant degrees of freedom of the unperturbed basis states $|\{x_{\square}\},\{z_{+}\},\{s_i\}\rangle$ are not only defined on the original sites i, but also on stars and plaquettes, we extend the term site to refer to original sites i but also to stars + and plaquettes □ from now on. These types of sites are termed spin sites, charge sites, and flux sites respectively. In this language any bond contains the spin site the charge sites and the flux sites on which the respective Pauli matrix acts. Note that it is important to distinguish the different types of sites within the bonds. Here it is necessary to distinguish spin sites from flux and charge sites, as the operators act differently on them.

Accordingly, a bond $b^{(z)}$ ($b^{(x)}$) includes a spin site and the neighboring charge sites (flux sites), whereas a bond $b^{(y)}$ contains a spin site and the four neighboring charge and flux sites. The effective Hamiltonian can then be exactly rewritten as

$$H_{\text{eff}} = H^{\text{tc}} + \sum_{k\equiv k_x+k_y+k_z=1}^{\infty} (-1)^k \, h_x^{k_x} h_y^{k_y} h_z^{k_z} \sum_{|\mathbf{m}|=k, M(\mathbf{m})=0} C(\mathbf{m}) \sum_{\mathbf{b}} T(\mathbf{m},\mathbf{b}) \,, \tag{4.19}$$

where $\mathbf{b} = (b_1,\ldots,b_k)$ and $T(\mathbf{m},\mathbf{b}) = T_{m_1,b^{(\alpha_1)_1}} \ldots T_{m_k,b_k^{(\alpha_k)}}$.

In order to determine prefactors of the normal ordered quasiparticle number conserving operators in H_{eff} via the calculation of matrix elements, one has to evaluate

$$\langle\Psi|\, T_{m_1,b_1^{(\alpha_1)}} T_{m_2,b_2^{(\alpha_2)}} \ldots T_{m_k,b_k^{(\alpha_k)}} \,|\Phi\rangle \,, \tag{4.20}$$

where $|\Phi\rangle$ and $|\Psi\rangle$ are canonical states on sufficiently large clusters with the same number of quasiparticles. One therefore has to specify the action of the local operators $T_{n,b^{(\alpha)}}$ on the canonical states $|\{x_{+}\},\{z_{\square}\},\{s_i\}\rangle$.

We stress that the action on the spin background depends on the choice of the specific reference state $|\text{ref}\rangle$. As an example, we list in Tab. 4.1 the different processes taking the fully polarized state $|\Rightarrow\rangle$ as the reference state.

As outlined in Sect. 4.1, for the perturbed topological phase of the toric code in a field, one has to take care that scalar products are made with canonical states. States arising from the action of the operators $T_{n,b^{(\alpha)}}$ are not necessarily canonical. In the following subsections we discuss how to evaluate these scalar products properly for the ground-state energy and for one-quasiparticle states on a single large cluster. In principle, the scalar products for higher quasiparticle states are based on the same principles and are described in the literature [238].

4.2.2 Ground-state energy

Let us start the discussion for the ground-state energy E_0 by focusing on a single term of the effective Hamiltonian H_{eff} in order k perturbation theory. Ignoring prefactors in Eq.(4.19), this demands to calculate expectation values of the following form

$$\langle\text{GS}|\, T_{m_1,b_1^{(\alpha_1)}} T_{m_2,b_2^{(\alpha_2)}} \ldots T_{m_k,b_k^{(\alpha_k)}} \,|\text{GS}\rangle \,, \tag{4.21}$$

where $|\mathrm{GS}\rangle$ represents the unique ground state of the toric code on the chosen open cluster.

$\sigma_i^x = T_{2,b^{(x)}} + T_{0,b^{(x)}} + T_{-2,b^{(x)}}$			$\sigma_i^z = T_{2,b^{(z)}} + T_{0,b^{(z)}} + T_{-2,b^{(z)}}$		
$\|00;0\rangle$	$\rightarrow$	$\|11;0\rangle$	$\|00;0\rangle$	$\rightarrow$	$\|11;1\rangle$
$\|00;1\rangle$	$\rightarrow$	$-\|11;1\rangle$	$\|00;1\rangle$	$\rightarrow$	$\|11;0\rangle$
$\|01;0\rangle$	$\rightarrow$	$\|10;0\rangle$	$\|01;0\rangle$	$\rightarrow$	$\|10;1\rangle$
$\|01;1\rangle$	$\rightarrow$	$-\|10;1\rangle$	$\|01;1\rangle$	$\rightarrow$	$\|10;0\rangle$
$\|10;0\rangle$	$\rightarrow$	$\|01;0\rangle$	$\|10;0\rangle$	$\rightarrow$	$\|01;1\rangle$
$\|10;1\rangle$	$\rightarrow$	$-\|01;1\rangle$	$\|10;1\rangle$	$\rightarrow$	$\|01;0\rangle$
$\|11;1\rangle$	$\rightarrow$	$-\|00;1\rangle$	$\|11;1\rangle$	$\rightarrow$	$\|00;0\rangle$
$\|11;0\rangle$	$\rightarrow$	$\|00;0\rangle$	$\|11;0\rangle$	$\rightarrow$	$\|00;1\rangle$

Table 4.1: On the left the action of σ_i^x on the local state configuration $|\tilde{z}_{\square_1}, \tilde{z}_{\square_2}; \tilde{s}_i\rangle$ on a $b^{(x)}$-bond, which contains two plaquette operators and the background spin s_i. On the right the action of σ^z on the local state $|\tilde{x}_{+_1}, \tilde{x}_{+_2}; \tilde{s}_i\rangle$ on a $b^{(z)}$-bond type is given, which contains two star operators and the same background spin. The action on the spin-background variables s_i depends on the reference states $|\mathrm{ref}\rangle$. Here we have used the fully polarized states $|\Rightarrow\rangle$ in x-direction. The upper, middle, and lower line refer to the processes of $T_{2,b^{(\alpha)}}$, $T_{0,b^{(\alpha)}}$, and $T_{-2,b^{(\alpha)}}$ with $\alpha \in \{x, z\}$, respectively. For the sake of clarity we use Boolean values $\tilde{z}_{\square} = \frac{1}{2}(1 - z_{\square})$ and $\tilde{x}_{+} = \frac{1}{2}(1 - x_{+})$, which count the number of excitations at a given $+$ or $\square$ and for the background spins $\tilde{s}_i = \frac{1}{2}(1 - s_i)$. Furthermore, $\sigma^y = \mathrm{i}\sigma^x\sigma^z$ acts on the background spin s_i as well as on the four eigenvalues of the star and plaquette operators which surround the spin site i.

The successive action of the T-operators in Eq. (4.21) is properly treated on the state level by the processes listed in Tab. 4.1. Because the product of T-operators is quasiparticle number conserving, it can not create any excitations. Instead, the final state $|\mathrm{f}\rangle \equiv T_{m_1,b_1^{(\alpha_1)}} T_{m_2,b_2^{(\alpha_2)}} \ldots T_{m_k,b_k^{(\alpha_k)}} |\mathrm{GS}\rangle$ is either zero or is the ground state $|\mathrm{GS}\rangle$ with an additional phase factor $[i^{n_a}]$ with $n_a \in \{0, 1, 2, 3\}$ resulting from the action of the T-operators. One can explicitly write down the final state $|\mathrm{f}\rangle$ as

$$|\mathrm{f}\rangle = \mathcal{N} \prod_{+} (1 + X_{+}) \prod_{\square} (1 + Z_{\square})\ \sigma_{i_1}^{\alpha_1} \sigma_{i_2}^{\alpha_2} \ldots \sigma_{i_k}^{\alpha_k} |\mathrm{ref}\rangle\ . \tag{4.22}$$

The non-contributing sequences are easily identified, so we restrict the discussion to the contributing ones. For the explicit reference state $|\Rightarrow\rangle$, the action of $\sigma_{i_1}^{\alpha_1} \sigma_{i_2}^{\alpha_2} \ldots \sigma_{i_k}^{\alpha_k}$ on the reference state is given as

$$\sigma_{i_1}^{\alpha_1} \sigma_{i_2}^{\alpha_2} \ldots \sigma_{i_k}^{\alpha_k} |\Rightarrow\rangle = [\mathrm{i}^{n_a}]\, |s^x\rangle = [\mathrm{i}^{n_a}] \prod_{\square \in \Gamma_z} Z_{\square} |\Rightarrow\rangle\ , \tag{4.23}$$

$|s^x\rangle$ is a product state in the σ^x-basis and $[\mathrm{i}^{n_a}]$ with $n_a \in \{0, 1, 2, 3\}$ is the phase factor resulting from the action of the Pauli matrices, whereas Γ_z is a set of plaquettes such that

$$|s^x\rangle = \prod_{\square \in \Gamma_z} Z_{\square} |\Rightarrow\rangle\, . \tag{4.24}$$

Note that we are in the ground-state sector, so $|s^x\rangle$ can at most contain several contractible loops of flipped spins in the spin background, which can be replaced by a product of operators $Z_{\square}$. Inserting Eq. (4.23) into Eq. (4.22) yields

$$[\mathrm{i}^{n_a}] \cdot \mathcal{N} \prod_{\square \in \Gamma_z} Z_{\square} \prod_{+} (1 + X_{+}) \prod_{\square} (1 + Z_{\square}) \, |\Rightarrow\rangle = [\mathrm{i}^{n_a}] \prod_{\square \in \Gamma_z} Z_{\square} \, |\mathrm{GS}\rangle = [\mathrm{i}^{n_a}] \, |\mathrm{GS}\rangle \, . \tag{4.25}$$

Using the operators defined in Tab. 4.1 results exactly in the middle part of Eq. (4.25), i.e., they yield the result in terms of the state $\prod_{\square \in \Gamma_z} Z_{\square} \, |\mathrm{GS}\rangle$ and correctly include the additional phase $[\mathrm{i}^{n_a}]$ within the amplitude of this state.

Interestingly, the state $|\mathrm{f}\rangle$ can also be evaluated for an arbitrary reference state. To this end we sort the product of Pauli matrices in Eq. (4.22) by their flavor taking into account the non-trivial commutation relations. Note that Pauli matrices σ^y can always be written as $\mathrm{i}\sigma^x\sigma^z$. In the ground-state sector one can always write the obtained sorted expression as the product of contractible loops of σ^z or σ^x. Each contractible loop operator can be replaced exactly by the product of plaquette or star operators contained in the respective loop

$$\sigma_{i_1}^{\alpha_1} \sigma_{i_2}^{\alpha_2} \ldots \sigma_{i_k}^{\alpha_k} = [\mathrm{i}^{n_a}] \prod_{+ \in \Gamma_x} X_{+} \prod_{\square \in \Gamma_z} Z_{\square} \, . \tag{4.26}$$

Since any product of star and plaquette operators yields identity on any ground state, one directly gets the canonical ground state $|\mathrm{GS}\rangle$ with an additional phase factor $[\mathrm{i}^{n_a}]$ with $n_a \in \{0, 1, 2, 3\}$, which stems from the sorting of the Pauli matrices

$$[\mathrm{i}^{n_a}] \cdot \mathcal{N} \prod_{+ \in \Gamma_x} X_{+} \prod_{\square \in \Gamma_z} Z_{\square} \prod_{+} (1 + X_{+}) \prod_{\square} (1 + Z_{\square}) \, |\mathrm{ref}\rangle = [\mathrm{i}^{n_a}] \, |\mathrm{GS}\rangle \, . \tag{4.27}$$

So once the phase factor is determined, no post-processing is necessary in the ground-state sector and one has $\langle \mathrm{GS}| \, T_{m_1, b_1^{(\alpha_1)}} T_{m_2, b_2^{(\alpha_2)}} \ldots T_{m_k, b_k^{(\alpha_k)}} \, |\mathrm{GS}\rangle = [\mathrm{i}^{n_a}]$. With this the ground-state expectation value of all the perturbation terms in the effective Hamiltonian (4.19) can be evaluated, and thus the perturbative corrections to the ground-state energy are obtained.

4.2.3 One-quasiparticle energies

The one-quasiparticle sector of the effective Hamiltonian H_{eff} represents two one-particle problems: One for a single charge quasiparticle and one for a single flux quasiparticle. Both problems are exactly decoupled since the magnetic field does not contain any process transforming a charge into a flux or vice versa due to parity conservation of fluxes and charges. Furthermore, there is an exact self-duality in the toric code in a field so that charge and flux excitation energies are identical up to an interchange of h_x and h_z.

Let $|\vec{r}\rangle$ be either a canonical one-charge state $|\vec{r}, +\rangle$ or a canonical one-flux state $|\vec{r}, \square\rangle$. In real space one then has to calculate the one-particle hopping amplitudes $t_{\vec{\delta}}$ given by

$$t_{\vec{\delta}} = \langle \vec{r} + \vec{\delta}| \, H_{\mathrm{eff}} - E_0 \, |\vec{r}\rangle \, . \tag{4.28}$$

As in Subsect. 3.3.3, one can define corresponding one-quasiparticle states $|\vec{k}\rangle$ in Fourier space and write the one-particle dispersion of charges and fluxes

$$\omega(\vec{k}) \equiv \langle \vec{k}| \, H_{\mathrm{eff}} - E_0 \, |\vec{k}\rangle = \sum_{\vec{\delta}} t_{\vec{\delta}} \exp(-\mathrm{i}k\vec{\delta}) \, . \tag{4.29}$$

The minimum of this dispersion is called the one-particle gap Δ located at momentum $\vec{k} = 0$ for charges and fluxes. In the following we call the charge gap Δ^{+} and the flux gap $\Delta^{\square}$.

Next, we discuss how to evaluate the matrix elements $t_{\vec{\delta}}$. As in the calculation of the ground-state energy, we can focus on the contribution of a single perturbative term

$$\langle \vec{r}_2 | \, T_{m_1,b_1^{(\alpha_1)}} T_{m_2,b_2^{(\alpha_2)}} \dots T_{m_k,b_k^{(\alpha_k)}} \, | \vec{r}_1 \rangle \equiv \langle \vec{r}_2 | \mathrm{f} \rangle \tag{4.30}$$

to the hopping amplitude $t_{\vec{\delta}}$ with $\vec{r}_2 \equiv \vec{r}_1 + \vec{\delta}$. In order to evaluate the scalar product $\langle \vec{r}_2 | \mathrm{f} \rangle$, one has to express $|\mathrm{f}\rangle$ in terms of a canonical one-quasiparticle state along the lines discussed in Sect. 4.1. First, let us rewrite a canonical one-charge state as

$$|\vec{r}_1, +\rangle = \prod_{i \in p_{\vec{r}_1}} \sigma_i^z \, |\mathrm{GS}\rangle = \mathcal{N}(1 - X_{+_1}) \prod_{+ \neq +_1} (1 + X_+) \prod_{\square} (1 + Z_\square) \prod_{i \in p_{\vec{r}_1}} \sigma_i^z \, |\mathrm{ref}\rangle \, . \tag{4.31}$$

For a given reference state $|\mathrm{ref}\rangle$ this defines a canonical spin background for one-charge states $\prod_{i \in p_{\vec{r}_1}} \sigma_i^z \, |\mathrm{ref}\rangle$. Next, we investigate the action of a non-vanishing quasiparticle number conserving operator sequence on a canonical one-charge state

$$\begin{aligned} |\mathrm{f}\rangle &= T_{m_1,b_1^{(\alpha_1)}} T_{m_2,b_2^{(\alpha_2)}} \dots T_{m_k,b_k^{(\alpha_k)}} \, |\vec{r}_1, +\rangle \\ &= \mathcal{N}(1 - X_{+_2}) \prod_{+ \neq +_2} (1 + X_+) \prod_{\square} (1 + Z_\square) \, \sigma_{i_1}^{\alpha_1} \sigma_{i_2}^{\alpha_2} \dots \sigma_{i_k}^{\alpha_k} \prod_{i \in p_{\vec{r}_1}} \sigma_i^z \, |\mathrm{ref}\rangle \, , \end{aligned} \tag{4.32}$$

where $+_2$ is the charge site at position $\vec{r}_2$. While it is clear that the charge moved from $\vec{r}_1$ to $\vec{r}_2$, the spin background is not necessarily in a canonical form.

At this point it is most instructive to use $|\Rightarrow\rangle$ as reference state and to bring the spin background into a canonical form. For this choice we have

$$|\mathrm{f}\rangle = \mathcal{N}(1 - X_{+_2}) \prod_{+ \neq +_2} (1 + X_+) \prod_{\square} (1 + Z_\square) \, \sigma_{i_1}^{\alpha_1} \sigma_{i_2}^{\alpha_2} \dots \sigma_{i_k}^{\alpha_k} \prod_{i \in p_{\vec{r}_1}} \sigma_i^z \, |\Rightarrow\rangle \, . \tag{4.33}$$

Using $\sigma^y = \mathrm{i}\sigma^x\sigma^z$, the action of the Pauli matrices on $|\Rightarrow\rangle$ is evaluated

$$\sigma_{i_1}^{\alpha_1} \sigma_{i_2}^{\alpha_2} \dots \sigma_{i_k}^{\alpha_k} \prod_{i \in p_{\vec{r}_1}} \sigma_i^z \, |\Rightarrow\rangle = [\mathrm{i}^{n_a}] \cdot |s^x\rangle = [\mathrm{i}^{n_a}] \cdot \prod_{\square \in \Gamma_z} Z_\square \prod_{i \in p_{\vec{r}_2}} \sigma_i^z \, |\Rightarrow\rangle \, , \tag{4.34}$$

where $|s^x\rangle$ is a product state in the σ^x-basis and the phase factor $[\mathrm{i}^{n_a}]$ with $n_a \in \{0, 1, 2, 3\}$ results from the action of the Pauli matrices.

The expression on the right results from the fact that any state $|s^x\rangle$ can be written as a product of σ^z matrices acting on the reference state $|\Rightarrow\rangle$. In the current case this product of σ^z can always be chosen as the canonical Pauli string operator on $p_{\vec{r}_2}$ of the one-charge state $|\vec{r}_2, +\rangle$ times some product of $Z_\square$ over the appropriate set Γ_z. With this the final state $|\mathrm{f}\rangle$ becomes

$$\begin{aligned} |\mathrm{f}\rangle &= [\mathrm{i}^{n_a}] \cdot \mathcal{N}(1 - X_{+_2}) \prod_{+ \neq +_2} (1 + X_+) \prod_{\square} (1 + Z_\square) \prod_{\square \in \Gamma_z} Z_\square \prod_{i \in p_{\vec{r}_2}} \sigma_i^z \, |\Rightarrow\rangle \\ &= [\mathrm{i}^{n_a}] \cdot \mathcal{N}(1 - X_{+_2}) \prod_{+ \neq +_2} (1 + X_+) \prod_{\square} (1 + Z_\square) \prod_{i \in p_{\vec{r}_2}} \sigma_i^z \, |\Rightarrow\rangle \\ &= [\mathrm{i}^{n_a}] \, |\vec{r}_2, +\rangle \, . \end{aligned} \tag{4.35}$$

Note that the result is again obtained in terms of a canonical state $|\vec{r}_2, \blacksquare\rangle$ and an additional phase factor $[\mathrm{i}^{n_a}]$ stemming from the action of the Pauli matrices on the reference state as detailed in Eq. 4.34. The operators given in Tab. 4.1 yield the result in terms of a state $|\tilde{\mathrm{f}}\rangle$ with a phase $[\mathrm{i}^{n_a}]$, i.e.,

$$|\mathrm{f}\rangle = [\mathrm{i}^{n_a}]\,|\tilde{\mathrm{f}}\rangle \ . \tag{4.36}$$

So although the spin background of $|\tilde{\mathrm{f}}\rangle$ is not necessarily canonical we have

$$|\tilde{\mathrm{f}}\rangle = |\vec{r}_2, \blacksquare\rangle \,, \tag{4.37}$$

reflecting that canonicalizing the state $|\tilde{\mathrm{f}}\rangle$ is a trivial operation due to the absence of fluxes.

Note that this is different if we choose the reference state $|\Uparrow\rangle$ and act with the Pauli matrices to the right

$$|\mathrm{f}\rangle = \mathcal{N}(1 - X_{\blacksquare_2}) \prod_{\blacksquare \neq \blacksquare_2} (1 + X_{\blacksquare}) \prod_{\square} (1 + Z_{\square})\ \sigma_{i_1}^{\alpha_1} \sigma_{i_2}^{\alpha_2} \dots \sigma_{i_k}^{\alpha_k} \prod_{i \in p_{\vec{r}_1}} \sigma_i^z \,|\Uparrow\rangle \ . \tag{4.38}$$

Then we can write

$$\sigma_{i_1}^{\alpha_1} \sigma_{i_2}^{\alpha_2} \dots \sigma_{i_k}^{\alpha_k} \prod_{i \in p_{\vec{r}_1}} \sigma_i^z \,|\Uparrow\rangle = [\mathrm{i}^{n_a}] \cdot |s^z\rangle = [\mathrm{i}^{n_a}] \cdot \prod_{\blacksquare \in \Gamma_x} X_{\blacksquare} \,|\Uparrow\rangle \ , \tag{4.39}$$

where the factor $[\mathrm{i}^{n_a}]$ comes from the action of the Pauli operators. Note that the state $|s^z\rangle$ can at most contain contractible loops of flipped spins because we consider the one-charge sector. We can then commute the product over $X_{\blacksquare}$ to the left

$$|\mathrm{f}\rangle = [\mathrm{i}^{n_a}] \cdot \left(\prod_{\blacksquare \in \Gamma_x} X_{\blacksquare} \right) \mathcal{N}(1 - X_{\blacksquare_2}) \prod_{\blacksquare \neq \blacksquare_2} (1 + X_{\blacksquare}) \prod_{\square} (1 + Z_{\square})\,|\Uparrow\rangle \,, \tag{4.40}$$

which is a product of $X_{\blacksquare}$ acting on a one-charge state. And hence, we get the following expression

$$|\mathrm{f}\rangle = \left[\mathrm{i}^{n_a + 2n_b}\right] \cdot \mathcal{N}(1 - X_{\blacksquare_2}) \prod_{\blacksquare \neq \blacksquare_2} (1 + X_{\blacksquare}) \prod_{\square} (1 + Z_{\square})\,|\Uparrow\rangle \,, \tag{4.41}$$

where

$$n_b = \begin{cases} 1 & \text{if} \quad \blacksquare_2 \in \Gamma_x \\ 0 & \text{else.} \end{cases} \tag{4.42}$$

Clearly, in this convention, the definition of the operators in Tab. 4.1 needs to be adapted. These adapted operators then also yield the result in the form

$$|\mathrm{f}\rangle = [\mathrm{i}^{n_a}]\,|\tilde{\mathrm{f}}\rangle \ . \tag{4.43}$$

However, in contrast to Eq. (4.37), we have

$$|\tilde{\mathrm{f}}\rangle = \left[\mathrm{i}^{2n_b}\right] |\vec{r}_2, \blacksquare\rangle \ . \tag{4.44}$$

So we still need to determine n_b from the spin background of the state $|\tilde{\mathrm{f}}\rangle$ by checking whether there are contractible loops surrounding the charge at $\vec{r}_2$. Physically, each such loop corresponds to the winding of a flux around the charge. As a consequence, the total effect of all these loops

depends only on the parity of the loop number. In case of even (odd) parity no (an) additional sign results which has to be included in this non-trivial postprocessing procedure.

In the previous part we used an explicit reference state because it is easy to act with sequences of Pauli operators on product states in the spin basis. But actually the arguments are independent of the reference state. Note that we effectively just sorted the Pauli operators by flavor. Splitting $\sigma^y = \mathrm{i}\sigma^x\sigma^z$ we arranged the product $\sigma_{i_1}^{\alpha_1}\sigma_{i_2}^{\alpha_2}\ldots\sigma_{i_k}^{\alpha_k}$ such that σ_i^x acts before σ_i^z or vice versa. Accordingly, on an operator level, the signs stem from the ordering of the Pauli operators. In this sense the T-operators implement a bookkeeping technique for the necessary reordering and yield the appropriate sign for the ordered product.

As for the ground-state energy, the state $|\mathrm{f}\rangle$ can then be written independently of the reference state as

$$|\mathrm{f}\rangle = \left[\mathrm{i}^{n_a}\right] \cdot \mathcal{N}(1 - X_{+_2}) \prod_{+\neq +_2} (1 + X_+) \prod_{\square} (1 + Z_\square) \varsigma^z \varsigma^x \, |\mathrm{ref}\rangle \ , \tag{4.45}$$

where ς^α is the part consisting of σ^α. The additional factor $\left[\mathrm{i}^{n_a}\right]$ stems from the commutation relations of the Pauli matrices.

It is clear that ς^x corresponds to contractible loop operators, and hence, we have

$$|\mathrm{f}\rangle = \left[\mathrm{i}^{n_a}\right] \cdot \mathcal{N}(1 - X_{+_2}) \prod_{+\neq +_2} (1 + X_+) \prod_{\square} (1 + Z_\square) \varsigma^z \prod_{+\in\Gamma_x} X_+ \, |\mathrm{ref}\rangle \ . \tag{4.46}$$

The product ς^z corresponds to a product of stabilizers over the set Γ_z with a canonical path going from $\vec{r}_2$ to infinity. One therefore has

$$|\mathrm{f}\rangle = \left[\mathrm{i}^{n_a}\right] \cdot \mathcal{N}(1 - X_{+_2}) \prod_{+\neq +_2} (1 + X_+) \prod_{\square} (1 + Z_\square) \prod_{\square\in\Gamma_z} Z_\square \prod_{i\in p_{\vec{r}_2}} \sigma_i^z \prod_{+\in\Gamma_x} X_+ \, |\mathrm{ref}\rangle \ . \tag{4.47}$$

As a next step we move the product of X_+ and Z_+ to the left

$$|\mathrm{f}\rangle = \left[\mathrm{i}^{n_a+2n_b}\right] \cdot \left(\prod_{+\in\Gamma_x} X_+\right) \left(\prod_{\square\in\Gamma_z} Z_\square\right) \mathcal{N}(1 - X_{+_2}) \prod_{+\neq +_2} (1 + X_+) \prod_{\square} (1 + Z_\square) \prod_{i\in p_{\vec{r}_2}} \sigma_i^z \, |\mathrm{ref}\rangle \ , \tag{4.48}$$

where n_b captures whether $\prod_{+\in\Gamma_x} X_+$ and $\prod_{i\in p_{\vec{r}_2}} \sigma_i^z$ commute or anticommute

$$n_b = \begin{cases} 1 & \text{if} \quad +_2 \in \Gamma_x \\ 0 & \text{else} \, . \end{cases} \tag{4.49}$$

What remains is the action of stabilizer operators on a canonical one-charge state

$$|\mathrm{f}\rangle = \left[\mathrm{i}^{n_a+2n_b}\right] \cdot \left(\prod_{+\in\Gamma_x} X_+\right) \left(\prod_{\square\in\Gamma_z} Z_\square\right) |\vec{r}_2, +\rangle = \left[\mathrm{i}^{n_a+2n_b+2n_c}\right] |\vec{r}_2, +\rangle \, , \tag{4.50}$$

where

$$n_c = n_b = \begin{cases} 1 & \text{if} \quad +_2 \in \Gamma_x \\ 0 & \text{else} \, . \end{cases} \tag{4.51}$$

As $n_b \in \{0, 1\}$ we have

$$|\mathrm{f}\rangle = \left[\mathrm{i}^{n_a+2n_b+2n_c}\right] |\vec{r}_2, +\rangle = \left[\mathrm{i}^{n_a+4n_b}\right] |\vec{r}_2, +\rangle = \left[\mathrm{i}^{n_a}\right] |\vec{r}_2, +\rangle \, , \tag{4.52}$$

which means that the phase factor stems from the sorting of the Pauli matrices.

Note that we did choose a convention on the sorting of the Pauli matrices in this calculation, by sorting σ^x to the right. The operators given in Tab. 4.1 take into account the signs arising from this reordering and yield the final state in the form

$$|\mathrm{f}\rangle = [\mathrm{i}^{n_a}]\,|\tilde{\mathrm{f}}\rangle \ . \tag{4.53}$$

Comparing to Eq. (4.52), one sees that the canonicalization of $|\tilde{\mathrm{f}}\rangle$ cannot yield an additional phase factor.

Overall, these considerations allow to set up series expansions of the perturbed topological phase in the zero- and one-particle sector using sufficiently large clusters. A generalization to many particles requires further considerations treating the spin background properly in the evaluation of scalar products between multi-particle states [37, 238]. Next we go beyond series expansions on large clusters by performing a full graph decomposition.

4.3 Hypergraph decomposition for the perturbed topological phase

In this section we describe how to execute linked-cluster expansions [96, 97] for the perturbed toric code in the topological phase at finite fields using a full hypergraph decomposition [130]. How to set up such a hypergraph decomposition is also explained in Sect. 3.6. In this section we restrict ourselves to the zero- and one-quasiparticle sector. In these sectors it turns out that the non-trival mutual statistics can be correctly included by taking the spin background into account within the hypergraph decomposition. However, this problem is slightly different to the setup specified in Sect. 3.2. So we discuss two important points to set up a full hypergraph decomposition for the toric code in a field.

First, we address how to calculate the reduced contribution of a subcluster to the ground-state energy or an irreducible one-quasiparticle hopping element by just taking into account the degrees of freedom within the respective cluster, and no degrees of freedom outside of the respective cluster. Note that, although this might seem counter-intuitive due to the non-trivial mutual statistics, it is a direct consequence of the considerations in Sect. 4.2, that this is actually possible.

Second, we address how to properly sort the clusters into equivalence classes within a calculation of the ground-state energy or an irreducible one-quasiparticle hopping element. Although the equivalence relations are based on hypergraph isomorphism, as described in Subsect. 3.6.2, we also need to properly include the information about the spin background into the representing graphs.

4.3.1 Contributions of individual subclusters

For the low-field limit of the toric code in a general uniform field the unperturbed energy depends on the eigenvalues x_{+}, $z_{\square}$ which are defined locally at the charge or flux sites. The general uniform field then acts as a perturbation on three different types of bonds as described in Sect. 4.2. These bonds correspond to the elementary building blocks of the clusters. Indeed, every connected cluster relevant for the perturbative calculations is determined by a set of bonds, which is a subset of all the bonds in the system. Clusters consisting of a single site are an exception. However, they are only relevant in zeroth order, so their reduced contributions can be easily calculated and thus they

are neglected in the following discussion. Note that in contrast to the hypergraph decomposition in Ref. [130], we have several types of sites in the current problem: The spin sites i, the flux sites $\square$, and the charge sites $+$.

In Sect. 4.2 we describe how to calculate the ground-state energy and irreducible one-quasiparticle matrix elements of the effective Hamiltonian on finite clusters. More precisely, we describe how any of these matrix elements can be calculated on a single finite cluster. Recall, that for any finite perturbation order these calculations are valid in the thermodynamic limit if this finite cluster is designed accordingly [103, 120–122]. In principle, each of these calculations can be decomposed as a sum over all connected subclusters of the chosen finite cluster [95, 96] as given in Eq. 3.12. However, for the sake of readability we recall that in practice the lattice is replaced by an appropriate finite cluster, and consider Eq. (3.115) [96]

$$O(\mathcal{L}) = \sum_{C \subseteq \mathcal{L}} o(C), \tag{4.54}$$

with the reduced contribution [95, 96]

$$o(C) = O(C) - \sum_{c \subset C} o(c)\,. \tag{4.55}$$

More concretely, for a calculation of the ground-state energy, $O(C)$ corresponds to

$$E_0(C) = \langle \mathrm{GS}|\, H_{\text{eff}}^C\, |\mathrm{GS}\rangle\ . \tag{4.56}$$

Instead, for the calculation of an irreducible one-quasiparticle matrix element $\langle \vec{r}_2|\, H_{\text{eff}} - E_0\, |\vec{r}_1\rangle$ of the effective Hamiltonian, $O(C)$ corresponds to

$$t_{\vec{r}_2,\vec{r}_1}(C) = \langle \vec{r}_2|\, H_{\text{eff}}^C - E_0(C)\, |\vec{r}_1\rangle\ , \tag{4.57}$$

where $|\vec{r}\rangle$ is a canonical state, with either a charge or a flux at position $\vec{r}$, defined on the full system. Note that this implies, that the respective sites can also be outside of the considered cluster C. Interestingly, for such an irreducible one-quasiparticle matrix element, the reduced contribution of an individual cluster can depend on particles residing outside of the respective cluster in the current case, which is counter-intuitive and a consequence of the non-local properties of topological phases[1]. Such effects are however absent in the ground-state sector. Indeed, we showed that for the ground-state energy it is sufficient to act with the operators $T_{n,b^{(\alpha)}}$ (see Tab. 4.1) to the right so that the result is given in terms of the canonical ground state $|\mathrm{GS}\rangle$ times an additional phase factor. So the ground-state energy can easily be evaluated on each individual cluster and does not depend on any degree of freedom which is outside of the respective cluster. As a consequence, also the reduced ground-state energy of a cluster can be calculated, without considering degrees of freedom outside of the respective cluster.

In the one-quasiparticle sector, the procedure depends on the choice of the reference state. First, there are the specific reference states where the strings of the considered quasiparticle are visible but the corresponding strings of the other quasiparticle type are not visible in the spin background. Let us consider the generic example of a single charge excitation taking the reference state $|\Rightarrow\rangle$. The phase factor $[\mathrm{i}^{n_a}]$ in the one-charge state in Eq. (4.35) originates from the action of the bond-local

[1] Interestingly, clusters with this property also occur in linked-cluster expansions for other models which feature topological order [187].

operators $T_{n,b^{(\alpha)}}$ on the canonical state. Due to the absence of fluxes and the specific choice of the reference state, this one-charge state is a canonical state up to the phase $[\mathrm{i}^{n_a}]$. As a consequence, we can evaluate the reduced contribution of each individual cluster to an irreducible one-charge hopping element without the necessity to take degrees of freedom outside the respective cluster into account.

In contrast, using the reference state $|\Uparrow\rangle$ as in Eq. (4.40), the phase factor $[\mathrm{i}^{n_a+2n_b}]$ stems from the evaluation of the $T_{n,b^{(\alpha)}}$ on this reference state and the canonicalization of the resulting state. In this case the state resulting from the action of the $T_{n,b^{(\alpha)}}$ may contain loops in the spin background which surround the charge, and hence, lead to an additional phase factor of -1. In the formulation for arbitrary reference states, these conventions correspond to different sorting of the product of Pauli matrices acting on the reference state. In the first convention σ^x is sorted to the right of σ^z, in the second convention it is the other way around. Overall, in the appropriate convention the evaluation of the sequence of operators $T_{n,b^{(\alpha)}}$ yields a state which is equivalent to a canonical state and an additional phase factor. So the reduced contributions of individual clusters to irreducible hopping elements are easily evaluated on each individual cluster and do not depend on any degree of freedom outside of the respective cluster. Clearly, by the duality of charges and fluxes also the reduced contributions of individual clusters to one-flux irreducible matrix elements can be determined on the respective clusters, by choosing the appropriate convention.

Note, however, that in order to evaluate the reduced contribution of a cluster we need to take into account all the degrees of freedom within the cluster including the spin-background variables. Especially for the irreducible one-quasiparticle hopping elements this leads to the observation, that subclusters which do not host any quasiparticles before and after the hopping can contribute because of a non-trivial spin background on the cluster. Due to this non-trivial spin background the reduced contribution of such a cluster to the respective matrix element of the effective Hamiltonian can differ from its reduced contribution to the ground-state energy, resulting in a non-vanishing reduced contribution to the irreducible matrix element.

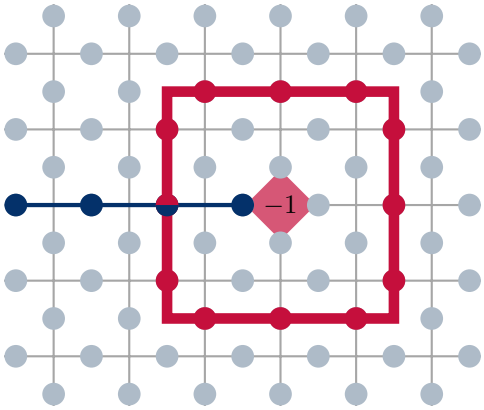

Figure 4.5: Example for a perturbation theory process which contributes to the excitation gap, although it does not directly act on the quasiparticle. The process consists of twelve σ^x operators which act on the red sites forming a loop around the excitation and interacting with the string operator. This operator consists of σ^z operators acting on the blue sites. Both operators, the loop and the string operator, act on the site which is red and blue. This image is taken from Ref. [23].

A physically simple, but enlightening example is a cluster which winds around a charge as illustrated in Fig. 4.5. It is clear, that a process winding a flux around the charge results in a different contribution, than the same process without the charge even though the process does not directly involve the respective charge site. So it is consistent that these clusters contribute to the irreducible hopping elements. Note that this type of process already occurs in order four perturbation theory.

Analogously to Subsect. 3.6.4, we can formulate selection rules to identify clusters or equivalence classes which have zero reduced contribution [97, 99]. Here, these are based on the observation, that any elementary perturbation operator either flips all stabilizer eigenvalues within the bond it acts on or results in zero. Basically, these selection rules correspond to the ones described in Subsect. 3.6.4 with the difference, that here we simply ignore the spin sites of the clusters. For a calculation of the ground-state energy this means that we consider the rule given in Eq. (3.166), but we replace the number of odd-degree sites in the considered cluster by the number of odd-degree stabilizer sites in the cluster. Further the maximum cardinality of a bond in the full system, is replaced by the maximum number of stabilizer sites within a bond in the entire system. Also the selection rule based on graph coloring given in Eq. (3.168) can be adapted by considering only the stabilizer sites of odd degree, instead of all sites of odd degree within the cluster. Similarly, one can adapt the rule in Eq. (3.167), by considering the number of bonds which have to be duplicated in the given cluster such that all stabilizer sites have even degree. The generalization for one-quasiparticle hopping elements is straightforward.

4.3.2 Identification of equivalent clusters

In the previous subsection we considered an expansion in the form of Eq. (4.54) for the desired quantities. We also explained that for the ground-state energy and the one-quasiparticle matrix elements we can always choose a reference state, such that we can evaluate the reduced contributions of the individual clusters without taking into account degrees of freedom which are not on the respective cluster. Throughout this subsection we assume to work in such a convention.

The next step is to exploit structural equivalence to identify clusters which have the same reduced contribution to the desired matrix element to arrive at an expansion of the form given in Eq. (3.152) [96–99]

$$O(\mathcal{L}) = \sum_{\mathcal{E}\subseteq\mathcal{L}} \mathcal{N}(\mathcal{E},\mathcal{L}) \cdot o(\mathcal{E})\,, \tag{4.58}$$

where we need an equivalence relation which guarantees, that all clusters of an equivalence class have the same reduced contribution [96, 105, 187]

$$o(\mathcal{E}) = o(C) \quad \forall C \in \mathcal{E}\,. \tag{4.59}$$

The equivalence relation is based on hypergraph isomorphism [130]. So the employed linked-cluster expansion corresponds to a hypergraph decomposition [130] which is explained in Sect. 3.6. In contrast to the hypergraph decomposition described in Ref. [130] and Sect. 3.6, we have several types of sites in the present problem: spin sites i, flux sites $\square$, and charge sites $+$. From a technical point of view it is interesting that a given perturbation operator can act differently on different types of degrees of freedom, namely the spin-background variables and the eigenvalues of the star and plaquette operators. So while a cluster still consists of sites and bonds, the bonds have some orientation. This means different sites have different roles in the bonds. While the eigenvalues of the stabilizer operators are always flipped, the action on the spin background can be different. So the

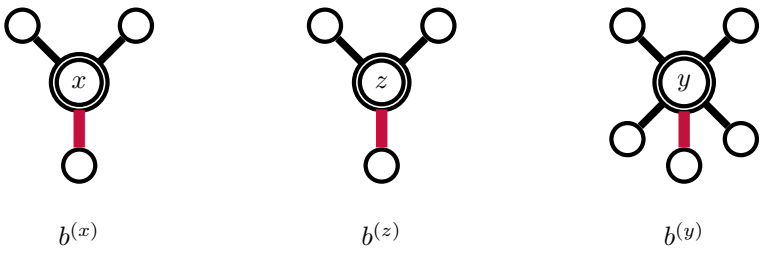

Figure 4.6: The König representation of the different bonds with the contained sites is shown. The double circles represent the bonds, and the single circles represent the sites, namely the charge-sites, the flux-sites and the spin-sites. Note that the vertices corresponding to spin-sites are connected to the double circles by a thick red edge. This image is taken from Ref. [23].

structure of the bonds cannot be captured by ordinary hyperedges, which are just subsets of the vertex set, in a hypergraph representation of the cluster. Interestingly, several definitions of oriented hypergraphs can be found in the literature [158, 159, 161, 176–178, 242]. Here, we use incidence-colored hypergraphs, where we assign a color to incident hyperedge-vertex pairs, to include the roles of the sites within the bonds as described in Subsect. 2.2.3. Hypergraphs can be represented by bipartite graphs, which are also referred to as the König representation of a hypergraph [132, 134]. The two parts of the bipartite König graph represent the edges (edge-part) and the vertices (vertex-part) of the hypergraph. Two vertices in the König representation are adjacent if and only if they correspond to an incident edge-vertex pair within the hypergraph. Importantly, two hypergraphs are isomorphic if and only if their König representations are isomorphic [132–134].

The colors of the incident hyperedge-vertex pairs can be incorporated using edge colors within the König representation. Note that this is consistent with the fact that the edges in the König representation correspond to incidences of edge-vertex pairs in the original hypergraph. Furthermore, we use vertex colors to distinguish the two parts of the bipartite graph and to incorporate the different bond types into the edge-part of the König representation.

As an example we give the König representation of the clusters which consist of a single bond in Fig. 4.6. In the end this enhanced König representation is the basis for the distinction of equivalence classes of clusters within the full hypergraph decomposition presented here. For calculations of the ground-state energy this representation of the clusters is indeed sufficient. For the calculation of hopping elements we need to explicitly incorporate the information about the involved states on the clusters, as the reduced contribution of a cluster also depends on the states considered within the matrix element. Finally, also this can be incorporated via vertex colors.

Ground-state energy

For the ground-state energy equivalent clusters are identified using hypergraph isomorphism accounting for the different roles of the vertices within the hyperedges and the different bond types $b^{(\alpha)}$ with $\alpha \in \{x, y, z\}$. In terms of the König representation this means that the isomorphism preserves the edge and the vertex colors. Note that one can reduce the König representation by omitting the vertices which represent the sites which are only contained in one bond within the cluster [130].

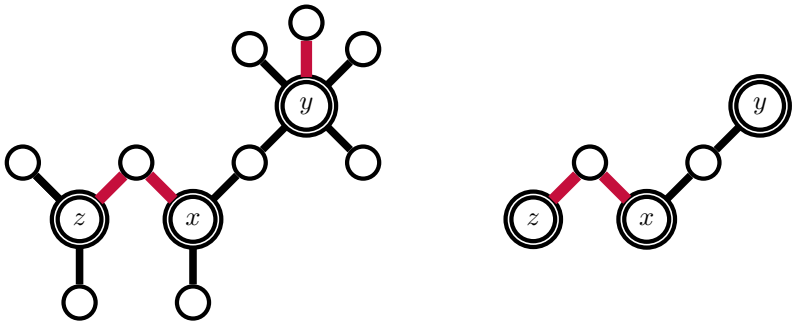

Figure 4.7: *L*eft: Example for the König representation of a cluster. The bonds are represented by double circles, where the bond types are explicitly given. The different labels x, y, z as well as double and single circles correspond to different vertex colors. The vertices corresponding to spin sites are explicitly distinguished as they are connected by red edges to the vertices representing the bonds. *R*ight: In the reduced König representation the vertices from the vertex-part are omitted if they have degree one, reducing the complexity of the graph representation. This image is taken from Ref. [23].

For each bond, the number and role of the omitted sites are easily deduced from the bond types. We do not distinguish flux and charge sites within the hypergraph representation, because they are treated on equal footing in the operators $T_{n,b^{(\alpha)}}$ and also in the unperturbed Hamiltonian.

So basically, the problem is decomposed into stabilizer eigenvalues which are relevant for the energetics, and spin-background variables, which we introduce to obtain the correct phases. It is clear that the additional phase depends only on the action of the Pauli matrices on the reference state. This is correctly taken into account, once we know which Pauli matrices act on which spin-background variable and in which order. From the edge colors in the König representation it is clear, which vertices correspond to the spin background. The order is given by the sequence of operators $T_{n,b^{(\alpha)}}$. Regarding the quasiparticles, the graph representation might result in graphs for which it is not clear whether vertices correspond to charge or flux sites. However, energetically this does not matter. In summary, we only separate the energetic degrees of freedom from the spin background within the graph representation exploiting that elementary fluxes and charges have the same energy. Finally, the embedding factor normalized to the number of spin sites $\mathcal{N}(\mathcal{E}, \mathcal{L})/N$ is calculated as explained in Subsubsect. 3.6.3. Note that this is equivalent to calculating the embedding factor normalized to a unit cell containing three bonds which share a given spin site.

Single-particle excitation gap

For the single particle irreducible matrix elements only minor modifications are necessary in the graph representation. Recall that we are aiming to calculate irreducible matrix elements of the form

$$t_{\vec{\delta}} = t_{\vec{r}_2,\vec{r}_1} = \langle \vec{r}_2 | \, H_{\text{eff}} - E_0 \, | \vec{r}_1 \rangle \tag{4.60}$$

with $\vec{\delta} = \vec{r}_2 - \vec{r}_1$. In Subsect. 4.3.1 we established that using appropriate conventions for the calculations we can evaluate the reduced contributions of individual clusters to these matrix elements, and the reduced contributions are not affected by any degrees of freedom outside of the respective

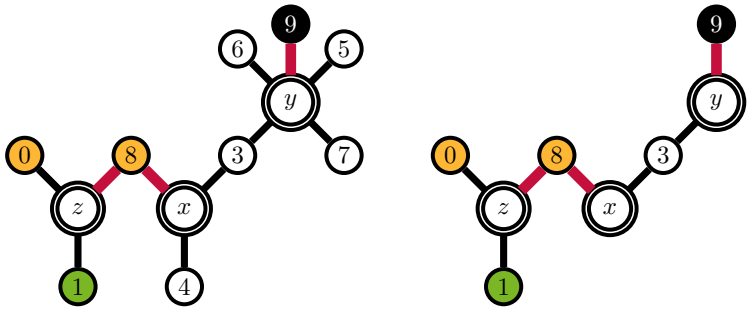

Figure 4.8: *Left*: Illustration of the König representation for the hopping element $\langle 01000000; 01|\, H^c_{\text{eff}} - E_0(c)\, |10000000; 11\rangle$. The i-th number in the states refers to the vertex with number i in the König representation. Note that the enumeration of site vertices is not part of the actual representation, whereas the label of the bond-vertices is. We do not explicitly distinguish charge and spin sites, e.g., we cannot deduce which types of sites the vertices $5, 6, 7$ represent. The label x, y, z of the bond vertices is part of the representation. *Right*: By omitting the white site-vertices of degree one we again obtain a reduced representation. This image is taken from Ref. [23].

cluster. So we can encode the product states on a given cluster using vertex colors for the vertices which represent sites. Note that these vertices must still be distinguishable from the vertices which represent bonds. Depending on the local state at a given site in the states $|\vec{r}_1\rangle$ and $|\vec{r}_2\rangle$ involved in the concrete matrix element we assign colors in the following way

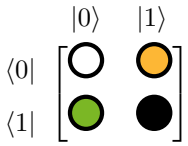

(4.61)

where the states label the values of $\tilde{x}_{+}$, $\tilde{z}_{\square}$ or $\tilde{s}_i$ at the respective site. A white filling of the vertex means, that the eigenvalue associated with the site is zero within both states $|\vec{r}_1\rangle$ and $|\vec{r}_2\rangle$, while an orange vertex indicates that the respective eigenvalue changes from 1 to 0. A specific example for this representation is shown in Fig. 4.8. In summary we distinguish seven different types of vertices with different colors: Three different types of vertices representing bonds $b^{(x)}, b^{(y)}, b^{(z)}$ and four different types of site vertices representing changes of the local states as indicated in Eq. (4.61).

Next, we address the question, which subclusters we need to consider. First of all, it is clear that a subcluster can only contribute if it contains all stabilizer sites, which change their local state within the matrix element. Next, any subcluster with a non-vanishing reduced contribution must include the sites which host excitations within the states $|\vec{r}_1\rangle$ and $|\vec{r}_2\rangle$, or the initial state $|\vec{r}_1\rangle$ must have a non-trivial spin background on the subcluster. Interestingly, the spin background of $|\vec{r}_2\rangle$ does not matter.

In order to determine the state $|\mathrm{f}\rangle$ resulting from the action of a sequence of operators $T_{n,b^{(\alpha)}}$ on a state $|\vec{r}_1\rangle$ the spin background of the state $|\vec{r}_1\rangle$ is crucial. Using an appropriate reference state the product of operators $T_{n,b^{(\alpha)}}$ yields the result in terms of a phase factor $[\mathrm{i}^{n_a}]$, and a state

equivalent to a canonical state $|\vec{r}''\rangle$. So the spin background of the state $|\vec{r}_2\rangle$ is not important, as

$$\langle \vec{r}_2 | \mathrm{f} \rangle = \langle \vec{r}_2 | \, [\mathrm{i}^{n_a}] \, |\vec{r}''\rangle = [\mathrm{i}^{n_a}] \cdot \delta_{\vec{r}_2, \vec{r}''} \, . \tag{4.62}$$

This also implies that the spin background of $|\vec{r}_2\rangle$ does not play a role in the representation and the selection of the subclusters. As a consequence, we can ignore the spin background of $|\vec{r}_2\rangle$ for the graph representation, while we still need to include the spin background of $|\vec{r}_1\rangle$ within the graphs. Accordingly, for vertices representing spin-background variables we only use two colors, based on the respective eigenvalue in the state $|\vec{r}_1\rangle$

$$\begin{array}{c} \\ \langle 0| \\ \langle 1| \end{array} \begin{array}{c} \begin{array}{cc} |0\rangle & |1\rangle \end{array} \\ \left[\begin{array}{cc} \circ & \bullet \\ \circ & \bullet \end{array} \right] \end{array} . \tag{4.63}$$

With this the König representation from Fig. 4.8 is replaced by the representation in Fig. 4.9. For the stabilizer degrees of freedom we keep the convention defined in Eq. (4.61) so we still distinguish seven different types of vertices. This way of coloring the vertices has the advantage that the rules which clusters need to be taken into account are formulated more easily. For off-diagonal elements $\langle \vec{r}_2 | \, H_{\text{eff}} - E_0 \, | \vec{r}_1 \rangle$ with $\vec{r}_2 \neq \vec{r}_1$ all sites represented by green or orange vertices need to be included in a cluster, otherwise its reduced contribution vanishes. Instead, for the diagonal elements the reduced contribution of a cluster is zero, if no site represented by a black vertex is contained in the cluster. A specific cluster on which the winding process of a flux around a charge

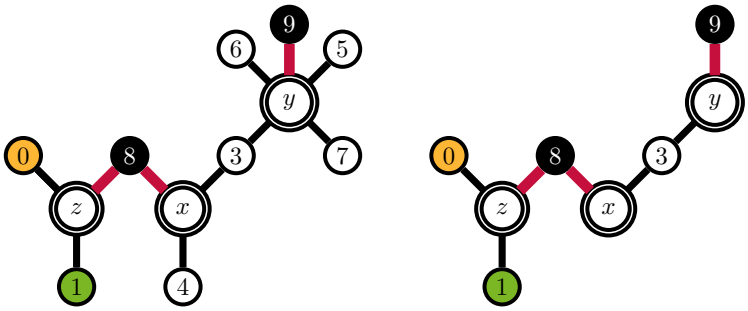

Figure 4.9: Illustration of the König representation of a hopping element, without taking into account the spin background of the state $|\vec{r}_2\rangle$. In contrast to Fig. 4.8 the vertex 8 is now black instead of orange. This image is taken from Ref. [23].

in Fig. 4.5 occurs is represented by the graph in Fig. 4.10. While this graph does not contain any vertices corresponding to excitations the non-trivial spin background suffices to take the effects of the charge (which is not on the cluster) into account. Note that this graph can only play a role within matrix elements $\langle \vec{r}_2, + | \, H_{\text{eff}} - E_0 \, | \vec{r}_1, + \rangle$ if $\vec{r}_2 = \vec{r}_1$. Interestingly, also clusters which do not enclose a charge can have a non-trivial spin background in such a hopping element. Currently, we simply consider the respective equivalence classes within the calculations. As in practice a large finite cluster is used instead of the lattice, there are only finitely many instances of these classes.

However, it is interesting whether a scheme to sort out these clusters can be devised and how it affects the efficiency of the method.

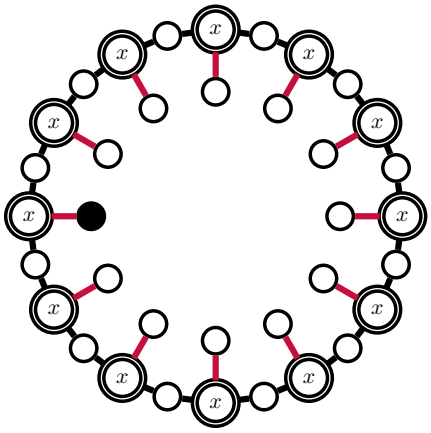

Figure 4.10: A graph which can only contribute to diagonal matrix elements $\langle \vec{r}, + | \, H_{\text{eff}} - E_0 \, | \vec{r}, + \rangle$. The spin background distinguishes this graph, representing a cluster which encloses a charge, from a graph which represents a cluster which does not enclose a charge. This image is taken from Ref. [23].

4.3.3 Series for ground-state energy and excitation gaps

Using the described hypergraph decomposition, we calculated the ground-state energy per spin up to order ten using the pCUT method. The ground-state energy, which is symmetric under the exchange of h_x and h_z due to self duality, can be written down by summarizing certain terms using the notation $S_j = h_x^j + h_z^j$ and $P_{2j} = h_x^j h_z^j$, which has been introduced in [238]. It reads

$$\begin{aligned} e_0 = &-1/2 - \frac{1}{2}S_2 - \frac{1}{4}h_y^2 - \frac{15}{8}S_4 - \frac{7}{32}S_2h_y^2 + \frac{1}{4}P_4 - \frac{13}{192}h_y^4 - \frac{147}{8}S_6 - \frac{371}{128}S_4h_y^2 \\ &+ \frac{113}{32}P_4S_2 - \frac{1045}{3456}S_2h_y^4 + \frac{2003}{384}P_4h_y^2 - \frac{197}{3072}h_y^6 - \frac{18003}{64}S_8 - \frac{1954879}{36864}S_6h_y^2 \\ &+ \frac{6685}{128}P_4S_4 - \frac{34054175}{3981312}S_4h_y^4 + \frac{146861}{2304}P_4S_2h_y^2 - \frac{15343549}{26542080}S_2h_y^6 + \frac{20869}{384}P_8 \\ &+ \frac{5020085}{497664}P_4h_y^4 - \frac{163885}{1769472}h_y^8 - \frac{5420775}{1024}S_{10} - \frac{1563459523}{1327104}S_8h_y^2 + \frac{39524033}{36864}P_4S_6 \\ &- \frac{1115105409427}{5733089280}S_6h_y^4 + \frac{10058235445}{7962624}P_4S_4h_y^2 - \frac{4219640835497}{191102976000}S_4h_y^6 \\ &+ \frac{5650925}{6912}P_8S_2 + \frac{20854097563}{143327232}P_4S_2h_y^4 - \frac{483890940281}{382205952000}S_2h_y^8 + \frac{1202498305}{1990656}P_8h_y^2 \\ &+ \frac{1994817656221}{71663616000}P_4h_y^6 - \frac{186734746441}{1146617856000}h_y^{10}. \end{aligned} \tag{4.64}$$

For the ground-state energy we do not exceed the highest available order of the previously known results [35, 238].

The one-particle excitation energies have been calculated in order nine for arbitrary field directions and in order ten for a parallel field direction with $h_y = 0$. Here we only focus on the charge and flux gap which is always located at $\vec{k} = (0, 0)$. Due to self-duality, we can constrain ourselves to the charge gap Δ^{+} which reads for arbitrary field direction

$$\begin{aligned}\Delta^{+} =&1 - 4h_z - 4h_z^2 - h_y^2 - 12h_z^3 + \frac{11}{4}h_y^2 h_z + 2h_x^2 h_z - 36h_z^4 - 9h_y^2 h_z^2 - \frac{15}{16}h_y^4 + 3h_x^2 h_z^2 \\ &+ 17h_x^2 h_y^2 + 5h_x^4 - 176h_z^5 + \frac{473}{64}h_y^2 h_z^3 + \frac{17}{4}h_y^4 h_z + \frac{83}{4}h_x^2 h_z^3 + \frac{9}{4}h_x^2 h_y^2 h_z + \frac{27}{2}h_x^4 h_z \\ &- \frac{2625}{4}h_z^6 - \frac{7971}{64}h_y^2 h_z^4 - \frac{135619}{3456}h_y^4 h_z^2 - \frac{575}{384}h_y^6 + 63h_x^2 h_z^4 + \frac{1305}{8}h_x^2 h_y^2 h_z^2 \\ &+ \frac{13621}{1152}h_x^2 h_y^4 + 71h_x^4 h_z^2 + \frac{14267}{96}h_x^4 h_y^2 + 92h_x^6 - \frac{14771}{4}h_z^7 - \frac{238621}{1152}h_y^2 h_z^5 \\ &+ \frac{1782929}{20736}h_y^4 h_z^3 + \frac{799973}{110592}h_y^6 h_z + \frac{28633}{64}h_x^2 h_z^5 + \frac{13807}{48}h_x^2 h_y^2 h_z^3 - \frac{3031}{13824}h_x^2 h_y^4 h_z \\ &+ \frac{925}{4}h_x^4 h_z^3 + \frac{1142149}{4608}h_x^4 h_y^2 h_z + \frac{495}{2}h_x^6 h_z - \frac{940739}{64}h_z^8 - \frac{4663837}{1728}h_y^2 h_z^6 \\ &- \frac{1760584999}{1990656}h_y^4 h_z^4 - \frac{1495320677}{19906560}h_y^6 h_z^2 - \frac{26492351}{7962624}h_y^8 + \frac{118029}{64}h_x^2 h_z^6 \\ &+ \frac{5186533}{1728}h_x^2 h_y^2 h_z^4 + \frac{24547709}{165888}h_x^2 h_y^4 h_z^2 + \frac{98263727}{3981312}h_x^2 h_y^6 + \frac{19263}{16}h_x^4 h_z^4 \\ &+ \frac{2199571}{4608}h_x^4 h_y^2 h_z^2 + \frac{3032191}{31104}h_x^4 h_y^4 + \frac{80999}{96}h_x^6 h_z^2 + \frac{7715431}{3072}h_x^6 h_y^2 + \frac{35649}{16}h_x^8 \\ &- \frac{11472297}{128}h_z^9 - \frac{4691521349}{442368}h_y^2 h_z^7 + \frac{538730849}{497664}h_y^4 h_z^5 + \frac{261699729407}{2388787200}h_y^6 h_z^3 \\ &+ \frac{43413180467}{2388787200}h_y^8 h_z + \frac{14650547}{1152}h_x^2 h_z^7 + \frac{2099164741}{165888}h_x^2 h_y^2 h_z^5 - \frac{215708093}{746496}h_x^2 h_y^4 h_z^3 \\ &+ \frac{41328278581}{597196800}h_x^2 h_y^6 h_z + \frac{918461}{144}h_x^4 h_z^5 + \frac{1791338425}{331776}h_x^4 h_y^2 h_z^3 - \frac{1255335587}{11943936}h_x^4 h_y^4 h_z \\ &+ \frac{18372481}{4608}h_x^6 h_z^3 + \frac{2913725647}{663552}h_x^6 h_y^2 h_z + \frac{162525}{32}h_x^8 h_z\,. \end{aligned} \tag{4.65}$$

Due to reduced computational time, in the parallel field case with $h_y = 0$, the charge gap was calculated up to order 10

$$\begin{aligned}\Delta^{+} =&1 - 4h_z - 4h_z^2 - 12h_z^3 + 2h_x^2 h_z - 36h_z^4 + 3h_x^2 h_z^2 + 5h_x^4 - 176h_z^5 + \frac{83}{4}h_x^2 h_z^3 \\ &+ \frac{27}{2}h_x^4 h_z - \frac{2625}{4}h_z^6 + 63h_x^2 h_z^4 + 71h_x^4 h_z^2 + 92h_x^6 - \frac{14771}{4}h_z^7 + \frac{28633}{64}h_x^2 h_z^5 + \frac{925}{4}h_x^4 h_z^3 \\ &+ \frac{495}{2}h_x^6 h_z - \frac{940739}{64}h_z^8 + \frac{118029}{64}h_x^2 h_z^6 + \frac{19263}{16}h_x^4 h_z^4 + \frac{80999}{96}h_x^6 h_z^2 + \frac{35649}{16}h_x^8 \\ &- \frac{11472297}{128}h_z^9 + \frac{14650547}{1152}h_x^2 h_z^7 + \frac{918461}{144}h_x^4 h_z^5 + \frac{18372481}{4608}h_x^6 h_z^3 + \frac{162525}{32}h_x^8 h_z \\ &- \frac{287258435}{768}h_z^{10} + \frac{96935975}{1728}h_x^2 h_z^8 + \frac{107740069}{3456}h_x^4 h_z^6 + \frac{21893537}{1536}h_x^6 h_z^4 \\ &+ \frac{43593271}{3072}h_x^8 h_z^2 + \frac{1873147}{32}h_x^{10}\,. \end{aligned} \tag{4.66}$$

The flux gap $\Delta^{\square}$ can be again obtained by exchanging h_x and h_z in these expressions. These results agree with previous high-order series expansions [35, 238]. In both the arbitrary and parallel field cases we were able to exceed the previously known results by one order.

4.4 Conclusions

In this work we presented how to treat non-local anyonic statistics with a high-order linked-cluster expansions using a full hypergraph decomposition. This has been exemplified for the topological phase of the toric code in the presence of a uniform field possessing Abelian charge and flux quasiparticles. Technically, we used the pCUT method to obtain series expansions for the ground-state energy and the one-quasiparticle charge and flux gap. Note that also other perturbative techniques like Takahashi's perturbation theory [192, 197] or Löwdin's partitioning technique [201, 205] can be applied to calculate these properties of the perturbed topological phase.

The improvement in terms of the achieved maximal perturbative order compared to calculations without a full graph decomposition [33, 35, 226, 238] is only moderate. Nevertheless, the explicit treatment of the non-locality of the fractional statistics of charges and fluxes within a full hypergraph decomposition is an asset on its own. Further, there can be a benefit of a full hypergraph decomposition when performing similar calculations for three-dimensional perturbed topological phases like the ones in the three-dimensional toric code [19, 20, 38] or the fractonic X-Cube model [26] in the presence of external perturbations. Indeed, in Subsect. 5.2.2, we employ such a calculation for the low-field limit of the X-Cube model in a parallel magnetic field.

Chapter 5

The X-Cube model in a magnetic field

The X-Cube model is a paradigmatic model for fracton topological order of type I [26, 27]. While elementary fracton excitations are fully immobile, topologically non-trivial composites of fractons have restricted mobility [26]. Furthermore, the model features a sub-extensive ground-state degeneracy which is dependent on real-space topology but also on geometrical properties like the system size or the lattice geometry [26, 28, 29]. The ground states have a non-trivial topological entanglement entropy [30] and the excitations feature a non-trivial mutual statistics [28, 222, 243].

The X-Cube model in an external magnetic field has been studied using quantum Monte Carlo (QMC) methods [84] and for two specific field directions with high-order series expansions [39]. In this chapter we extend the series expansion results for these specific field directions and additionally calculate series expansions for a general parallel field using the variant of linked-cluster expansions (LCEs) [130] introduced in Sect. 3.6. Unfortunately, the series expansions from the high-field limit are hard to extrapolate, and in general do not converge quickly enough to determine the expected first-order phase transition point reliably with the calculated perturbation orders.

5.1 The X-Cube model

The X-Cube model [26] is defined on a three dimensional cubic lattice with spin-$1/2$ degrees of freedom on the edges of the lattice. The Hamiltonian

$$H^{\mathrm{xc}} = -J_{\square} \sum_{\square} X_{\square} - J_{+} \sum_{+} Z_{+} \tag{5.1}$$

is composed of two different types of stabilizer operators and we assume the couplings $J_{\square}, J_{+}$ to be non-negative. First, there are the twelve-spin cube operators

$$X_{\square} = \prod_{i \in \square} \sigma_i^x \,, \tag{5.2}$$

where the product runs over all twelve spins at the edges of a cube. Second, there are the four-spin vertex operators

$$Z_{+} = \prod_{i \in +} \sigma_i^z \,. \tag{5.3}$$

where the product runs over all four spins surrounding a vertex within a given lattice plane. These vertex operators Z_{+} are defined in all three possible orientations, so at each vertex one has three operators Z_{+}, defined on the three different crosses + containing the respective vertex. Interestingly, the product of the three operators Z_{+} at each vertex equals identity as [244, 245]

$$\prod_{+\subset *} Z_{+} = \prod_{i \in *} (\sigma_i^z)^2 = \mathbb{1}\,, \tag{5.4}$$

where the star $*$ contains the six spins surrounding the vertex, and thus also the three differently oriented crosses + containing this vertex. Both types of operators are illustrated in Fig. 5.1. All these stabilizer operators commute mutually

$$[X_{\square}, X_{\square'}] = 0\,, \quad [X_{\square}, Z_{+}] = 0\,, \quad [Z_{+}, Z_{+'}] = 0\,. \tag{5.5}$$

As these operators are composed of Pauli matrices they have eigenvalues $x_{\square} \pm 1$ and $z_{+} = \pm 1$.

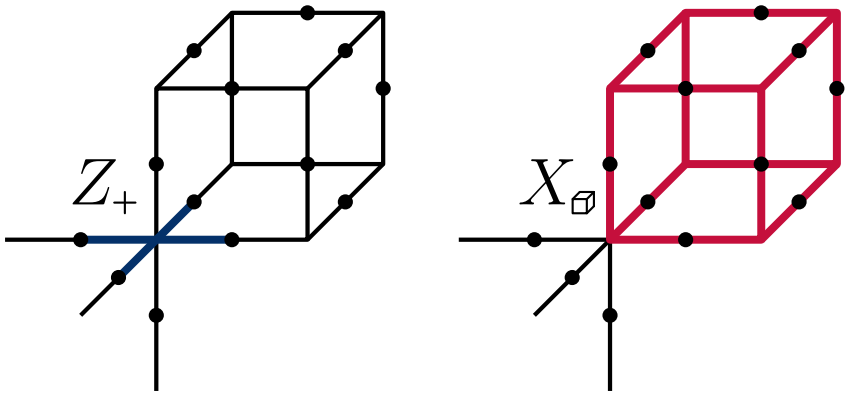

Figure 5.1: In the left (right) part of the image a vertex operator Z_{+} (cube operator $X_{\square}$) is illustrated. The respective operators act with σ^z (σ^x) on every spin which is touched by a blue (red) line. This figure is based on Fig. 1 in Ref. [118].

5.1.1 Ground state

A ground state $|\mathrm{GS}\rangle$ of the X-Cube model is an eigenstate of all operators $X_{\square}$, Z_{+} with eigenvalue $+1$, and can be constructed as [222]

$$|\mathrm{GS}\rangle = \mathcal{N} \prod_{\square} (1 + X_{\square}) \prod_{+} (1 + Z_{+}) \, |\Uparrow\rangle = \mathcal{N} \prod_{\square} (1 + X_{\square}) \, |\Uparrow\rangle \;, \tag{5.6}$$

where $|\Uparrow\rangle$ is a fully polarized state with all spins pointing in positive z-direction and $\mathcal{N}$ is a normalization factor. The degeneracy of this ground state depends on topological and geometrical properties of the system [26, 28, 29], e.g., on the $L \times L \times L$-torus it is [26, 28, 243]

$$\log_2(\mathrm{GSD}) = 6L - 3\,. \tag{5.7}$$

This result can be obtained by counting the number of independent logical operators [28, 243].

5.1.2 Excitations

Excitations can be created by acting with Pauli operators on the ground state [26]. Acting with σ_i^z on an eigenstate of the Hamiltonian (5.1) flips the eigenvalues $x_{\square}$ of the four cube operators $X_{\square}$ which contain the operator σ_i^x [39,221]. An eigenvalue $x_{\square} = -1$ corresponds to a fracton excitation [26]. While a fracton in isolation is unable to move (without creating additional excitations), aligned pairs of these fractons can move in the plane orthogonal to their alignment axis and adjacent pairs of these fractons are thus called planons [221, 222]. One the other hand, acting with σ_i^x on an eigenstate of the Hamiltonian (5.1) flips the eigenvalues z_{+} of all four operators Z_{+} which contain σ_i^z [39, 221]. Note that it is not possible that only one eigenvalue z_{+} at a given vertex of the cubic lattice equals -1 due to Eq. (5.4). Two eigenvalues $z_{+} = -1$ at a vertex correspond to an excitation, called lineon, which can only move along a straight line [26, 221, 222]. This straight line is given by the intersection of the planes containing the crosses + on which the operators Z_{+} with negative eigenvalues are defined [245]. Importantly, one distinguishes three types of lineons depending on the direction (x, y or z) in which they can move without creating additional excitations [30, 222, 245]. More generally, one can formulate non-trivial fusion rules for these lineon excitations [30, 222, 244]. Interestingly, there are pair configurations of adjacent lineons which are mobile in a plane and are also called planons [222]. Analogously to Ref. [222], we refer to cube excitations as magnetic excitations and vertex excitations as electric excitations when it is not clear from the context. Interestingly, these excitations obey a non-trivial mutual statistics. A simple process is a magnetic planon which moves around an (electric) lineon within the same plane and acquires a phase of π [26,28]. On the other hand, also electric planons can be moved around fracton excitations counting the number of negative $x_{\square}$-eigenvalues inside the enclosed volume [222].

5.2 The X-Cube model in a homogeneous magnetic field

In this section we consider the effect of an additional homogeneous magnetic field on the X-Cube model, which is reflected by the Hamiltonian

$$H^{\text{xcf}} = -J_{\square} \sum_{\square} X_{\square} - J_{+} \sum_{+} Z_{+} - \sum_{i} \vec{h} \cdot \vec{\sigma}_i \tag{5.8}$$

with $\vec{\sigma}_i = (\sigma_i^x, \sigma_i^y, \sigma_i^z)^T$. The additional magnetic field leads to quantum phase transitions between the fracton phase and the respective polarized phase [39, 84]. In [39] we investigated the cases $\vec{h} = (h_x, 0, 0)^T$ and $\vec{h} = (0, 0, h_z)^T$. We review these cases and extend some of the results making use of LCEs via hypergraph decompositions as introduced in Sect. 3.6 and Ref. [130]. Afterwards, we consider parallel fields, i.e., fields of the form $\vec{h} = (h_x, 0, h_z)$ as investigated in [84, 221]. For such parallel fields, series expansions for the excitation gaps of lineons and magnetic planons have been calculated about the limit of low fields [246]. In the case of parallel fields, the exotic mutual statistics of excitations has to be taken into account in the calculation of series expansions about the low-field limit [33,35,238]. How to setup a full hypergraph decomposition, which incorporates the exotic mutual statistics is explained in Chap. 4 and Ref. [23].

For series expansions about the high-field limit we align the quantization axis with the field direction, such that the unperturbed part is diagonal [238]. In general, the Hamiltonian in this basis results to be complicated due to the twelve-spin products in the operators $X_{\square}$. Notwithstanding, we manage to calculate series expansions up to order five for the ground-state energy using a full

hypergraph decomposition [118]. The phase diagram of the X-Cube model in a parallel magnetic field has been determined with QMC in Ref. [84]. For specific field directions, i.e., a field pointing in x- or z-direction, high-order series expansions have been derived [39], which are in good agreement with QMC data [247]. Nevertheless, we fail to obtain reliable results for the first-order phase transition in the general case of parallel fields, due to convergence issues of the series and because the high-field limit of general parallel magnetic fields is computationally challenging to approach with series expansions.

5.2.1 Specific field directions

Here we consider the specific field directions $\vec{h} = (h_x, 0, 0)^T$ and $\vec{h} = (0, 0, h_z)^T$, which have been extensively treated in Ref. [39]. Accordingly, this subsection is based on Ref. [39] in large parts. For these cases a first-order quantum phase transition occurs at $h_x/J_{\blacksquare} \approx 0.92$ or $h_z/J_{\blacksquare} \approx 0.29$ respectively [39, 84]. For these specific field directions, series expansions for the ground-state energy are relatively easy to tackle with LCEs as the mutual quasiparticle statistics do not play any role. This is due to the fact, that σ_i^x (σ_i^z) and thus also the field term commute with all operators $X_{\square}$ (Z_{+}). In the low-field limit, we are either in the sector without cube excitations or in the sector without vertex excitations, and in both cases one can find relatively simple dual descriptions [27,39], which we address below. In the high-field limit stabilizer operators with Pauli matrices parallel to the field direction act as identity on the polarized unperturbed ground state, and hence just result in a constant offset. Accordingly, for these field directions high-order series expansion results in good agreement with QMC data [247] are available [39].

Let us begin with the field which points in x-direction. In this case the Hamiltonian reads

$$H^{\text{xcx}} = -J_{\square} \sum_{\square} X_{\square} - J_{+} \sum_{+} Z_{+} - h_x \sum_i \sigma_i^x \,. \tag{5.9}$$

It is obvious that $[X_{\square}, \sigma_i^x] = 0 \; \forall i, \square$, so we concentrate on the sector where $x_{\square} = 1 \; \forall \square$. Due to the absence of cube excitations in this sector we do not need to consider any exotic mutual statistics of the excitations. The Hamiltonian in this sector reads

$$H^{\text{xcx}}_{x_{\square}=1} = -J_{\square} N_{\square} - J_{+} \sum_{+} Z_{+} - h_x \sum_i \sigma_i^x, \tag{5.10}$$

where $N_{\square}$ is the number of elementary cubes in the lattice. A given operator Z_{+} anticommutes with any σ^x acting on one of the spins affected by the operator Z_{+}.

Let us consider the case $h_x \gg J_{+}$, where we treat the term including the operators Z_{+} as perturbation and the field term as unperturbed part. The unperturbed ground state is given by the polarized state $|\Rightarrow\rangle$, where all spins are pointing in positive x-direction. A single spin flip is an elementary excitation of the unperturbed model with the energy $2h_x$. An operator Z_{+} acts on an unperturbed eigenstate by flipping all four σ^x-eigenvalues of the spins it acts on. We summarize these four eigenvalues as $\vec{m}^x$, and rewrite the action of Z_{+} on these eigenvalues as

$$Z_{+} \; : \quad |\vec{m}^x\rangle \quad \mapsto \quad |-\vec{m}^x\rangle \,. \tag{5.11}$$

For the perturbative expansion from the other limit $h_x \ll J_{+}$, we treat the field term as perturbation, and the Z_{+}-term as unperturbed part. The unperturbed ground state is characterized by $z_{+} = 1 \; \forall +$ and the elementary excitations of the unperturbed model are the lineons of the X-Cube

model. However, it is easier to denote the action of σ^x on an unperturbed eigenstate in terms of the eigenvalues z_{+}

$$\sigma_i^x \;:\quad |\vec{z}_{+}\rangle \quad\mapsto\quad |-\vec{z}_{+}\rangle\;, \tag{5.12}$$

where $\vec{z}_{+}$ denotes the four eigenvalues z_{+} at the crosses which contain the spin i. In terms of pseudospin operators an isospectral dual model reads [246]

$$H^{\text{xcx,dual}}_{x_{\square}=1} = -J_{\square}N_{\square} - J_{+}\sum_{+}\tau^z_{+} - h_x\sum_i\prod_{+\ni i}\tau^x_{+}\,, \tag{5.13}$$

where the τ^x_{+}, τ^z_{+} are the respective Pauli matrices. The eigenvalues of τ^z_{+} reflect the cube eigenvalues, and the four-pseudospin products in the second term represent the action of σ^x_i on the eigenvalues of the four adjacent vertex operators (which contain the spin i). Note that these dual mappings do not preserve the degeneracy of states, e.g., the unperturbed ground state of the dual model is unique on the torus, while the ground state of the X-Cube model is not.

Due to Eq. 5.4 the three z_{+} eigenvalues at a vertex can either all be equal to one or form one of three lineons where two of the eigenvalues z_{+} equal -1. In the language of lineons, acting with σ^x on a link pointing in direction α will fuse the actual state at each incident vertex with a lineon ℓ^α according to the fusion rules of lineons [243]

$$\ell^\alpha \times \ell^\beta = \begin{cases} \ell^\gamma & \text{if } \alpha \neq \beta \\ 1 & \text{if } \alpha = \beta\,, \end{cases} \tag{5.14}$$

where ℓ^α denotes a lineon which is able to move in direction α, γ is the direction orthogonal to α and β and 1 denotes no lineon. A dual model in terms of lineons can be found in Ref. [39].

Now let us consider the case where the magnetic field is pointing in z-direction. As the operators Z_{+} commute with all operators σ^z_i, we can concentrate on the sector $z_{+} = 1\ \forall{+}$ and rewrite the Hamiltonian in this sector as

$$H^{\text{xcz}}_{z_{+}=1} = -J_{\square}\sum_{\square} X_{\square} - J_{+}N_{+} - h_z\sum_i \sigma^z_i, \tag{5.15}$$

where $N_{+} = 3N_{\square}$ is the total number of operators Z_{+} in the system. Also in this case we discuss the action of the operators in the two limiting cases. For the case $h_z \gg J_{+}$ the field-term is the unperturbed part and the $X_{\square}$-term corresponds to the perturbation. The unperturbed ground state is a polarized state $|\Uparrow\rangle$ where all spins point in positive z-direction. The elementary excitation of the unperturbed model is again given by a single spin flip, which has energy $2h_z$. Acting with an operator $X_{\square}$ on an unperturbed eigenstate flips the σ^z-eigenvalues of all the twelve spins it acts on

$$X_{\square} \;:\quad |\vec{m}^z\rangle \quad\mapsto\quad |-\vec{m}^z\rangle\;, \tag{5.16}$$

where $\vec{m}^z$ labels the twelve σ^z-eigenvalues affected by the action of $X_{\square}$. Conversely, in the low-field limit the unperturbed part is the $X_{\square}$-term and the perturbation corresponds to the field-term. The unperturbed ground state is given by a state with $x_{\square} = 1\ \forall{\square}$ and an elementary excitation of the unperturbed model is a single fracton $x_{\square} = -1$. An operator σ^z_i acting on an unperturbed eigenstate flips all the four eigenvalues of the cube operators containing the site i

$$\sigma^z \;:\quad |\vec{x}_{\square}\rangle \quad\mapsto\quad |-\vec{x}_{\square}\rangle\;, \tag{5.17}$$

where $\vec{x}_{\square}$ stands for the eigenvalues of the four affected cube operators. Interestingly, up to a constant offset, the resulting isospectral dual model corresponds to the plaquette Ising model in a transverse field on the three dimensional cubic lattice [27]

$$H^{\text{xcz, dual}}_{z_{+}=1} = -J_{+}N_{+} - J_{\square}\sum_{i}\tau^{z}_{\square} - h_{z}\sum_{i}\prod_{\square\ni i}\tau^{x}_{\square}\,. \tag{5.18}$$

Again the pseudospin operators $\tau^{x}_{\square}, \tau^{z}_{\square}$ are Pauli matrices. The eigenvalues of $\tau^{z}_{\square}$ represent the cube eigenvalues, and the four-pseudospin products in the second term represent the action of σ^{z}_{i} on the eigenvalues of the four adjacent cube operators. With the hypergraph decomposition method [130] we manage to expand the available series expansions for the ground-state energy per site [39] significantly. For the field pointing in z-direction the low field limit can be deduced from the result for the plaquette Ising model obtained in Ref. [130] and Sect. 3.7. We give the series expansions together with the discussion of some details in App. A.2.

Let us conclude by briefly discussing selection rules for the clusters which need to be considered in an LCE via a full hypergraph decomposition. For the limit of a small field pointing in x-direction we can formulate a dual model in terms of lineons or in terms of z_{+} eigenvalues. As expected, the selection rules to reduce the number of clusters depend on the choice of the dual model. For the formulation in terms of lineons one can reduce the number of clusters using the fact that the perturbation has to act at least twice on every site in order to reobtain the unperturbed ground state. Furthermore, one can exploit that the perturbation has to act twice on bridges, which are bonds whose removal would lead to a disconnected cluster [108, 215]. This selection rule is also considered in Subsect. 3.5.4. Employing the formulation in terms of eigenvalues z_{+}, the perturbation has to act an even number of times on every site in order to get back to the unperturbed ground state. This also holds for both the high-field limit and the dual model for a field pointing in z-direction. For models with this property, very strict selection rules to sort out non-contributing clusters exist [97,99,130]. A description of these rules in the context of hypergraph decompositions is given in Subsect. 3.6.4 and Ref. [130]. Actually, for the high-field limit of the X-Cube model in a magnetic field pointing in z-direction only the clusters up to six bonds are relevant for a calculation of the ground-state energy up to order twelve due to the double-touch property mentioned in Ref. [39].

5.2.2 The X-Cube model in a parallel magnetic field

In the next step we investigate the X-Cube model in a parallel field. A phase diagram for this case has been obtained using QMC [84]. The Hamiltonian of the X-Cube model in a parallel magnetic field can be written as [84, 221]

$$H^{\text{xcp}} = -J_{\square}\sum_{\square} X_{\square} - J_{+}\sum_{+} Z_{+} - h_{x}\sum_{i}\sigma^{x}_{i} - h_{z}\sum_{i}\sigma^{z}_{i}\,. \tag{5.19}$$

Furthermore, we set $J_{\square} = J_{+} = J$ and $h = \sqrt{h_{x}^{2} + h_{z}^{2}}$ for the sake of simplicity. The perturbative limits we investigate are the low-field $h \ll J$ and the high-field limit $h \gg J$. In the low-field limit the exotic mutual statistics of the excitations has to be taken into account [33, 35, 238]. In the high-field limit one uses a rotation of the quantization axis to bring the Hamiltonian into a form where the field term is diagonal [238]. How to deal with these technical difficulties is already known from perturbative investigations of the two-dimensional toric code [33, 35, 238] and explained in large

detail in Ref. [238]. How to setup a full hypergraph decomposition for the low-field limit of the two-dimensional toric code in a parallel magnetic field is described in Ref. [23] and Sect. 4.2.

The low-field limit

In the low-field limit the unperturbed part of the Hamiltonian is given by

$$H_0 = -J \sum_{\square} X_{\square} - J \sum_{+} Z_{+} \,, \tag{5.20}$$

which has a discrete equidistant spectrum which is bounded from below. So the excitations in this spectrum can be interpreted as quasiparticles. The operators σ_i^x and σ_i^z create and annihilate these quasiparticles, depending on the state they act on. As in the case of specific field directions acting with σ_i^z on an unperturbed eigenstate flips the four adjacent $x_{\square}$ eigenvalues while σ_i^x flips the four adjacent z_{+} eigenvalues as described in Subsect. 5.2.1. However, we need to consider the interplay of the different perturbation operators, taking into account an additional spin background [33] as detailed in Ref. [238] and Sect. 4.2 to correctly take into account the mutual statistics of the excitations. Here, we use a full hypergraph decomposition [23, 130] to obtain the ground-state energy per spin of the original lattice

$$\begin{aligned} e_0(h_x, h_z) = &- \frac{4}{3} - \frac{h_x^2}{8} - \frac{h_z^2}{8} - \frac{11h_x^4}{1536} + \frac{h_x^2 h_z^2}{256} - \frac{113h_z^4}{1536} \\ &- \frac{349h_x^6}{221184} + \frac{353h_x^4 h_z^2}{491520} + \frac{205h_x^2 h_z^4}{24576} - \frac{21427h_z^6}{163840} \\ &- \frac{902473h_x^8}{1698693120} + \frac{3588071h_x^6 h_z^2}{14155776000} + \frac{1036909h_x^4 h_z^4}{619315200} + \frac{1129088161h_x^2 h_z^6}{49545216000} \\ &- \frac{879593848 93h_z^8}{254803968000} - \frac{13009537783h_x^{10}}{58706834227200} + \frac{44233090201h_x^8 h_z^2}{380507258880000} \\ &+ \frac{435920117618 59h_x^6 h_z^4}{69918208819200000} + \frac{141189499612457h_x^4 h_z^6}{34959104409600000} \\ &+ \frac{943259562859 51h_x^2 h_z^8}{1165303480320000} - \frac{115181804621864639h_z^{10}}{102736959897600000} \,. \end{aligned} \tag{5.21}$$

This series is obtained using pCUTs [103, 120] on 6826 non-isomorphic clusters with one up to ten bonds within a full hypergraph decomposition. We use selection rules as explained in Subsect. 3.6.4 adapted for the problem at hand to identify non-contributing clusters as early as possible. Note that, after proper adjustment of the units, the terms containing only h_x or only h_z correspond to the terms of the series of the magnetic field pointing in x- or z-direction, respectively given in App. A.2 which agree with the terms from Ref. [39]. In the case $h_x = h_z$ these results are in good agreement to QMC data for a system of $6 \times 6 \times 6$ cubes [247]. For comparison, the QMC data and the series are illustrated in Fig. 5.2 for the case $h_x = h_z$.

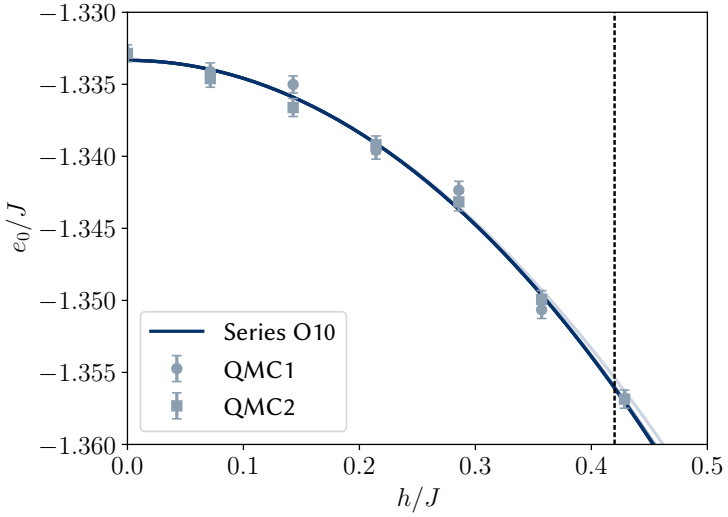

Figure 5.2: The ground-state energy per spin of the X-Cube model in a parallel magnetic field with $h_x = h_z$ and $h = \sqrt{h_x^2 + h_z^2}$. The different QMC datasets [247] correspond to different sweeps: QMC1 corresponds to a sweep from high to low fields, and QMC2 to a sweep in the opposite direction. The series is in good agreement with the QMC results and well convergent up to the phase transition point which is indicated by the dashed vertical line.

The high-field limit

For the X-Cube model in an parallel magnetic field the Hamiltonian can be written as

$$H^{\text{xcp}} = -J \sum_{\square} X_{\square} - J \sum_{+} Z_{+} - \sum_{i} \vec{h} \cdot \vec{\sigma}_i, \tag{5.22}$$

where $\vec{h} = (h_x, 0, h_z)^T$ and $\vec{\sigma}_i = (\sigma^x, \sigma^y, \sigma^z)^T$. Here we consider the perturbative limit of high magnetic fields $h \gg J$. We follow the idea of Ref. [238] and use a different basis of Pauli matrices

$$\tilde{\vec{\sigma}}_i = (\tilde{\sigma}_i^x, \tilde{\sigma}_i^y, \tilde{\sigma}_i^z)^T. \tag{5.23}$$

This basis is chosen such, that the unperturbed part of the Hamiltonian is diagonal

$$\vec{h} \cdot \vec{\sigma}_i = h\tilde{\sigma}_i^z \,. \tag{5.24}$$

Recalling that the vector $\vec{h}$ is in the xz-plane, it can be rewritten as

$$\vec{h} = h \cdot R_y(\varphi) \cdot \vec{e}_z = h \cdot \left[\cos(\varphi)\vec{e}_z + \sin(\varphi)\vec{e}_x \right], \tag{5.25}$$

where $R_y(\varphi)$ rotates a vector by an angle of φ around the y-axis

$$R_y(\varphi) = \begin{pmatrix} \cos(\varphi) & 0 & \sin(\varphi) \\ 0 & 1 & 0 \\ -\sin(\varphi) & 0 & \cos(\varphi) \end{pmatrix}. \tag{5.26}$$

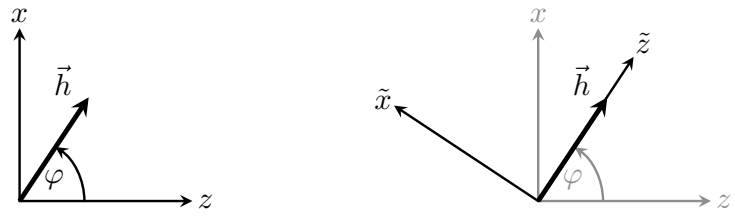

Figure 5.3: Illustration of the employed rotation to the coordinates (with tilde in the right part of the figure) where the field points in $\tilde{z}$-direction.

Applying this rotation to the canonical basis vectors gives a new rotated basis

$$\tilde{\vec{e}}_x = R_y(\varphi)\vec{e}_x = \cos(\varphi)\vec{e}_x - \sin(\varphi)\vec{e}_z \,, \tag{5.27}$$

$$\tilde{\vec{e}}_y = R_y(\varphi)\vec{e}_y = \vec{e}_y \,, \tag{5.28}$$

$$\tilde{\vec{e}}_z = R_y(\varphi)\vec{e}_z = \sin(\varphi)\vec{e}_x + \cos(\varphi)\vec{e}_z \,. \tag{5.29}$$

The Pauli matrices in this basis are defined by

$$\tilde{\sigma}_i^\alpha = \vec{e}_\alpha \cdot \vec{\sigma}_i \qquad \alpha \in \{x, y, z\} \,. \tag{5.30}$$

Using the inverse rotation $R_y^{-1}(\varphi)$ one obtains the Pauli operators σ_i^x, σ_i^z in terms of $\tilde{\sigma}_i^x, \tilde{\sigma}_i^z$

$$\sigma_i^z = \cos(\varphi)\tilde{\sigma}_i^z - \sin(\varphi)\tilde{\sigma}_i^x \,, \tag{5.31}$$

$$\sigma_i^x = \sin(\varphi)\tilde{\sigma}_i^z + \cos(\varphi)\tilde{\sigma}_i^x \,. \tag{5.32}$$

Now, we can replace the operators σ_i^x and σ_i^z in the Hamiltonian by the above expressions. By construction, the field term becomes diagonal. This gives rise to a new unperturbed basis, which consists of product states of eigenstates of $\tilde{\sigma}_i^z$. We denote the eigenstates of $\tilde{\sigma}_i^z$ associated with the eigenvalue $+1$ by $|\uparrow\rangle$ and the eigenstate with the negative eigenvalue -1 by $|\downarrow\rangle$. For the product states we employ the conventional notation

$$|\uparrow\downarrow \ldots \downarrow\rangle = |\uparrow\rangle \otimes |\downarrow\rangle \otimes \ldots \otimes |\uparrow\rangle \,. \tag{5.33}$$

For a given basis state $|\Psi\rangle$ we write $\tilde{s}_i^z(\Psi)$ to refer to the eigenvalue of $\tilde{\sigma}_i^z$ of this state

$$\tilde{\sigma}_i^z |\Psi\rangle = \tilde{s}_i^z(\Psi) |\Psi\rangle \,. \tag{5.34}$$

In contrast to the field term, the operators $X_{\square}$ and Z_{+}, which act as local perturbations, become more complicated. They are obtained inserting the respective expressions in Eqs. (5.31) and (5.32) for σ_i^x and σ_i^z in the operators $X_{\square}$ and Z_{+}

$$X_{\square} = \prod_{i \in \square} \sigma_i^x = \prod_{i \in \square} \left[\sin(\varphi)\tilde{\sigma}_i^z + \cos(\varphi)\tilde{\sigma}_i^x\right] \,, \tag{5.35}$$

$$Z_{+} = \prod_{i \in +} \sigma_i^z = \prod_{i \in +} \left[\cos(\varphi)\tilde{\sigma}_i^z - \sin(\varphi)\tilde{\sigma}_i^x\right] \,. \tag{5.36}$$

Let us now consider the matrix elements of the operators $X_{\square}$ and Z_{+} with respect to product states in the $\tilde{\sigma}^z$ basis which involve only the sites the respective operator $X_{\square}$ or Z_{+} acts on. These states are defined on twelve sites for $X_{\square}$ and on four sites for Z_{+}. Importantly, in both cases any such basis state is mapped to each of these basis states at the respective bond. For twelve spins on the edges of a cube any of the 2^{12} basis states is mapped to each of these 2^{12} basis states by the action of the respective operator $X_{\square}$. This means that for $X_{\square}$ we have $2^{24} = 16777216$ such matrix elements at a single cube. Instead, Z_{+} has only $2^8 = 256$ matrix elements at a single cross.

As a next step, we assign the correct amplitudes to these matrix elements of the operators $X_{\square}$ and Z_{+}. First, we consider the matrix element $\langle \Phi^{\square} | X_{\square} | \Psi^{\square} \rangle$ where $|\Phi^{\square}\rangle$ and $|\Psi^{\square}\rangle$ are unperturbed eigenstates defined on the twelve sites $X_{\square}$ acts on. The amplitude of a matrix element of $X_{\square}$ with respect to these states reads

$$\langle \Phi^{\square} | X_{\square} | \Psi^{\square} \rangle = (-1)^{a_1} \sin^{a_2}(\varphi) \cos^{a_3}(\varphi) \,, \tag{5.37}$$

where a_1 is the number of sites $i \in \square$ with

$$\tilde{s}_i^z(\Phi^{\square}) = \tilde{s}_i^z(\Psi^{\square}) = -1 \,. \tag{5.38}$$

Similarly, a_2 is the number of sites $i \in \square$ which fulfill

$$\tilde{s}_i^z(\Phi^{\square}) = \tilde{s}_i^z(\Psi^{\square}) \tag{5.39}$$

and a_3 counts the number of sites $i \in \square$ for which

$$\tilde{s}_i^z(\Phi^{\square}) \neq \tilde{s}_i^z(\Psi^{\square}) \,. \tag{5.40}$$

For the local matrix element $\langle \Psi^{+} | Z_{+} | \Phi^{+} \rangle$, with the unperturbed eigenstates $|\Phi^{+}\rangle$ and $|\Psi^{+}\rangle$ on the four sites where the operator Z_{+} acts, one can write the amplitude as

$$\langle \Phi^{+} | Z_{+} | \Psi^{+} \rangle = (-1)^{a_4 + a_5} \sin^{a_5}(\varphi) \cos^{a_6}(\varphi) \,, \tag{5.41}$$

where a_4 is the number of sites $i \in +$ which obey

$$\tilde{s}_i^z(\Phi^{+}) = \tilde{s}_i^z(\Psi^{+}) = -1 \,. \tag{5.42}$$

Similarly, a_5 is the number of sites $i \in +$ with

$$\tilde{s}_i^z(\Phi^{+}) \neq \tilde{s}_i^z(\Psi^{+}) \tag{5.43}$$

and a_6 counts the number of sites $i \in +$ which fulfill

$$\tilde{s}_i^z(\Phi^{+}) = \tilde{s}_i^z(\Psi^{+}) \,. \tag{5.44}$$

These amplitudes can be implemented into a computer program to obtain the local perturbation operators $\mathcal{T}_{n,b}$ and $\mathcal{V}_b$.

From the vast number of local matrix elements within the operators $X_{\square}$ in the rotated $\tilde{\sigma}^z$ basis it is clear that the problem is difficult to tackle directly even when using an LCE via a full hypergraph decomposition. One quickly notes that most of the clusters have many sites which are only

contained in one bond, and the resulting vertices in the König representation have only degree one. We refer to these sites as *open sites* and to the respective vertices as *open vertices*.

Now, we define a set of permutations Π of the open sites of a cluster with the constraint that sites are only mapped to sites within the same bond. Importantly, all the other sites are not affected. We define the action of a permutation $\rho \in \Pi$ on a product state $|\Psi\rangle$ as

$$\rho\,|\Psi\rangle = \rho\,(|\Psi_0\rangle \otimes \ldots \otimes |\Psi_n\rangle) = |\Psi_{\rho(0)}\rangle \otimes \ldots \otimes |\Psi_{\rho(n)}\rangle\ . \tag{5.45}$$

where $\rho(i)$ obeys $\rho(i) = i$ for all sites which are contained in more than one bond, while for all open sites $i \in b$ implies $\rho(i) \in b$.

Interestingly, these permutations commute with the local unperturbed Hamiltonian $H_{0,i}$, all the operators $\mathcal{T}_{n,b}$, and hence, also the perturbation operators $\mathcal{V}_b$. Indeed, one can consider the amplitudes 5.37 and 5.41 and convince oneself that

$$\langle\Phi^{\blacksquare}|\,\rho^\dagger X_{\blacksquare}\rho\,|\Psi^{\blacksquare}\rangle = \langle\Phi^{\blacksquare}|\,X_{\blacksquare}\,|\Psi^{\blacksquare}\rangle\ , \quad \langle\Phi^{+}|\,\rho^\dagger Z_{+}\rho\,|\Psi^{+}\rangle = \langle\Phi^{+}|\,Z_{+}\,|\Psi^{+}\rangle \quad \forall\rho\in\Pi\,, \tag{5.46}$$

by observing that a permutation $\rho \in \Pi$ acting to the left and right states of the expressions in Eqs. 5.37 and 5.41 does neither affect the change in the number of quasiparticles nor the numbers a_1 to a_6. On the level of the operators $\mathcal{T}_{n,b}$ this leads to

$$\langle\Phi^b|\,\rho^\dagger\mathcal{T}_{n,b}\rho\,|\Psi^b\rangle = \langle\Phi^b|\,\mathcal{T}_{n,b}\,|\Psi^b\rangle\ , \tag{5.47}$$

where again the superscript b on the states indicate that they are defined only on the sites contained in the bond b. The action of an operator $\mathcal{T}_{n,b}$ on a state $\rho\,|\Psi^b\rangle$ results in

$$\mathcal{T}_{n,b}\rho\,|\Psi^b\rangle = \sum_{\Phi^b}\rho\,|\Phi^b\rangle\,\langle\Phi^b|\,\rho^\dagger\mathcal{T}_{n,b}\rho\,|\Psi^b\rangle \overset{(5.47)}{=} \rho\sum_{\Phi^b}|\Phi^b\rangle\,\langle\Phi^b|\,\mathcal{T}_{n,b}\,|\Psi^b\rangle = \rho\mathcal{T}_{n,b}\,|\Psi^b\rangle\ , \tag{5.48}$$

which shows that $\mathcal{T}_{n,b}$, and hence also $\mathcal{V}_b$, commutes with all permutations in Π. Note that the permutations do not affect the sites which are contained in multiple bonds, so this result also extends to clusters consisting of multiple bonds.

The fully polarized unperturbed ground state is obviously an eigenstate of all permutations $\rho \in \Pi$ with eigenvalue $+1$. Note that the permutations do not necessarily commute among each other, so in general it is not possible to find a common eigenbasis for all the permutations in Π. However, as all operators $\mathcal{T}_{n,b}$, $\mathcal{V}_b$ and $H_{0,i}$ commute with all permutations in Π the eigenvalue of each permutation ρ is conserved by the perturbative processes. Consequently, we can execute perturbation theory calculations for the ground-state energy solely in terms of states which are eigenstates of every $\rho \in \Pi$ with eigenvalue $+1$. These states read

$$|\Pi(\Psi)\rangle = \mathcal{N}\sum_{\rho\in\Pi}\rho\,|\Psi\rangle\,, \tag{5.49}$$

where $|\Psi\rangle$ is a product state in the $\tilde{\sigma}^z$-basis, on a finite cluster and $\mathcal{N}$ is a normalization constant. Evaluating this for all product states in the $\tilde{\sigma}^z$-basis obviously results in duplicate states. In fact it is sufficient to consider one representative state for each Π-*equivalence class* of states. We refer to two basis states as Π-*equivalent* states if they can be obtained from each other via a permutation in Π. To be as concrete as possible let us consider the cluster given in Fig. 5.4. We label the states on this cluster by a product state in the $\tilde{\sigma}^z$-basis. We denote a permutation ρ explicitly as

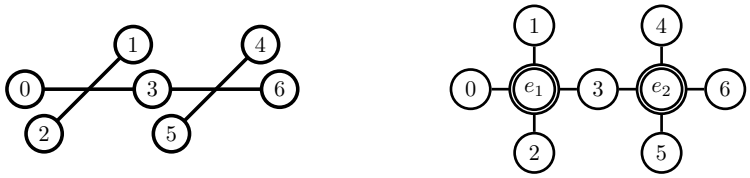

Figure 5.4: In the left part of the image a cluster consisting of two four-spin bonds which we use as an example in order to explain how we use the symmetries of the clusters. The König representation of the cluster is given in the right part.

$(\rho(0), \rho(1), \dots \rho(6))$, where we specify the image of all sites under ρ for the sake of readability. Recall, that the operator ρ acts on the basis states assigning the local state at site $\rho(i)$ to site i. As an example we define the states

$$|1;0\rangle := |\downarrow\uparrow\uparrow\uparrow\uparrow\uparrow\uparrow\rangle \ , \quad |1;1\rangle := |\uparrow\downarrow\uparrow\uparrow\uparrow\uparrow\uparrow\rangle \ , \quad |1;2\rangle := |\uparrow\uparrow\downarrow\uparrow\uparrow\uparrow\uparrow\rangle \ . \tag{5.50}$$

Now, consider the permutations of open vertices such that these are always mapped to open vertices at the same bond. These permute the sites $0, 1, 2$ as well as the sites $4, 5, 6$ among each other. The sites $4, 5, 6$ do not host any excitation, within the states $|1;0\rangle, |1;1\rangle, |1;2\rangle$ so any permutation on them leaves the states invariant. So we concentrate on the sites $1, 2, 3$ and keep the sites $3, 4, 5, 6$ fixed. For these permutations the resulting states are given in Tab. 5.1. The eigenstates

Permutation ρ	$\rho\,\|1;0\rangle$	$\rho\,\|1;1\rangle$	$\rho\,\|1;2\rangle$
$(0,1,2,3,4,5,6)$	$\|1;0\rangle$	$\|1;1\rangle$	$\|1;2\rangle$
$(0,2,1,3,4,5,6)$	$\|1;0\rangle$	$\|1;2\rangle$	$\|1;1\rangle$
$(1,0,2,3,4,5,6)$	$\|1;1\rangle$	$\|1;0\rangle$	$\|1;2\rangle$
$(2,0,1,3,4,5,6)$	$\|1;2\rangle$	$\|1;0\rangle$	$\|1;1\rangle$
$(2,1,0,3,4,5,6)$	$\|1;2\rangle$	$\|1;1\rangle$	$\|1;0\rangle$
$(1,2,0,3,4,5,6)$	$\|1;1\rangle$	$\|1;2\rangle$	$\|1;0\rangle$

Table 5.1: The permutations which fix the sites $3, 4, 5, 6$, together with the states resulting after the permutation. In the following columns we give the states which result from the action of ρ on the respective state.

(5.49) with eigenvalue $+1$ of the permutations are basically the sum over any of the columns $\rho\,|1;i\rangle$ in Tab. 5.1 with an appropriate normalization.

Next, we represent the states $|1;0\rangle, |1;1\rangle$, and $|1;2\rangle$ as graphs. To this sake we use the König representation of the cluster and color occupied vertices in orange. The representations of the Π-equivalent states $|1;0\rangle, |1;1\rangle$ and $|1;2\rangle$ are given in Fig. 5.5. Note, that these Π-equivalent states coincide on all sites except the open sites and the number of occupied open sites coincides for all bonds. For the problem of the X-Cube model in a magnetic field in the limit of high fields a single

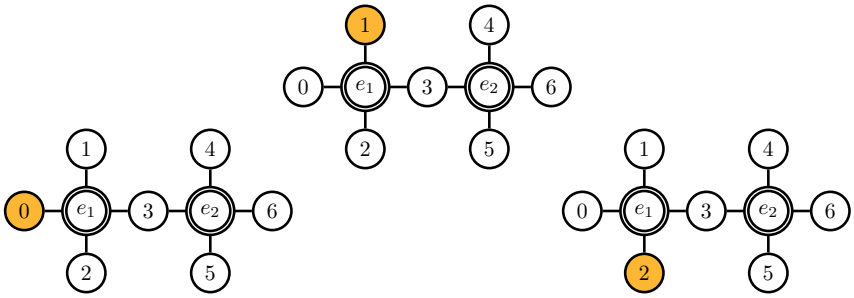

Figure 5.5: The three states $|1;0\rangle$, $|1;1\rangle$, and $|1;2\rangle$ are represented by isomorphic graphs.

bond can have up to twelve open sites, and even in connected clusters consisting of multiple bonds a single bond can have eleven open sites. As an example consider that the number of basis states with five excitations at the open sites of such a bond (and no excitations elsewhere) is already 462. Now consider the perturbation acting on the ground state. As the operators $\mathcal{T}_{n,b}$ commute with the permutations ρ, the action of the perturbation will result in an equal amplitude superposition of all states within the class, and any intermediate state in perturbation theory is an eigenstate of all these permutations with eigenvalue $+1$, like the ground state.

As we did the perturbative calculation of the ground-state energy with pCUT, it might be instructive to consider a simple example, namely the evaluation of the ground-state expectation value of the operator sequence $\mathcal{T}_{-1,b}\mathcal{T}_{1,b}$ on a single cross ($b = +$) with sites $0, 1, 2$ and 3. Using the normalized symmetric states

$$|\Pi(1;i)\rangle \equiv |\Pi(1)\rangle = \frac{1}{2}\sum_{i=0}^{3}|1;i\rangle \quad \forall i. \tag{5.51}$$

the expectation value can be written as

$$\begin{aligned}\langle 0|\,\mathcal{T}_{-1,+}\mathcal{T}_{1,+}\,|0\rangle = &\left[\sum_{i=0}^{3}A^*\,\langle 1;i|\right]\left[\sum_{i=0}^{3}A\,|1;i\rangle\right]\\ =&2A^*\,\langle\Pi(1)|\,2A\,|\Pi(1)\rangle\\ =&4|A|^2\,,\end{aligned} \tag{5.52}$$

where $A \in \mathbb{C}$ is a complex number and A^* denotes its complex conjugate. From a practical perspective we define canonical representative basis states for the Π-equivalence classes. When we act with the perturbation to the right all Π-equivalent basis states, which result from the action of the perturbation, are cast to the same canonical basis state, reducing the number of basis states in the resulting superposition. The left action of the perturbation is executed normally, without this procedure. In the resulting state on the right side the amplitude of any canonical basis state is actually the sum of the amplitudes of all the states within the class it represents. Whereas on the left side, all Π-equivalent basis states have the same amplitude because the resulting state must be an eigenstate of all permutations in Π with eigenvalue $+1$. Accordingly, accumulating all the amplitudes in one representative basis state for each Π-equivalence class on the right side does not

affect the outcome of the scalar product. In the example above this looks like

$$\begin{aligned}\langle 0|\, \mathcal{T}_{-1,+}\mathcal{T}_{1,+}\, |0\rangle &= \left[\sum_{i=0}^{3} A^* \langle 1;i|\right]\left[\sum_{i=0}^{3} A\, |1;i\rangle\right] \\ &= \left[\sum_{i=0}^{3} A^* \langle 1;i|\right]\cdot 4A\, |1;0\rangle \\ &= 4|A|^2.\end{aligned} \tag{5.53}$$

In the first line we consider the normal action of the operators $\mathcal{T}_{n,+}$ to both sides. Then we replace all states $|1;i\rangle$ by the representative state $|1;0\rangle$, as described for right actions of the operators $\mathcal{T}_{n,+}$, which leads to the same result. In our implementation, we do not cast the resulting basis states to the representative basis states for the last action of an operator $\mathcal{T}_{n,b}$ before taking the scalar product, in order to keep the implementation simple.

With this exploitation of the symmetry we manage to obtain a series expansion for the ground-state energy e_0/h about the high-field limit up to order five in J/h with pCUTs [103,120] and a full hypergraph decomposition [130], which is already remarkable for such a complicated problem. Although it is possible to obtain series expansions as a function of the angle φ we restrict the discussion here to the results for $h_x = h_z$ with $h = \sqrt{h_x^2 + h_z^2}$. The series for general φ can be found in [248]. For this case the ground-state energy $e_0/J = e_0/h \cdot h/J$ per spin reads

$$\begin{aligned}e_0/J = &\frac{3451108380478794155560524767624561079 49J^4}{1419160244849872849986524977456742400 00h^4} \\ &-\frac{1084981903155727091990353J^3}{3585688399999081119744000h^3} \\ &-\frac{805704681223949J^2}{1208586181017600h^2} - \frac{90085675J}{136249344h} - \frac{49}{192} - \frac{h}{J}.\end{aligned} \tag{5.54}$$

However, this series diverges long before it approaches the phase transition point at $h/J \approx 0.42$ [84]. Hence, determining the intersection of the obtained series for the low-field and high-field limit in order to find the phase transition point is not reasonable, and thus we cannot extract any information about a possible phase transition. An illustration of the series together with QMC data obtained for a system of $6 \times 6 \times 6$ cubes [247] can be found in Fig. 5.6. It is apparent that the convergence of the series is not sufficiently good to get reliable information about the ground-state energy in the vicinity of the phase transition. However, one also notes that in the region where the series starts to strongly diverge also the sweeps of QMC do not agree any more, which indicates that also for QMC obtaining the ground-state energy in this domain is challenging.

5.2.3 Summary and discussion

For the case $h_x = h_z$ the obtained series expansions are illustrated in Fig. 5.7. This figure also includes QMC data for a system of $6 \times 6 \times 6$ cubes [247]. Actually, the series results fit quite well to the QMC data in the limiting cases, so it seems improbable that the series result are flawed by a mistake. In particular the convergence of the low-field series as well as its agreement with the QMC data is good from $h = 0$ up to the phase transition as illustrated in Fig. 5.2. Unfortunately, the series about the high-field limit does not converge well, as illustrated in Fig. 5.6. In the domain where the series expansions are badly behaved one also notes that the two different QMC sweeps do not

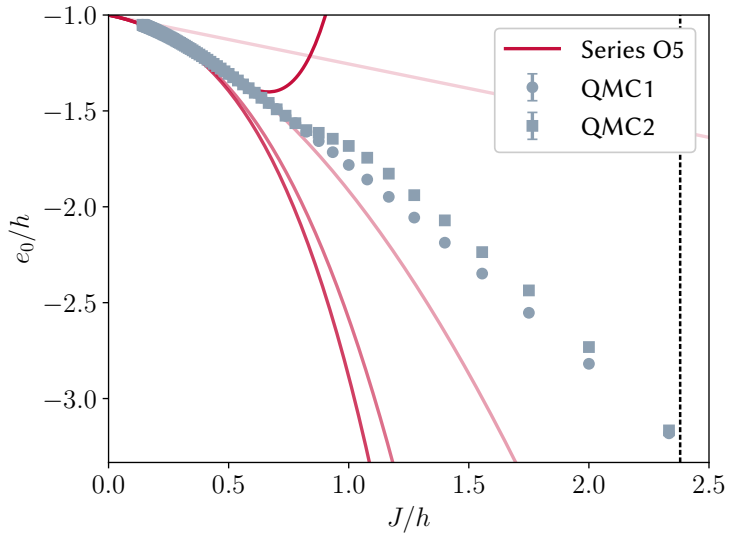

Figure 5.6: The high-field series for the ground-state energy per spin for $h_x = h_z$ as a function of the original perturbation parameter J/h. The series from order five to order one are shown with decreasing opacity. The series results start to diverge already far away from the phase transition point, indicated by the vertical dashed line. The QMC datasets [247] correspond to different sweeps: QMC1 corresponds to a sweep from high to low fields, and QMC2 to a sweep in the opposite direction. The vertical dashed line indicates the phase transition, which occurs at $h/J \approx 0.42$ [84].

agree. With the calculated perturbation order only one of the Padé extrapolants where both, the denominator and the numerator degree, are larger than one is non-defective. This is the diagonal Padé extrapolant where the degrees of the numerator and denominator both equal two. However, it still fails to correctly capture the ground-state energy, as shown in Fig. 5.7. Note that order five is a very low order for a Padé analysis and there is only a very limited amount of reasonable Padé extrapolations.

It is difficult to quantify the deviation of the series from the correct ground-state energy in the limiting cases due to the statistical error of the QMC data. To further check the correctness of our approach, we calculate the ground-state energy about the high-field limit for $h_x = h_z$ on a cluster which consists of a cube ⧈ and a cross + which share two spins with pCUT up to order six in J/h as well as with ED. As this cluster has only 14 sites, an ED calculation for the ground-state energy is easily feasible. Here, we used an ARPACK wrapper provided by the python library scipy to obtain the smallest eigenvalue of the matrix representing the cluster Hamiltonian. Importantly, while the series expansion for the ground-state energy on this cluster is obtained in the rotated $\tilde{\sigma}^z$-basis, we perform the ED calculations in the original σ^z-basis. We plot the absolute difference $|E_0^{\mathrm{SE}} - E_0^{\mathrm{ED}}|$ between the ground-state energy obtained with series expansions and the ED results in Fig. 5.8. for small values of J/h one observes numerical noise, as the deviation of the series from the ED results is extremely small. For slightly larger values of J/h we obtain a straight line in the double logarithmic plot in Fig. 5.8. The slope of this straight line indicates that the dominating deviations

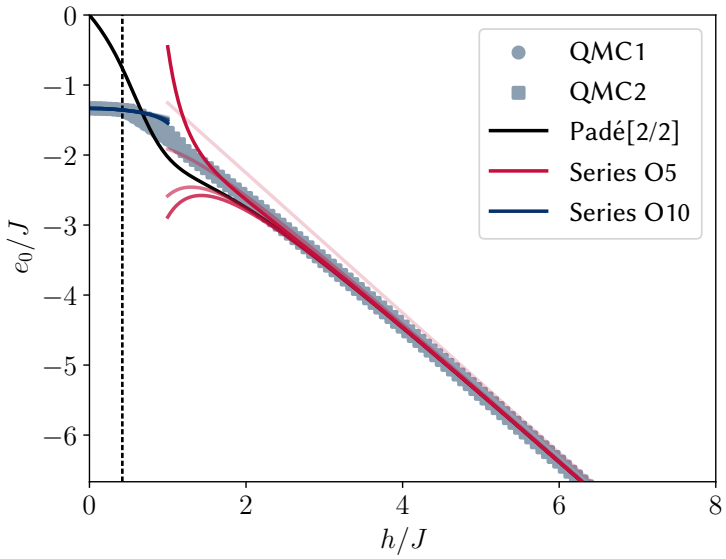

Figure 5.7: The ground-state energy per spin of the X-Cube model in a parallel magnetic field with $h_x = h_z$ and $h = \sqrt{h_x^2 + h_z^2}$. The QMC datasets [247] correspond to different sweeps: QMC1 corresponds to a sweep from high to low fields, and QMC2 to a sweep in the opposite direction. The vertical dashed line indicates the phase transition, which occurs at $h/J \approx 0.42$ [84].

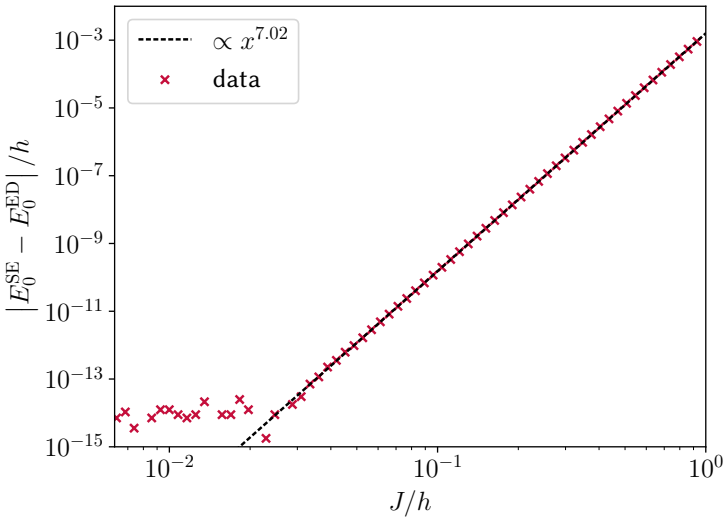

Figure 5.8: The absolute difference between the ground-state energy obtained with ED and the ground-state energy determined with series expansions for the cluster described in the main text.

of the two approaches close to zero are of order seven in J/h, and hence, that the series expansion on the finite cluster appears to be correct up to order six.

This check on a small finite system confirms the implementation of the model in the $\tilde{\sigma}^z$-basis for the perturbation theory calculations. As a consequence, we attribute the significant deviations of the high-field series in the thermodynamic limit from the QMC results to convergence issues of the series. Unfortunately, obtaining the series up to order six is not computationally feasible with the series expansion approach presented here. In contrast, we are convinced that deriving a series expansion up to order five for this challenging problem is a notable achievement. The low-field series is in good agreement with the received QMC data [247]. However, as we need to determine the intersection with the high-field series, the bad convergence of the latter prevents us from determining the phase transition point. For the cases, where the magnetic field is pointing either in x- or z-direction we managed to extend the known series [39] for the ground-state energy in the low- and high-field limit from order six or order eight, respectively, to order twelve. Note that in these cases already the previously known series are in good agreement with QMC data [39, 247] in the respective domains and suffice to determine the corresponding first-order phase transition points quantitatively with good accuracy [39].

Chapter 6

Competing topological orders in three dimensions

This chapter basically reproduces the content of Ref. [118]. However, the parts about variational approaches presented in this chapter are not contained in Ref. [118]. Nevertheless, we actually investigated variational approaches to the problem, during the work on this project. The corresponding variational calculations were done by M. R. Walther and me under the supervision of K. P. Schmidt and J. Vidal. So, also the variational calculations and results presented in this chapter should be regarded as an outcome of this collaboration.

In this chapter we study the competition between the fractonic X-Cube model [26] and the topologically ordered 3D toric code [19, 20]. We compute high-order series expansions from different starting points in order to obtain a full phase diagram. This phase diagram features four different phases, the fractonic order of the X-Cube model (XC-phase), the topologically ordered 3D toric-code phase (TC-phase), and two further phases. In the respective limiting case these two phases have an x- or z-polarized ground-state, and thus we call them X- and Z-phase respectively. All phase transitions are found to be first order. The ground-states of these phases are in general not unique but they feature a sub-extensive degeneracy. In all four limiting cases degenerate ground states are separated by non-local logical operators [28, 118, 249].

We begin this chapter by briefly reviewing the basic properties of the 3D toric code [19, 20, 38, 249]. An introduction to the X-Cube model can be found in Sect. 5.1. After this we investigate the full model, starting with a decomposition of the full Hamiltonian into two commuting parts. This results in two different Hamiltonians which we can treat separately. Next, we perturbatively calculate the ground-state energy of these Hamiltonians about the limiting cases, and show that also in the X- and Z-phase different degenerate ground states are separated by non-local operators. As a consequence, we can do the perturbative calculations on finite systems such that the ground-state degeneracy is not lifted up to the desired perturbation order and the degenerate ground states are well separated, in the sense that there are no matrix elements between different ground states within the effective Hamiltonian. For the perturbative treatment of the ground-state energy we introduce dual models which actually have a unique ground state. The resulting perturbative problems are then suited for linked-cluster expansions (LCEs) via a full hypergraph decomposition as presented in Ref. [130] and Sect. 3.6. To integrate the perturbative result we also treat the ground-

state energy by variational methods as described in Ref. [250]. Finally, we conclude the chapter by presenting and discussing the results of both approaches.

6.1 The 3D toric code

The 3D toric code [19, 20] is defined on a cubic lattice with spin-$1/2$ degrees of freedom located at the edges of the lattice. The Hamiltonian reads

$$H^{\mathrm{tc}} = -J_{\text{✱}} \sum_{\text{✱}} Z_{\text{✱}} - J_{\square} \sum_{\square} X_{\square} \,, \tag{6.1}$$

where the six-spin star operators $Z_{\text{✱}}$ are defined as follows

$$Z_{\text{✱}} = \prod_{i \in \text{✱}} \sigma_i^z, \tag{6.2}$$

and the product runs over the six spins surrounding a vertex of the cubic lattice. The four-spin plaquette operators read

$$X_{\square} = \prod_{i \in \square} \sigma_i^x \,, \tag{6.3}$$

where the product runs over the spins at the edges of a plaquette. The operators $X_{\square}$ and $Z_{\text{✱}}$ are visualized in Fig. 6.1. Note that in the literature one typically finds a different convention for the

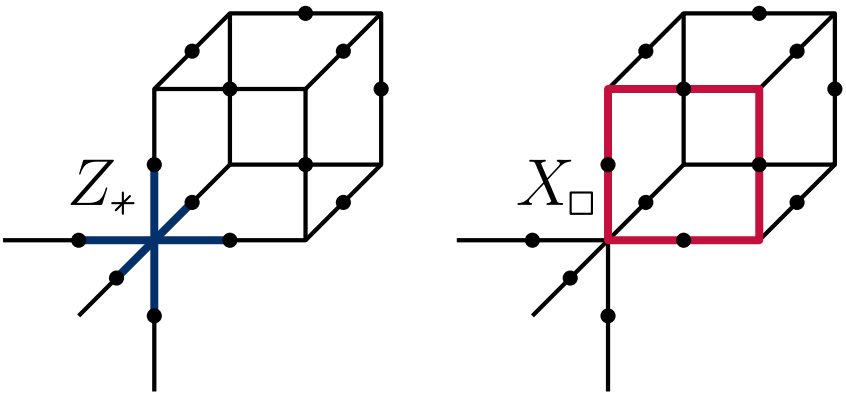

Figure 6.1: In the left (right) part a star operator $Z_{\text{✱}}$ (plaquette operator $X_{\square}$) is illustrated. The respective operators act with σ^z (σ^x) on every spin which is touched by a blue (red) line. This figure is based on Fig. 1 in Ref. [118].

operators ($\sigma^x \leftrightarrow \sigma^z$) [20, 38, 118]. As the operators $X_{\square}$ and $Z_{\text{✱}}$ are products of Pauli matrices, and hence, square to identity, they have eigenvalues $x_{\square} = \pm 1$ and $z_{\text{✱}} = \pm 1$ [38]. Furthermore, all these operators commute mutually

$$[Z_{\text{✱}}, Z_{\text{✱}'}] = 0 \,, \quad [X_{\square}, Z_{\text{✱}}] = 0 \,, \quad [X_{\square}, X_{\square'}] = 0 \,. \tag{6.4}$$

as the intersection of stars and plaquettes can contain either zero or two sites [38]. As a consequence, a ground-state can be written as [38]

$$|\mathrm{GS}\rangle = \mathcal{N} \prod_{\square} (1 + X_{\square}) \prod_{\text{✱}} (1 + Z_{\text{✱}}) \, |\Uparrow\rangle = \mathcal{N} \prod_{\square} (1 + X_{\square}) \, |\Uparrow\rangle \ , \tag{6.5}$$

where $\mathcal{N}$ is a normalization constant and $|\Uparrow\rangle$ is a fully polarized state with all spins pointing in positive z-direction. The ground-state features a non-vanishing topological entanglement entropy [38, 249]. The ground-state degeneracy depends on the real space topology of the system, where different ground-state sectors are distinguished by eigenvalues of non-local operators [249]. Furthermore, the excitations of the model feature exotic mutual statistics [38].

6.2 Competition between the X-Cube model and the 3D toric code

In order to investigate the competition between the fractonic X-Cube model and the 3D toric code we first combine the Hamiltonians of both models [118]

$$H = H^{\mathrm{xc}} + H^{\mathrm{tc}} = -J_{\square} \sum X_{\square} - J_{+} \sum_{+} Z_{+} - J_{*} \sum_{*} Z_{*} - J_{\square} \sum_{\square} X_{\square} \,, \tag{6.6}$$

where we assume all coupling constants $J_{\square}$, J_{+}, J_{*} and $J_{\square}$ to be non-negative. Due to consistency with the definition of the X-Cube model in Sect. 5.1 the choice within this thesis is different than in the original publication [118]. Concretely, σ^x and σ^z have been exchanged, which just corresponds to a rotation of the quantization axis and does not alter the physical results.

Note that there are several possibilities to choose the flavors of the Pauli matrices within the stabilizer operators. The presented choice contains only operators which are products of σ^x or σ^z. Furthermore, it is interesting that the operators Z_{+} and $X_{\square}$ form layers of 2D toric codes.

As a first step we recall that all operators belonging to the same model commute with each other

$$[X_{*}, Z_{\square}] = 0 \,, \quad [X_{\square}, Z_{+}] = 0 \,, \tag{6.7}$$

as well as all the operators which are composed of the same type of Pauli matrices

$$[Z_{*}, Z_{+}] = 0 \,, \quad [X_{\square}, X_{\square}] = 0 \,. \tag{6.8}$$

Indeed, the only operators which do not generally commute are

$$[Z_{*}, X_{\square}] \neq 0 \,, \quad [X_{\square}, Z_{+}] \neq 0 \,. \tag{6.9}$$

More precisely, a commutator of the form $[Z_{*}, X_{\square}]$ is nonzero if the $*$ and $\square$ overlap, while a commutator of the form $[X_{\square}, Z_{+}]$ is nonzero if $\square$ and $+$ overlap in a single spin, i.e., they overlap and are not in the same plane. If they are in the same plane they always commute. As a consequence, we can decompose the Hamiltonian into two commuting parts H_A and H_B

$$H = H_A + H_B \,, \qquad [H_A, H_B] = 0 \,, \tag{6.10}$$

with the two Hamiltonians

$$H_A = -J_{\square} \sum_{\square} X_{\square} - J_{*} \sum_{*} Z_{*}, \tag{6.11}$$

$$H_B = -J_{\square} \sum_{\square} X_{\square} - J_{+} \sum_{+} Z_{+}. \tag{6.12}$$

We aim to treat the Hamiltonians H_A and H_B separately using a hypergraph decomposition [130] as introduced in Sect. 3.6 and a variational approach [250] to obtain the ground-state energies per cube e_0^A and e_0^B of the Hamiltonians H_A and H_B. For both Hamiltonians we consider both limiting cases, where one of the couplings is zero and the other one is finite, as perturbative starting points. For the perturbative studies we define isospectral dual models for these cases in Sect. 6.4. Obviously, these dual models do not take into account degeneracies. So we give arguments that the degenerate ground states are not coupled in the perturbative orders we investigate.

6.3 Ground-state degeneracies

For the topological and the fracton phase which are realized in two limiting cases, it is known that the ground-state sectors are separated by non-local logical operators [28, 249]. For the other two limiting cases we investigated the ground-state degeneracy in Ref. [118] and found as well that the ground states are separated by non-local logical operators. We use all four of these limiting cases as starting points for perturbative considerations later, so we review the argument from [118] about the ground-state degeneracy for the limiting cases of the X- and the Z-phase.

6.3.1 X-phase

In the limiting case $J_{\textcolor{black}{+}} = 0$, $J_{\textcolor{black}{+}} = 0$ the ground state is given by a state with the eigenvalues $x_{\textcolor{black}{\square}} = 1$ and $x_{\textcolor{black}{\square}} = 1$ for all $\square, \square$. Obviously, a state with all spins pointing in x-direction fulfills this requirement, and is a ground state of the model in this limiting case.

Now, we are aiming to find a set of operators which leave the eigenvalues $x_{\textcolor{black}{\square}}$ and $x_{\textcolor{black}{\square}}$ invariant, and form a complete set of commuting observables together with the operators $X_{\textcolor{black}{\square}}$ and $X_{\textcolor{black}{\square}}$. Obviously, these operators must commute with all operators $X_{\textcolor{black}{\square}}, X_{\textcolor{black}{\square}}$. For the case of the $L_1 \times L_2 \times L_3$ torus, we find the operators given in Fig. 6.2. These operators are products of σ^z along tubes which circumvent the torus (*tube operators*) and products of all the spins between two adjacent parallel lattice planes (*plane operators*). Alternatively, one can interpret the tube operators as a line of operators $Z_{\textcolor{black}{+}}$ going around the torus. However, not all of these operators are independent. Two parallel plane operators correspond exactly to the product of all the tube operators lying between these planes. In particular, two adjacent plane operators, correspond to the product over a layer of tube operators. So for a layer of width L only $L-1$ of these tube operators are actually independent. Counting these operators for an $L_1 \times L_2 \times L_3$ torus leads to a ground-state degeneracy of

$$\log_2(\mathrm{GSD}) = \sum_{i=1}^{3} \sum_{\substack{j=1 \\ i<j}}^{3} (L_i - 1)(L_j - 1) + \sum_{i=1}^{3} L_i. \tag{6.13}$$

We checked this ground-state degeneracy numerically for small finite systems. To this end one can consider all spins in the σ^x-basis and find all configurations of σ^x-eigenvalues which correspond to the ground state. This can be done in a brute-force way for very small systems, just considering all possible basis-states in the σ^x basis. As the operators $X_{\textcolor{black}{\square}}, X_{\textcolor{black}{\square}}$ commute with all operators σ^x any ground state can be expressed as a product state of eigenstates of σ^x. In practice it is advantageous to assign the spins which are contained in the same operators $X_{\textcolor{black}{\square}}$ or $X_{\textcolor{black}{\square}}$ first, and prune configurations that cannot lead to a ground state early on. This is again an example where simple

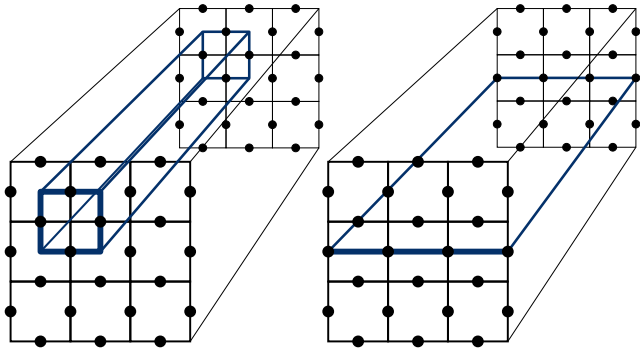

Figure 6.2: Illustration of the tube (left) and plane (right) operators. These operators correspond to products of σ^z along a tube or a plane. The figure is adapted from Ref. [118].

backtracking algorithms with some heuristics to prune away unfeasible solutions early one result useful.

6.3.2 Z-phase

In the limiting case $J_{\blacksquare} = 0$, $J_{\square} = 0$ the ground state is given by a state with the eigenvalues $z_{\ast} = 1$ and $z_{+} = 1$ for all $+, \ast$. Obviously, a state with all spins pointing in z-direction fulfills this requirement, and is a ground state of the model in this limiting case. Now, we are aiming to

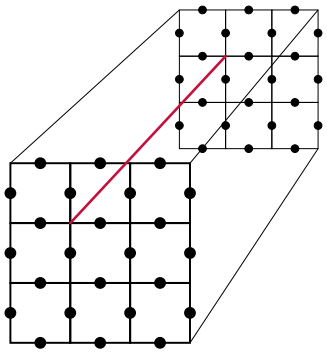

Figure 6.3: Illustration of a line-like logical operator, which corresponds to a product of σ^x along the indicated line. This figure is adapted from Ref. [118].

find operators which form a set of independent operators together with Z_{+}, $Z_{\ast}$. For the case of the $L_1 \times L_2 \times L_3$ torus, we found the operators given in Fig. 6.3. These operators are products of σ^x along straight lines (given by the intersection of two orthogonal lattice planes) which circumvent the torus. The operators are all independent and thus counting them for an $L_1 \times L_2 \times L_3$ torus

leads to a ground state degeneracy of

$$\log_2(\mathrm{GSD}) = \sum_{i=1}^{3} \sum_{\substack{j=1 \\ i<j}}^{3} L_i L_j, \tag{6.14}$$

Also this result was checked numerically for small periodic systems. Here one considers product states of σ^z eigenstates. Finally, note that all obtained operators which separate the degenerate ground states are non-local.

6.4 Isospectral dual models

All unperturbed ground states are separated by non-local operators, so we can design a system where the effective Hamiltonian has no matrix elements between degenerate ground states in the considered perturbation order. In this section we write down dual models which are isospectral to the original model for four different perturbative limits. Conversely to the original model, these models have a unique ground state, and hence we can employ non-degenerate perturbation theory.

For H_A in the limiting case $J_{\ast} = 0$ the ground state is characterized by $x_{\square} = 1$ for all $\square$ and an operator $Z_{\ast}$ acting on an unperturbed eigenstate is flipping all $x_{\square}$ eigenvalues at the eight cubes surrounding a vertex. Accordingly, an isospectral dual model using pseudospin operators $\tau^x_{\square}$ and $\tau^z_{\square}$, given by the respective Pauli matrices, reads

$$H_A^{\mathrm{dual}} = -J_{\square} \sum_{\square} \tau^z_{\square} - J_{\ast} \sum_{\ast} \prod_{\square, \square \cap \ast \neq \emptyset} \tau^x_{\square}\,, \tag{6.15}$$

where the eigenvalues of $\tau^z_{\square}$ correspond to the eigenvalues $x_{\square}$ in the original model. These pseudospin degrees of freedom are located at the vertices of the dual cubic lattice formed by the centers of the cubes of the original lattice. The products in the second term acting on unperturbed eigenstates flip the eigenvalues of the eight operators $\tau^z_{\square}$ at the corners of a cube of the dual lattice.

Interestingly, for the case $J_{\square} \ll J_{\ast}$ the action of a cube operator on an unperturbed eigenstate flips the eigenvalues $z_{\ast}$ at the eight vertices surrounding a cube. The isospectral dual model reads

$$H_A^{\mathrm{dual}} = -J_{\ast} \sum_{\ast} \tau^z_{\ast} - J_{\square} \sum_{\square} \prod_{\ast, \ast \cap \square \neq \emptyset} \tau^x_{\ast}\,, \tag{6.16}$$

which just corresponds to Eq. (6.15) with $\square \leftrightarrow \ast$, so H_A is self-dual.

For H_B we find no exact self-duality but we can again write down isospectral models. For $J_{\square} \gg J_{+}$ the unperturbed part is given by the $X_{\square}$ term and the perturbation corresponds to the operators Z_{+}. An operator Z_{+} acting on an unperturbed eigenstate flips all the eigenvalues $x_{\square}$ of the plaquettes which share a single spin with the respective cross $+$. These are the eight plaquettes which touch the cross but are orthogonal to the plane in which the cross is lying. Incorporating the eigenvalues $x_{\square}$ into the pseudospins $\tau^z_{\square}$ leads to the isospectral dual model

$$H_B^{\mathrm{dual}} = -J_{\square} \sum_{\square} \tau^z_{\square} - J_{+} \sum_{+} \prod_{\square, |\square \cap +| = 1} \tau^x_{\square}\,. \tag{6.17}$$

For the other limiting case $J_{+} \gg J_{\square}$ the unperturbed part is given by the Z_{+}-term and the operators $X_{\square}$ act as perturbation. The action of a $X_{\square}$ flips the z_{+} eigenvalues at the crosses which share a single spin with the plaquette. As a consequence, the isospectral model in terms of pseudospins can be written as

$$H_B^{\mathrm{dual}} = -J_{+} \sum_{+} \tau_{+}^{z} - J_{+} \sum_{\square} \prod_{+,|+\cap\square|=1} \tau_{+}^{x} \,. \tag{6.18}$$

The excitations $z_{+} = -1$ can also be understood in terms of lineon excitations of the X-Cube model, together with the corresponding fusion rules [243]. There is no self-duality in this case, as three Z_{+} operators at a vertex recombine to identity [244] while this is not possible for three $X_{\square}$ operators.

All these dual models are easily treatable with LCEs as introduced in Sect. 3.6 and Ref. [130]. The results are presented together with the variational results in Sect. 6.6.

6.5 Variational approach

In this section we use a variational approach introduced in Ref. [250] in order to obtain the ground-state energy for the Hamiltonians H_A and H_B. Although we did not explicitly include variational calculations in Ref. [118] we also applied variational approaches to the problem at hand while working on the respective project. The corresponding variational calculations were done by M. R. Walther and me under the supervision of K. P. Schmidt and J. Vidal. So, also the variational calculations and results presented in this chapter should be regarded as an outcome of this collaboration. Here, we define variational states and obtain the expectation values of the Hamiltonians H_A and H_B with respect to these states. These expectation values will depend on variational parameters. A minimization of the expectation value with respect to the variational parameters is expected to approximate the ground-state energy, while the variational state at this minimum is expected to approximate the ground state. All the ansätze in this section are single-parameter variational functions, designed such that the variational parameters are between zero and one. Thus after evaluating the expectation values, the variational ground-state energy can be obtained by minimizing a function of one variable in the interval $[0, 1]$. Technically, we use numerical minimization from several starting points within the interval to minimize the variational energy. Here, we have two ansätze for each of the Hamiltonians H_A and H_B, and we suppose that the one which yields the lower energy after minimization is closer to the correct ground state. It is important to state that the variational calculations for the 3D toric code explained in Ref. [38] were very helpful for our calculations, and actually some of the calculations are identical. During the following calculations we assume an infinite system with open boundaries. First, we consider two ansätze for the ground-state wave function of H_A

$$|\Psi_1^A\rangle = \mathcal{N}_1^A \prod_{+} (1 + \alpha_1 Z_{+}) \, |\Rightarrow\rangle \,, \tag{6.19}$$

$$|\Psi_2^A\rangle = \mathcal{N}_2^A \prod_{\square} (1 + \alpha_2 X_{\square}) \, |\Uparrow\rangle \,, \tag{6.20}$$

where $\mathcal{N}_1^A$ and $\mathcal{N}_2^A$ are normalization factors and α_1 and α_2 are variational parameters. The states $|\Rightarrow\rangle$ and $|\Uparrow\rangle$ are fully polarized such that all spins point in x- or z-direction, respectively. Note that the state $|\Psi_1^A\rangle$ is also used and investigated in Ref. [38]. Importantly, both limiting cases of H_A are

correctly included in the variational states $|\Psi_1^A\rangle$ and $|\Psi_2^A\rangle$.

$$X_{\square} |\Psi_1^A\rangle = |\Psi_1^A\rangle \quad \text{for } \alpha_1 = 0 \tag{6.21}$$
$$Z_{+} |\Psi_1^A\rangle = |\Psi_1^A\rangle \quad \text{for } \alpha_1 = 1 \tag{6.22}$$
$$Z_{+} |\Psi_2^A\rangle = |\Psi_2^A\rangle \quad \text{for } \alpha_2 = 0 \tag{6.23}$$
$$X_{\square} |\Psi_2^A\rangle = |\Psi_2^A\rangle \quad \text{for } \alpha_2 = 1 \tag{6.24}$$

Furthermore, for $\alpha_1 = 1$ the variational state $|\Psi_1^A\rangle$ corresponds to the ground state of the 3D toric code while for $\alpha_1 = 0$ it is just an x-polarized state. Similarly, the state $|\Psi_2^A\rangle$ corresponds to the ground state of the X-Cube model or a z-polarized state for the respective values of α_2. These states are sensible limiting cases in the full phase diagram.

Most of the calculations for $|\Psi_1^A\rangle$ are actually included in [38]. So we concentrate on the calculations for $|\Psi_2^A\rangle$ which are, nevertheless, still analogous. As a first step, we calculate the normalization factor of the variational state

$$\begin{aligned}(1/\mathcal{N}_2^A)^2 &= \langle\Uparrow| \prod_{\square}(1 + \alpha_2 X_{\square}) \prod_{\square}(1 + \alpha_2 X_{\square}) |\Uparrow\rangle \\ &= \langle\Uparrow| \prod_{\square}(1 + 2\alpha_2 X_{\square} + \alpha_2^2) |\Uparrow\rangle \\ &= (1 + \alpha_2^2)^{N_{\square}} ,\end{aligned} \tag{6.25}$$

where $N_{\square}$ is the number of elementary cubes in the system. In the first step we use that $X_{\square}^2 = 1$, whereas in the last step we exploit that no non-empty product of different $X_{\square}$ acts trivially (as identity) on the z-polarized state $|\Uparrow\rangle$, so we can drop the term linear in $X_{\square}$ within the product. For the other normalization factor $\mathcal{N}^A$ an analogous calculation gives [38]

$$(1/\mathcal{N}_1^A)^2 = (1 + \alpha_1^2)^{N_{\square}} . \tag{6.26}$$

Now we proceed with the calculation of $\langle X_{\square}\rangle$ and $\langle Z_{+}\rangle$ with respect to the two variational states. Evaluating $\langle Z_{+}\rangle$ with respect to $|\Psi_1^A\rangle$ yields [38]

$$\langle\Psi_1^A| Z_{+} |\Psi_1^A\rangle = \frac{2\alpha_1}{1 + \alpha_1^2} \tag{6.27}$$

for any operator Z_{+}. Again, a completely analogous calculation to evaluate $\langle X_{\square'}\rangle$ with respect to $|\Psi_2^A\rangle$ yields

$$\begin{aligned}\langle X_{\square'}\rangle_{\Psi_2^A} &= \langle\Psi_2^A| X_{\square'} |\Psi_2^A\rangle \\ &= \mathcal{N}_2^A \langle\Uparrow| (X_{\square'} + 2\alpha_2 + \alpha_2^2 X_{\square'}) \prod_{\square \neq \square'} (1 + 2\alpha_2 X_{\square} + \alpha_2^2) |\Uparrow\rangle \\ &= \frac{2\alpha_2}{1 + \alpha_2^2} .\end{aligned} \tag{6.28}$$

Clearly, this expectation value is the same for all cube operators in the system. The expectation

value of an operator $X_{\square}$ with respect to the state $|\Psi_1^A\rangle$ can also be calculated

$$\begin{aligned}
\langle X_{\square}\rangle_{\Psi_1^A} &= \langle\Psi_1^A|\, X_{\square}\, |\Psi_1^A\rangle \\
&= \mathcal{N}_2^A \,\langle\Rightarrow| \prod_{\star}(1+\alpha_1 Z_{\star}) X_{\square} \prod_{\star}(1+\alpha_1 Z_{\star})\,|\Rightarrow\rangle \\
&= \mathcal{N}_2^A \,\langle\Rightarrow| \prod_{\star}(1+\alpha_1 Z_{\star}) \prod_{\star,\ \star\cap\square=\emptyset}(1+\alpha_1 Z_{\star}) \prod_{\star,\ \star\cap\square\neq\emptyset}(1-\alpha_1 Z_{\star})\,|\Rightarrow\rangle \\
&= \mathcal{N}_2^A \,\langle\Uparrow| \prod_{\star,\ \star\cap\square=\emptyset}(1+2\alpha_1 Z_{\star}+\alpha_1^2) \prod_{\star,\ \star\cap\square\neq\emptyset}(1-\alpha_1^2)\,|\Uparrow\rangle \\
&= \left(\frac{1-\alpha_1^2}{1+\alpha_1^2}\right)^8,
\end{aligned} \tag{6.29}$$

where the notation $\star, \star\cap\square=\emptyset$ indicates that the product runs only over the stars which do not intersect with the cube on which $X_{\square}$ is defined. In these cases $X_{\square}$ commutes with $Z_{\star}$, in the other cases the commutation yields an additional minus sign. Again, a completely analogous calculation yields [38]

$$\langle\Psi_2^A|\, Z_{\star}\, |\Psi_2^A\rangle = \left(\frac{1-\alpha_2^2}{1+\alpha_2^2}\right)^8. \tag{6.30}$$

Combining all these expectation values, it is possible to evaluate the expectation value of the full Hamiltonian with respect to these variational states. The results are expressions for the variational ground-state energies. Normalized to the number of elementary cubes they read

$$e_0^A(\alpha_1) = -J_{\star}\frac{2\alpha_1}{1+\alpha_1^2} - J_{\square}\left(\frac{1-\alpha_1^2}{1+\alpha_1^2}\right)^8, \tag{6.31}$$

$$e_0^A(\alpha_2) = -J_{\square}\frac{2\alpha_2}{1+\alpha_2^2} - J_{\star}\left(\frac{1-\alpha_2^2}{1+\alpha_2^2}\right)^8. \tag{6.32}$$

Note that these expression have the same form, and only the variables are different. This result reflects the exact self-duality of H_A.

Now, we consider the other Hamiltonian H_B with the following ansätze

$$|\Psi_1^B\rangle = \mathcal{N}_1^B \prod_{\square}(1+\beta_1 X_{\square})\,|\Uparrow\rangle \tag{6.33}$$

$$|\Psi_2^B\rangle = \mathcal{N}_2^B \prod_{+}(1+\beta_2 Z_{+})\,|\Rightarrow\rangle\,. \tag{6.34}$$

Again the limiting cases of H_B are correctly included. The variational state $|\Psi_1^B\rangle$ corresponds to the ground state of the 3D toric code for $\beta_1 = 1$ and to a z-polarized state for $\beta_1 = 0$. Similarly, $|\Psi_2^B\rangle$ corresponds to the ground state of the X-Cube model for $\beta_2 = 1$ and to an x-polarized state for $\beta_2 = 0$. For the following calculations it is useful to define the function [38, 250]

$$\zeta(x) = \frac{2x}{1+x^2}\,. \tag{6.35}$$

First we use Eq. (6.35) to rearrange the expression for the normalization factor

$$\begin{aligned}\frac{1}{(\mathcal{N}_2^B)^2} &= \langle\Rightarrow| \prod_{\color{orange}+}(1+2\beta_2 Z_{\color{orange}+}+\beta_2^2)\,|\Rightarrow\rangle \\ &= (1+\beta_2^2)^{3N_{\color{orange}\square}}\,\langle\Rightarrow| \prod_{\color{orange}+}(1+\zeta(\beta_2)Z_{\color{orange}+})\,|\Rightarrow\rangle\ .\end{aligned} \tag{6.36}$$

Now recall that the product of all three operators $Z_{\color{orange}+}$ at a vertex is equal to identity. So we cannot just discard the linear terms in $Z_{\color{orange}+}$ in the first line of the calculation as products of operators $Z_{\color{orange}+}$ can be equal to identity. Accordingly, we need to take these products in account. The key insight is that we need n local products (of three operators $Z_{\color{orange}+}$) on n different vertices out of $N_{\color{orange}\square}$ vertices, in order to realize identity with a product of $3n$ different operators $Z_{\color{orange}+}$ on an open system. The number of possibilities to realize a product of $3n$ different operators $Z_{\color{orange}+}$ equal to identity is given by the binomial coefficient $\binom{N_{\color{orange}\square}}{n}$. Considering such products on 0 to $N_{\color{orange}\square}$ vertices yields

$$\begin{aligned}\frac{1}{(\mathcal{N}_2^B)^2} &= (1+\beta_2^2)^{3N_{\color{orange}\square}} \sum_{i=0}^{N_{\color{orange}\square}} \binom{N_{\color{orange}\square}}{i} \zeta^{3i}(\beta_2) \\ &= (1+\beta_2^2)^{3N_{\color{orange}\square}} (1+\zeta^3(\beta_2))^{N_{\color{orange}\square}},\end{aligned} \tag{6.37}$$

where in the last step we just evaluated the binomial series. Now, we continue with the expectation value

$$\begin{aligned}\langle Z_{\color{orange}+'}\rangle_{\Psi_2^B} &= \mathcal{N}_2^B (1+\beta_2^2)^{3N_{\color{orange}\square}}\,\langle\Rightarrow|\, Z_{\color{orange}+'} \prod_{\color{orange}+}(1+\zeta(\beta_2)Z_{\color{orange}+})\,|\Rightarrow\rangle \\ &= \mathcal{N}_2^B (1+\beta_2^2)^{3N_{\color{orange}\square}} \sum_{i=0}^{N_{\color{orange}\square}-1} \binom{N_{\color{orange}\square}-1}{i} \left[\zeta^{3i+2}(\beta_2)+\zeta^{3i+1}(\beta_2)\right] \\ &= \frac{\zeta^2(\beta_2)+\zeta(\beta_2)}{1+\zeta^3(\beta_2)},\end{aligned} \tag{6.38}$$

where from the first to the second line we used that there can be two types of products which are proportional to identity. One of them contains $Z_{\color{orange}+'}$ twice and does not contain the other operators at this vertex. From this product we obtain the terms proportional to $\zeta^{3i+1}(\beta_2)$. The other one contains $Z_{\color{orange}+'}$ once together with the two other operators $Z_{\color{orange}+}$ at the same vertex. From this product we obtain the terms proportional to $\zeta^{3i+2}(\beta_2)$. The change from $N_{\color{orange}\square}$ to $N_{\color{orange}\square}-1$ in the binomial coefficient comes from the fact, that after considering these products we can only choose out of $N_{\color{orange}\square}-1$ other vertices, because the vertex at $Z_{\color{orange}+'}$ has already been combined with at least one operator out of the product over all $\color{orange}+$. The next expectation value is given by

$$\begin{aligned}\langle X_{\color{orange}\square}\rangle_{\Psi_2^B} &= \mathcal{N}_2^B\,\langle\Rightarrow| \prod_{\color{orange}+}(1+\beta_2 Z_{\color{orange}+}) \prod_{\substack{{\color{orange}+},\\ [X_{\color{orange}\square},Z_{\color{orange}+}]=0}} (1+\beta_2 Z_{\color{orange}+}) \prod_{\substack{{\color{orange}+},\\ [X_{\color{orange}\square},Z_{\color{orange}+}]\neq 0}} (1-\beta_2 Z_{\color{orange}+})\,|\Rightarrow\rangle \\ &= \mathcal{N}_2^B (1+\beta_2^2)^{3N_{\color{orange}\square}-8}(1-\beta_2^2)^8\,\langle\Rightarrow| \prod_{\substack{{\color{orange}+},\\ [X_{\color{orange}\square},Z_{\color{orange}+}]=0}} (1+\zeta(\beta_2)Z_{\color{orange}+})\,|\Rightarrow\rangle \\ &= \left(\frac{1-\beta_2^2}{1+\beta_2^2}\right)^8 (1+\zeta^3(\beta_2))^{-N_{\color{orange}\square}} \sum_{i=0}^{N_{\color{orange}\square}-4} \binom{N_{\color{orange}\square}-4}{i} \zeta^{3i}(\beta_2) \\ &= \left(\frac{1-\beta_2^2}{1+\beta_2^2}\right)^8 (1+\zeta^3(\beta_2))^{-4}.\end{aligned} \tag{6.39}$$

In the first line we commuted $X_{\square}$ to the right, where it acts trivially on the polarized state. From the commutation relations we obtain additional minus signs for operators Z_{+} which do not commute with $X_{\square}$. Combining these with terms from the product over all $+$ leads to the term $(1-\beta_2^2)^8$. The expectation value of the remaining product can then again be evaluated using the binomial series. Note that here only for $N_{\blacksquare}-4$ vertices all operators Z_{+} are contained in the product. Combining the variational expectation values of $X_{\square}$ and Z_{+} results in the variational energy

$$e_0^B(\beta_2) = -J_{\square}\left(\frac{1-\beta_2^2}{1+\beta_2^2}\right)^8 (1-\zeta^3(\beta_2))^{-4} - 3J_{+}\frac{\zeta^2(\beta_2)+\zeta(\beta_2)}{1+\zeta^3(\beta_2)}. \tag{6.40}$$

Now, we come to the last variational ansatz $|\Psi_1^B\rangle$ which is also the most difficult one, as products of plaquette operators over closed surfaces equal identity [38]. The simplest example is the product of the six plaquettes including an elementary cube of the lattice. Clearly, any product of several such products also results in identity [38] In contrast to the case of the operators Z_{+}, two products over six plaquettes at different cubes can contain the same operator $X_{\square}$.

In Ref. [38] these products are treated explicitly, and results in the limit $N_{\blacksquare}\to\infty$ are derived. In the end the relevant expectations values correspond to the results which would be obtained by simply ignoring the additional identities stemming from these products. Motivated by this we ignore the presence of the additional identities stemming from these products in the following calculations. With this the normalization factor reads

$$\frac{1}{(\mathcal{N}_1^B)^2} = (1+\beta_1^2)^{3N_{\blacksquare}} \langle\Uparrow| \prod_{\square}(1+\zeta(\beta_1)X_{\square})\,|\Uparrow\rangle \quad \approx (1+\beta_1^2)^{3N_{\blacksquare}}\,. \tag{6.41}$$

The expectation value of $X_{\square}$ is [38]

$$\begin{aligned}\langle X_{\square}\rangle_{\Psi_1^B} &= \langle\Uparrow|\,(\zeta(\beta_1)+X_{\square'})\prod_{\square\neq\square'}(1+\zeta(\beta_1)X_{\square})\,|\Uparrow\rangle \\ &\approx \zeta(\beta_1)\,.\end{aligned} \tag{6.42}$$

and finally

$$\begin{aligned}\langle Z_{+}\rangle_{\Psi_1^B} &= (1+\beta_1^2)^{-8}\,\langle\Uparrow|\prod_{[Z_{+},X_{\square}]=0}(1+\zeta(\beta_1)X_{\square})\prod_{[Z_{+},X_{\square}]\neq 0}(1-\beta_1^2X_{\square})\,|\Uparrow\rangle \\ &\approx \left(\frac{1-\beta_1^2}{1+\beta_1^2}\right)^8\,.\end{aligned} \tag{6.43}$$

With these expressions we can write the variational energy as

$$e_0^B(\beta_1) \approx -3J_{\square}\zeta(\beta_1) - 3J_{+}\left(\frac{1-\beta_1^2}{1+\beta_1^2}\right)^8 \tag{6.44}$$

Let us note again that we did not obtain the variational energy rigorously as this would be very difficult, due to the combinations of plaquettes which one would have to take into account. Moreover, our approach is not even a controlled approximation. However, we have two arguments to motivate this approximation. First, we did the error to neglect similar products of star operators in calculations for the X-Cube model [39, 246]. In this case, the products can actually be treated exactly using binomial series (see App. B). However, the improved result and the approximation resulting from neglecting these products deviate only moderately. Second, in Sect. 6.6 we compare the obtained results to the series expansions and see a good agreement.

6.6 Results

Using LCEs for multi-site interactions as explained in Chap. 3 we were able to obtain series expansion up to order ten for the ground-state energies from four different limits. For H_A these limits are $J_{\star} \ll J_{\square}$ and $J_{\square} \ll J_{\star}$. As H_A features an exact self-duality the series for the ground-state energies $e_{0,A}^{J_{\star} \ll J_{\square}}$ and $e_{A,0}^{J_{\square} \ll J_{\star}}$ are identical up to an exchange of $J_{\star}$ and $J_{\square}$. Another consequence of the exact self-duality is that the series intersect at $J_{\square}/J_{\star} = \eta_A = 1$. The series are given in App. A.1 and plotted in Fig. 6.4.

For H_B these limits are $J_{+} \ll J_{\square}$ and $J_{\square} \ll J_{+}$. As already indicated H_B does not have a self-duality and hence two series expansions have to be calculated. These series expansions are also given in App. A.1 and plotted in Fig. 6.5. They intersect at $J_{+}/J_{\square} = \eta_B \approx 1.012$.

In order to obtain the ground-state energy per vertex e_0 of the full Hamiltonian H we simply add up the ground-state energies of H_A and H_B

$$e_0 = e_{0,A} + e_{0,B} \,, \tag{6.45}$$

because $e_{0,A}$ is completely independent of J_{+} and $J_{\square}$ and $e_{0,B}$ does also not depend on $J_{\square}$ and $J_{\star}$. So the crossing points of the ground-state energies in the full phase diagram are also just $J_{\square}/J_{\star} = \eta_A$ and $J_{+}/J_{\square} = \eta_B$ as illustrated in Fig. 6.6. These intersection lines divide the phase diagram into four different sectors. Two of them are connected to the X-Cube and the toric-code phases as expected, and are referred to as XC- and TC-phase, respectively. Interestingly, two further phases can be found. One of these phases is found at $J_{\square}/J_{\star} > \eta_A$ and $J_{+}/J_{\square} < \eta_B$. This phase is referred to as X-phase, because in the liming case $J_{\star} = 0, J_{+} = 0$ only the operators $X_{\square}, X_{\square}$ have nonzero prefactors, and hence the Hamiltonian has two obvious x-polarized ground states. Analogously, for the case $J_{\square} = 0, J_{\square} = 0$ the model has two z-polarized ground states, and thus the corresponding phase is referred to as Z-phase. Let us conclude with the remark that we cannot exclude the existence of intermediate phases with our approach. Although this scenario seems unlikely to us, further investigations would be interesting.

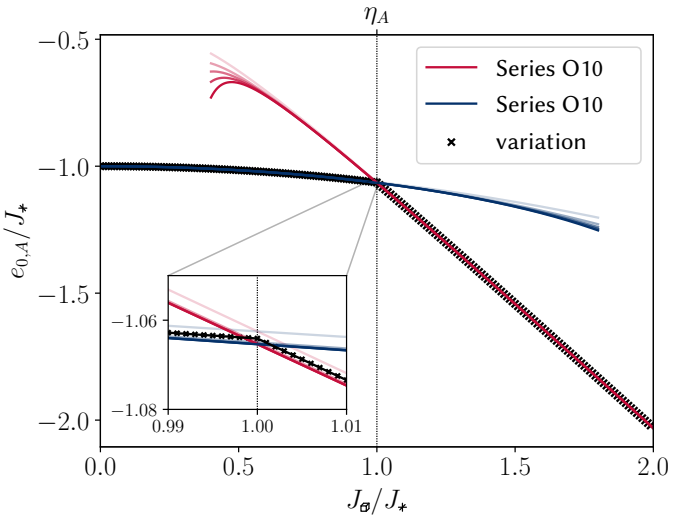

Figure 6.4: Perturbative expansion for the ground-state energy per vertex $e_{0,A}$ of H_A from two different perturbative limits. The perturbation orders $2, 4, 6, 8, 10$ are given with increasing opacity. The black crosses indicate the variational ground-state energy obtained for H_A. This figure is based on Fig. 2 in Ref. [118].

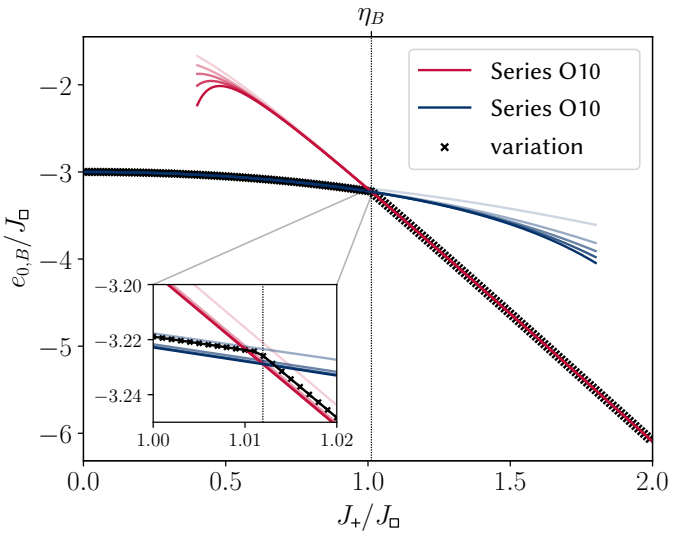

Figure 6.5: Perturbative expansion for the ground-state energy per vertex $e_{0,B}$ of H_B from two different perturbative limits. The perturbation orders $2, 4, 6, 8, 10$ are given with increasing opacity. The black crosses correspond to the variational ground-state energy obtained H_B. This figure is based on Fig. 2 in Ref. [118].

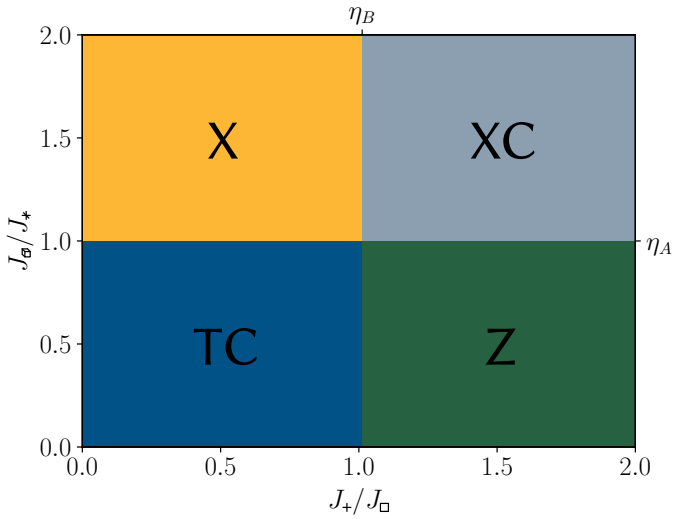

Figure 6.6: The resulting phase diagram consists of the XC-phase, the TC-phase, the X-phase and the Z-phase. All phase transitions have been found to be first order. Note that the positions of the X- and Z-phase are exchanged compared to the phase diagram in Ref. [118] due to the different conventions used in the definition of the operators. This figure is based on Fig. 3 in Ref. [118].

Chapter 7

Numerical linked-cluster expansions for the ferromagnetic transverse-field Ising model in the low-field limit

In the previous chapters we evaluated the reduced contributions of the clusters within a linked-cluster expansion (LCE) perturbatively. Instead, one can also use methods like exact diagonalization to evaluate these contributions exactly [125, 127, 179, 185]. The combination of LCEs with ED was termed exact linked cluster expansions (ELCE) [127, 179]. Later this method was used to determine thermal expectation values and called numerical linked-cluster expansions (NLCE) [125, 185]. A review can be found in [126]. Here, we are considering NLCE at $T = 0$. Typically, NLCEs target extensive quantities like the ground-state energy, but it is also possible to obtain results for higher particle sectors [127, 128, 181]. Conversely to perturbative LCEs, the truncation in NLCEs is not perturbative. Instead, the choice of the considered clusters is usually the only truncation [127]. Of course, one can simply use the same clusters as for perturbative LCEs. However, schemes with different choices of clusters proved more successful in a number of cases [209, 251, 252].

In this chapter we show that NLCEs for the low-field limit of the ferromagnetic transverse-field Ising model (TFIM) on the triangular lattice and the square lattice can be done with the formalism presented in Sect. 3.6, i.e., with a LCE of the high-field type. It is not expected that one can do an expansion of the high-field type to obtain the ground-state energy of the ferromagnetic TFIM in the low-field limit, because a perturbative expansion of the TFIM about the low-field limit is not of the form specified in Sect. 3.2, as the unperturbed part is not composed of strictly local operators. In principle, this setup requires LCEs of the low-field type [96–98, 100, 115] and perturbative results for the problems considered in this chapter obtained with low-field type expansions can be found in Ref. [100]. Note that several types of NLCEs for ordered quantum phases are also considered in Ref. [251]. While these expansions share some important properties with the low-field type expansions, there is the difference that the considered Hamiltonians do not contain strictly local terms at all.

Instead of using LCEs of the low-field type, we use a dual model which maps the Hamiltonian of the TFIM in the low-field limit to an isospectral Hamiltonian where the unperturbed energy is again defined in terms of strictly local operators [121]. Note that this duality mapping does not preserve the degeneracies of the states. For example, the unperturbed ground-state of the original model is two-fold degenerate on the infinite lattice, whereas the unperturbed ground-state of the dual model is unique. With the hypergraph decomposition [130] described in Sect. 3.6 and this dual model one can straightforwardly calculate a perturbative expansion of the ground-state energy about the low-field limit of the TFIM using LCEs of the high-field type. The results are in agreement with the series obtained from LCEs of the low-field type [100]. In addition, we also use a non-perturbative evaluation of the reduced contributions of the individual clusters, and hence, we employ an NLCE, for the dual model. Interestingly, there are also recent perturbative and non-perturbative results for one-particle states and two-particle bound states of this model in the literature [181].

7.1 Expansions of the low-field type

Another application of the LCEs for many site interactions [130] is that one can employ LCEs of the high-field type in cases where typically LCEs of the low-field type are used. The characteristic feature of the low-field type expansions is that the perturbation is given by local field terms, while the interactions are part of the unperturbed Hamiltonian [100]. This setup is opposed to the setup for LCEs of the high-field type, were the unperturbed part is a sum over local operators, and the perturbation terms correspond to the couplings [96, 99]. As an example, we consider the ferromagnetic TFIM in the low-field limit, where we rescale the Hamiltonian as

$$\frac{H^{\mathrm{TFIM}}}{2J} = -\frac{1}{2}\sum_{\langle i,j\rangle}\sigma_i^x\sigma_j^x - \frac{h}{2J}\sum_i \sigma_i^z\,, \tag{7.1}$$

where again σ^x and σ^z are the usual Pauli matrices, $\langle i,j\rangle$ indicates that the sum runs over pairs of next neighbors, h and $J>0$ are real numbers and $h/(2J)$ is used as a tuning parameter. In a perturbative setting, low-field type expansions are a bit more cumbersome compared to high-field type expansions, because the change in the unperturbed energy caused by fluctuations can not be evaluated naively on the individual subclusters, but one needs to account for all the bonds connecting the subcluster to the environment [96]. As one also needs to consider all bonds connecting sites of the cluster, only induced subclusters which contain all the bonds of the lattice which join sites of the subcluster are considered. In the language of graph theory one considers only the induced subgraphs - i.e., we are interested in the strong embeddings [96–98, 100, 115]. As an example two subclusters are illustrated in Fig. 7.1, one of them is an induced subcluster the other one not.

This is actually very consistent with the change of the role of sites and bonds compared to high-field type expansions. For the TFIM such a high-field type expansion corresponds to an expansion about the high-field limit $h/J\to\infty$. In such an expansion the perturbation acts on the bonds, so perturbative processes are defined on sets of bonds and accordingly the connected subclusters are already specified by their bonds, as their sites are just the sites contained in these bonds. Of course, subclusters consisting of a single site and no bond can not be defined in terms of bonds, though they are typically only relevant for the zeroth order contribution. As the unperturbed energy is defined as a sum of strictly local operators, changes in the unperturbed energy resulting from the action

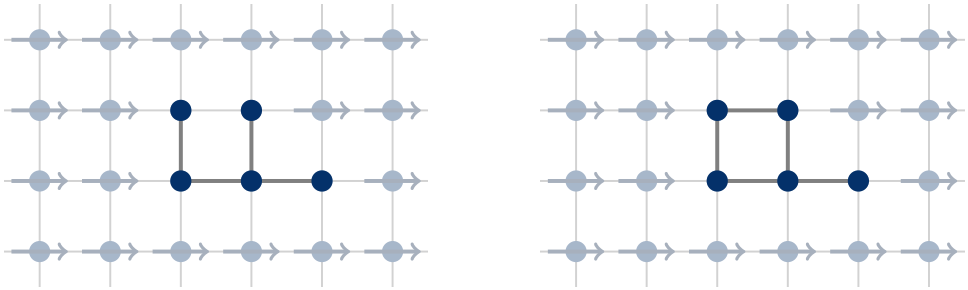

Figure 7.1: The subcluster illustrated in the left part (with dark blue sites opaque gray bonds), needs to be considered only in a high-field type expansion. Note that this subcluster is a subgraph but not an induced subgraph of the lattice graph. In the low-field type expansion, one would only use the subcluster illustrated in the right part. This subcluster contains all bonds of the lattice which exclusively contain sites of the subcluster (dark blue).

of the perturbation on a subcluster are easily evaluated on the sites contained in the respective cluster.

Conversely, for the low-field type expansions, each elementary perturbation operator acts locally on a single site. For the TFIM such a low-field type expansion corresponds to an expansion about the low-field limit. So, perturbative processes are defined on sets of sites, not on sets of bonds. Accordingly, the relevant connected subclusters are already specified by their set of sites, as their bonds can be deduced from these sites. The zeroth order contributions are hardly associated to subclusters, as the only cluster with zero sites, would be the empty cluster. So for the actual calculation we set the unperturbed ground-state energy to zero without loss of generality and only calculate the corrections due to the perturbation. Formally, a constant offset can be introduced to the unperturbed part of the Hamiltonian, such that the unperturbed ground-state energy equals zero [98, 100]. After the corrections to the unperturbed ground-state energy have been calculated, the contribution of the unperturbed part can be easily added.

As the unperturbed energy is defined as a sum of operators acting on the bonds of the lattice, in principle, one needs to consider all the bonds which contain at least one site of the respective subcluster in order to access the changes in the unperturbed energy caused by the action of the perturbation on this subcluster. For bonds which join sites of a given subcluster with sites outside of the respective subcluster (see Fig. 7.2), the states on the sites outside of the cluster are not affected by actions of the perturbation on the cluster, and remain as in the unperturbed ground-state [96]. As a consequence the contributions of these bonds to the unperturbed energy can be deduced from the states on the sites of the subcluster, e.g., by adding local field terms to the cluster Hamiltonian [96, 251]. Accordingly, any relevant connected subcluster in the expansion is defined by a set of sites from the lattice and all the bonds within the lattice which exclusively join sites from this set. As a consequence, one needs to consider strong embeddings (induced subgraph isomorphism), instead of weak embeddings (subgraph monomorphism) to obtain the embedding factor of a given subcluster into another cluster (or the lattice) [96–98, 100, 115]. This also implies, that during the subcluster subtraction to obtain the reduced contribution of a given cluster only induced subclusters are considered. Furthermore, the cluster Hamiltonian is designed such, that

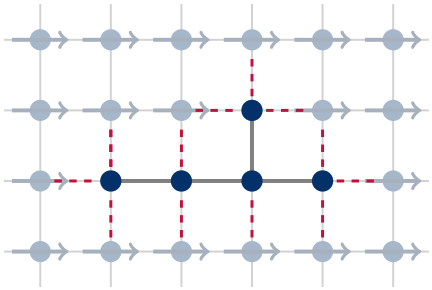

Figure 7.2: An induced subcluster (with dark blue sites and opaque gray bonds) within the square lattice. While this subcluster corresponds to a strong embedding there are many bonds to the environment (dashed red). Changing the state on the subcluster also affects the contributions of these bonds to the unperturbed energy of the system.

it correctly takes the unperturbed energies of bonds between the cluster and its environment into account [96]. Overall, this makes sure to consider all bonds (within the lattice) which contain a site from the considered subcluster for the calculation of the unperturbed energy of the system. Hence, the changes in the unperturbed energy of the entire system caused by perturbative fluctuations on a given subcluster, can also be evaluated on the respective subcluster.

7.2 The duality mapping

In contrast to the high-field type expansions, in the low-field type formalism the evaluation of the changes in the unperturbed energy appears more complicated due to the interactions within H_0 which accordingly is not a sum of strictly local operators. While it is known how to efficiently handle this difficulty [96, 100] it is still tempting to formulate the problem in terms of a high-field type expansion.

Interestingly, a duality mapping exists which maps the Hamiltonian of the TFIM in the low-field limit to an isospectral Hamiltonian where the unperturbed energy is again defined in terms of strictly local operators [121]. In this mapping the products $\sigma_i^z \sigma_j^z$ on the links $\langle i,j\rangle$ of the original problem are mapped to pseudospins $\tau^z_{\langle i,j\rangle}$, and the sites of the original model are mapped to bonds which contain the surrounding links

$$\frac{H^{\mathrm{TFIM}}_{\mathrm{dual}}}{2J} = -\frac{1}{2}\sum_{\langle i,j\rangle} \tau^z_{\langle i,j\rangle} - \lambda \sum_i \prod_{\langle i,j\rangle \ni i} \tau^x_{\langle i,j\rangle} = -\frac{1}{2}\sum_l \tau^z_l - \lambda \sum_b \prod_{l\in b} \tau^x_l, \tag{7.2}$$

where $\lambda = h/(2J)$ and the sum runs over all bonds b of the dual model. Each of these bonds couples all pseudospins on the links of the original lattice which contain a given vertex of the original lattice. For the TFIM on the square lattice the bonds in the dual model would be crosses containing the four pseudospins which surround the respective vertices of the square lattice. A ground state of the original model and the unique ground state of the dual model are illustrated in Fig. 7.3. Note that this mapping increases the number of degrees of freedom, and hence, the Hilbert space of the dual model would be larger than the Hilbert space of the original model [121]. In the original model each basis state of the σ^x-basis can be obtained by a series of spin-flip operations

(actions of σ^z operators) on one of the x-polarized unperturbed ground states. In the dual model this corresponds to the action of the perturbation at a single bond on the unique ground state. Systematically repeating the actions of the perturbation at different bonds, the physically relevant sector of the Hilbert space can be obtained. Formally, this sector is associated to plaquette operators having eigenvalue $+1$ [121].

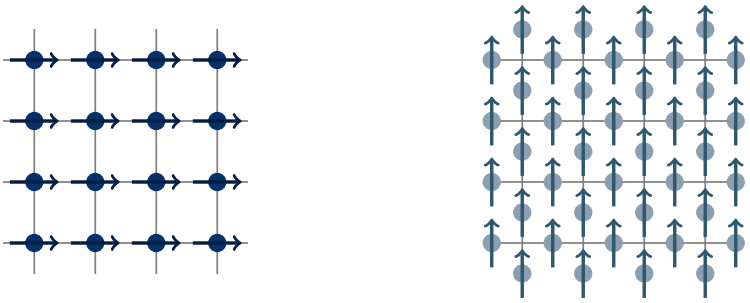

Figure 7.3: The dual mapping for the square lattice. In the left one ground state in the original formulation is shown. The ground state in the dual formulation is illustrated in the right part. Note that in the dual formulation the ground-state is unique and the two ground states of the original formulation cannot be distinguished.

Thanks to the duality mapping, Eq. (7.2) has exactly the form described in Sect. 3.2 and we can do LCEs of the high-field type with many-site interactions in the perturbation to tackle the TFIM in the low-field limit, which originally required a low-field type expansion. Interestingly, a cluster in the original formulation can be transformed to a cluster in the dual formulation and vice versa, as shown in Fig. 7.4. After appropriate rearrangements the perturbative results for the ground-state energy of the respective dual models agree with the results for the TFIM on the square lattice and the triangular lattice from Ref. [100].

Figure 7.4: In the left part a cluster from a low-field type expansion is shown. The bonds to the surrounding system which have to be taken into account are given by dashed red lines. In the right part the corresponding cluster in the dual formulation is shown. Here, the unperturbed energy can be determined on the sites which are part of the cluster.

7.3 Exact diagonalization

In this subsection we focus on the evaluation of the reduced contributions of the individual clusters in the dual formulation. Accordingly, in this chapter sites and bonds refer to sites and bonds of the system within the dual formulation, where sites host pseudospin degrees of freedom and bonds contain all sites surrounding a given vertex of the original lattice.

In order to obtain the ground-state energy per bond we evaluate the reduced contributions of all non-isomorphic connected subclusters up to 13 bonds and sum them up weighed with the appropriate embedding factors. Note that by shifting the ground-state energy at $h = 0$ to zero [98, 100] we do not need to take into account the clusters which consist of only a single site. The lowest eigenvalue of the cluster Hamiltonian of individual clusters is calculated using the Lanczos method [41–43]. We used the C++ library Eigen to implement the Lanczos algorithm and find the lowest eigenvalue of the occurring tridiagonal matrices.

In order to find the lowest energy eigenvalue on a cluster, we need to construct the matrix representing the cluster Hamiltonian in the product basis formed by the eigenstates of the pseudospins τ_l^z. To this end we start from the unique ground state at $h = 0$ on the considered cluster and collect the basis states we encounter when we repeatedly act with

$$V = \sum_b \prod_{l \in b} \tau_l^x \tag{7.3}$$

on this state. Whenever we encounter a new basis state we add this state to a list of relevant basis states. We then act with V (restricted to the given cluster) on all newly discovered basis states. This procedure continues until no new basis states are found. Note that this procedure will in general not find all basis states on a given cluster, but only all basis states of the block of the cluster Hamiltonian which contains the ground state at $h = 0$. After all relevant states have been found we calculate all matrix elements of the cluster Hamiltonian with respect to these states.

As an example consider the cluster consisting of a single bond and the four sites it contains. From the unique ground state at $h = 0$ on this cluster we can obtain two basis states by acting with V, although in principle there would be $2^4 = 16$ basis states. The relevant block of the cluster Hamiltonian reads

$$\frac{[H_{\text{dual}}^{\text{TFIM}}]_0^c}{2J} = \begin{array}{c} \begin{matrix} |0000\rangle & |1111\rangle \end{matrix} \\ \begin{bmatrix} -2 & -\lambda \\ -\lambda & 2 \end{bmatrix} \end{array} \begin{matrix} |0000\rangle \\ |1111\rangle \end{matrix} . \tag{7.4}$$

In the present problem, the ground-state sector is the only physically relevant sector. However, this is not necessarily true, for other problems. For example consider the TFIM in the high-field limit where the perturbation conserves the parity of spin-flips. With this approach one obtains the Hamiltonian with respect to states with an even number of spin-flips. The block with odd-parity is not obtained. If one can be sure that the selected block of the Hamiltonian contains the actual ground-state, this method to generate the cluster Hamiltonian is helpful to reduce the complexity of the problem. We also used this approach within the calculations for the quantum Newman-Moore model presented in Ref. [105].

7.4 Results

Here, we present the results for the ground-state energy of the TFIM in the low-field limit on the square lattice (Fig. 7.5) and the triangular lattice (Fig. 7.7). In order to access convergence of the NLCE results we show the results for expansions up to various numbers of bonds, where the highest number of bonds has the largest opacity. We also add values of Wynn extrapolations [116, 253], which are commonly used in the field of NLCEs to improve convergence [125, 126, 185, 252, 254]. The data for the plots can be found in [248]. In both cases we display the known series expansions from the low-field [100] and the high-field limit [99] in the plots and indicate the phase transition point as obtained in Ref. [99] by a vertical line. One quickly observes that the NLCE results are in good agreement with the low-field expansions where these expansions are convergent. In this range the NLCE results are also well converged. Remarkably, after the phase transition they are still in agreement with the high-field expansions. This is expected as an NLCE does not have a perturbative truncation, but the truncation is of topological nature, determined by the choice of the clusters in the expansion [127]. However, the convergence of the NLCE results is worse than before the phase transition. This is probably due to the fact that the expansion is better suited for the low-field limit of the TFIM.

In Figs. 7.6 and 7.8 we explicitly access the convergence of the NLCE. To this end we consider two specific values of the tuning parameter $h/(2J)$. One is very close to the phase transition and another one is far in the low-field limit. In the plot we display the absolute change of the ground-state energy when we consider an NLCE up to x bonds instead of an NLCE up to $x-1$ bonds. At the point close to the phase transition one observes a slow convergence, which is expected due to diverging correlation lengths at the phase transition [8, 125, 255]. We inserted a straight line into the double logarithmic plots in order to illustrate the algebraic nature of the convergence. In some works critical behavior was investigated using the convergence of suitable quantities with the number of bonds [256] or the perturbation order [257]. For the point far in the low-field limit the convergence is much faster. At some point numerical errors start to accumulate and grow with the number of bonds considered in the expansion (these points are less opaque in the plots). This analysis can help to get a rough estimate of the numerical errors. At some point considering clusters with more bonds will essentially add numeric noise. In this case it does not make sense to push the expansion to higher numbers of bonds.

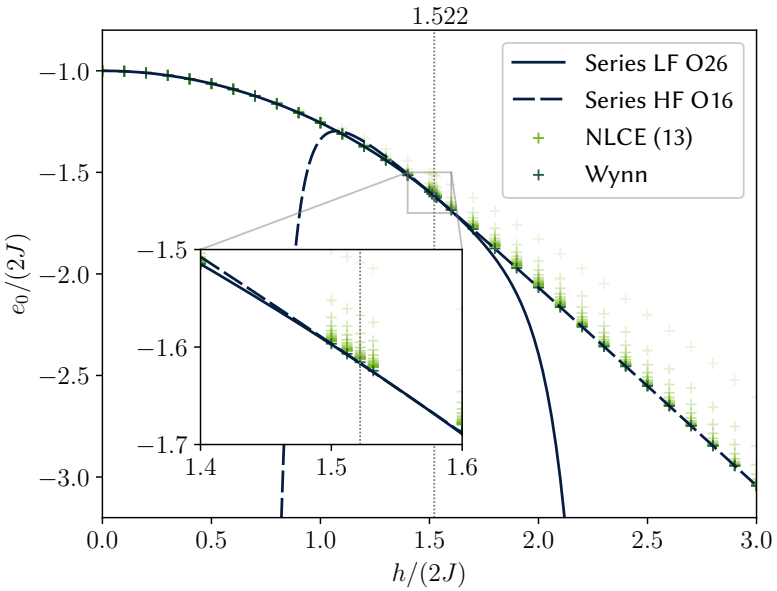

Figure 7.5: The results from NLCE for the square lattice match the known results from series expansions [99, 100] well. HF and HL indicate series expansions about the high-field and low-field limit, respectively. The dashed gray line indicates the phase transition as obtained in Ref. [99].

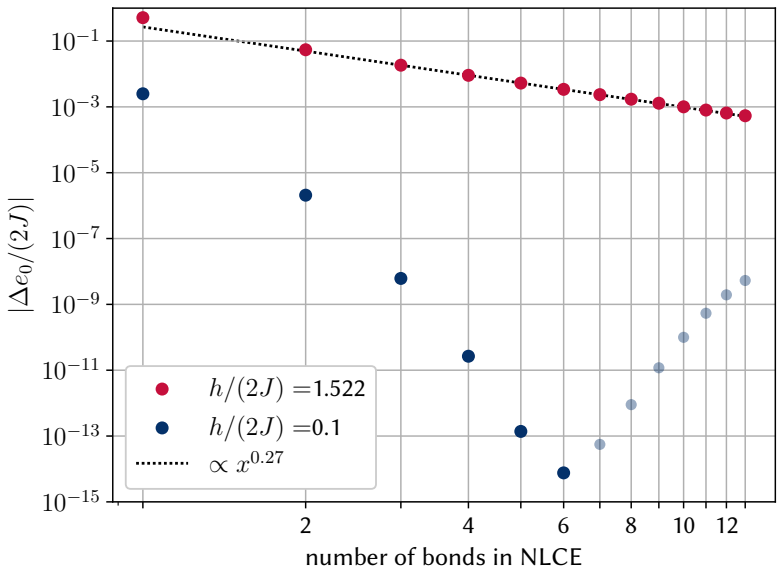

Figure 7.6: Convergence of the NLCE for the square lattice. The y-value is the absolute change of the ground-state energy at a given value of $h/(2J)$ by considering an NLCE with clusters up to x bonds instead of clusters up to $x-1$ bonds.

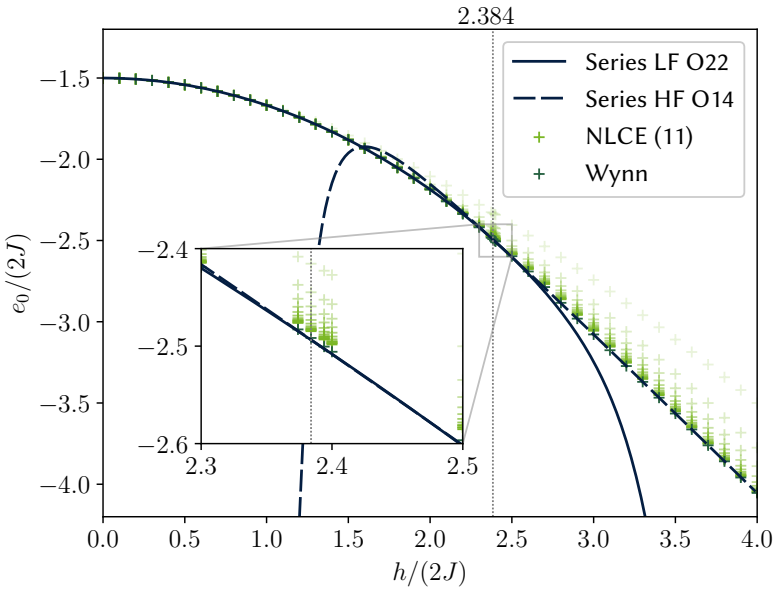

Figure 7.7: The results from NLCE for the triangular lattice match the known results from series expansions [99, 100] well. HF and HL indicate series expansions about the high-field and low-field limit, respectively. The dashed gray line indicates the phase transition as obtained in Ref. [99].

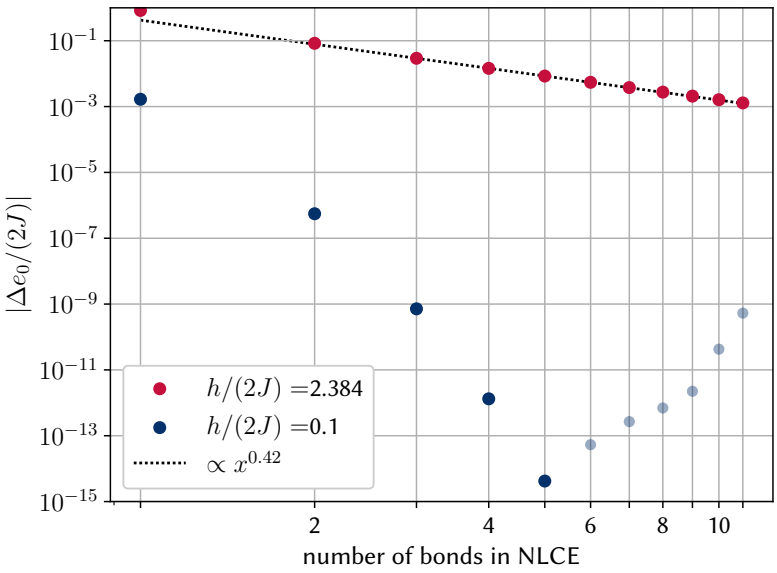

Figure 7.8: Convergence of the NLCE for the square lattice. The y-value is the absolute change of the ground-state energy at a given value of $h/(2J)$ by considering an NLCE with clusters up to x bonds instead of clusters up to $x-1$ bonds.

Chapter 8

Summary and Outlook

In this thesis we introduced linked-cluster expansions via a full hypergraph decomposition [130] in Sect. 3.6 and applied this method to several physical problems. The applications considered in this thesis clearly show that the presented method successfully extends the method of linked-cluster expansions via full graph decompositions [95–98] to the realm of perturbations with multi-spin interactions at least for the calculations of the ground-state energy and matrix elements of a quasi-particle number conserving effective Hamiltonian in few-quasi-particle sectors.

One remarkable application of the method is the formulation of a full graph decomposition for the low-field phase of Kitaev's toric code [18] in a parallel magnetic field on the square lattice which correctly takes into account the exotic mutual statistics in the ground-state and one-quasiparticle sector [23] as described in Chap. 4. Interestingly, only some minor tweaks had to be applied in order to apply hypergraph decompositions to this problem. While the problem has already been treated successfully with linked-cluster expansions [33, 35, 238], to the best of our knowledge a full graph decomposition has not been applied to the problem before.

We also extended the series expansions for the ground-state energy of the X-Cube model [26] about the high- and the low-field limit for the specific field directions considered in Ref. [39]. For the perturbative treatment of a general parallel field in the low-field limit we were able to obtain high-order series expansions which converge well up to the known phase transition point, using a variant of the hypergraph approach which has been explained in Chap. 4 and Ref. [23]. The obtained series expansions are in good agreement with the QMC data we received from Trithep Devakul [84]. For the challenging problem of a perturbative expansion of the ground-state energy of the X-Cube model about the high-field limit for general parallel fields, series expansions up to order five could be obtained. Though, these expansions apparently have serious convergence issues far before approaching the phase transition point, which accordingly could not be determined from these series expansions.

For the competition of the X-Cube model [26] with the 3D toric code [19, 20] described in Ref. [118] and Chap. 6 we were able to derive high-order series expansions about all four limits, which converge well up to the respective phase transition points, so we could determine the ground-state phase diagram [118]. This diagram holds under the assumption that no further intermediate phase transitions occur [118]. The perturbative calculations from Ref. [118] have been complemented with some variational considerations using the method of Ref. [250]. Although these calculations are not expected to be as quantitatively accurate as high-order series expansions

it is still interesting to see that the obtained variational results match the series expansion very well.

At last, we moved to the realm of expansions of the low-field type, investigating the low-field limit of the TFIM on the square and the triangular lattice. In this chapter we used hypergraph decompositions to execute NLCEs [125,127,185], evaluating the reduced contributions of the clusters with ED instead of perturbation theory. While our results are in good agreement with the perturbative results [100], we used a duality mapping [121] to formulate the expansions in terms of high-field type expansions. In this formulation the introduction of boundary fields into the cluster Hamiltonian, as commonly done in the low-field type formalism [96, 251], is not necessary.

The results presented in this thesis are not the only applications of hypergraph decompositions, which further proves the value of the method. Other applications in the literature include the investigation of the phase transition in the quantum Newman-Moore-model [105] and series expansions for the toric code in a field on the honeycomb lattice, which together with QMC simulations permitted a quantitative investigation of the quantum phase diagram of this model [119].

From a technical point of view it is an achievement to have set up a rather general tool-chain to apply the method to various physical problems with only small effort for adaptation. However, the development of the method is still in progress, and especially on the algorithmic side improvements are likely possible. For example, when we determine the clusters needed for the calculation of the ground-state energy we still generate multiple clusters related by translational symmetry. Typically, we test several of these clusters for isomorphism against the representative clusters of the equivalence classes which have been obtained so far. For conventional graph decompositions a scheme without this drawback is presented in Ref. [258]. Also for hypergraph decompositions such a scheme would be highly desirable. On the level of the evaluation of reduced contributions of equivalence classes of clusters, an obvious next step is to combine the hypergraph decomposition method with pCAT [181], which generates a cluster additive effective Hamiltonian as MBOT or pCUT, but with a much better performance, comparable to the TBOT method. Another obvious step is to use schemes to directly evaluate all hopping elements [96, 97, 124] within a single linked-cluster expansion, instead of doing separate expansions for each desired hopping element, reducing the repeated computation of equivalent matrix elements.

Still with all of this room for improvement left on the technical and conceptional side, we obtained competitive scientific results. Accordingly, we are convinced that the presented method is a valuable extension of the commonly used graph decomposition techniques for quantum many body systems at zero temperature [95–99]. In particular, it provides a straightforward way to set up a full graph decomposition for perturbation theory problems where elementary perturbations couple more than two sites. Finally, we are convinced that the method of linked-cluster expansions via hypergraph decompositions [130] will continue to be useful for the investigation of quantum spin systems with multi-spin interactions.

Appendix A

Series expansions

A.1 Series expansions for competing topological orders

This section is basically a slight adaptation of the respective appendix in Ref. [118], though we omitted some parts which are already covered in Chap. 6. We give the series expansions for the ground-state energies of H_A and H_B in the different limits which have been obtained using the Löwdin method [201] (see Subsect. 3.4.3) together with a hypergraph decomposition [130] which is also explained in Sect. 3.6. For the ground-state energy $e_{0,A}$ of H_A per vertex up to order ten one obtains [118]

$$\begin{aligned} e_{0,A}^{J_{\bigstar}\ll J_{\bigcirc}} = &- J_{\bigcirc} - \frac{J_{\bigstar}^2/J_{\bigcirc}}{16} - \frac{71J_{\bigstar}^4/J_{\bigcirc}^3}{28672} - \frac{5357137J_{\bigstar}^6/J_{\bigcirc}^5}{16184770560} \\ &- \frac{15573579216301097J_{\bigstar}^8/J_{\bigcirc}^7}{235160106814144512000} \\ &- \frac{2377281942167559599461133495 9J_{\bigstar}^{10}/J_{\bigcirc}^9}{14658112233383615100402794496000 00}\,. \end{aligned} \tag{A.1}$$

The series in the limit $J_{\bigstar} \gg J_{\bigcirc}$ is the same up to an exchange of $J_{\bigstar}$ and $J_{\bigcirc}$ due to the exact self-duality. For the ground-state energy $e_{0,B}$ of H_B per vertex up to order ten one finds [118]

$$\begin{aligned} e_{0,B}^{J_{\square}\ll J_{+}} = &- 3J_{+} - \frac{3J_{\square}^2/J_{+}}{16} - \frac{195J_{\square}^4/J_{+}^3}{28672} - \frac{7052113J_{\square}^6/J_{+}^5}{6936330240} \\ &- \frac{2392948067252749J_{\square}^8/J_{+}^7}{10853543391422054400} \\ &- \frac{5879767026395403486947158 43J_{\square}^{10}/J_{+}^9}{99715049206691259186413568000 00}, \end{aligned} \tag{A.2}$$

and for the other limit $J_{+} \ll J_{\square}$ one gets [118]

$$\begin{aligned} e_{0,B}^{J_{+} \ll J_{\square}} = &-3J_{\square} - \frac{3J_{+}^2/J_{\square}}{16} - \frac{3J_{+}^3/J_{\square}^2}{128} - \frac{195J_{+}^4/J_{\square}^3}{28672} - \frac{4455J_{+}^5/J_{\square}^4}{1605632} \\ &- \frac{14445391J_{+}^6/J_{\square}^5}{12138577920} - \frac{286541706167J_{+}^7/J_{\square}^6}{489427461734400} \\ &- \frac{21431205246868721J_{+}^8/J_{\square}^7}{70548032044243353600} \\ &- \frac{16855520449846227741465 1J_{+}^9/J_{\square}^8}{10169075530985413961318400 00} \\ &- \frac{43066666341130689979363310 17J_{+}^{10}/J_{\square}^9}{45806600729323797188758732800000}\,. \end{aligned} \tag{A.3}$$

Note that in order to reach high perturbation orders, it is important to use appropriate selection rules [97, 99, 108, 130, 215] to identify non-contributing clusters as early as possible within the linked-cluster expansions as described in Subsect. 3.6.4.

A.2 Series expansion for the X-Cube model

In this section we give the series expansions for the ground-state energy per spin obtained for several perturbative limits of the X-Cube model in a magnetic field pointing in x or z direction. We manage to expand the available series expansions for the ground-state energy per spin [39] significantly using hypergraph decompositions [130] (see Sect. 3.6) together with matrix perturbation theory [95–97] (see Subsect. 3.4.4). For the field pointing in z-direction the series in the low-field limit can be directly deduced from the respective series for the plaquette Ising model in a transverse field given in Ref. [130] or Sect. 3.7 without further calculation. For the magnetic field pointing in x-direction we obtain

$$\begin{aligned} \frac{e_0}{J_{+}} = &-\frac{J_{\blacksquare}}{3J_{+}} - 1 - \frac{\lambda_x^2}{8} - \frac{11\lambda_x^4}{1536} - \frac{349\lambda_x^6}{221184} - \frac{902473\lambda_x^8}{1698693120} \\ &- \frac{13009537783\lambda_x^{10}}{58706834227200} - \frac{13170313859088551\lambda_x^{12}}{118352977802035200000} \end{aligned} \tag{A.4}$$

for the low-field limit $h_x \ll J_{+}$ where $\lambda_x = h_x/J_{+}$. Here we can execute the calculation in two different ways. One possibility is to use a dual model which is formulated in terms of lineon excitations [39]. As the elementary perturbation only acts on two sites, this problem can be tackled by a normal graph decomposition. These lineon excitations have the property that three different lineons recombine to the the local unperturbed ground state [222], though we still have the property that the perturbation needs to act at least twice on each site in order to reobtain the unperturbed ground state state at this site. So one can use a transitive selection rule based on counting vertices of degree one, and a non-transitive rule based on the detection of bridges as explained in Subsect. 3.5.4. However, one can also use the dual model in terms of the eigenvalues z_{+} [246], also described in Subsect. 5.2.1, where each elementary perturbation operator acts on four eigenvalues z_{+} at a time. Clearly, this model can be treated using linked-cluster expansions via a full hypergraph decomposition described in Ref. [130] and Sect. 3.6. In this formulation the perturbation simply flips four eigenvalues z_{+} and accordingly in order to reobtain the unperturbed ground state it has to act an even number of times on each site in the considered cluster, which makes the selection rules based on odd-degree vertices viable. These are described in Subsect. 3.6.4 and in the

literature [97, 99, 130]. For all the remaining three dual models these selection rules apply as well, so we just give the results. For the high-field limit $h_x \gg J_{\boldsymbol{+}}$ we obtain

$$\begin{aligned}\frac{e_0}{h_x} = -\frac{J_{\boldsymbol{\bullet}}}{3h_x} - 1 - \frac{\tilde{\lambda}_x^2}{8} - \frac{\tilde{\lambda}_x^3}{32} - \frac{11\tilde{\lambda}_x^4}{1536} - \frac{55\tilde{\lambda}_x^5}{18432} - \frac{733\tilde{\lambda}_x^6}{442368} - \frac{9403\tilde{\lambda}_x^7}{10616832} \\ - \frac{2605817\tilde{\lambda}_x^8}{5096079360} - \frac{98715107\tilde{\lambda}_x^9}{305764761600} - \frac{61822221557\tilde{\lambda}_x^{10}}{293534171136000} \\ - \frac{4975292628523\tilde{\lambda}_x^{11}}{35224100536320000} - \frac{11529979136214041\tilde{\lambda}_x^{12}}{118352977802035200000},\end{aligned} \tag{A.5}$$

where $\tilde{\lambda}_x = 1/\lambda_x = J_{\boldsymbol{+}}/h_x$. For the field pointing in z-direction the series in the low-field limit can be directly deduced from the result for the plaquette Ising model in a transverse field on the cubic lattice given in Ref. [130] and Sect. 3.7 without further calculations. Adjusting the units and adding another zeroth order term, the series results in

$$\begin{aligned}\frac{e_0}{J_{\boldsymbol{\bullet}}} = -\frac{J_{\boldsymbol{+}}}{J_{\boldsymbol{\bullet}}} - \frac{1}{3} - \frac{\lambda_z^2}{8} - \frac{113\lambda_z^4}{1536} - \frac{21427\lambda_z^6}{163840} - \frac{87959384893\lambda_z^8}{254803968000} \\ - \frac{1151818046218646 39\lambda_z^{10}}{102736959897600000} - \frac{11998648200089619699404 51\lambda_z^{12}}{28996479561498624000000 0},\end{aligned} \tag{A.6}$$

where $\lambda^z = h_z/J_{\boldsymbol{\bullet}}$. In the high-field limit $h_z \gg J_{\boldsymbol{\bullet}}$ we find

$$\begin{aligned}\frac{e_0}{h_z} = -\frac{J_{\boldsymbol{+}}}{h_z} - 1 - \frac{\tilde{\lambda}_z^2}{72} - \frac{17\tilde{\lambda}_z^4}{228096} - \frac{2307925\tilde{\lambda}_z^6}{1653327396864} \\ - \frac{34882117854510041 53\tilde{\lambda}_z^8}{88061074183163574484992000} \\ - \frac{12052987831402811783290917253466780 53\tilde{\lambda}_z^{10}}{87809194698991269281663926146395359150080000 0} \\ - \frac{27034291901360779965540812488395096478245464034736838963011 9\tilde{\lambda}_z^{12}}{50289930649023171224364298253321890732866187971389894846054400000000 00},\end{aligned} \tag{A.7}$$

where $\tilde{\lambda}^z = J_{\boldsymbol{\bullet}}/h_z$.

Appendix B

Variational calculation for the X-Cube model in a magnetic field in x-direction

In this appendix we show variational calculations for the X-Cube model in a uniform magnetic field in x-direction using the approach presented in Ref. [250]. These calculations are analogous to the ones presented in Sect. 6.5. Here, we use the variational state (6.34)

$$|\Psi_2^B\rangle = \mathcal{N}_2^B \prod_{+} (1 + \beta_2 Z_{+}) \, |\Rightarrow\rangle \, . \tag{B.1}$$

and calculate the expectation values of the operators contained in the Hamiltonian (5.10)

$$H^{\text{xcx}} = -J_{\square} N_{\square} - J_{+} \sum_{+} Z_{+} - h_x \sum_i \sigma_i^x, \tag{B.2}$$

the normalization factor $\mathcal{N}_2^B$ has already been calculated in Eq. (6.37)

$$\frac{1}{(\mathcal{N}_2^B)^2} = (1 + \beta_2^2)^{3N_{\square}} (1 + \zeta^3(\beta_2))^{N_{\square}}, \tag{B.3}$$

The expectation value of Z_{+} with respect to the variational state has already been calculated in (6.38)

$$\langle Z_{+} \rangle_{\Psi_2^B} = \frac{\zeta^2(\beta_2) + \zeta(\beta_2)}{1 + \zeta^3(\beta_2)}, \tag{B.4}$$

with $\zeta(x) = 2x/(1+x^2)$. The expectation value of σ_i^x with respect to the variational state remains to be calculated

$$\begin{aligned}
\langle \sigma_i^x \rangle_{\Psi_2^B} =& \mathcal{N}_B^2 \langle \Rightarrow | \prod_{+} (1+\beta_2 Z_{+}) \, \sigma_i^x \prod_{+} (1+\beta_2 Z_{+}) \, | \Rightarrow \rangle \\
=& \mathcal{N}_B^2 (1+\beta^2)^{3N_{\square}-4} \langle \Rightarrow | \prod_{+ \ni i} (1-\beta_2^2) \prod_{+ \not\ni i} (1+\zeta(\beta_2) Z_{+}) \, | \Rightarrow \rangle \\
=& \left(\frac{1-\beta_2^2}{1+\beta_2^2} \right)^4 \cdot \frac{1}{(1+\zeta^3(\beta_2))^{N_{\square}}} \sum_{i=0}^{N_{\square}-2} \binom{N_{\square}-2}{i} \zeta^{3i}(\beta_2) \\
=& \left(\frac{1-\beta_2^2}{1+\beta_2^2} \right)^4 \cdot \frac{1}{(1+\zeta^3(\beta_2))^2}.
\end{aligned} \tag{B.5}$$

With this we can write down the variational ground-state energy per cube

$$e_0^{\mathrm{xcx,binom}}(\beta_2) = -J_{\square} - 3J_{+} \frac{\zeta^2(\beta_2) + \zeta(\beta_2)}{1+\zeta^3(\beta_2)} - \frac{3h_x}{(1+\zeta^3(\beta_2))^2} \left(\frac{1-\beta_2^2}{1+\beta_2^2} \right)^4 \tag{B.6}$$

In order to obtain the data presented in Ref. [39] we did a slight error in the calculation [246], neglecting that the product of the three different operators Z_{+} at a vertex equals identity [244,245]. In the units used here this would result in [246]

$$e_0^{\mathrm{xcx,approx}}(\beta_2) = -J_{\square} - 3J_{+}\zeta(\beta_2) - 3h_x \left(\frac{1-\beta_2^2}{1+\beta_2^2} \right)^4 . \tag{B.7}$$

One easily sees that for $\zeta(\beta_2) \ll 1$ this approximates the variational ground-state energy from Eq. (B.6). From now on we set $J_{\square} = J_{+} = J$ for simplicity. In Figs. B.1 and B.2 we explore the quantitative differences of both approaches from the polarized limit of large h_x. In the topological phase the variational energies do only incorporate the zeroth order effects in h_x which is a known problem for these kind of variational ansätze [250]. The energies in the polarized phase are a far better approximation. Indeed, the variational energy with the binomial coefficients matches the series expansions about the high field-limit up to order three in J/h_x, while the approximation still matches up to order two as illustrated in Fig. B.2.

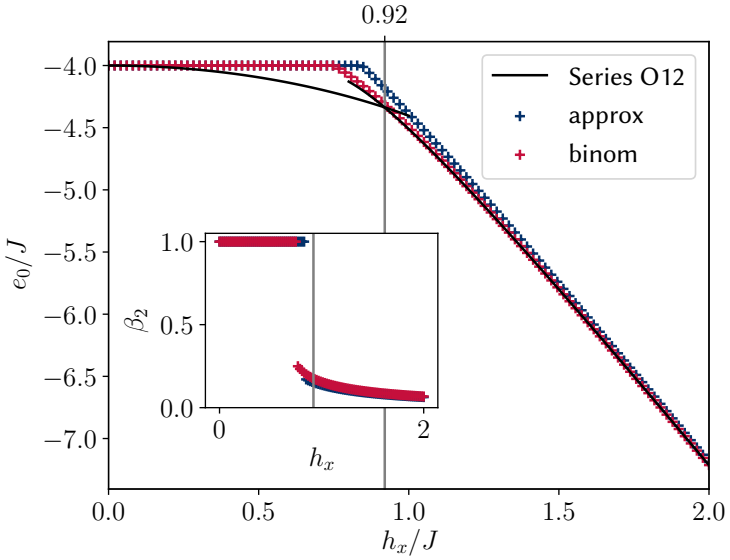

Figure B.1: The ground-state energy per cube of the X-Cube model in a x-directed magnetic field. Comparison of the two different variational energies and the series expansion results. The inset shows the variational parameter β_2 for which $e_0^{\mathrm{xcx}}(\beta_2)$ is minimal.

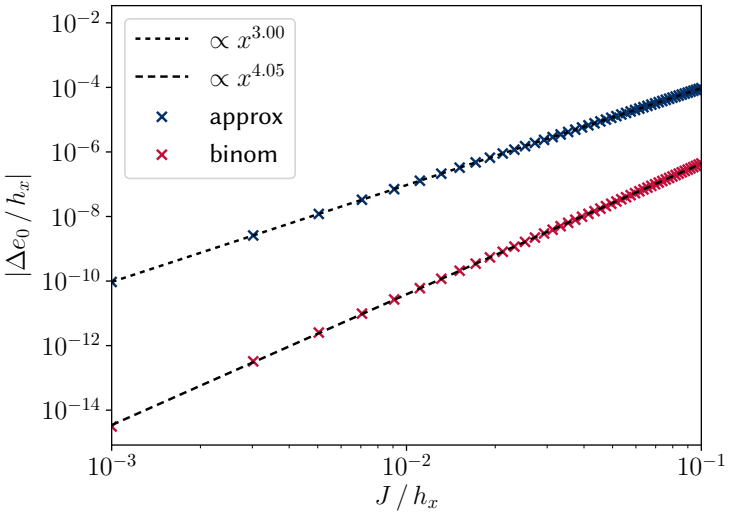

Figure B.2: The absolute value of the difference between the series expansion result about the limit of $J/h_x \ll 1$ and the variational energies. While the approximative variational energy $e_0^{\mathrm{xcx,approx}}$ already differs significantly from the series expansion in order three, the correct variational energy $e_0^{\mathrm{xcx,binom}}$ starts to differ in order four.

List of publications

This is a list of all research papers I have contributed to during the work on this thesis. The contents of the publications listed as most relevant for this thesis are at least partially included in this thesis.

Most relevant publications for this thesis

Quantum robustness of fracton phases

Matthias Mühlhauser, Matthias R. Walther, David A. Reiß, Kai P. Schmidt.
Phys. Rev. B **101**, 054426 (2020). doi:10.1103/PhysRevB.101.054426

The project was initiated by D. A. Reiß and K. P. Schmidt. The part about the X-Cube model is based on my master's thesis [246], and the series expansions for the X-Cube model have been calculated by me. The part on Haah's cubic code is based on the master's thesis of M. R. Walther [259], and the respective series expansions have been calculated by him. Both of these theses have been written under the supervision of K. P. Schmidt. The manuscript has been prepared in cooperation of all authors.

Competing topological orders in three dimensions

Matthias Mühlhauser, Kai P. Schmidt, Julien Vidal, Matthias R. Walther.
SciPost Phys. **12**, 069 (2022). doi:10.21468/SciPostPhys.12.2.069

The project was initiated by K. P. Schmidt, J. Vidal and M. R. Walther. I calculated the series expansions for the ground-state energy. The ground-state degeneracies on the three-torus given in the appendix were determined by M. R. Walther and me. The manuscript has been prepared and approved by all authors. It is also important to mention that during the work for this publication we worked on variational calculations for the problem. These calculations were done by M. R. Walther and me under the supervision of K. P. Schmidt and J. Vidal.

Linked cluster expansions via hypergraph decompositions

Matthias Mühlhauser, Kai P. Schmidt.
Phys. Rev. E **105**, 064110 (2022). doi:10.1103/PhysRevE.105.064110

The development of the presented hypergraph approach to linked-cluster expansions its implementation into a computer program and application including the calculation of the presented series expansions for the plaquette Ising model on the cubic lattice have been done by me under the supervision of K. P. Schmidt. The final manuscript has been written by both authors.

Absence of fractal quantum criticality in the quantum Newman-Moore model

Raymond Wiedmann, Lea Lenke, Matthias Mühlhauser, Kai P. Schmidt.
Phys. Rev. Research **6**, 013191 (2024). doi:10.1103/PhysRevResearch.6.013191

The publication is based on the master's thesis of R. Wiedmann [260] which has been supervised by K. P. Schmidt. I contributed the numerical linked-cluster expansion results and drafted the section about linked-cluster expansions in the appendix. The final manuscript has been prepared in collaboration of all authors.

Incorporating non-local anyonic statistics into a graph decomposition

Matthias Mühlhauser, Viktor Kott, Kai P. Schmidt
SciPost Phys. Core **7**, 031 (2024). doi:10.21468/SciPostPhysCore.7.2.031

The insights on how to set up a full hypergraph decomposition in the low-field limit of the toric code in a homogeneous magnetic field should be attributed to all three authors. However, most of the conceptual and technical work regarding the hypergraph decomposition in this particular case has been done by me under the supervision of K. P. Schmidt. The presented series expansions have been calculated by V. Kott. All authors have been involved in the preparation of the final manuscript.

Further publications

Quantum critical phase transition between two topologically ordered phases in the Ising toric code bilayer

Raymond Wiedmann, Lea Lenke, Matthias R. Walther, Matthias Mühlhauser, Kai P. Schmidt.
Phys. Rev. B **102**, 214422 (2020). doi:10.1103/PhysRevB.102.214422

Fine grained tensor network methods

Philipp Schmoll, Saeed S. Jahromi, Max Hörmann, Matthias Mühlhauser, Kai P. Schmidt, Román Orús.
Phys. Rev. Lett. **124**, 200603 (2020). doi:10.1103/PhysRevLett.124.200603

High-order series expansion of non-Hermitian quantum spin models

Lea Lenke, Matthias Mühlhauser, Kai P. Schmidt.
Phys. Rev. B **104**, 195137 (2021), doi:10.1103/PhysRevB.104.195137

Quantum phase transitions in the K-layer Ising toric code

Lukas Schamriß, Lea Lenke, Matthias Mühlhauser, Kai P. Schmidt.
Phys. Rev. B **105**, 184425 (2022). doi:10.1103/PhysRevB.105.184425

Order-by-disorder and long-range interactions in the antiferromagnetic transverse-field Ising model on the triangular lattice – A perturbative point of view

Jan A. Koziol, Matthias Mühlhauser, Kai P. Schmidt.
Results in Physics **61** 107794 (2024). doi:10.1016/j.rinp.2024.107794

Quantum robustness of the toric code in a parallel field on the honeycomb and triangular lattice

Viktor Kott, Matthias Mühlhauser, Jan A. Koziol, Kai P. Schmidt.
SciPost Phys. **17** 053 (2024). doi:10.21468/SciPostPhys.17.2.053

Preprints

Order-by-disorder in the antiferromagnetic J_1-J_2-J_3 transverse-field Ising model on the ruby lattice

Antonia Duft, Jan A. Koziol, Patrick Adelhardt, Matthias Mühlhauser, Kai P. Schmidt. arXiv:2312.12941 (2023). doi:10.48550/arXiv.2312.12941

List of Acronyms

CUT: Continuous unitary transformation
DMRG: Density matrix renormalization group
ED: Exact diagonalization
ELCE: Exact linked-cluster expansion
GSD: Ground-state degeneracy
LCE: Linked-cluster expansion
MBOT: Multi-block orthogonal transformation
MPS: Matrix product state
NLCE: Numerical linked-cluster expansion
pCAT: Projective cluster additive transformation
pCUT: Perturbative continuous unitary transformation
QPT: Quantum phase transition
SSE: Stochastic series expansions
PEPS: Projected entangled pair states
TBOT: Two-block orthogonal transformation
TFIM: Transverse-field Ising model
TFPIM: Transverse-field plaquette Ising model
TN: Tensor network
QMC: Quantum Monte Carlo
VQE: Variational Quantum Eigensolver

Bibliography

[1] I. Bloch, J. Dalibard, and W. Zwerger. Many-body physics with ultracold gases. Rev. Mod. Phys. **80** 885 (2008). doi:10.1103/RevModPhys.80.885.

[2] J. W. Britton, B. C. Sawyer, A. C. Keith, C.-C. J. Wang, J. K. Freericks, H. Uys, M. J. Biercuk, and J. J. Bollinger. Engineered two-dimensional Ising interactions in a trapped-ion quantum simulator with hundreds of spins. Nature **484** 489 (2012). doi:10.1038/nature10981.

[3] C. Gross and I. Bloch. Quantum simulations with ultracold atoms in optical lattices. Science **357** 995 (2017). doi:10.1126/science.aal3837.

[4] P. Schauss. Quantum simulation of transverse Ising models with Rydberg atoms. Quantum Science and Technology **3** 023001 (2018). doi:10.1088/2058-9565/aa9c59.

[5] R. Liao, F. Xiong, and X. Chen. Simulating an exact one-dimensional transverse Ising model in an optical lattice. Phys. Rev. A **103** 043312 (2021). doi:10.1103/PhysRevA.103.043312.

[6] T. Vojta. Quantum phase transitions in electronic systems. Ann. Phys. **512** 403 (2000). doi:10.1002/andp.20005120601.

[7] M. Vojta. Quantum phase transitions. Reports on Progress in Physics **66** 2069 (2003). doi:10.1088/0034-4885/66/12/R01.

[8] S. Sachdev. *Quantum Phase Transitions*. Cambridge University Press, Cambridge, second ed. (2011). doi:10.1017/CBO9780511973765.

[9] A. Dutta, G. Aeppli, B. K. Chakrabarti, U. Divakaran, T. F. Rosenbaum, and D. Sen. *Quantum Phase Transitions in Transverse Field Spin Models: From Statistical Physics to Quantum Information*. Cambridge University Press, Cambridge (2015). doi:10.1017/CBO9781107706057.

[10] P. Pfeuty. The one-dimensional Ising model with a transverse field. Ann. Phys. (NY) **57** 79 (1970). doi:10.1016/0003-4916(70)90270-8.

[11] X. G. Wen. Vacuum degeneracy of chiral spin states in compactified space. Phys. Rev. B **40** 7387 (1989). doi:10.1103/PhysRevB.40.7387.

[12] X. G. Wen and Q. Niu. Ground-state degeneracy of the fractional quantum Hall states in the presence of a random potential and on high-genus Riemann surfaces. Phys. Rev. B **41** 9377 (1990). doi:10.1103/PhysRevB.41.9377.

[13] X. G. Wen. Topological orders in rigid states. Int. J. Mod. Phys B **04** 239 (1990). doi:10.1142/S0217979290000139.

[14] X.-G. Wen. *Quantum Field Theory of Many-Body Systems.* Oxford University Press, Oxford (2004).

[15] M. Levin and X.-G. Wen. Detecting topological order in a ground state wave function. Phys. Rev. Lett. **96** 110405 (2006). doi:10.1103/PhysRevLett.96.110405.

[16] A. Kitaev and J. Preskill. Topological entanglement entropy. Phys. Rev. Lett. **96** 110404 (2006). doi:10.1103/PhysRevLett.96.110404.

[17] D. Arovas, J. R. Schrieffer, and F. Wilczek. Fractional statistics and the quantum Hall effect. Phys. Rev. Lett. **53** 722 (1984). doi:10.1103/PhysRevLett.53.722.

[18] A. Y. Kitaev. Fault-tolerant quantum computation by anyons. Ann. Phys. (NY) **303** 2 (2003). doi:10.1016/S0003-4916(02)00018-0.

[19] A. Hamma, P. Zanardi, and X.-G. Wen. String and membrane condensation on three-dimensional lattices. Phys. Rev. B **72** 035307 (2005). doi:10.1103/PhysRevB.72.035307.

[20] Z. Nussinov and G. Ortiz. Autocorrelations and thermal fragility of anyonic loops in topologically quantum ordered systems. Phys. Rev. B **77** 064302 (2008). doi:10.1103/PhysRevB.77.064302.

[21] A. Kitaev. Anyons in an exactly solved model and beyond. Ann. Phys. (NY) **321** 2 (2006). doi:10.1016/j.aop.2005.10.005.

[22] K. J. Satzinger, Y.-J. Liu, A. Smith, C. Knapp, M. Newman, C. Jones, Z. Chen, C. Quintana, X. Mi, A. Dunsworth, C. Gidney, I. Aleiner, F. Arute, K. Arya, J. Atalaya, R. Babbush, J. C. Bardin, R. Barends, J. Basso, A. Bengtsson, A. Bilmes, M. Broughton, B. B. Buckley, D. A. Buell, B. Burkett, N. Bushnell, B. Chiaro, R. Collins, W. Courtney, S. Demura, A. R. Derk, D. Eppens, C. Erickson, L. Faoro, E. Farhi, A. G. Fowler, B. Foxen, M. Giustina, A. Greene, J. A. Gross, M. P. Harrigan, S. D. Harrington, J. Hilton, S. Hong, T. Huang, W. J. Huggins, L. B. Ioffe, S. V. Isakov, E. Jeffrey, Z. Jiang, D. Kafri, K. Kechedzhi, T. Khattar, S. Kim, P. V. Klimov, A. N. Korotkov, F. Kostritsa, D. Landhuis, P. Laptev, A. Locharla, E. Lucero, O. Martin, J. R. McClean, M. McEwen, K. C. Miao, M. Mohseni, S. Montazeri, W. Mruczkiewicz, J. Mutus, O. Naaman, M. Neeley, C. Neill, M. Y. Niu, T. E. O'Brien, A. Opremcak, B. Pató, A. Petukhov, N. C. Rubin, D. Sank, V. Shvarts, D. Strain, M. Szalay, B. Villalonga, T. C. White, Z. Yao, P. Yeh, J. Yoo, A. Zalcman, H. Neven, S. Boixo, A. Megrant, Y. Chen, J. Kelly, V. Smelyanskiy, A. Kitaev, M. Knap, F. Pollmann, and P. Roushan. Realizing topologically ordered states on a quantum processor. Science **374** 1237 (2021). doi:10.1126/science.abi8378.

[23] M. Mühlhauser, V. Kott, and K. P. Schmidt. Incorporating non-local anyonic statistics into a graph decomposition. SciPost Phys. Core **7** 031 (2024). doi:10.21468/SciPostPhysCore.7.2.031.

[24] J. Haah. Local stabilizer codes in three dimensions without string logical operators. Phys. Rev. A **83** 042330 (2011). doi:10.1103/PhysRevA.83.042330.

[25] S. Vijay, J. Haah, and L. Fu. A new kind of topological quantum order: A dimensional hierarchy of quasiparticles built from stationary excitations. Phys. Rev. B **92** 235136 (2015). doi:10.1103/PhysRevB.92.235136.

[26] S. Vijay, J. Haah, and L. Fu. Fracton topological order, generalized lattice gauge theory, and duality. Phys. Rev. B **94** 235157 (2016). doi:10.1103/PhysRevB.94.235157.

[27] R. M. Nandkishore and M. Hermele. Fractons. Annu. Rev. Condens. Matter Phys. **10** 295 (2019). doi:10.1146/annurev-conmatphys-031218-013604.

[28] K. Slagle and Y. B. Kim. Quantum field theory of X-cube fracton topological order and robust degeneracy from geometry. Phys. Rev. B **96** 195139 (2017). doi:10.1103/PhysRevB.96.195139.

[29] K. Slagle and Y. B. Kim. X-cube model on generic lattices: Fracton phases and geometric order. Phys. Rev. B **97** 165106 (2018). doi:10.1103/PhysRevB.97.165106.

[30] H. Ma, A. T. Schmitz, S. A. Parameswaran, M. Hermele, and R. M. Nandkishore. Topological entanglement entropy of fracton stabilizer codes. Phys. Rev. B **97** 125101 (2018). doi:10.1103/PhysRevB.97.125101.

[31] H. He, Y. Zheng, B. A. Bernevig, and N. Regnault. Entanglement entropy from tensor network states for stabilizer codes. Phys. Rev. B **97** 125102 (2018). doi:10.1103/PhysRevB.97.125102.

[32] M. Pretko, X. Chen, and Y. You. Fracton phases of matter. Int. J. Mod. Phys A **35** 2030003 (2020). doi:10.1142/S0217751X20300033.

[33] J. Vidal, S. Dusuel, and K. P. Schmidt. Low-energy effective theory of the toric code model in a parallel magnetic field. Phys. Rev. B **79** 033109 (2009). doi:10.1103/PhysRevB.79.033109.

[34] I. S. Tupitsyn, A. Kitaev, N. V. Prokof'ev, and P. C. E. Stamp. Topological multicritical point in the phase diagram of the toric code model and three-dimensional lattice gauge Higgs model. Phys. Rev. B **82** 085114 (2010). doi:10.1103/PhysRevB.82.085114.

[35] S. Dusuel, M. Kamfor, R. Orús, K. P. Schmidt, and J. Vidal. Robustness of a perturbed topological phase. Phys. Rev. Lett. **106** 107203 (2011). doi:10.1103/PhysRevLett.106.107203.

[36] F. Wu, Y. Deng, and N. Prokof'ev. Phase diagram of the toric code model in a parallel magnetic field. Phys. Rev. B **85** 195104 (2012). doi:10.1103/PhysRevB.85.195104.

[37] M. Kamfor, S. Dusuel, J. Vidal, and K. P. Schmidt. Spectroscopy of a topological phase. Phys. Rev. B **89** 045411 (2014). doi:10.1103/PhysRevB.89.045411.

[38] D. A. Reiss and K. P. Schmidt. Quantum robustness and phase transitions of the 3D Toric Code in a field. SciPost Phys. **6** 078 (2019). doi:10.21468/SciPostPhys.6.6.078.

[39] M. Mühlhauser, M. R. Walther, D. A. Reiss, and K. P. Schmidt. Quantum robustness of fracton phases. Phys. Rev. B **101** 054426 (2020). doi:10.1103/PhysRevB.101.054426.

[40] H. Q. Lin. Exact diagonalization of quantum-spin models. Phys. Rev. B **42** 6561 (1990). doi:10.1103/PhysRevB.42.6561.

[41] A. W. Sandvik. Computational Studies of Quantum Spin Systems. AIP Conf. Proc. **1297** 135 (2010). doi:10.1063/1.3518900.

[42] C. Lanczos. An iteration method for the solution of the eigenvalue problem of linear differential and integral operators. Journal of Research of the National Bureau of Standards **45** 255 (1950). doi:10.6028/jres.045.026.

[43] C. C. Paige. Accuracy and effectiveness of the Lanczos algorithm for the symmetric eigenproblem. Linear Algebra and its Applications **34** 235 (1980). doi:10.1016/0024-3795(80)90167-6.

[44] A. M. Läuchli, J. Sudan, and R. Moessner. $S = \frac{1}{2}$ kagome Heisenberg antiferromagnet revisited. Phys. Rev. B **100** 155142 (2019). doi:10.1103/PhysRevB.100.155142.

[45] S. R. White. Density matrix formulation for quantum renormalization groups. Phys. Rev. Lett. **69** 2863 (1992). doi:10.1103/PhysRevLett.69.2863.

[46] S. R. White. Density-matrix algorithms for quantum renormalization groups. Phys. Rev. B **48** 10345 (1993). doi:10.1103/PhysRevB.48.10345.

[47] U. Schollwöck. The density-matrix renormalization group. Rev. Mod. Phys. **77** 259 (2005). doi:10.1103/RevModPhys.77.259.

[48] K. Hallberg. New trends in density matrix renormalization. arXiv:cond-mat/0609039 (2006). doi:10.48550/arxiv.cond-mat/0609039.

[49] M.-C. Chung and I. Peschel. Density-matrix spectra for two-dimensional quantum systems. Phys. Rev. B **62** 4191 (2000). doi:10.1103/PhysRevB.62.4191.

[50] H. C. Jiang, Z. Y. Weng, and D. N. Sheng. Density matrix renormalization group numerical study of the kagome antiferromagnet. Phys. Rev. Lett. **101** 117203 (2008). doi:10.1103/PhysRevLett.101.117203.

[51] R. Hagymási, I.and Schäfer, R. Moessner, and D. J. Luitz. Possible inversion symmetry breaking in the $S = 1/2$ Pyrochlore Heisenberg magnet. Phys. Rev. Lett. **126** 117204 (2021). doi:10.1103/PhysRevLett.126.117204.

[52] S. Östlund and S. Rommer. Thermodynamic limit of density matrix renormalization. Phys. Rev. Lett. **75** 3537 (1995). doi:10.1103/PhysRevLett.75.3537.

[53] U. Schollwöck. The density-matrix renormalization group in the age of matrix product states. Ann. Phys. (NY) **326** 96 (2011). doi:10.1016/j.aop.2010.09.012.

[54] T. Xiang. *Density Matrix and Tensor Network Renormalization.* Cambridge University Press, Cambridge (2023).

[55] R. Orús. A practical introduction to tensor networks: Matrix product states and projected entangled pair states. Ann. Phys. (NY) **349** 117 (2014). doi:10.1016/j.aop.2014.06.013.

[56] F. Verstraete and J. I. Cirac. Renormalization algorithms for quantum-many body systems in two and higher dimensions. arXiv:cond-mat/0407066 (2004). doi:10.48550/arXiv.cond-mat/0407066.

[57] J. I. Cirac, D. Pérez-García, N. Schuch, and F. Verstraete. Matrix product states and projected entangled pair states: Concepts, symmetries, theorems. Rev. Mod. Phys. **93** 045003 (2021). doi:10.1103/RevModPhys.93.045003.

[58] R. Orús. Tensor networks for complex quantum systems. Nature Reviews Physics **1** 538 (2019). doi:10.1038/s42254-019-0086-7.

[59] J. Jordan, R. Orús, G. Vidal, F. Verstraete, and J. I. Cirac. Classical simulation of infinite-size quantum lattice systems in two spatial dimensions. Phys. Rev. Lett. **101** 250602 (2008). doi:10.1103/PhysRevLett.101.250602.

[60] S.-J. Ran, E. Tirrito, C. Peng, X. Chen, L. Tagliacozzo, G. Su, and M. Lewenstein. *Tensor Network Approaches for Higher-Dimensional Quantum Lattice Models*, page 87. Springer, Cham (2020). doi:10.1007/978-3-030-34489-4_4.

[61] M. P. Zaletel and F. Pollmann. Isometric tensor network states in two dimensions. Phys. Rev. Lett. **124** 037201 (2020). doi:10.1103/PhysRevLett.124.037201.

[62] M. S. J. Tepaske and D. J. Luitz. Three-dimensional isometric tensor networks. Phys. Rev. Res. **3** 023236 (2021). doi:10.1103/PhysRevResearch.3.023236.

[63] K. Sfairopoulos, L. Causer, J. F. Mair, and J. P. Garrahan. Boundary conditions dependence of the phase transition in the quantum Newman-Moore model. Phys. Rev. B **108** 174107 (2023). doi:10.1103/PhysRevB.108.174107.

[64] G.-Y. Zhu, J.-Y. Chen, P. Ye, and S. Trebst. Topological fracton quantum phase transitions by tuning exact tensor network states. Phys. Rev. Lett. **130** 216704 (2023). doi:10.1103/PhysRevLett.130.216704.

[65] D. C. Handscomb. The Monte Carlo method in quantum statistical mechanics. Math. Proc. Cambridge Philos. Soc. **58** 594 (1962). doi:10.1017/S0305004100040639.

[66] M. Suzuki. Quantum statistical Monte Carlo methods and applications to spin systems. J. Stat. Phys. **43** 883 (1986). doi:10.1007/bf02628318.

[67] M. Suzuki, S. Miyashita, and A. Kuroda. Monte Carlo simulation of quantum spin systems. i. Progress of Theoretical Physics **58** 1377 (1977). doi:10.1143/PTP.58.1377.

[68] A. W. Sandvik and J. Kurkijärvi. Quantum Monte Carlo simulation method for spin systems. Phys. Rev. B **43** 5950 (1991). doi:10.1103/PhysRevB.43.5950.

[69] A. W. Sandvik. A generalization of handscomb's quantum Monte Carlo scheme-application to the 1D Hubbard model. J. Phys. A: Math. Gen. **25** 3667 (1992). doi:10.1088/0305-4470/25/13/017.

[70] A. W. Sandvik. Finite-size scaling of the ground-state parameters of the two-dimensional Heisenberg model. Phys. Rev. B **56** 11678 (1997). doi:10.1103/PhysRevB.56.11678.

[71] P. Adelhardt, J. A. Koziol, A. Langheld, and K. P. Schmidt. Monte Carlo based techniques for quantum magnets with long-range interactions (2024). doi:10.3390/e26050401.

[72] J. A. Koziol, A. Langheld, S. C. Kapfer, and K. P. Schmidt. Quantum-critical properties of the long-range transverse-field Ising model from quantum Monte Carlo simulations. Phys. Rev. B **103** 245135 (2021). doi:10.1103/PhysRevB.103.245135.

[73] A. Langheld, J. A. Koziol, P. Adelhardt, S. C. Kapfer, and K. P. Schmidt. Scaling at quantum phase transitions above the upper critical dimension. SciPost Phys. **13** 088 (2022). doi:10.21468/SciPostPhys.13.4.088.

[74] E. Y. Loh, J. E. Gubernatis, R. T. Scalettar, S. R. White, D. J. Scalapino, and R. L. Sugar. Sign problem in the numerical simulation of many-electron systems. Phys. Rev. B **41** 9301 (1990). doi:10.1103/PhysRevB.41.9301.

[75] P. Henelius and A. W. Sandvik. Sign problem in Monte Carlo simulations of frustrated quantum spin systems. Phys. Rev. B **62** 1102 (2000). doi:10.1103/PhysRevB.62.1102.

[76] M. Troyer and U.-J. Wiese. Computational complexity and fundamental limitations to fermionic quantum Monte Carlo simulations. Phys. Rev. Lett. **94** 170201 (2005). doi:10.1103/PhysRevLett.94.170201.

[77] G. Pan and Z. Y. Meng. The sign problem in quantum Monte Carlo simulations. In *Encyclopedia of Condensed Matter Physics*, pages 879–893. Academic Press, Oxford, second edition ed. (2024). doi:10.1016/b978-0-323-90800-9.00095-0.

[78] T. Nakamura. Vanishing of the negative-sign problem of quantum Monte Carlo simulations in one-dimensional frustrated spin systems. Phys. Rev. B **57** R3197 (1998). doi:10.1103/PhysRevB.57.R3197.

[79] A. Honecker, S. Wessel, R. Kerkdyk, T. Pruschke, F. Mila, and B. Normand. Thermodynamic properties of highly frustrated quantum spin ladders: Influence of many-particle bound states. Phys. Rev. B **93** 054408 (2016). doi:10.1103/PhysRevB.93.054408.

[80] F. Alet, K. Damle, and S. Pujari. Sign-problem-free Monte Carlo simulation of certain frustrated quantum magnets. Phys. Rev. Lett. **117** 197203 (2016). doi:10.1103/PhysRevLett.117.197203.

[81] S. Wessel, B. Normand, F. Mila, and A.Honecker. Efficient Quantum Monte Carlo simulations of highly frustrated magnets: the frustrated spin-1/2 ladder. SciPost Phys. **3** 005 (2017). doi:10.21468/SciPostPhys.3.1.005.

[82] L. Weber, N. Caci, and S. Wessel. Cluster quantum Monte Carlo study of two-dimensional weakly coupled frustrated trimer antiferromagnets. Phys. Rev. B **106** 035141 (2022). doi:10.1103/PhysRevB.106.035141.

[83] A. Honecker, L. Weber, P. Corboz, F. Mila, and S. Wessel. Quantum Monte Carlo simulations of highly frustrated magnets in a cluster basis: The two-dimensional Shastry-Sutherland model. J. Phys.: Conf. Ser. **2207** 012032 (2022). doi:10.1088/1742-6596/2207/1/012032.

[84] T. Devakul, S. A. Parameswaran, and S. L. Sondhi. Correlation function diagnostics for type-I fracton phases. Phys. Rev. B **97** 041110 (2018). doi:10.1103/PhysRevB.97.041110.

[85] C. Zhou, M.-Y. Li, Z. Yan, P. Ye, and Z. Y. Meng. Evolution of dynamical signature in the X-cube fracton topological order. Phys. Rev. Res. **4** 033111 (2022). doi:10.1103/PhysRevResearch.4.033111.

[86] Z. Zhou, X.-F. Zhang, F. Pollmann, and Y. You. Fractal quantum phase transitions: Critical phenomena beyond renormalization. arXiv:2105.05851 (2021). doi:10.48550/arXiv.2105.05851.

[87] F. Wegner. Flow-equations for Hamiltonians. Ann. Phys. **506** 77 (1994). doi:10.1002/andp.19945060203.

[88] S. D. Glazek and K. G. Wilson. Perturbative renormalization group for Hamiltonians. Phys. Rev. D **49** 4214 (1994). doi:10.1103/PhysRevD.49.4214.

[89] S. Dusuel and G. S. Uhrig. The quartic oscillator: a non-perturbative study by continuous unitary transformations. J. Phys. A: Math. Gen. **37** 9275 (2004). doi:10.1088/0305-4470/37/39/014.

[90] G. Carleo and M. Troyer. Solving the quantum many-body problem with artificial neural networks. Science **355** 602 (2017). doi:10.1126/science.aag2302.

[91] A. Valenti, E. Greplova, N. H. Lindner, and S. D. Huber. Correlation-enhanced neural networks as interpretable variational quantum states. Phys. Rev. Res. **4** L012010 (2022). doi:10.1103/PhysRevResearch.4.L012010.

[92] M. Machaczek, L. Pollet, and K. Liu. Neural quantum state study of fracton models. arXiv:2406.11677 (2024). doi:10.48550/arXiv.2406.11677.

[93] A. Peruzzo, J. McClean, P. Shadbolt, M.-H. Yung, X.-Q. Zhou, P. J. Love, A. Aspuru-Guzik, and J. L. O'Brien. A variational eigenvalue solver on a photonic quantum processor. Nat. Commun. **5** 4213 (2014). doi:10.1038/ncomms5213.

[94] J. Tilly, H. Chen, S. Cao, D. Picozzi, K. Setia, Y. Li, E. Grant, L. Wossnig, I. Rungger, G. H. Booth, and J. Tennyson. The Variational Quantum Eigensolver: A review of methods and best practices. Physics Reports **986** 1 (2022). doi:10.1016/j.physrep.2022.08.003. The Variational Quantum Eigensolver: a review of methods and best practices.

[95] M. P. Gelfand, R. R. P. Singh, and D. A. Huse. Perturbation expansions for quantum many-body systems. J. Stat. Phys. **59** 1093 (1990). doi:10.1007/bf01334744.

[96] M. P. Gelfand and R. R. P. Singh. High-order convergent expansions for quantum many particle systems. Adv. Phys. **49** 93 (2000). doi:10.1080/000187300243390.

[97] J. Oitmaa, C. Hamer, and W. Zheng. *Series Expansion Methods for Strongly Interacting Lattice Models*. Cambridge University Press, Cambridge (2006). doi:10.1017/CBO9780511584398.

[98] L. G. Marland. Series expansions for the zero-temperature transverse Ising model. J. Phys. A: Math. Gen. **14** 2047 (1981). doi:10.1088/0305-4470/14/8/027.

[99] H.-X. He, C. J. Hamer, and J. Oitmaa. High-temperature series expansions for the (2+1)-dimensional Ising model. J. Phys. A: Math. Gen. **23** 1775 (1990). doi:10.1088/0305-4470/23/10/018.

[100] J. Oitmaa, C. J. Hamer, and Z. Weihong. Low-temperature series expansions for the (2+1)-dimensional Ising model. J. Phys. A: Math. Gen. **24** 2863 (1991). doi:10.1088/0305-4470/24/12/024.

[101] C. Hamer, J. Oitmaa, and Z. Weihong. Series analysis of the 3-state Potts model in (2+1) dimensions. J. Phys. A: Math. Gen. **25** 1821 (1992). doi:10.1088/0305-4470/25/7/023.

[102] A. Koga and N. Kawakami. Quantum phase transitions in the Shastry-Sutherland model for $SrCu_2(BO_3)_2$. Phys. Rev. Lett. **84** 4461 (2000). doi:10.1103/PhysRevLett.84.4461.

[103] C. Knetter and G. Uhrig. Perturbation theory by flow equations: dimerized and frustrated S = 1/2 chain. Eur. Phys. J. B **13** 209 (2000). doi:10.1007/s100510050026.

[104] J. Röchner, L. Balents, and K. P. Schmidt. Spin liquid and quantum phase transition without symmetry breaking in a frustrated three-dimensional Ising model. Phys. Rev. B **94** 201111 (2016). doi:10.1103/PhysRevB.94.201111.

[105] R. Wiedmann, L. Lenke, M. Mühlhauser, and K. P. Schmidt. Absence of fractal quantum criticality in the quantum Newman-Moore model. Phys. Rev. Res. **6** 013191 (2024). doi:10.1103/PhysRevResearch.6.013191.

[106] Z. Weihong, J. Oitmaa, and C. J. Hamer. Series expansions for the 3d transverse Ising model at T=0. J. of Phys. A: Math. Gen. **27** 5425 (1994). doi:10.1088/0305-4470/27/16/010.

[107] M. D. Schulz, S. Dusuel, K. P. Schmidt, and J. Vidal. Topological phase transitions in the golden string-net model. Phys. Rev. Lett. **110** 147203 (2013). doi:10.1103/PhysRevLett.110.147203.

[108] K. Coester, D. G. Joshi, M. Vojta, and K. P. Schmidt. Linked-cluster expansions for quantum magnets on the hypercubic lattice. Phys. Rev. B **94** 125109 (2016). doi:10.1103/PhysRevB.94.125109.

[109] S. Fey and K. P. Schmidt. Critical behavior of quantum magnets with long-range interactions in the thermodynamic limit. Phys. Rev. B **94** 075156 (2016). doi:10.1103/PhysRevB.94.075156.

[110] S. Fey, S. C. Kapfer, and K. P. Schmidt. Quantum criticality of two-dimensional quantum magnets with long-range interactions. Phys. Rev. Lett. **122** 017203 (2019). doi:10.1103/PhysRevLett.122.017203.

[111] P. Adelhardt, J. A. Koziol, A. Schellenberger, and K. P. Schmidt. Quantum criticality and excitations of a long-range anisotropic xy chain in a transverse field. Phys. Rev. B **102** 174424 (2020). doi:10.1103/PhysRevB.102.174424.

[112] L. Lenke, M. Mühlhauser, and K. P. Schmidt. High-order series expansion of non-Hermitian quantum spin models. Phys. Rev. B **104** 195137 (2021). doi:10.1103/PhysRevB.104.195137.

[113] L. Schamriß, L. Lenke, M. Mühlhauser, and K. P. Schmidt. Quantum phase transitions in the K-layer Ising toric code. Phys. Rev. B **105** 184425 (2022). doi:10.1103/PhysRevB.105.184425.

[114] P. Adelhardt and K. P. Schmidt. Continuously varying critical exponents in long-range quantum spin ladders. SciPost Phys. **15** 087 (2023). doi:10.21468/SciPostPhys.15.3.087.

[115] C. Domb and M. S. Green, eds. *Series expansions for Lattice Models*, vol. 3. Academic Press, London (1974).

[116] A. J. Guttmann. Asymptotic Analysis of Power-Series expansions. In C. Domb and J. L. Lebowitz, eds., *Phase Transitions and Critical Phenomena*, vol. 13. Academic Press, London (1989).

[117] M. Powalski, K. Coester, R. Moessner, and K. P. Schmidt. Disorder by disorder and flat bands in the kagome transverse field Ising model. Phys. Rev. B **87** 054404 (2013). doi:10.1103/PhysRevB.87.054404.

[118] M. Mühlhauser, K. P. Schmidt, J. Vidal, and M. R. Walther. Competing topological orders in three dimensions. SciPost Phys. **12** 069 (2022). doi:10.21468/SciPostPhys.12.2.069.

[119] V. Kott, M. Mühlhauser, J. A. Koziol, and K. P. Schmidt. Quantum robustness of the toric code in a parallel field on the honeycomb and triangular lattice. SciPost Phys. **17** 053 (2024). doi:10.21468/SciPostPhys.17.2.053.

[120] C. Knetter, K. P. Schmidt, and G. S. Uhrig. The structure of operators in effective particle-conserving models. J. Phys. A: Math. Gen. **36** 7889 (2003). doi:10.1088/0305-4470/36/29/302.

[121] S. Dusuel, M. Kamfor, K. P. Schmidt, R. Thomale, and J. Vidal. Bound states in two-dimensional spin systems near the Ising limit: A quantum finite-lattice study. Phys. Rev. B **81** 064412 (2010). doi:10.1103/PhysRevB.81.064412.

[122] M. D. Schulz, S. Dusuel, R. Orús, J. Vidal, and K. P. Schmidt. Breakdown of a perturbed $\mathbb{Z}_N$ topological phase. New J. Phys. **14** 025005 (2012). doi:10.1088/1367-2630/14/2/025005.

[123] K. Coester and K. P. Schmidt. Optimizing linked-cluster expansions by white graphs. Phys. Rev. E **92** 022118 (2015). doi:10.1103/PhysRevE.92.022118.

[124] M. P. Gelfand. Series expansions for excited states of quantum lattice models. Solid State Communications **98** 11 (1996). doi:10.1016/0038-1098(96)00051-8.

[125] M. Rigol, T. Bryant, and R. R. P. Singh. Numerical linked-cluster approach to quantum lattice models. Phys. Rev. Lett. **97** 187202 (2006). doi:10.1103/PhysRevLett.97.187202.

[126] B. Tang, E. Khatami, and M. Rigol. A short introduction to numerical linked-cluster expansions. Comput. Phys. Commun. **184** 557 (2013). doi:10.1016/j.cpc.2012.10.008.

[127] C. J. Hamer and A. C. Irving. Cluster expansions in the (2+1)D Ising model. J. Phys. A: Math. Gen. **17** 1649 (1984). doi:10.1088/0305-4470/17/8/021.

[128] H. Y. Yang and K. P. Schmidt. Effective models for gapped phases of strongly correlated quantum lattice models. EPL **94** 17004 (2011). doi:10.1209/0295-5075/94/17004.

[129] Sumeet, M. Hörmann, and K. P. Schmidt. Hybrid quantum-classical algorithm for the transverse-field Ising model in the thermodynamic limit. arXiv:2310.07600 (2023). doi:10.48550/arXiv.2310.07600.

[130] M. Mühlhauser and K. P. Schmidt. Linked cluster expansions via hypergraph decompositions. Phys. Rev. E **105** 064110 (2022). doi:10.1103/PhysRevE.105.064110.

[131] C. Berge. *Graphs and Hypergraphs*. North-Holland, Amsterdam (1973).

[132] A. A. Zykov. HYPERGRAPHS. Russian Mathematical Surveys **29** 89 (1974). doi:10.1070/RM1974v029n06ABEH001303.

[133] B. D. McKay. Practical graph isomorphism. Congressus Numerantium **30** 45 (1981).

[134] E. V. Konstantinova and V. A. Skorobogatov. Molecular hypergraphs: The new representation of nonclassical molecular structures with polycentric delocalized bonds. J. Chem. Inf. Comput. Sci. **35** 472 (1995). doi:10.1021/ci00025a015.

[135] E. V. Konstantinova and V. A. Skoroboratov. Graph and hypergraph models of molecular structure: A comparative analysis of indices. Journal of Structural Chemistry **39** 958 (1998). doi:10.1007/bf02903615.

[136] E. V. Konstantinova and V. A. Skorobogatov. Application of hypergraph theory in chemistry. Discrete Mathematics **235** 365 (2001). doi:10.1016/S0012-365X(00)00290-9.

[137] The plaquette Ising model is a limiting case of a gonihedric Ising model [261–266].

[138] A. Lipowski. Glassy behaviour and semi-local invariance in Ising model with four-spin interaction. J. Phys. A: Math. Gen. **30** 7365 (1997). doi:10.1088/0305-4470/30/21/012.

[139] S. Davatolhagh, D. Dariush, and L. Separdar. Nature of the glassy transition in simulations of the ferromagnetic plaquette Ising model. Phys. Rev. E **81** 031501 (2010). doi:10.1103/PhysRevE.81.031501.

[140] D. A. Johnston, M. Mueller, and W. Janke. Plaquette Ising models, degeneracy and scaling. Eur. Phys. J. Spec. Top. **226** 749 (2017). doi:10.1140/epjst/e2016-60329-4.

[141] R. C. Read and D. G. Corneil. The graph isomorphism disease. Journal of Graph Theory **1** 339 (1977). doi:10.1002/jgt.3190010410.

[142] V. Bonnici, R. Giugno, A. Pulvirenti, D. Shasha, and A. Ferro. A subgraph isomorphism algorithm and its application to biochemical data. BMC Bioinformatics **14** S13 (2013). doi:10.1186/1471-2105-14-s7-s13.

[143] M. Grohe and P. Schweitzer. The graph isomorphism problem. Communications of the ACM **63** 128 (2020). doi:10.1145/3372123.

[144] P. T. Darga, M. H. Liffiton, K. A. Sakallah, and I. L. Markov. Exploiting structure in symmetry detection for CNF. In *Proceedings of the 41st Annual Design Automation Conference*, page 530. ACM, New York (2004). doi:10.1145/996566.996712.

[145] T. Junttila and P. Kaski. *Engineering an Efficient Canonical Labeling Tool for Large and Sparse Graphs*, page 135. Society for Industrial and Applied Mathematics (2007). doi:10.1137/1.9781611972870.13.

[146] J. L. López-Presa and A. Fernández Anta. Fast algorithm for graph isomorphism testing. In J. Vahrenhold, ed., *Experimental Algorithms*, page 221. Springer, Berlin (2009).

[147] B. D. McKay and A. Piperno. Practical graph isomorphism, II. Journal of Symbolic Computation **60** 94 (2014). doi:10.1016/j.jsc.2013.09.003.

[148] J. R. Ullmann. An algorithm for subgraph isomorphism. Journal of the ACM **23** 31 (1976). doi:10.1145/321921.321925.

[149] L. P. Cordella, P. Foggia, C. Sansone, and M. Vento. Performance evaluation of the VF graph matching algorithm. In *Proceedings. 10th International Conference on Image Analysis and Processing*, page 1172 (1999). doi:10.1109/ICIAP.1999.797762.

[150] L. Cordella, P. Foggia, C. Sansone, and M. Vento. A (sub)graph isomorphism algorithm for matching large graphs. IEEE Trans. Pattern Anal. Mach. Intell. **26** 1367 (2004). doi:10.1109/TPAMI.2004.75.

[151] C. Solnon. AllDifferent-based filtering for subgraph isomorphism. Artificial Intelligence **174** 850 (2010). doi:10.1016/j.artint.2010.05.002.

[152] M. Houbraken, S. Demeyer, T. Michoel, P. Audenaert, D. Colle, and M. Pickavet. The Index-Based Subgraph Matching Algorithm with General Symmetries (ISMAGS): Exploiting Symmetry for Faster Subgraph Enumeration. PLOS ONE **9** 1 (2014). doi:10.1371/journal.pone.0097896.

[153] V. Carletti, P. Foggia, A. Saggese, and M. Vento. Challenging the time complexity of exact subgraph isomorphism for huge and dense graphs with VF3. IEEE Trans. Pattern Anal. Mach. Intell. **40** 804 (2018). doi:10.1109/TPAMI.2017.2696940.

[154] C. McCreesh, P. Prosser, and J. Trimble. The glasgow subgraph solver: Using constraint programming to tackle hard subgraph isomorphism problem variants. In *Graph Transformation*, pages 316–324. Springer (2020). doi:10.1007/978-3-030-51372-6_19.

[155] F. Harary. *Graph theory*. Addison Wesley, Reading, Massachusetts (1969).

[156] J. Harris, J. L. Hirst, and M. Mossinghoff. *Combinatorics and Graph Theory*. Springer, New York, second ed. (2008). doi:10.1007/978-0-387-79711-3.

[157] M. S. Rahman. *Basic Graph Theory*. Springer, Cham (2017). doi:10.1007/978-3-319-49475-3.

[158] G. Gallo, G. Longo, S. Pallottino, and S. Nguyen. Directed hypergraphs and applications. Discrete Applied Mathematics **42** 177 (1993). doi:10.1016/0166-218X(93)90045-P.

[159] K. Böhmová, J. Chalopin, M. Mihalák, G. Proietti, and P. Widmayer. Sequence hypergraphs. In P. Heggernes, ed., *Graph-Theoretic Concepts in Computer Science*, page 282. Springer, Berlin (2016).

[160] N. Reff and L. J. Rusnak. An oriented hypergraphic approach to algebraic graph theory. Linear Algebra and its Applications **437** 226 (2012). doi:10.1016/j.laa.2012.06.011.

[161] J. Jost and R. Mulas. Normalized Laplace operators for hypergraphs with real coefficients. J. Complex Netw. **9** cnab009 (2021). doi:10.1093/comnet/cnab009.

[162] R. Balakrishnan and K. Ranganathan. *A Textbook of Graph Theory*. Springer, New York (2012). doi:10.1007/978-1-4614-4529-6.

[163] R. M. R. Lewis. *A Guide to Graph Colouring*. Springer, Cham (2016). doi:10.1007/978-3-319-25730-3.

[164] V. Bonnici and R. Giugno. On the variable ordering in subgraph isomorphism algorithms. IEEE/ACM Trans. Comput. Biol. Bioinform. **14** 193 (2017). doi:10.1109/TCBB.2016.2515595.

[165] F. V. Fomin, D. Lokshtanov, V. Raman, S. Saurabh, and B. V. R. Rao. Faster algorithms for finding and counting subgraphs. J. Comput. Syst. Sci. **78** 698 (2012). doi:10.1016/j.jcss.2011.10.001.

[166] M. Dehmer, M. Grabner, A. Mowshowitz, and F. Emmert-Streib. An efficient heuristic approach to detecting graph isomorphism based on combinations of highly discriminating invariants. Advances in Computational Mathematics **39** 311 (2012). doi:10.1007/s10444-012-9281-0.

[167] M. Dehmer, F. Emmert-Streib, and M. Grabner. A computational approach to construct a multivariate complete graph invariant. Information Sciences **260** 200 (2014). doi:10.1016/j.ins.2013.11.008.

[168] P. Boldi. Graph Invariants. In *Encyclopedia of Big Data Technologies*, page 848. Springer, Cham (2019). doi:10.1007/978-3-319-77525-8_77.

[169] D. Neuen. *The power of algorithmic approaches to the graph isomorphism problem*. Ph.D. thesis, RWTH Aachen (2019). doi:10.18154/RWTH-2020-00160.

[170] M. Grohe, D. Neuen, and D. Wiebking. Isomorphism testing for graphs excluding small minors. SIAM Journal on Computing **52** 238 (2023). doi:10.1137/21m1401930.

[171] J. D. Dixon and B. Mortimer. *Permutation Groups*. Springer, New York (1996).

[172] C. Berge. *Hypergraphs*. North-Holland, Amsterdam (1989).

[173] A. Bretto. *Hypergraph Theory*. Springer, Cham (2013). doi:10.1007/978-3-319-00080-0.

[174] L. Wang, E. K. Egorova, and A. V. Mokryakov. Development of hypergraph theory. Journal of Computer and Systems Sciences International **57** 109 (2018). doi:10.1134/s1064230718010136.

[175] X. Ouvrard. Hypergraphs: an introduction and review. arXiv:2002.05014 (2020). doi:10.48550/arXiv.2002.05014.

[176] G. Ausiello and L. Laura. Directed hypergraphs: Introduction and fundamental algorithms—a survey. Theoretical Computer Science **658** 293 (2017). doi:10.1016/j.tcs.2016.03.016.

[177] H. Müller. Oriented hypergraphs, stability numbers and chromatic numbers. Discrete Mathematics **34** 319 (1981). doi:10.1016/0012-365X(81)90011-X.

[178] P. Frankl. What must be contained in every oriented k-uniform hypergraph. Discrete Mathematics **62** 311 (1986). doi:10.1016/0012-365X(86)90219-0.

[179] A. C. Irving and C. J. Hamer. Methods in hamiltonian lattice field theory (II). linked-cluster expansions. Nucl. Phys. B **230** 361 (1984). doi:10.1016/0550-3213(84)90218-9.

[180] A. C. Irving and C. J. Hamer. Linked cluster expansions for U(1) lattice gauge theory in 2 + 1 and 3 + 1 dimensions. Nucl. Phys. B **235** 358 (1984). doi:10.1016/0550-3213(84)90504-2.

[181] M. Hörmann and K. P. Schmidt. Projective cluster-additive transformation for quantum lattice models. SciPost Phys. **15** 097 (2023). doi:10.21468/SciPostPhys.15.3.097.

[182] S. Trebst, H. Monien, C. J. Hamer, Z. Weihong, and R. R. P. Singh. Strong-coupling expansions for multiparticle excitations: Continuum and bound states. Phys. Rev. Lett. **85** 4373 (2000). doi:10.1103/PhysRevLett.85.4373.

[183] W. Zheng, C. J. Hamer, R. R. P. Singh, S. Trebst, and H. Monien. Linked cluster series expansions for two-particle bound states. Phys. Rev. B **63** 144410 (2001). doi:10.1103/PhysRevB.63.144410.

[184] C. J. Hamer, W. Zheng, and R. R. P. Singh. Dynamical structure factor for the alternating Heisenberg chain: A linked cluster calculation. Phys. Rev. B **68** 214408 (2003). doi:10.1103/PhysRevB.68.214408.

[185] M. Rigol, T. Bryant, and R. R. P. Singh. Numerical linked-cluster algorithms. I. spin systems on square, triangular, and kagomé lattices. Phys. Rev. E **75** 061118 (2007). doi:10.1103/PhysRevE.75.061118.

[186] K. Cöster. *Quasiparticle pictures and graphs - from perturbative to non-perturbative linked-cluster expansions*. Ph.D. thesis, TU Dortmund (2015). doi:10.17877/DE290R-16955.

[187] M. D. Schulz. *Topological phase transitions driven by non-Abelian anyons*. Ph.D. thesis, TU Dortmund (2014). doi:10.17877/DE290R-13177.

[188] A. Syropoulos. Mathematics of multisets. In C. S. Calude, G. Păun, G. Rozenberg, and A. Salomaa, eds., *Multiset Processing*, page 347. Springer, Berlin (2001). doi:10.1007/3-540-45523-X_17.

[189] A. Schellenberger, M. Hörmann, and K. P. Schmidt. Dynamic structure factor of the antiferromagnetic Kitaev model in large magnetic fields. Phys. Rev. B **106** 104403 (2022). doi:10.1103/PhysRevB.106.104403.

[190] J. J. Sakurai. *Modern Quantum Mechanics*. Addison-Wesley, Reading, Massachussets, revised ed. (1994).

[191] C. C. Tannoudji, B. Diu, and F. Laloë. *Quantum Mechanics*, vol. II: Angular Momentun, Spin and Approximation Methods. Wiley-VCH, Weinheim, second ed. (2020).

[192] M. Takahashi. Half-filled Hubbard model at low temperature. J. Phys. C: Solid State Phys. **10** 1289 (1977). doi:10.1088/0022-3719/10/8/031.

[193] To the best of our knowledge an implementation of a bookkeeping technique to directly obtain the reduced contributions with Takahashi's method was first done by Patrick Adelhardt.

[194] K. P. Schmidt. *Spectral properties of quasi one-dimensional quantum antiferromagnets. Perturbative continuous unitary transformations.* Ph.D. thesis, Universität zu Köln (2004).

[195] A. Mielke. Flow equations for band-matrices. Eur. Phys. J. B **5** 605 (1998). doi:10.1007/s100510050485.

[196] C. Knetter. *Perturbative Continuous Unitary Transformations: Spectral Properties of Low Dimensional Spin Systems.* Ph.D. thesis, Universiät zu Köln (2003).

[197] D. Klagges and K. P. Schmidt. Constraints on measurement-based quantum computation in effective cluster states. Phys. Rev. Lett. **108** 230508 (2012). doi:10.1103/PhysRevLett.108.230508.

[198] T. Kato. On the Convergence of the Perturbation Method. I. Progress of Theoretical Physics **4** 514 (1949). doi:10.1143/ptp/4.4.514.

[199] F. Mila and K. P. Schmidt. Strong-Coupling Expansion and Effective Hamiltonians. In C. Lacroix, P. Mendels, and F. Mila, eds., *Introduction to Frustrated Magnetism: Materials, Experiments, Theory*, page 537. Springer, Berlin (2011). doi:10.1007/978-3-642-10589-0_20.

[200] M. Hörmann. *Effects of quenched disorder on spectral densities of gapped quantum antiferromagnets.* Ph.D. thesis, FAU Erlangen-Nürnberg (2022).

[201] P.-O. Löwdin. Studies in Perturbation Theory. IV. Solution of Eigenvalue Problem by Projection Operator Formalism. J. Math. Phys. **3** 969 (2004). doi:10.1063/1.1724312.

[202] D. Yao and J. Shi. Projection operator approach to time-independent perturbation theory in quantum mechanics. Am. J. Phys. **68** 278 (2000). doi:10.1119/1.19419.

[203] T. Griffin and S. D. Bartlett. Spin lattices with two-body Hamiltonians for which the ground state encodes a cluster state. Phys. Rev. A **78** 062306 (2008). doi:10.1103/PhysRevA.78.062306.

[204] D. Klagges. *Effektive Zweispinmodelle für Cluster-State-Hamilton-Operatoren.* Diploma thesis, TU Dortmund (2011). German.

[205] H. Kalis, D. Klagges, R. Orús, and K. P. Schmidt. Fate of the cluster state on the square lattice in a magnetic field. Phys. Rev. A **86** 022317 (2012). doi:10.1103/PhysRevA.86.022317.

[206] J. Oitmaa and Z. Weihong. Two-parameter expansions for quantum spin systems. J. Phys. A: Math. Gen. **25** 5849 (1992). doi:10.1088/0305-4470/25/22/013.

[207] Daniel Klagges provided very generic and efficient computer implementations of Takahashi's perturbation theory, Löwdin's partitioning technqiue and pCUT.

[208] M. Powalski. *Quantum paramagnetism in the kagome and triangular transverse field Ising model.* Master's thesis, TU Dortmund (2016).

[209] R. Schäfer, I. Hagymási, R. Moessner, and D. J. Luitz. Pyrochlore $S = \frac{1}{2}$ Heisenberg antiferromagnet at finite temperature. Phys. Rev. B **102** 054408 (2020). doi:10.1103/PhysRevB.102.054408.

[210] A. R. Hehn. *Series Expansion Methods for Quantum Lattice Models.* Ph.D. thesis, ETH Zürich (2016). doi:10.3929/ETHZ-A-010742232.

[211] B. D. McKay. Isomorph-free exhaustive generation. Journal of Algorithms **26** 306 (1998). doi:10.1006/jagm.1997.0898.

[212] M. I. Stankevitch, S. S. Tratch, and N. S. Zefirov. Combinatorial models and algorithms in chemistry. search for isomorphisms and automorphisms of molecular graphs. J. Comput. Chem. **9** 303 (1988). doi:10.1002/jcc.540090405.

[213] X. Liu and D. J. Klein. The graph isomorphism problem. J. Comput. Chem. **12** 1243 (1991). doi:10.1002/jcc.540121012.

[214] M. Müller. *Clusterentwicklungen für dimerisierte Spinsysteme.* Ph.D. thesis, Universität Hannover (2002). doi:10.15488/6072.

[215] D. G. Joshi, K. Coester, K. P. Schmidt, and M. Vojta. Nonlinear bond-operator theory and $1/d$ expansion for coupled-dimer magnets. I. paramagnetic phase. Phys. Rev. B **91** 094404 (2015). doi:10.1103/PhysRevB.91.094404.

[216] K. Cöster. *Series expansions for dimerized quantum spin systems.* Diploma thesis, TU Dortmund (2011).

[217] L. M. Vasiloiu, T. H. E. Oakes, F. Carollo, and J. P. Garahan. Trajectory phase transitions in noninteracting spin systems. Phys. Rev. E **101** 042115 (2020). doi:10.1103/PhysRevE.101.042115.

[218] M. D. Schulz, S. Dusuel, G. Misguich, K. P. Schmidt, and J. Vidal. Ising anyons with a string tension. Phys. Rev. B **89** 201103 (2014). doi:10.1103/PhysRevB.89.201103.

[219] G. Rücker. and C. Rücker. Automatic enumeration of all connected subgraphs. MATCH Commun. Math. Comput. Chem. **41** 145 (2000).

[220] G. Rücker and C. Rücker. On finding nonisomorphic connected subgraphs and distinct molecular substructures. J. Chem. Inf. Comput. Sci. **41** 314 (2001). doi:10.1021/ci000092b.

[221] A. Prem, J. Haah, and R. Nandkishore. Glassy quantum dynamics in translation invariant fracton models. Phys. Rev. B **95** 155133 (2017). doi:10.1103/PhysRevB.95.155133.

[222] W. Shirley, K. Slagle, and X. Chen. Fractional excitations in foliated fracton phases. Ann. Phys. (NY) **410** 167922 (2019). doi:10.1016/j.aop.2019.167922.

[223] S. Trebst, P. Werner, M. Troyer, K. Shtengel, and C. Nayak. Breakdown of a topological phase: Quantum phase transition in a loop gas model with tension. Phys. Rev. Lett. **98** 070602 (2007). doi:10.1103/PhysRevLett.98.070602.

[224] A. Hamma and D. A. Lidar. Adiabatic preparation of topological order. Phys. Rev. Lett. **100** 030502 (2008). doi:10.1103/PhysRevLett.100.030502.

[225] J. Yu, S.-P. Kou, and X.-G. Wen. Topological quantum phase transition in the transverse Wen-plaquette model. Eur. Phys. Lett. **84** 17004 (2008). doi:10.1209/0295-5075/84/17004.

[226] J. Vidal, R. Thomale, K. P. Schmidt, and S. Dusuel. Self-duality and bound states of the toric code model in a transverse field. Phys. Rev. B **80** 081104 (2009). doi:10.1103/PhysRevB.80.081104.

[227] M. Iqbal and N. Schuch. Entanglement order parameters and critical behavior for topological phase transitions and beyond. Phys. Rev. X **11** 041014 (2021). doi:10.1103/PhysRevX.11.041014.

[228] S. C. Morampudi, C. W. von Keyserlingk, and F. Pollmann. Numerical study of a transition between $\mathbb{Z}_2$ topologically ordered phases. Phys. Rev. B **90** 035117 (2014). doi:10.1103/PhysRevB.90.035117.

[229] Y. Zhang, R. G. Melko, and E.-A. Kim. Machine learning $\mathbb{Z}_2$ quantum spin liquids with quasiparticle statistics. Phys. Rev. B **96** 245119 (2017). doi:10.1103/PhysRevB.96.245119.

[230] L. Vanderstraeten, M. Mariën, J. Haegeman, N. Schuch, J. Vidal, and F. Verstraete. Bridging perturbative expansions with tensor networks. Phys. Rev. Lett. **119** 070401 (2017). doi:10.1103/PhysRevLett.119.070401.

[231] R. Alicki, M. Fannes, and M. Horodecki. On thermalization in Kitaev's 2D model. J. Phys. A: Math. Theor. **42** 065303 (2009). doi:10.1088/1751-8113/42/6/065303.

[232] C. Castelnovo and C. Chamon. Entanglement and topological entropy of the toric code at finite temperature. Phys. Rev. B **76** 184442 (2007). doi:10.1103/PhysRevB.76.184442.

[233] Z. Nussinov and G. Ortiz. Symmetry and topological order. Proc. Nat. Acad. Sci. **106** 16944 (2009). doi:10.1073/pnas.0803726105.

[234] G. B. Halász and A. Hamma. Probing topological order with Rényi entropy. Phys. Rev. A **86** 062330 (2012). doi:10.1103/PhysRevA.86.062330.

[235] S. Santra, A. Hamma, L. Cincio, Y. Subasi, P. Zanardi, and L. Amico. Local convertibility of the ground state of the perturbed toric code. Phys. Rev. B **90** 245128 (2014). doi:10.1103/PhysRevB.90.245128.

[236] D. I. Tsomokos, A. Hamma, W. Zhang, S. Haas, and R. Fazio. Topological order following a quantum quench. Phys. Rev. A **80** 060302 (2009). doi:10.1103/PhysRevA.80.060302.

[237] A. Rahmani and C. Chamon. Exact results on the quench dynamics of the entanglement entropy in the toric code. Phys. Rev. B **82** 134303 (2010). doi:10.1103/PhysRevB.82.134303.

[238] M. Kamfor. *Robustness and spectroscopy of the toric code in a magnetic field.* Ph.D. thesis, TU Dortmund (2013). doi:10.17877/DE290R-5590.

[239] T. de Neef and I. G. Enting. Series expansions from the finite lattice method. J. Phys. A: Math. Gen. **10** 801 (1977). doi:10.1088/0305-4470/10/5/013.

[240] C. Xu and J. E. Moore. Strong-weak coupling self-duality in the two-dimensional quantum phase transition of $p + ip$ superconducting arrays. Phys. Rev. Lett. **93** 047003 (2004). doi:10.1103/PhysRevLett.93.047003.

[241] Z. Nussinov and E. Fradkin. Discrete sliding symmetries, dualities, and self-dualities of quantum orbital compass models and $p+ip$ superconducting arrays. Phys. Rev. B **71** 195120 (2005). doi:10.1103/PhysRevB.71.195120.

[242] L. J. Rusnak. Oriented hypergraphs: Introduction and balance. The Electronic Journal of Combinatorics **20** (2013). doi:10.37236/2763.

[243] H. Ma, E. Lake, X. Chen, and M. Hermele. Fracton topological order via coupled layers. Phys. Rev. B **95** 245126 (2017). doi:10.1103/PhysRevB.95.245126.

[244] S. Pai and M. Hermele. Fracton fusion and statistics. Phys. Rev. B **100** 195136 (2019). doi:10.1103/PhysRevB.100.195136.

[245] E. Lake and M. Hermele. Subdimensional criticality: Condensation of lineons and planons in the X-cube model. Phys. Rev. B **104** 165121 (2021). doi:10.1103/PhysRevB.104.165121.

[246] M. Mühlhauser. *Robustness of fracton phases under external magnetic fields.* Master's thesis, FAU Erlangen-Nürnberg (2018).

[247] The QMC data has been provided by Trithep Devakul. A description how to set up QMC simulations for the X-Cube model in a parallel magnetic field can be found in Ref. [84].

[248] M. Mühlhauser. Supplementary data for the doctoral thesis "Graph decomposition techniques for quantum spin systems with multi-spin interactions". Zenodo (2024). doi:10.5281/zenodo.13482029.

[249] C. Castelnovo and C. Chamon. Topological order in a three-dimensional toric code at finite temperature. Phys. Rev. B **78** 155120 (2008). doi:10.1103/PhysRevB.78.155120.

[250] S. Dusuel and J. Vidal. Mean-field ansatz for topological phases with string tension. Phys. Rev. B **92** 125150 (2015). doi:10.1103/PhysRevB.92.125150.

[251] D. Ixert and K. P. Schmidt. Nonperturbative linked-cluster expansions in long-range ordered quantum systems. Phys. Rev. B **94** 195133 (2016). doi:10.1103/PhysRevB.94.195133.

[252] M. Abdelshafy and M. Rigol. L-based numerical linked cluster expansion for square lattice models. Phys. Rev. E **108** 034126 (2023). doi:10.1103/PhysRevE.108.034126.

[253] P. Graves-Morris, D. Roberts, and A. Salam. The epsilon algorithm and related topics. J. Comput. Appl. Math. **122** 51 (2000). doi:10.1016/S0377-0427(00)00355-1.

[254] M. Rigol, T. Bryant, and R. R. P. Singh. Numerical linked-cluster algorithms. II. $t-J$ models on the square lattice. Phys. Rev. E **75** 061119 (2007). doi:10.1103/PhysRevE.75.061119.

[255] C. J. Hamer and M. N. Barber. Finite-lattice methods in quantum Hamiltonian field theory. I. The Ising model. J. Phys. A: Math. Gen. **14** 241 (1981). doi:10.1088/0305-4470/14/1/024.

[256] M. Pirke. *Numerical linked cluster expansions for the transverse field Ising model.* Bachelor's thesis, FAU Erlangen-Nürnberg (2022).

[257] L. Schamriß, M. R. Walther, and K. P. Schmidt. Extracting quantum-critical properties from directly evaluated enhanced perturbative continuous unitary transformations. arXiv:2402.18989 (2024). doi:10.48550/arXiv.2402.18989.

[258] L. Pierre, B. Bernu, and L. Messio. High temperature series expansions of S = 1/2 Heisenberg spin models: algorithm to include the magnetic field with optimized complexity. arXiv:2404.02271 (2024). doi:10.48550/arXiv.2404.02271.

[259] M. R. Walther. *Breakdown of topological type-II fracton phases.* Master's thesis, FAU Erlangen-Nürnberg (2019).

[260] R. Wiedmann. *Fractal Quantum Criticality in the Newman-Moore Model in a transverse field investigated using linked cluster expansions.* Master's thesis, FAU Erlangen-Nürnberg (2022).

[261] G. K. Savvidy and K. G. Savvidy. Self-avoiding surfaces and spin systems. Phys. Lett. B **324** 72 (1994). doi:10.1016/0370-2693(94)00114-6.

[262] G. K. Savvidy, K. G. Savvidy, and F. J. Wegner. Geometrical string and dual spin systems. Nucl. Phys. B **443** 565 (1995). doi:10.1016/0550-3213(95)00151-H.

[263] D. A. Johnston and R. P. K. C. Malmini. Gonihedric 3D Ising actions. Phys. Lett. B **378** 87 (1996). doi:10.1016/0370-2693(96)00391-7.

[264] M. Baig, D. Espriu, D. A. Johnston, and R. P. K. C. Malmini. String tension in gonihedric three-dimensional Ising models. J. Phys. A: Math. Gen. **30** 7695 (1997). doi:10.1088/0305-4470/30/22/009.

[265] D. Espriu, M. Baig, D. A. Johnston, and R. P. K. C. Malmini. Evidence for a first-order transition in a plaquette three-dimensional Ising-like action. J. Phys. A: Math. Gen. **30** 405 (1997). doi:10.1088/0305-4470/30/2/008.

[266] M. Mueller, W. Janke, and D. A. Johnston. Planar ordering in the plaquette-only gonihedric Ising model. Nucl. Phys. B **894** 1 (2015). doi:10.1016/j.nuclphysb.2015.02.020.

Acknowledgments

First of all, I would like to thank Professor Kai Phillip Schmidt for supervising my thesis. In particular, I appreciate that he gave me the freedom to follow own ideas while providing the necessary guidance at the same time. Moreover, I am grateful that he has always been available for questions and that he has been very supportive and motivating also in the more difficult phases of my PhD. I would also like to thank all my collaborators for the stimulating and appreciating discussions which contributed to widen my horizon.

Furthermore, I would like to thank Max Hörmann, Lea Lenke, Jan Koziol, Andreas Schellenberger, and Matthias Walther for their valuable feedback on some parts of this thesis. I am also very grateful to Matthias and Lea for creating a friendly but still productive atmosphere in our office. In general, I wish to thank all the people at Theoretische Physik I and V for providing such a friendly, supportive and stimulating working environment. In particular, I wish to thank the computer administration team for always being available for technical questions, and Ingrid for helping with all possible administrative issues.

I also would like to express my gratitude towards the administration team of QuCoLiMa and the RTG for the good collaboration and for always being kind and supportive. Moreover, I am grateful to the researchers of the RTG, which were helping with tasks during events or conferences, at times even without the need to ask them.

I also wish to thank my friends, not only for the good times spent together, but also for being there in more challenging times. Finally, I would like to express my deep gratitude towards my family for their continuous and unconditional support.

Eigenständigkeitserklärung

Hiermit erkläre ich, die vorliegende Arbeit eigenständig verfasst, und keine anderen als die angegebenen Quellen und Hilfsmittel verwendet zu haben.

Erlangen, September 2024

Matthias Mühlhauser